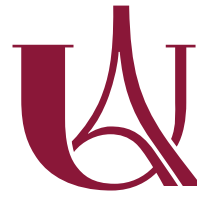




POLITECNICO
DI TORINO



Université
de Paris

Master double degree course in
Nanotechnologies for ICTs and Quantum Devices

Master Degree Thesis

Quantum toolbox for cavity quantum electrodynamics

Supervisors

Prof. Carlo Ricciardi

Prof. Maria Luisa Della Rocca

Candidate
Fabrizio Berritta

Internship Tutor
Center for Nanoscience and Nanotechnology (C2N)
Dr. Loïc Lanco

June 2020

This thesis is licensed under a Creative Commons License, Attribution – NonCommercial – NoDerivative Works 4.0 International: see www.creativecommons.org. The text may be reproduced for non-commercial purposes, provided that credit is given to the original author.

I hereby declare that the contents and organization of this dissertation constitute my own original work and does not compromise in any way the rights of third parties, including those relating to the security of personal data.

Fabrizio Berritta

Paris, 8 of July 2020

Abstract

This Thesis describes a custom-made cavity quantum electrodynamics (QED) toolbox for a quantum dot (QD) emitter in an optical micropillar. The toolbox has been developed for MATLAB® and it allows using either a full cavity-QED model or an effective adiabatic Hamiltonian to work only with the QD subspace. The toolbox simulates output intensities, first- and second-order correlations, and flux spectral densities both in continuous and pulsed wave regime. The results show that the adiabatic model reduces the computational cost in comparison to the full model, and allows performing accurate quantum optics simulations in the weak coupling regime between the QD and the cavity. For the approximation to yield satisfactory results, the cavity must decay at a faster timescale than the other subsystems, including the QD dynamics and the incoming field: the Rabi frequency of the QD must be much slower than the cavity damping rate, whereas, for the incoming field, its evolution must be slow compared to the photon lifetime in the cavity. This work also finds applications in the more general context of excited dipoles in 1-D photonic crystal waveguides and nanocavities, and it can be generalized to more complex and realistic systems. This includes the description of anisotropic neutral quantum dots, described by 3-level systems, or charged quantum dots with a spin degree of freedom, modeled by 4-level systems, taking into account the polarization degree of freedom for the cavity and input/output fields.

Acknowledgements

I would like to express my uttermost gratitude to my supervisor Dr. Loïc Lanço of the C2N laboratory, for his persistent guidance and help. I acknowledge the great effort that he has given to my internship. His relentless, yet thoughtful, perseverance has contributed greatly to making my thesis more accurate, comprehensible, and thorough.

I am very thankful to the Ph.D. students Clément Millet and Elham Mehdi for being always available to answer my questions and for having introduced me to the laboratory. Indeed, I would also like to thank all the members of the Solid-State Quantum Optics group for all the interesting and fruitful discussions that have kept me company during a worldwide lockdown.

The people that I am going to mention should stop reading right now. They could easily choose something more exciting for them to read or to do. Then, I would love to hear about it. However if you are one of them, unfortunately, you have decided to continue, not listening to my warning.

I thank the members of *L'Associazione*, with whom I share my dreams, literally and figuratively. I recognize their unconditional support during these last five years, drown into a carousel of emotions and experiences that have greatly outlined my way of thinking.

I would like to mention Eleonora Cappuccio. Although she has not contributed directly to this work, she has played a major role in all my life decisions that have led to this manuscript.

I am grateful to Gabriele Caliri and Lorenzo Giannì for their presence and all the valuable discussions, no matter the subject and the distance.

It goes without saying, I thank my Family.

Contents

List of Figures	5
1 Introduction	7
1.1 Photons and Quantum dots	7
1.2 Internship Presentation & State of The Art	8
1.3 Outline of the Thesis	9
2 Quantum Dots in Micropillar Cavities	11
2.1 The Quantum Dot and Pseudo-spin Systems	14
2.2 The Micropillar as a Cavity-QED	15
2.3 Jaynes–Cummings Model	17
2.4 Open Quantum Systems	18
2.4.1 Master equation	19
2.4.2 Input-output formalism	20
2.4.3 The “full” model	21
3 Cavity-QED Quantum Toolbox	23
3.1 Nonlinear Optics with CQED	24
3.2 First-order Coherence and Spectrum	27
3.2.1 Continuous wave regime	28
3.2.2 Pulsed wave regime	29
3.3 Second-order Coherence	35
4 Adiabatic Elimination	41
4.1 Approximations from the “Full Model”	43
4.2 Adiabatic Hamiltonian and Output Operators	44
4.3 Comparing Adiabatic and Full Model	45
4.3.1 Mollow triplets	45
4.3.2 Reflectivity in pulsed wave regime	48
5 Conclusions	51
A Correlations in Time Domain	53
A.1 First-order Coherence and Quantum Regression Theorem	53
A.2 Custom Wigner Distribution Function Script	54

B Supplementary Figures	57
C MATLAB® Scripts	61
C.1 Main scripts	61
C.1.1 Reflectivity spectrum in CW	61
C.1.2 Photon flux evolution and QD occupation in PW	65
C.1.3 First-order correlation and spectral densities in CW	70
C.1.4 First-order correlation and Wigner Distribution Function in PW	81
C.1.5 Second-order correlation in CW	96
C.1.6 Second-order correlation in PW	105
C.2 CQED device parameters	119
C.3 Subprograms	120
C.3.1 mesolve	120
C.3.2 Init 2level Hilbert space and operators	121
C.3.3 Init lists 2level CW scan laser frequency	124
C.3.4 Init lists 2level PW vs time	125
C.3.5 Init lists 2level g1SD CW vs delay and frequency	126
C.3.6 Init maps 2level g1 WDF PW	129
C.3.7 Interpolation 2level G1 WDF PR	132
C.3.8 Init maps 2level g2 PR vs t1 t2	136
C.3.9 plot 2level CW vs laser frequency	138
C.3.10 plot 2level PW vs time	140
C.3.11 plot 2level g1SD CW vs delay and frequency	142
C.3.12 plot 2level g1 WDF PW	146
C.3.13 plot 2level g2 CW vs delay	155
C.3.14 plot 2level g2 PR vs t1 t2	159

List of Figures

2.1	Main properties of an ideal single photon (SP) source.	12
2.2	QD in the micropillar, schematics.	13
2.3	TEM image of a single InGaAs QD embedded into GaAs material and energy levels in the InGaAs QD.	14
2.4	Micropillar and CQED parameters.	16
2.5	Eigenstates of Jaynes-Cummings Hamiltonian.	18
2.6	Total system composed of the system of interested and a reservoir.	19
2.7	Input-output field formalism with a 1-D atom.	20
3.1	Custom Cavity QED Quantum toolbox.	24
3.2	Reflectivity spectra in continuous wave excitation.	25
3.3	Results from pulsed-wave excitation script.	26
3.4	First order coherence of the reflected light in continuous wave regime, compared to a coherent field.	28
3.5	Simulated spectral density of the reflected flux for increasing input power. .	30
3.6	Degeneracy splitting in strong field regime, leading to Mollow triplets spectrum.	30
3.7	Reflected photon flux computed by the output operator and by the Wigner Distribution Function.	32
3.8	Absolute value of the normalized-first order coherence.	33
3.9	First-order correlation function of the reflected field in pulsed wave excitation. .	34
3.10	Wigner Distribution Functions in time-frequency axes given an input Gaussian pulse.	35
3.11	Reflected flux spectral density obtained from the Wigner Distribution Function.	36
3.12	Photon statistics and simulated second-order correlation for the QD spontaneously emitted field.	37
3.13	Second order correlation function, correlated and uncorrelated coincidences in pulsed wave excitation.	38
4.1	A fast sub-system, the cavity, is coupled to the slow sub-system, the neutral QD. The cavity acts as a perturbation and it is adiabatically eliminated. .	41
4.2	Comparing Mollow triplets spectra of the spontaneously emitted field, obtained with adiabatic and full model, for different input powers.	46
4.3	Mollow triplets of the emitted field spectrum, with the cavity detuned from the QD.	47
4.4	Adiabatic and full model comparison of the reflected photon flux in pulsed wave regime.	49
A.1	Discrete first order correlation function	55

B.1	Experimental and simulated reflectivity as a function of the incident laser energy.	57
B.2	Fraction of photons emitted outside the mode.	58
B.3	Laser detuning dependent resonance fluorescence spectra at increasing power, showing Mollow triplets.	58
B.4	Correlated and uncorrelated coincidences of the emitted field in pulsed wave excitation.	59
B.5	Experimental second order correlation of the emission from a QD in a micropillar.	59

Chapter 1

Introduction

Quantum technology is based on the development and control of systems governed by the laws of quantum physics, while conventional technology can be understood in the context of classical mechanics. The first practical reason that drives quantum technology is the miniaturization of devices down to the nanometer scale [1], where Planck's constant becomes comparable with the action scales. The second reason, more fundamental, is that quantum mechanics may improve the performances of the classical picture. In the *first quantum revolution*, quantum mechanics was used to model and understand something that already existed. It was possible to explain the different behavior of metals and semiconductors, but not to design and build "artificial atoms". In the *second quantum revolution*, we are not passive observers anymore. It is possible to generate quantum states of matter and energy that would not likely exist elsewhere.

1.1 Photons and Quantum dots

Photons are of particular interest being the smallest units of energy of the quantized electromagnetic field and it is possible to manipulate them separately. They propagate at the speed of light, hence they are ideal as *flying qubits* for long-range information transfer. The fundamental difference, compared to a classical bit of information, is that a *qubit* can be prepared in a coherent superposition of states. Photons are promising also to interconnect different physical systems. The nodes of the quantum network are interrelated by quantum channels and at each node, the information is processed [2]. To exploit the quantum mechanical properties of photons, bright, efficient, and integrable quantum light sources are needed, as well as efficient detectors and two-photon gates. Superconducting nanowires detectors already show efficiencies close to unity in a wide spectral range and high spatial resolution [3]. Previously single-photon based technologies were based on heralded single-photon techniques, based on probabilistic generation in non-linear crystals. However, one problem of these devices is the source brightness scaling linearly with the multi-photon pairs probability. Possible solutions include neutral atoms and ions in traps, solid-state emitters such as quantum dots and defects and molecules, without excluding hybrid systems to optimize wavelength and bandwidth [4]. Still, currently available sources have intrinsically limited efficiencies of a few percents.

When light of a certain frequency is directed onto a semiconductor, an electron-hole pair may be generated. The latter is bound by the Coulomb interaction and it is called an exciton. Moreover, if the exciton is confined in a QD, then the exciton acts like an artificial atom with complex spectra. It is possible to obtain bound excitons also by injecting electrons and holes into a quantum dot. QD excitons act as a bridge between quantum electronics and the world of quantum optics, paving the way to quantum optoelectronics. Much attention in this field has been focused on the development of a single-photon source that generates pulses of light, with each pulse containing one and only one photon, starting from almost twenty years ago [4]. Besides, the spin of a single charge carrier in the QD can be used as a stationary qubit and can be optically manipulated [5]. Finally, QDs are compatible with the III-V semiconductor nanofabrication techniques. More specifically, it is possible to couple QDs to a variety of photonic structures, such as waveguides, microlenses, microcavities, etc. for large scale applications [4].

1.2 Internship Presentation & State of The Art

This Master's thesis has been realized in the group of Prof. Pascale Senellart at Centre for Nanoscience and Nanotechnology (C2N/CNRS) under the supervision of Dr. Loïc Lanco. The group activity is focused on the development of quantum devices based on single QDs in cavity quantum electrodynamics (CQED) systems. The research team developed a new technology in 2008, called *in-situ* optical lithography [6], which allows for the deterministic and scalable fabrication of CQED devices by a single QD coupled to a micropillar cavity. Through this technique, it is possible to work both in the weak and strong coupling regimes [6; 7]. Afterward, an ultrabright source of entangled photon pairs was fabricated in 2010 [8]. In 2013, bright source QD-micropillar devices were realized, with indistinguishability ranging from 70% to 90% [9]. In 2016 a brightness 20 times brighter than any source of equal quality [10] was obtained with near-unity indistinguishability. Nowadays, a key challenge is the source operation wavelength variability [11] because of inhomogeneities during the growth process across the wafer. Another quest is controlling the temporal profile of a single photon wavepacket, since it requires control of the fine-structure splitting and the axes' orientation between the cavity and the neutral QD.

My internship was expected to be experimental, however, because of the Covid-19 lockdown, I worked on the modeling and simulation of CQED open systems. For this reason, I have chosen here to enter more in the details of quantum system simulations rather than the devices themselves. The choice of the quantum dot in the micropillar will be discussed more thoroughly in the next chapter, in comparison with other quantum emitter systems. In quantum optics, it is often required to simulate the physical properties of a system coupled to a reservoir. The system of interest has in general much fewer degrees of freedom compared to the environment, e.g. phonons, photons, nuclear spins, etc. Quantum dissipative systems in general require numerical integrations to be solved, but they are still a delicate task. For an arbitrary system, there exist *path-integral* expressions [12] for density matrix evolution, but they suffer from instability at long times. In the Schrödinger picture approach, a solution is to integrate the *Master equation* for the density matrix [13] or by

using *quantum Monte Carlo* simulations [14].

If a system is described by an n dimensional Hilbert space, the number of matrix elements is n^2 for Schrödinger equation and n^4 for the density matrix equations. This polynomial computational memory is further reduced by considering that many of the previous coefficients are zero, hence making viable the integration of systems of $10^2 : 10^3$ equations numerically by using sparse matrices, within a few hours on an average personal computer. Moreover, when CQED simulations require few photons and atoms, it is possible to truncate the Fock space basis for the light field modes with satisfactory results. Even so, sometimes it may be required to increase the dimension of the Fock space to better reproduce higher photon number experiments, resulting in much longer simulation times.

A possible way to overcome this problem is offered in quantum systems composed of several interacting subsystems [15]. One may be interested in the dynamics of one subsystem, getting rid of the others by making some approximations. This operation is called *adiabatic elimination* and it offers an accurate model as long as the selected subsystem has much slower dissipation rates than the others, to which it is weakly coupled. In the specific case of a cavity interacting with an electromagnetic field, the total Hilbert space is given by the tensor product of the spaces of the two individual systems, increasing the number of variables. This is where *adiabatic elimination* may become a useful tool to simplify the problem numerically or to get a better physical understanding of some phenomenon, or both. Indeed, by adiabatic elimination one works only with the QD sub-space, taking the cavity sub-space into account by an effective Hamiltonian.

The aim of my internship was the implementation of adiabatic elimination of the light modes Fock space in high-loss cavities for several quantum optics simulations, concerning mainly the simplest model of a QD as ground and excited state. It was also expected to investigate the validity and differences of the adiabatic elimination relating to the “full model” and literature. Moreover, my work was to be included in a new quantum toolbox to simulate CQED multi-level systems.

1.3 Outline of the Thesis

In Chapter 2 the QD is introduced as a simple ground and excited state inside a micropillar, first as a closed quantum system by recalling the Jaynes-Cummings Hamiltonian. In the following, to treat the cavity QED as an open quantum system, the input-output formalism and Lindblad Master equation are reviewed. In Chapter 3 the custom made cavity-QED Quantum Toolbox is presented, showing some simulations regarding output intensities, first- and second-order correlations, and time-frequency analysis. Some results are related to previous ones in literature for referring theory to past experiments. The adiabatic elimination is presented in Chapter 4, where the key approximations from the full model are discussed, followed by possible criteria for its domain of validity. Finally, generalizations of this work are suggested, with applications on more complex CQED models.

Chapter 2

Quantum Dots in Micropillar Cavities

This chapter aims to develop a quantum mechanical description of a neutral quantum dot (QD) in a micropillar cavity. The most important approximations will be outlined, at the end of which the Hamiltonian will fully describe the closed quantum system evolution. Dissipation and decoherence will be briefly mentioned in the following section. They will be addressed more thoroughly at the end of this chapter, focused on the system coupling with the environment.

Why Cavity-QED with Quantum Dots? A single-photon (SP) source is necessary to perform quantum communication. It will be shown why optical microcavities are studied nowadays for the realization of a SP source. For that purpose, it is important to briefly review the main properties that an ideal SP source should satisfy. They are presented in figure 2.1, where each slot corresponds to a time bin.

The first row (a) represents a source that emits identical single-photon wavepackets at each excitation pulse. The following rows represent deviations from the perfect situation when the source lacks one or more properties that label the corresponding row. For instance, in (b), when an emitted photon is lacking given an excitation, then the brightness is lower than 100%, lowering the overall efficiency. Another important property is the SP purity (c), which is related to the probability of having a second photon in the emitted wavepacket. This is a flaw for instance in quantum key distribution since secure communications would require only a stream of single photons to avoid photon-number splitting attack [16]. The purity is measured by a Hanbury Brown and Twiss (HBT) experiment, which evaluates the second-order correlation function of a given source. For a pure SP source $g^{(2)}(0) = 0$, whereas when $g^{(2)}(0) > 0$ there is a non-zero probability to have at least a second emitted photon after the excitation pulse.

As for classical fields, the coherence of a SP source describes the light phase stability and in (d) it is represented by a phase jump in the wavepacket. The total coherence time T_2 is given by

$$\frac{1}{T_2} = \frac{1}{2T_1} + \frac{1}{T_2^*}, \quad (2.1)$$

where T_1 is the transition radiative lifetime and T_2^* is the pure dephasing time, i.e. a loss of coherence due to the interaction with the environment without recombination. Equivalently, equation (2.1) can be written for the total dephasing rate γ as

$$\gamma = \frac{\gamma_{\text{sp}}}{2} + \gamma^*, \quad (2.2)$$

being γ_{sp} the damping rate of the population due to spontaneous emission in the external environment and γ^* the damping rate of the phase amplitude.

When the rate of pure dephasing is low enough in equation (2.1), then the so-called Fourier transform-limit is obtained:

$$\frac{T_2}{2T_1} \rightarrow 1 \quad . \quad (2.3)$$

This limit is a necessary condition for photons indistinguishability (e), which occurs

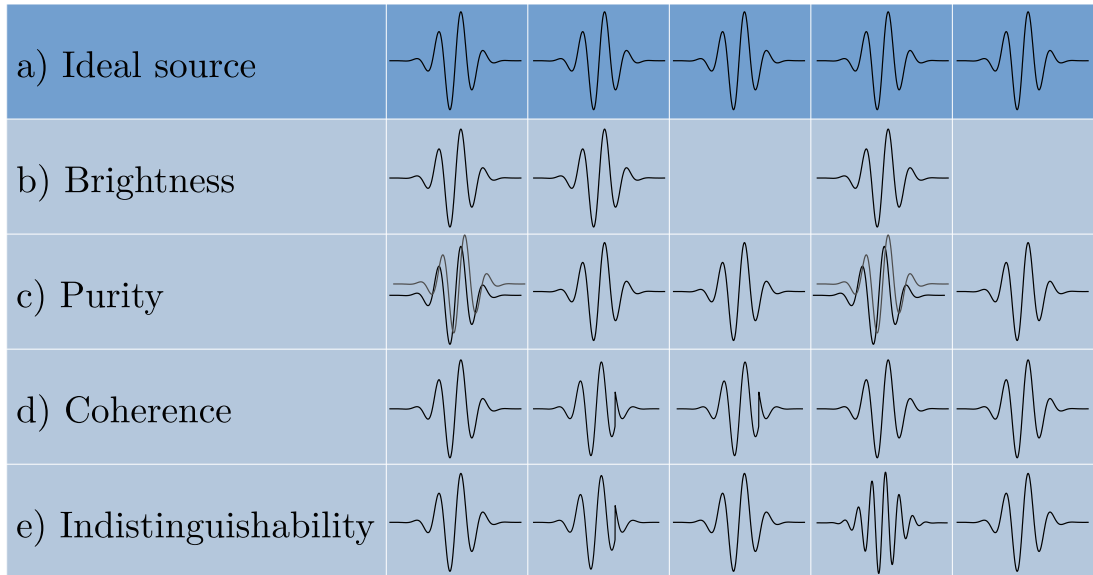


Figure 2.1: (a) An ideal source with identical, single photons generated per excitation pulse. (b) When the brightness is lower than unity, sometimes no photon emission occurs. (c) As a second identical photon is present in the wavepacket, the purity is degraded. (d) Coherence loss for phase instability due to $T_2 \leq 2T_1$. (e) Indistinguishability $V < 1$ because of decoherence and spectral wandering.

when two photons have the same spectral bandwidth, pulse width, polarization, carrier frequency, and mode profile. In such a case, when they impinge at the same time at the two ports of a beamsplitter (BS), quantum mechanics predicts they both will leave the BS from the same output port. This phenomenon was first measured by Hong-Ou-Mandel. Spectral wandering is another process contributing to distinguishability because of the environmental fluctuations. It is characterized by a shift of the photon wavelength, spoiling indistinguishability which is important for low-error quantum computation.

The main limitation for brightness is the refractive index mismatch between the QD layer

and air ($n \approx 3.5$ for GaAs), confining most of the light inside the semiconductor. It is possible to improve the extraction efficiency by inserting the QD between two Distributed Bragg Reflectors (DBRs), realizing a 3-D microcavity to redirect spontaneous emission toward the surface. The brightness can be defined as [4]

$$\text{brightness} = p \times \eta, \quad (2.4)$$

where η is the extraction efficiency and, in a two-level system, p is the occupation probability for the excited state

$$\eta = \eta_{\text{out}} \times \beta = \eta_{\text{out}} \times \frac{\Gamma_m}{\Gamma_m + \gamma_{\text{sp}}}. \quad (2.5)$$

Here η_{out} is the output extraction efficiency and the *spontaneous emission coupling factor* β measures the fraction of photons emitted into the cavity mode Γ_m , considering also the other radiative modes γ_{sp} . The *increase* of spontaneous emission in the mode of interest can be achieved through the Purcell effect, in the domain of cavity quantum electrodynamics (CQED) in the weak coupling regime [17]. This is employed for instance in micropillars, whose first lens brightness nowadays is about 14% with 91% indistinguishability [11]. Because of the Purcell-enhanced emission in the cavity, the inverse of the QD lifetime is now given by $1/T_1 = \Gamma_{\text{tot}} \equiv \Gamma_m + \gamma_{\text{sp}}$, with Γ_{tot} the total emission rate taking into account both emissions into and outside the cavity mode. It also improves the ratio $T_2 / (2T_1)$, since the coherence time T_2 is now given by

$$\frac{1}{T_2} = \frac{\Gamma_{\text{tot}}}{2} + \gamma^*. \quad (2.6)$$

A simple schematic of the micropillar used at C2N is shown in figure 2.2. The InGaAs is at

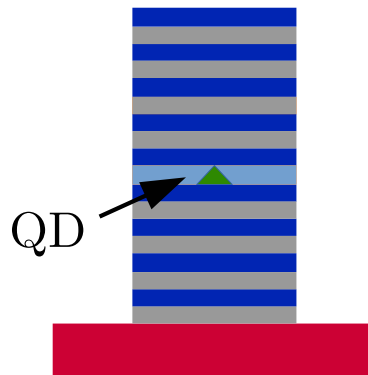


Figure 2.2: In green, the QD sandwiched between two Bragg mirrors of the micropillar, standing on the substrate.

the center of a cavity with a cylindrical shape. The GaAs spacer is sandwiched between the top and bottom AlGaAs/GaAs DBRs. The latter confine light along the vertical direction, while total internal reflection guarantees lateral confinement.

2.1 The Quantum Dot and Pseudo-spin Systems

Quantum dots are structures confining charge carriers in regions of space over the nanometer scale. In general direct-bandgap semiconductors are used for optical applications to have direct transitions in reciprocal space. The aim here is to show why a QD can be seen as an artificial atom, interacting with an electromagnetic field in the dipole approximation. The analysis will be restricted to two energy levels, to be described in terms of Pauli spin algebra.

In self-assembled QDs, quantum confinement generates localized states, having shells in the conduction and valence band with discrete energy levels. These quantization effects become relevant when the confinement dimensions are comparable with De Broglie wavelength of the charge carrier. At low temperatures, λ_{DB} is of the order of $10 \div 100$ nm [18]. For the QD fabricated at C2N/CNRS, a Transmission Electron Microscopy (TEM) image and the energy levels are shown in figure 2.3. The InGaAs QD is separated by the GaAs bulk by an InAs wetting layer, originated by the growth process. The energy levels have been computed in a non-interacting charge picture; electrons and holes fill the shells according to the Pauli exclusion principle.

The fundamental state is when the valence band is filled and the conduction band is empty. Among the possible excited states, the neutral exciton will be of interest, with an electron in the conduction band and a hole in the valence band. For the CQED simulation toolbox, without loss of generality, it is assumed that the interband transition between the two lowest energy levels is dipole allowed.

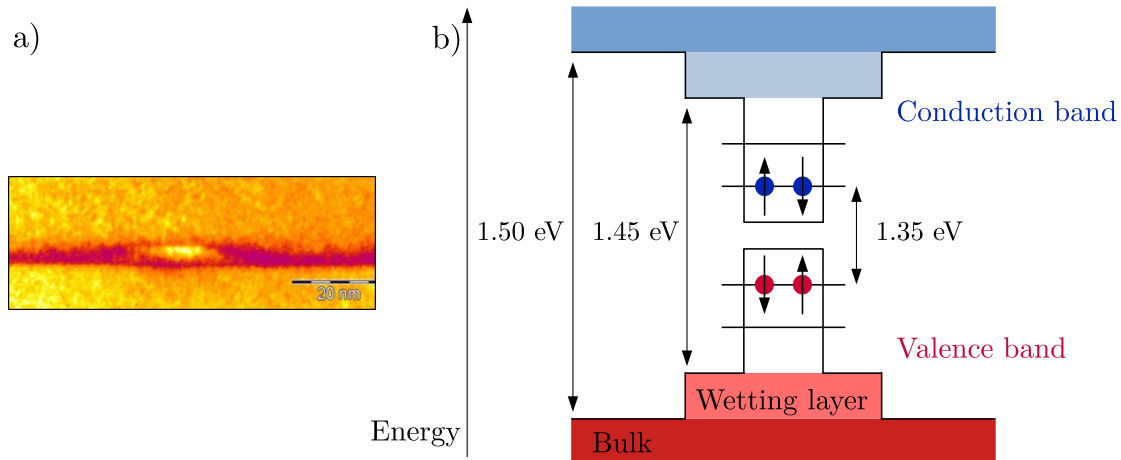


Figure 2.3: (a) Transmission Electron Microscope image of a single InGaAs QD embedded into GaAs. Image measured by A. Lemaitre and C. Gomez at C2N. (b) Schematics of energy levels of non-interacting charge in the InGaAs QD, including the InAs wetting material and GaAs bulk. The lowest states in energy are filled according to the Pauli exclusion principle.

For the quantum mechanical description, the unexcited state of the QD is the state $|g\rangle$, whereas the exciton is $|e\rangle$, according to Dirac notation. At this point it is favorable to

define the so-called *atomic transition operators* [16]

$$\hat{\sigma}_+ \equiv |e\rangle\langle g|, \quad \hat{\sigma}_- \equiv |g\rangle\langle e| = \hat{\sigma}_+^\dagger, \quad (2.7)$$

being $\hat{\sigma}_+^\dagger$ the hermitian conjugate of $\hat{\sigma}_+$. The *projection operator* in the excited state is

$$|e\rangle\langle e| = \hat{\sigma}_+\hat{\sigma}_-. \quad (2.8)$$

The zero energy is referred to the ground state $|g\rangle$, thus the free atomic Hamiltonian is

$$\hat{H}_d = (E_e - E_g)\hat{\sigma}_+\hat{\sigma}_- = \hbar\omega_d\hat{\sigma}_+\hat{\sigma}_-, \quad (2.9)$$

Throughout this manuscript, “quantum dot” and “two-level atom” will be used interchangeably, since only the two-level system will be addressed.

2.2 The Micropillar as a Cavity-QED

In this section a model of the micropillar will be shown based on common CQED parameters, that will be reviewed shortly based on [17]. The same arguments can be applied to different micro-optical cavities, to be possibly implemented in the Cavity-QED Quantum Toolbox. It is assumed that the atom in the cavity is a two-level system with fixed energies and that it can radiatively decay, emitting a photon in the cavity, or absorb one from the latter. The parameters that describe the interaction between the atom, that will represent our QD, and the cavity field (see figure 2.4, left) are:

- the photon decay rate of the cavity (damping rate) κ , given by $\kappa = \omega/Q$, where ω is the angular frequency and Q is the quality factor. Higher quality factors will reduce the cavity losses.
- the coupling strength g between the atom and the electromagnetic field;
- the dephasing rate γ , taking into account only the interaction with the external environment, i.e. emission outside the cavity mode and pure dephasing : $\gamma = \gamma_{sp}/2 + \gamma^*$.

Before commenting more on the previous parameters, for the following discussion, it is important to distinguish between two possible regimes of the atom interacting with the cavity. In the so-called *strong coupling* limit $g \gg (\kappa, \gamma)$ the coupling strength is much greater than the highest value between the cavity decay rate κ and the non-resonant decay rate γ . In this regime, the atom strongly interacts with the cavity, and a *reversible* process occurs. Indeed, the losses are so low that the emitted photon from the atom instead of escaping from the cavity, it is readily absorbed by the atom. Viceversa is the *weak coupling* limit, $g \ll (\kappa, \gamma)$: it describes an irreversible process, as the emitted photon is promptly lost and no re-absorption can occur.

As mentioned before, in this manuscript the weak coupling regime will be of interest because of the Purcell effect, to increase spontaneous emission in the mode of interest. Before describing how this phenomenon affects the micropillar, it is crucial to outline the coupling strength g . Differently from the case when a two-level atom interacts with a resonant light field originating from an external source, here there is no external source that gives the

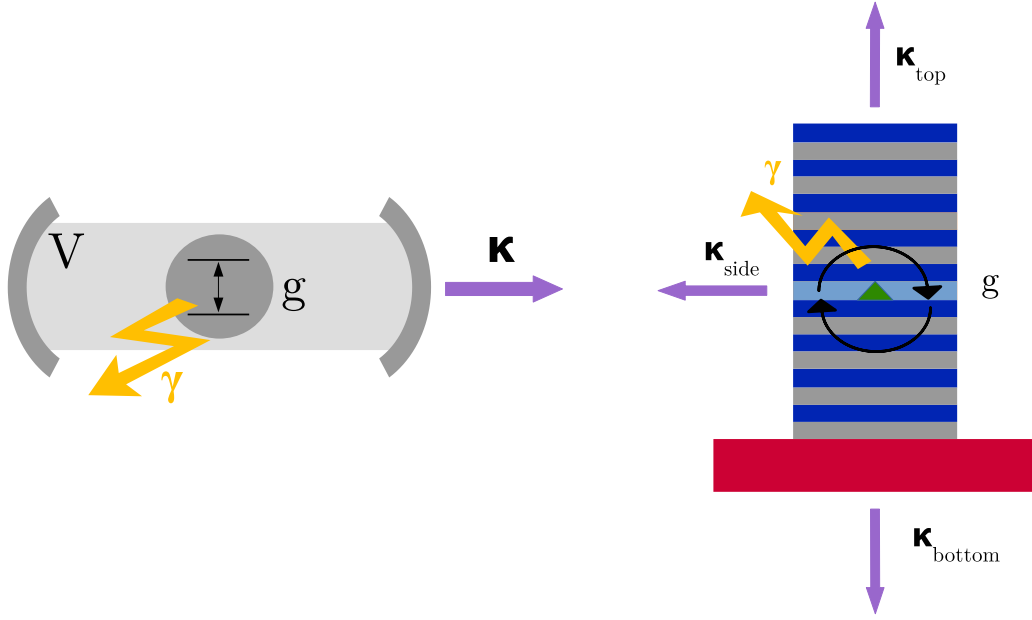


Figure 2.4: (Left) A two-level atom is in a resonant cavity. The cavity parameters are g , κ , γ , and V . They are respectively the atom-cavity coupling, the photon decay rate from the cavity, the dephasing rate, and the modal volume. (Right) Micropillar with QD and corresponding cavity parameters.

field strength.

In the weak coupling regime, since the effect of the cavity is relatively small, the atom-cavity interaction can be modeled by perturbation theory. Distinctively from the free space case, the emission rate in the cavity can be tuned since the cavity changes the photon number density of states that appears in Fermi's golden rule. By considering an atom coupled resonantly to a single mode of a high-Q cavity, it is found that the ratio between the cavity emission rate Γ_m and the one in a homogeneous medium γ_{sp} , is

$$F_P \equiv \frac{\Gamma_m}{\gamma_{sp}} = \frac{4g^2}{\kappa\gamma_{sp}}. \quad (2.10)$$

In the previous equation, the Purcell factor F_P has been defined and it emerges that high-quality factor and low mode volume are required to get a strong emission rate in the cavity mode. By introducing the Purcell factor in equation (2.5), one gets

$$\beta = \frac{F_P}{F_P + 1}. \quad (2.11)$$

So as $F_P \gg 1$, the coupling factor β approaches unity, increasing the brightness of the optical cavity.

The micropillar cavity In the micropillar (figure 2.4, right) g describes the time scales at which energy can be coherently exchanged between the cavity field and the exciton. The

dephasing rate is $\gamma = \gamma_{\text{sp}}/2 + \gamma^*$. It models the rate at which the QD leaks information in the external (i.e. not including the cavity) environment. The total cavity damping rate is $\kappa = \kappa_{\text{top}} + \kappa_{\text{side}} + \kappa_{\text{bottom}}$, being κ_{top} and κ_{bottom} accounting for the photons escaping the cavity from the top and bottom mirror, respectively, while κ_{side} through the sidewalls of the cavity.

Three important parameters describe the performances of a QD-micropillar device [19] and they will be used in the Quantum Toolbox:

- the *cooperativity* $C = g^2/\kappa\gamma$, which quantifies the coherent processes component over the incoherent one;
- the top-mirror *output coupling efficiency* $\eta_{\text{top}} = \kappa_{\text{top}}/\kappa$, identifying the fraction of photons escaping the cavity through the top mirror and to be collected;
- the *input coupling efficiency* η_{in} , which is the probability for an incoming photon to be coupled to the cavity mode.

2.3 Jaynes–Cummings Model

Here the Jaynes-Cummings Hamiltonian in the dressed states formalism is reviewed to model the interaction of a two-level atom with the single mode of an electromagnetic field. Experimentally it is indeed possible to have the optical cavities supporting only a single mode, as in the version of the micropillar of figure 2.2. The consequence of introducing an interaction term with the field is that in general $|e\rangle$ and $|g\rangle$ will not be eigenstates anymore of the Hamiltonian, leading to the so-called Rabi oscillations [16].

In the *dipole approximation* [16] the interaction Hamiltonian with a quantized field $\hat{\mathbf{E}} \propto (\hat{a} - \hat{a}^\dagger)$ is:

$$\hat{H}_{\text{int}} \approx -\hat{\mathbf{d}} \cdot \hat{\mathbf{E}}, \quad (2.12)$$

being $\hat{\mathbf{d}}$ the dipole moment of the quantum emitter. The free-field Hamiltonian, to be added to the free-atom one and the interaction term, is

$$\hat{H}_{\text{cav}} = \hbar\omega_c \hat{a}^\dagger \hat{a}, \quad (2.13)$$

having neglected the zero-point energy. By making the *rotating wave approximation* (RWA), the Jaynes-Cummings Hamiltonian [16] is

$$\begin{aligned} \hat{H}_{\text{JC}} &\approx \hat{H}_{\text{d}} + \hat{H}_{\text{cav}} + \hat{H}_{\text{int}} \\ &= \hbar\omega_d \hat{\sigma}_+ \hat{\sigma}_- + \hbar\omega_c \hat{a}^\dagger \hat{a} - i\hbar g (\hat{\sigma}_- \hat{a}^\dagger - \hat{\sigma}_+ \hat{a}), \end{aligned} \quad (2.14)$$

The interaction term \hat{H}_{int} causes only transitions of the kind

$$|e\rangle |n\rangle \longleftrightarrow |g\rangle |n+1\rangle, \quad (2.15)$$

between two product states, where the second kets n are labeled by the number of photons in the mode. These states are also called “bare” states of the Jaynes-Cummings model. By

letting $n \geq 0$ and expressing \hat{H}_{JC} in the basis $|\Psi_{1n}\rangle = |e\rangle|n\rangle$ and $|\Psi_{2n}\rangle = |g\rangle|n+1\rangle$, the eigenvalues are

$$E_{\pm}(n) = \hbar\omega_c \left(n + \frac{1}{2} \right) + \frac{\hbar\omega_d}{2} \pm \frac{\hbar}{2}\Omega_n(\Delta), \quad (2.16)$$

where

$$\Omega_n(\Delta) = \left[\Delta^2 + 4g^2(n+1) \right]^{1/2} \quad (\Delta = \omega_d - \omega_c) \quad (2.17)$$

is the Rabi frequency comprising half the detuning. An example at resonance, i.e. $\omega_c = \omega_d \equiv \omega_0$, is shown in figure 2.5. In (a) the detuning is null and the atom is decoupled

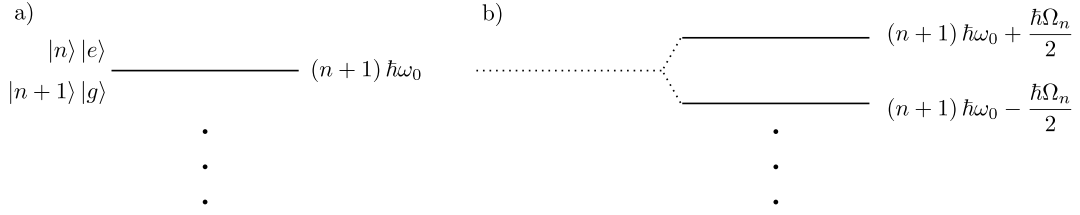


Figure 2.5: (a) Degenerate energy levels for an uncoupled atom-field system at resonance, $\omega_c = \omega_d \equiv \omega_0$. (b) Level splitting due to the atom-field interaction, Ω_n is the Rabi frequency.

from the field, i.e. $g = 0$. The energy levels are degenerate. The degeneracy is lifted by introducing coupling ($g > 0$), splitting the original two degenerate eigenstates into two new ones separated by the energy $\hbar\Omega_n$. This phenomenon is known also as dynamic or AC Stark effect. The perturbed eigenstates $|n, \pm\rangle$ are called the “dressed states” of the Jaynes-Cummings model.

2.4 Open Quantum Systems

Quantum states that are described by state vectors are called *pure* states. States that cannot be described by state vectors are called *mixed* states. Both are described in terms of the density operator $\hat{\rho}$ in the following way:

$$\hat{\rho} \equiv \sum_i p_i |\psi_i\rangle\langle\psi_i|, \quad (2.18)$$

where the sum is over a statistical ensemble such that p_i is the probability of the system of being in the state $|\psi_i\rangle$, given the normalized state $\langle\psi_i|\psi_i\rangle = 1$. A density matrix $\hat{\rho}$ has unit trace, i.e. $\text{tr}(\hat{\rho}) = 1$, and it is positive. Moreover, if and only if the state is pure, $\text{tr}(\hat{\rho}^2) = 1$. Similarly for $\text{tr}(\hat{\rho}^2) < 1$, the system is a mixed state. For a general quantum state, the average of some operator \hat{A} is given by

$$\langle \hat{A} \rangle = \text{tr}(\hat{\rho}\hat{A}) = \sum_i p_i \langle \psi_i | \hat{A} | \psi_i \rangle. \quad (2.19)$$

In the absence of dissipative interactions and in the case of no explicitly time dependent interaction, the density operator evolves following the unitary transformation, called the *Von Neumann equation* [16]:

$$\frac{d\hat{\rho}}{dt} = \frac{i}{\hbar} [\hat{\rho}, \hat{H}], \quad (2.20)$$

whereas the *Heisenberg equation of motion* is given by

$$\frac{d\hat{A}^{(H)}}{dt} = -\frac{i}{\hbar} [\hat{A}^{(H)}, \hat{H}]. \quad (2.21)$$

2.4.1 Master equation

The density matrix formalism is useful for the description of incoherent and dissipative processes that occur mainly when the system is coupled to a reservoir, figure 2.6. The aim is to describe the dynamics of the system of interest with the reservoir entering only as parameters, reviewing the approximations stated in [20]. The total Hamiltonian of the reservoir and the system is given by

$$\hat{H} = \hat{H}_S + \hat{H}_R + \hat{H}_{SR}, \quad (2.22)$$

where \hat{H}_S and \hat{H}_R are Hamiltonians for the undamped system (S) and the reservoir (R), respectively, and \hat{H}_{SR} is the interaction Hamiltonian. The density operator $\hat{\rho}(t)$ of the

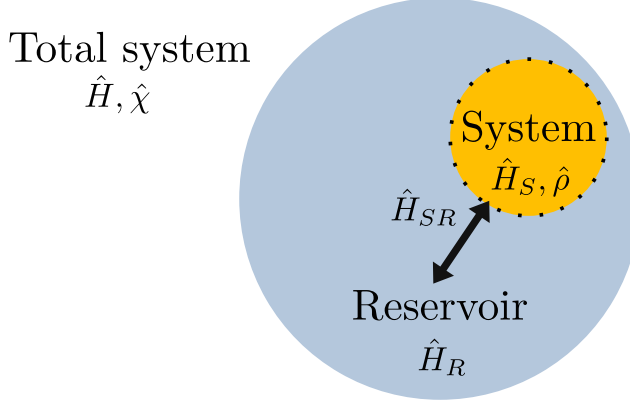


Figure 2.6: Total system with Hamiltonian \hat{H} and density operator $\hat{\chi}$ divided into the system of interest, “System”, and the Reservoir.

system is given by tracing the density matrix $\hat{\chi}(t)$ of the composite system $S \otimes R$ over all possible states of the reservoir, i.e.

$$\hat{\rho}(t) \equiv \text{tr}_R [\hat{\chi}(t)]. \quad (2.23)$$

It is assumed that the interaction is turned on at $t = 0$, with no correlation between S and R at this initial time. Then it is possible to factorize the density operator of the composite system as

$$\hat{\chi}(0) = \hat{\rho} \otimes \hat{R}_0, \quad (2.24)$$

being R_0 the initial reservoir density operator. In general, at later times the correlations between S and R will couple the system and the reservoir. By assuming that the coupling is very weak and that R is a very large system weakly affected by S , it is legit to write

$$\hat{\chi}(t) = \hat{\rho}(t) \otimes \hat{R}_0 + \mathcal{O}(\hat{H}_{SR}). \quad (2.25)$$

Notice that the previous expression is still exact, based on the previous assumptions. The first Born approximation consists of neglecting terms higher than the second order in H_{SR} . Still, the evolution of $\hat{\rho}(t)$ depends on its history [20]. The second major approximation is the Markov approximation, which is based on the existence of two very different time scales: a slow time scale for the system dynamics, compared to the decay of the reservoir correlation functions.

Under these approximations, in the special case where there is a single initial state $|i\rangle$ and final state $|f\rangle$, the incoherent process are described in terms of collapse operators \hat{C}_{if} with rate γ_{if} :

$$\hat{C}_{if} = \sqrt{\gamma_{if}} |f\rangle\langle i|. \quad (2.26)$$

For each collapse operator, a superoperator called Lindbladian $\hat{\mathcal{L}}_{if}$ is defined such that

$$\hat{\mathcal{L}}_{if}(\hat{\rho}) \equiv \hat{C}_{if}\hat{\rho}\hat{C}_{if}^\dagger - \frac{1}{2}\{\hat{C}_{if}^\dagger\hat{C}_{if}, \hat{\rho}\}, \quad (2.27)$$

being the last term the anticommutator defined as $\{\hat{A}, \hat{B}\} \equiv \hat{A}\hat{B} + \hat{B}\hat{A}$. The density matrix evolution in the RWA is given by the *Lindblad master equation*:

$$\frac{d\hat{\rho}}{dt} = \frac{i}{\hbar} [\hat{\rho}, \hat{H}] + \sum_{if} \hat{\mathcal{L}}_{if}(\hat{\rho}), \quad (2.28)$$

where the coherent processes are described by the first term on the RHS and the Lindbladian operators account for the ensemble of the possible incoherent processes.

2.4.2 Input-output formalism

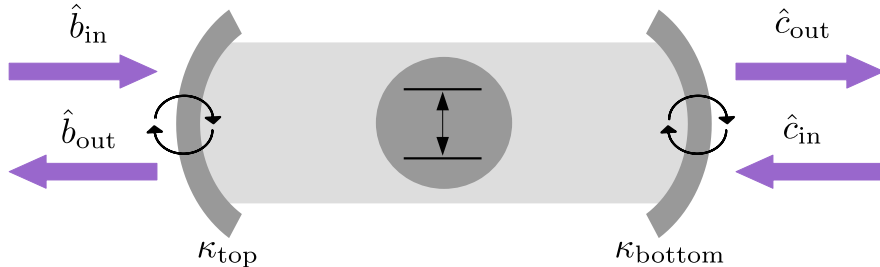


Figure 2.7: Input-output field formalism with a 1-D atom.

In the previous section the master-equation has been introduced to calculate the physical properties of a damped system, in this thesis the cavity with an artificial atom. In this section the aim is to treat explicitly the external field as the reservoir, in order to determine the effect of the internal and external cavity dynamics. In the input-output formalism the properties of the field exiting the system can be determined based upon information on the dynamics of the atom-cavity and the input field. The following results have been derived assuming the RWA and system-bath interactions that are linear in the bath operators. Moreover, the coupling constant is assumed to be a constant independent of frequency [21].

In the ideal case of a one-dimensional cavity as in figure 2.7, the first port (top-mirror) is associated to the operators \hat{b}_{in} and \hat{b}_{out} , whereas \hat{c}_{in} and \hat{c}_{out} for the second port (bottom-mirror). In the 1D-atom limit, where the dominant atomic radiative interactions are via the cavity mode, the side losses are much lower than the ones from the mirrors ($\kappa_{\text{side}} \ll \kappa_{\text{top}} + \kappa_{\text{bottom}}$) and the cooperativity ($C \gg 1$) [22].

Given an input or output operator \hat{s} , the expected value $\langle \hat{s}^\dagger \hat{s} \rangle$ is the associated photon flux defined as *number of photons per unit time*. Thus the unit of each operator is $\text{s}^{-1/2}$. Given the single confined mode of annihilation operator \hat{a} , the continuity relations of the fields are:

$$\hat{b}_{\text{out}} = \hat{b}_{\text{in}} + \sqrt{\kappa_{\text{top}}} \hat{a}, \quad (2.29\text{a})$$

$$\hat{c}_{\text{out}} = \hat{c}_{\text{in}} + \sqrt{\kappa_{\text{bottom}}} \hat{a}, \quad (2.29\text{b})$$

reflecting the interference between the incoming field and the one escaping from the cavity. The interaction Hamiltonian between the cavity and the external electromagnetic field is given by:

$$\hat{H}_{\text{pump}} = -i\hbar\sqrt{\kappa_{\text{top}}} (\hat{b}_{\text{in}} \hat{a}^\dagger - \hat{b}_{\text{in}}^\dagger \hat{a}). \quad (2.30)$$

A useful simplification is the specific case of a coherent beam at resonant excitation. In such case the input fields are fully described by the mean input field amplitudes, namely $b_{\text{in}} = \langle \hat{b}_{\text{in}} \rangle$ and $c_{\text{in}} = \langle \hat{c}_{\text{in}} \rangle$. This approximation has simplified the computational costs of the numerical results of the CQED Quantum Toolbox, to be addressed in the next chapter. It is anticipated here that the numerical simulations are based on an input field b_{in} solely from the top-mirror. Therefore, $c_{\text{in}} = 0$ and in this limit equations (2.29, 2.30) become

$$\hat{b}_{\text{out}} = b_{\text{in}} \hat{I} + \sqrt{\kappa_{\text{top}}} \hat{a}, \quad (2.31\text{a})$$

$$\hat{c}_{\text{out}} = \sqrt{\kappa_{\text{bottom}}} \hat{a}, \quad (2.31\text{b})$$

and

$$\hat{H}_{\text{pump}} = -i\hbar\sqrt{\kappa_{\text{top}}} (b_{\text{in}} \hat{a}^\dagger - b_{\text{in}}^* \hat{a}), \quad (2.32)$$

where the \hat{I} on the right-hand side of equation (2.31a) must be understood as the identity operator. These relations will be exploited to evaluate the properties of the output fields both in the continuous wave (CW) or pulsed wave (PW) laser regime.

2.4.3 The “full” model

At this point it is possible to model the time evolution of the exciton in the micropillar, starting from the Lindblad Master equation (2.28). It is thus necessary to define the Hamiltonian of interest and the collapse operators. In the following the rotating frame of reference will be considered, centered at the laser frequency ω . The Hamiltonian is given by

$$\hat{H} = \hat{H}_{\text{d}} + \hat{H}_{\text{cav}} + \hat{H}_{\text{int}} + \hat{H}_{\text{pump}}, \quad (2.33)$$

where

$$\hat{H}_d = (\omega_d - \omega) \hat{\sigma}_+ \hat{\sigma}_-, \quad (2.34a)$$

$$\hat{H}_{\text{cav}} = (\omega_c - \omega) \hat{a}^\dagger \hat{a}, \quad (2.34b)$$

$$\hat{H}_{\text{int}} = ig (\hat{\sigma}_+ \hat{a} - \hat{\sigma}_- \hat{a}^\dagger), \quad (2.34c)$$

$$\hat{H}_{\text{pump}} = -i\sqrt{\kappa_{\text{top}}} (b_{\text{in}} \hat{a}^\dagger - b_{\text{in}}^* \hat{a}), \quad (2.34d)$$

where the \hbar constant has been dropped. At last, the collapse operators are required to describe the dissipative processes. The *cavity damping* $\hat{C}_{\text{cav}} = \sqrt{\kappa} \hat{a}$, with κ the total damping rate, models the cavity optical losses. The QD *spontaneous emission in the leaky modes* is given by $\hat{C}_{\text{QD}} = \sqrt{\gamma_{\text{sp}}} \hat{\sigma}_-$, being γ_{sp} the spontaneous emission rate. Last, the QD pure dephasing is described by $\hat{C}_{\text{deph}} = \sqrt{2\gamma^*} \hat{\sigma}_+ \hat{\sigma}_-$, where the population is preserved during the dephasing. From equation (2.27), the overall Lindbladian becomes then:

$$\hat{\mathcal{L}} = \hat{\mathcal{L}}_{\text{cav}} + \hat{\mathcal{L}}_{\text{QD}} + \hat{\mathcal{L}}_{\text{deph}}, \quad (2.35)$$

whose labels reflect the recently defined collapse operators.

Conclusions

This chapter has presented the main properties that single-photon quantum emitters should satisfy and the potential of QDs in microcavities. The micropillar solution, in the weak coupling regime, is known to guarantee simultaneously high brightness and degree of indistinguishability. After having introduced a pseudo-spin formalism to model the two-level system of an exciton in the QD, the main parameters characterizing an optical cavity have been briefly reviewed and translated to the micropillar. For the following simulations, the Jaynes-Cummings Hamiltonian has been introduced to model the coupling between the exciton and the micropillar as closed quantum systems. At last, to describe the system dissipation, an open quantum system description based on the Master Equation has been presented with its approximations. In the following chapter, the **CQED Quantum Toolbox** will be presented with the implemented quantum optics simulations.

Chapter 3

Cavity-QED Quantum Toolbox

Given a quantum emitter in an optical cavity interacting with an external field, one may be interested in some physical properties such as output intensities, first- and second-order correlations, flux spectral densities, etc. In this manuscript the `Quantum Optics Toolbox` [23] has been exploited to numerically solve the Master Equation on `MATLAB®`. A custom made `Cavity QED Quantum Toolbox` has been developed to efficiently organize different simulations for two-level systems coupled to a microcavity mode. For instance, even though field spectrum processing under stationary resonant excitation and second-order correlations require different approaches to be simulated, they both share the same device, i.e. the QD in the micropillar, and they are modeled by the same Hilbert space and Master Equation formalism.

The scripts for the two-level system are contained in Appendix C and, based on figure 3.1, they are divided in the following sections:

Main programs It contains the main scripts, for both continuous wave (CW) and pulsed wave (PW) regime. They incorporate parameters commonly set by an experimentalist, the field input-output operators and the core of the code to let the reader understand which quantities are actually computed and how they are defined.

CQED device parameters The parameters of the device are imported from a file `Init 2level device parameters`. It includes the atom-cavity coupling, the photon decay rate from the micropillar, the spontaneous emission rate, the pure dephasing rate, the resonance frequencies etc., which characterize a given QD-cavity device.

CQED subprograms The subroutine `Init 2level Hilbert space and operators` defines the Hilbert space and some of the operators introduced in the previous chapter. Mainly two other kinds of subroutines are present. The ones that start by `Init...` contain the initialization of some additional variables and they allow to preallocate memory. The `plot...` scripts generate plots based on the choice set by the user in the associated main script.

Each program contained in the main folder can be executed by choosing the *full model* presented at the end of the previous chapter, or by selecting the *adiabatic model*, where the cavity mode Fock space is not explicitly considered (see Chapter 4) by proper redefinition of some of the full model operators. Before introducing the several quantum optics simulations,

it is instructive to briefly introduce the “matrix representation” of Lindblad Master equation, required for the numerical integration.

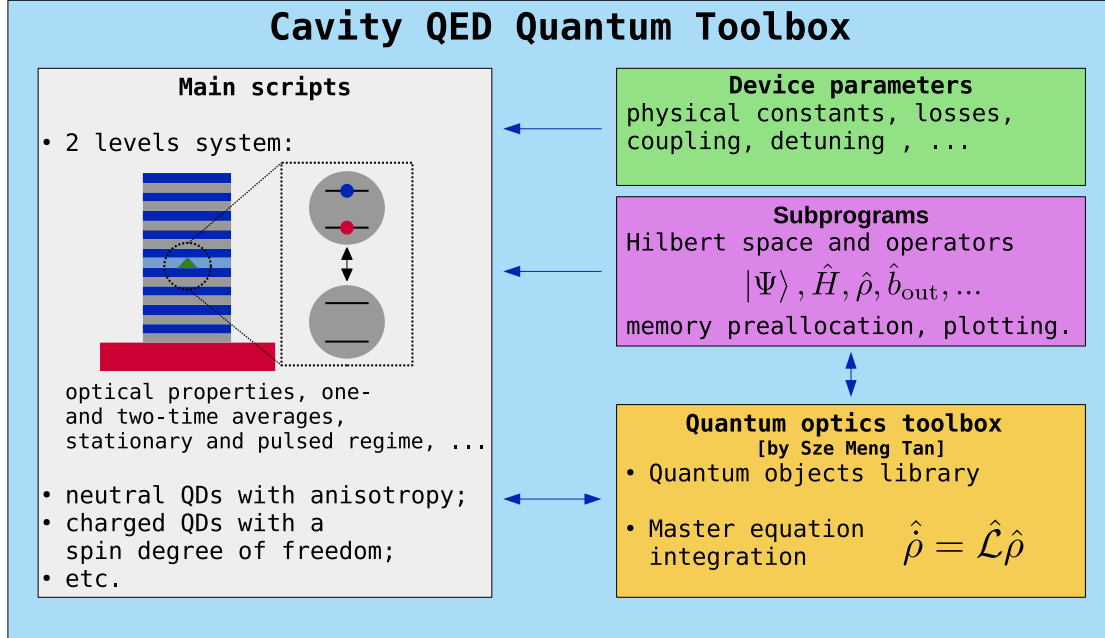


Figure 3.1: Custom Cavity QED toolbox. Here $A \leftarrow B$ means that B sends data to A .

The Fock-Liouville Hilbert space Some linear combinations of density matrices are still density matrices as long as they have unit trace and positivity. A Hilbert space of density matrices can be defined converting the matrices into vectors of the so called *Fock-Liouville space* (FLS). The corresponding scalar product between $\hat{\phi}$ and $\hat{\rho}$ is defined as $\langle\langle\phi|\rho\rangle\rangle \equiv \text{tr}(\hat{\phi}^\dagger \hat{\rho})$. The Liouville superoperator $\hat{\mathcal{L}}$ of equation (2.27) is now an operator $\tilde{\mathcal{L}}$ acting on the FLS. For instance, it is possible to define for a two-level system:

$$|\rho\rangle\rangle \equiv \begin{pmatrix} \rho_{00} \\ \rho_{01} \\ \rho_{10} \\ \rho_{11} \end{pmatrix}, \quad (3.1)$$

where ρ_{ij} is an element of the density matrix in the chosen representation basis. At last, the time evolution of the system corresponds to a system of first order differential equations $\frac{d|\rho\rangle\rangle}{dt} = \tilde{\mathcal{L}}|\rho\rangle\rangle$, to be numerically solved.

3.1 Nonlinear Optics with CQED

In this section the spectral response of an atom-cavity device will be addressed based on the parameters that have been introduced in Chapter 2. Before showing the simulation results of

the reflection coefficient as a function of the laser energy ω , some features of the reflectivity can be predicted based on the analytical formula [19] obtained in the semi-classical approach, valid only for low power and $\gamma^* = 0$. It is found that for the reflection coefficient

$$r(\omega) \equiv \langle \hat{b}_{\text{out}} \rangle / b_{\text{in}} = 1 - \frac{\kappa_{\text{top}}}{\frac{\kappa}{2} - i \left(\omega - \omega_c - \frac{g^2}{(\omega - \omega_d + i\gamma)} \right)}, \quad (3.2)$$

being ω the energy of the excitation laser, ω_c and ω_d the energy of the cavity and the quantum dot resonance, respectively. As in the previous chapter, g is the coupling strength, γ is the total dephasing rate and κ the cavity damping rate. The reflectivity in the simulation is given by $R \equiv \langle \hat{b}_{\text{out}}^\dagger \hat{b}_{\text{out}} \rangle / |b_{\text{in}}|^2$ and for the uncoupled cavity ($g = 0$), a Lorentzian dip in the reflectivity spectrum, at the cavity frequency ω_c , is described from equation (3.2). The following curves have been obtained by simulating at resonance, $\omega_d = \omega_c$, with null pure dephasing, $\gamma_{\text{sp}} = 0.6 \mu\text{eV}$, $\gamma^* = 0$, $\kappa = 100 \mu\text{eV}$ and extraction efficiency of the top mirror $\eta_{\text{top}} = \frac{\kappa_{\text{top}}}{\kappa} = 0.7$. The reflectivity spectrum of an uncoupled cavity ($g = 0$) is the expected

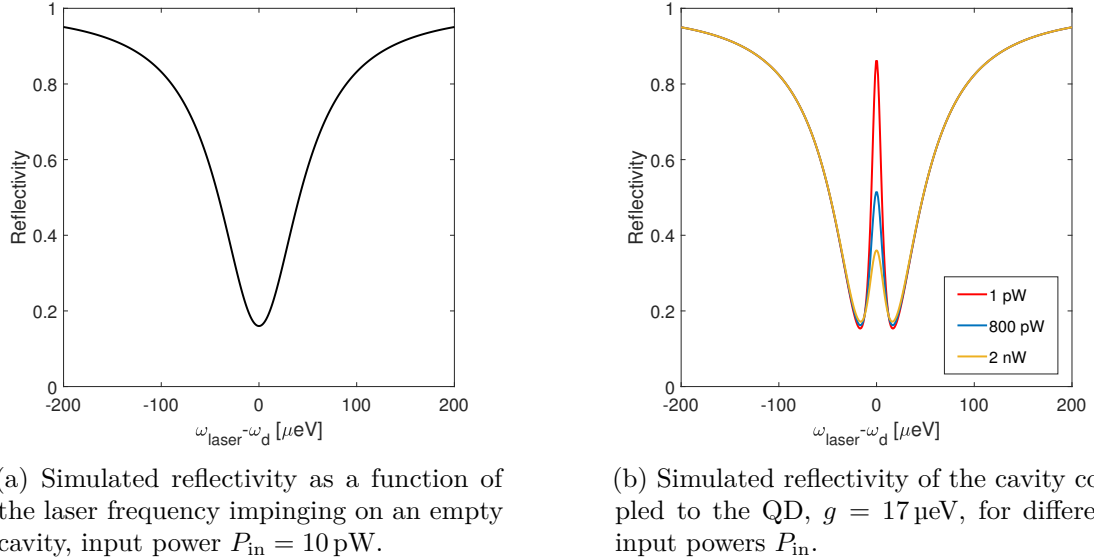


Figure 3.2: Reflectivity spectra in continuous wave excitation.

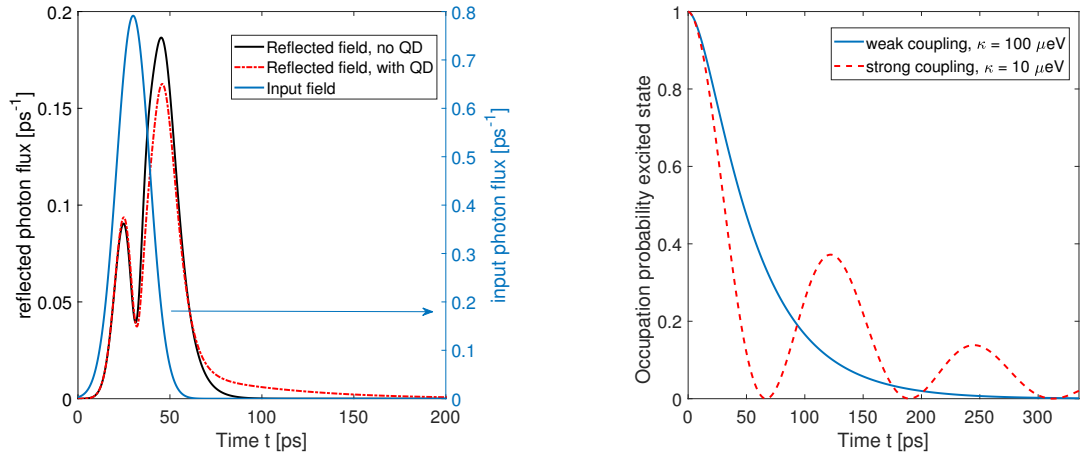
Lorentzian curve centered at the cavity resonance, see figure 3.2a. The two-level atom strongly modifies the reflectivity with a peak because of light being resonantly scattered. In the particular case of weak coupling regime, setting $g = 17 \mu\text{eV}$ in figure 3.2b, the light intensity tunes the light-atom coupling because when the transition is saturated, the atom has equal probability to be in the ground or excited state, and it becomes transparent to the optical field since it has the same probability to experience absorption or stimulated emission. This phenomenon has been verified experimentally, for instance in figure B.1 in Appendix B. As the contribution of the emission in the mode of interest decreases, also the fraction of photons emitted outside the mode reduces with increasing input power, as shown in figure B.2.

In *pulsed wave* (PW) regime one can analyze the temporal evolution of a reflected wavepacket. In the following simulation, it has been considered an input Gaussian pulse of 15 ps Full Width Half Maximum (FWHM), longer than the cavity lifetime of approximately 7 ps. The coherent laser pulse has a fixed center frequency, temporal width and average number of photons.

In figure 3.3a it is shown the response of the micropillar with and without the QD. In the case of an empty cavity, the first peak is the light being directly reflected from the top mirror. It is followed by partially-destructive interference with the light escaping from the cavity through the same top mirror, according to equation (2.31a). The second peak is mostly due to the light which exits the cavity at the end of the excitation pulse, so that no interference occurs and the decay time corresponds to the cavity damping rate.

As the exciton is coupled to the cavity mode, the second peak height is reduced because of light absorbed by the artificial atom. Moreover, the reflected photon flux tail decays at a lower rate than before because of the exciton spontaneous emission and the light slowly being emitted by the QD in the cavity mode. The last process occurs through Purcell-enhanced single-photon emission, with a typical decay time Γ_{tot} , and the light is extracted from the cavity mode by the top-mirror.

By using the same program, it is possible to describe a non-resonant excitation experiment



(a) Reflected field as a function of the time evolution. The input field has 15 ps FWHM and the average photon number is $N_P = 10$.

(b) Occupation probability as a function of time for the QD in the initial excited state, in the weak and strong coupling regime.

Figure 3.3: Results from pulsed-wave excitation script.

where the exciton state $|e\rangle$ is populated at time zero. To simulate such an effect, one can simply change the initial state and use a very small value for the pulse average photon number, to ensure that the output fields are almost entirely induced by the initial excitation. The result is shown in figure 3.3b. For the blue curve, the high value of the cavity damping rate $\kappa = 100 \mu\text{eV}$ determines that the QD-cavity system is in the weak coupling regime, being the merit factor $S \equiv 4g/\kappa = 0.68 < 1$ [24]. Vice-versa, for the dashed red curve, the lower damping rate $\kappa = 10 \mu\text{eV}$ implies that the system is in the strong-coupling regime. In this figure, the Rabi oscillations are visible, with damping mainly caused by spontaneous

emission outside the cavity mode and intracavity photon losses. If not stated otherwise, the default simulation parameters of this chapter will be those defined in this section, in the weak coupling regime, i.e. $g = 17 \mu\text{eV}$, $\gamma_{\text{sp}} = 0.6 \mu\text{eV}$ and $\kappa = 100 \mu\text{eV}$.

3.2 First-order Coherence and Spectrum

In this section the quantum-mechanical first-order coherence functions will be briefly reviewed, highlighting how they evaluate the coherent and incoherent contributions to the reflected photon flux. In the CW regime the first-order temporal coherence has been obtained by the *quantum regression theorem* [25], which greatly simplifies the task of computing two-time correlation functions as one-time averages. The incoherent flux component has been Fourier transformed to obtain the incoherent spectral density of the field. On the other hand, in PW regime the Wigner Distribution Function of the first-order correlation has been evaluated, yielding information on both the photon flux and energy spectral densities. In the dipole interaction, mentioned in Chapter 2, using the Heisenberg picture, the general first-order correlation function [16] for a scalar field is defined as:

$$G^{(1)}(t_1, t_2) = \text{tr} \left(\hat{\rho} \hat{E}^{(-)}(t_2) \hat{E}^{(+)}(t_1) \right), \quad (3.3)$$

with normal ordering and where, summing over the modes k of frequency ω_k , electric constant ε_0 and cavity volume V ,

$$\hat{E}^{(+)}(t_i) = i \sum_k \left(\frac{\hbar \omega_k}{\varepsilon_0 V} \right)^{1/2} \hat{a}_k(t_i). \quad (3.4)$$

The normalized first-order quantum coherence function is

$$g^{(1)}(t_1, t_2) = \frac{G^{(1)}(t_1, t_2)}{[G^{(1)}(t_1, t_1) G^{(1)}(t_2, t_2)]^{1/2}}, \quad (3.5)$$

such that three possible degrees of coherence are defined:

$$|g^{(1)}(t_1, t_2)| = 1 \quad \text{complete coherence}, \quad (3.6a)$$

$$0 < |g^{(1)}(t_1, t_2)| < 1 \quad \text{partial coherence}, \quad (3.6b)$$

$$|g^{(1)}(t_1, t_2)| = 0 \quad \text{incoherent}. \quad (3.6c)$$

Such a quantity plays a major role in any experiment using an interference between two time-delayed components of an optical field, as in a Michelson or Mach-Zender setup. Notice that complete coherence is obtained when the expectation value of the numerator can be factorized, i.e. $\langle \hat{E}^{(-)}(t_2) \hat{E}^{(+)}(t_1) \rangle \equiv \langle \hat{E}^{(-)}(t_2) \rangle \langle \hat{E}^{(+)}(t_1) \rangle$, where the right hand side is the coherent contribution.

3.2.1 Continuous wave regime

For the following discussion, it is assumed a CW excitation. Being at stationary regime, one may set a general reference time $t_1 = 0$, and define the delay $\tau \equiv t_2 - t_1$ so that equation (3.5) reduces to

$$g^{(1)}(\tau) = \frac{\langle \hat{E}^{(-)}(t + \tau) \hat{E}^{(+)}(t) \rangle}{\langle \hat{E}^{(-)}(t) \hat{E}^{(+)}(t) \rangle}. \quad (3.7)$$

The details on the normalized-first order coherence computation by the *quantum regression*

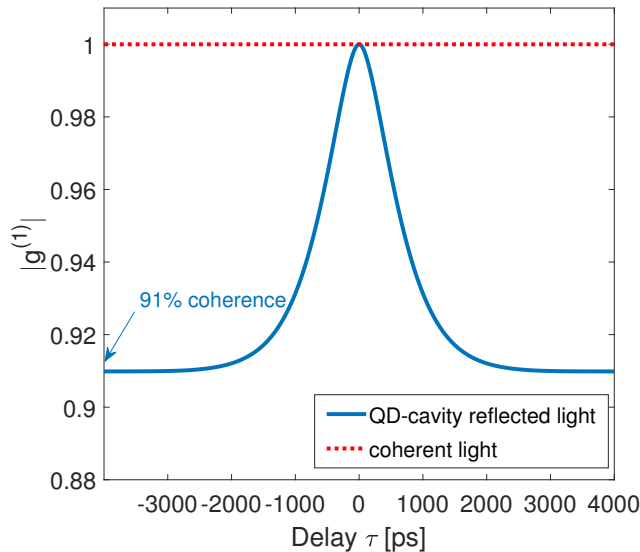


Figure 3.4: First order coherence of the reflected light in continuous wave regime, compared to a coherent field. The input power is $P_{in} = 10 \text{ pW}$ and $\kappa = 400 \mu\text{eV}$. The reflected field is partially coherent.

theorem are discussed in Appendix A. As before, the reflected flux is given by $\langle \hat{b}_{out}^\dagger(t) \hat{b}_{out}(t) \rangle$, in Heisenberg picture. Being here in the CW regime, the flux takes a constant value $\Phi_R = \langle \hat{b}_{out}^\dagger \hat{b}_{out} \rangle$ in the stationary state. Given that \hat{b}_{out} is a fluctuating operator, due to the random nature of spontaneous emission, it should become uncorrelated with itself at very distant times. Mathematically speaking,

$$\lim_{\tau \rightarrow \infty} \langle \hat{b}_{out}^\dagger(t + \tau) \hat{b}_{out}(t) \rangle = \langle \hat{b}_{out}^\dagger \rangle \langle \hat{b}_{out} \rangle = \Phi_{R,coh}, \quad (3.8)$$

where $\Phi_{R,coh}$ is the coherent photon flux reflected by the micropillar with the QD inside. By comparing equation (3.8) with the definition of the normalized first-order correlation function (3.7), it follows that $\lim_{\tau \rightarrow \infty} g^{(1)}(\tau) = \Phi_{R,coh}/\Phi_R$, being the total reflected flux the sum of the coherent and incoherent components, $\Phi_R = \Phi_{R,coh} + \Phi_{R,incoh}$. An example is shown in figure 3.4, where the $g^{(1)}(\tau)$ of a coherent field is compared to the reflected light

from the optical micropillar. At zero delay the normalized-first order coherence has unit modulus as expected from the definition. For positive infinite delay, and negative, being $g^{(1)}(-\tau) = g^{(1)}(\tau)^*$, the coherent percentage $\Phi_{R,\text{coh}}/\Phi_R$ of the reflected light is recovered, in this example about 91 %.

Resonance fluorescence spectrum and Mollow triplets In this paragraph the radiation due to an isolated atom driven by a monochromatic field will be addressed. The optical spectrum of a CW optical field is characterized by its spectral density of flux, $S(\omega)$, whose integral over the whole spectrum returns the total photon flux. Given a field operator, e.g. the reflected field \hat{b}_{out} , the Wiener-Khinchin theorem [25] states that its spectrum is the Fourier transform of the related correlation function $G^{(1)}(\tau)$. In the rotating frame at the laser frequency ω_s , the spectrum of the reflected field is

$$S_R(\omega) = \frac{1}{2\pi} \int_{-\infty}^{+\infty} \langle \hat{b}_{\text{out}}^\dagger(\tau) \hat{b}_{\text{out}}(0) \rangle e^{i(\omega - \omega_s)\tau} d\tau, \quad (3.9)$$

normalized such that its integral over the whole spectrum gives the total reflected flux:

$$\int_{-\infty}^{+\infty} S_R(\omega) d\omega = \langle \hat{b}_{\text{out}}^\dagger(0) \hat{b}_{\text{out}}(0) \rangle = \Phi_R. \quad (3.10)$$

As stated before, the quantity $\langle \hat{b}_{\text{out}}^\dagger(\tau) \hat{b}_{\text{out}}(0) \rangle$ is the sum of the coherent component $\langle \hat{b}_{\text{out}}^\dagger(0) \rangle \langle \hat{b}_{\text{out}}(0) \rangle$ and a varying contribution that tends towards zero for larger delays. Correspondingly, the total spectrum $S_R(\omega)$ will be the sum of two contributions: $S_R(\omega) = S_{R,\text{coh}}(\omega) + S_{R,\text{incoh}}(\omega)$. The coherent contribution has a DC value which, when Fourier transformed over time, leads to a monochromatic spectrum centered at the laser frequency, described by $S_{R,\text{coh}}(\omega) = \langle \hat{b}_{\text{out}}^\dagger \rangle \langle \hat{b}_{\text{out}} \rangle \times \delta(\omega - \omega_s)$. On the other hand, the varying contribution leads, after Fourier Transform, to a continuous spectrum $S_{R,\text{incoh}}(\omega)$ which is denoted as the spectrum of the incoherent component of the photon flux. Such a component is called incoherent since, not being monochromatic, it cannot interfere with the incoming laser. In the weak-coupling regime this incoherent spectrum has the shape of a Lorentzian at low power, but of a Mollow triplet at high power, see figure 3.5. Experimental curves from literature are shown in Appendix B, figure B.3.

The laser frequency is $\omega_s = \omega_d$, so it is at resonance with the QD driven at the Rabi frequency Ω . At the low power or weak field limit, $\Omega \ll \gamma_{\text{sp}}$ and the Rabi frequency of the driving field is much smaller than the spontaneous emission rate. The atom behaves as an over-damped quantum harmonic oscillator and the spectrum is a Lorentzian. Yet, when the Rabi frequency becomes comparable to the exciton linewidth in the strong excitation limit $\Omega \gg \gamma_{\text{sp}}$, the energy level splitting described in section 2.3 occurs. This generates two side-bands at $\omega_s \pm \Omega$ in addition to the transition at ω_s , resulting in the Mollow triplet.

3.2.2 Pulsed wave regime

Constant CW regime can be used to design a two-level system single photon source. However, one would be interested in deterministic sources that can be triggered on-demand. This is in general done by an optical pulse, which requires a quantum dynamical treatment of

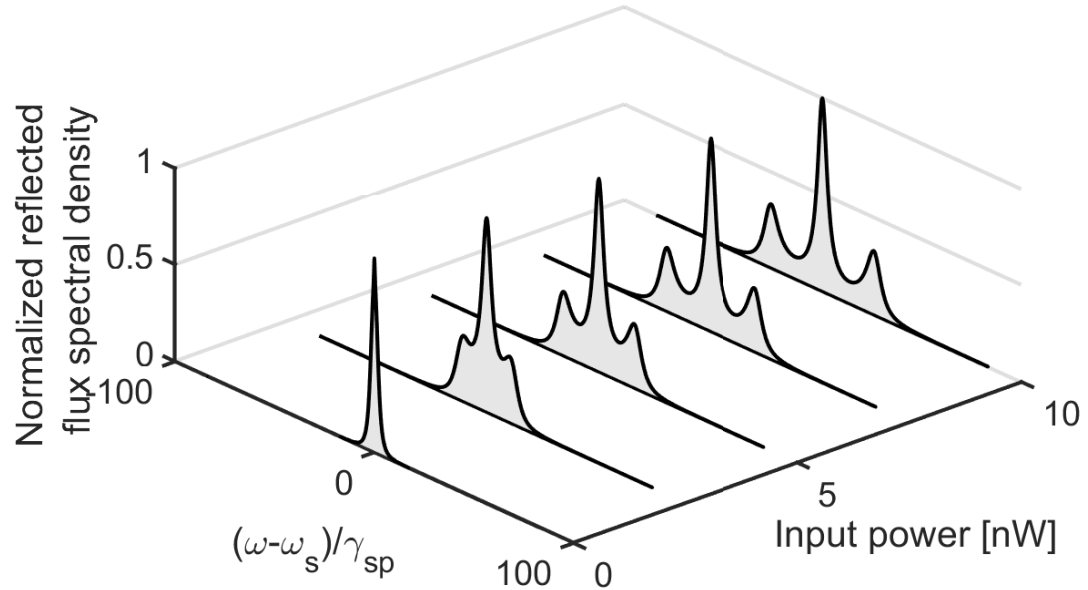


Figure 3.5: Simulated spectral density of the reflected flux in the rotating frame, $S_R(\omega)$, for increasing input power. The Lorentzian profile turns into the Mollow triplet at higher powers. Image for section 3.2.1.

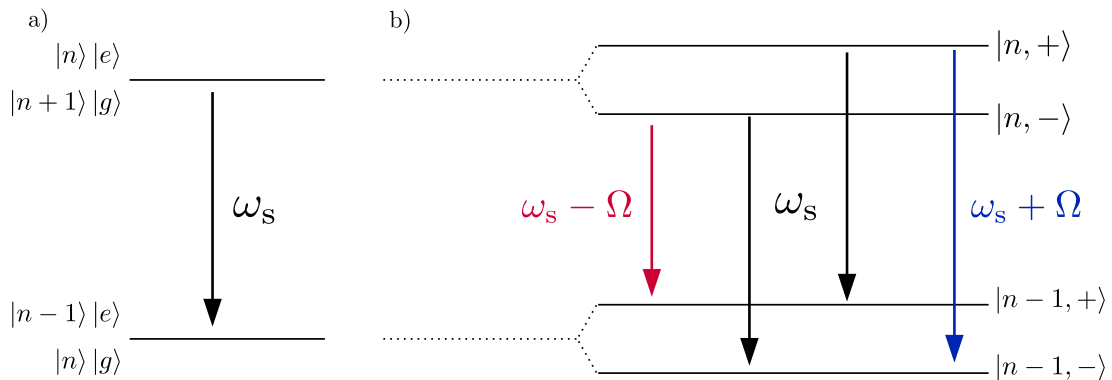


Figure 3.6: (a) Two-level system resonant with the cavity field ω_s , weak field and weak coupling regime. (b) Degeneracy splitting due to strong field regime. The four dressed states add two side-bands transitions at $\omega_s \pm \Omega$, in addition to the transition at ω_s , leading to the Mollow triplet. Image for section 3.2.1.

resonance fluorescence. In pulsed regime two time evolution must be numerically computed to obtain, e.g. for the reflected field

$$G^{(1)}(t_1, t_2) = \langle \hat{b}_{\text{out}}^\dagger(t_2) \hat{b}_{\text{out}}(t_1) \rangle, \quad (3.11)$$

which is the first-order correlation evaluated at two different times, t_1 and t_2 .

The aim has been to compute the energy spectral density and to check, as in all the simulations, the proper normalization of the spectrum. Assuming a transform-limited¹ Gaussian pulse shape, the electric field can be represented in the time domain and the rotating frame as

$$\mathcal{E}(t) = \exp \left[-\frac{t^2}{2\sigma_t^2} \right], \quad (3.12)$$

where σ_t characterizes the standard deviation of the pulse.

A common tool for time-frequency analysis is the Wigner distribution function (WDF), which is used as transform in time-frequency analysis. It provides the highest possible temporal and frequency resolutions, mathematically limited by the uncertainty principle in quantum wave theory. Information on the single photon wavepacket can be obtained by calculating the associated Wigner-Ville function (WVF, also known as chronocyclic Wigner distribution), which is the quantum analogue of the WDF, the latter being the name chosen in this text. In the rotating frame centered at the average pulse frequency ω_p , its expression [27] for a field mode of annihilation operator \hat{s} is:

$$W(t, \omega) = \frac{1}{2\pi} \int_{-\infty}^{\infty} \left\langle s^\dagger \left(t + \frac{\tau}{2} \right) s \left(t - \frac{\tau}{2} \right) \right\rangle e^{-i(\omega - \omega_p)\tau} d\tau. \quad (3.13)$$

Indeed, it is the Fourier transform of the electric field correlations as a function of time. In the following only the reflected field will be shown. Due to the projection property of the WDF function, the following holds:

$$\int_{-\infty}^{+\infty} W(t, \omega) d\omega = \langle \hat{b}_{\text{out}}^\dagger(t) \hat{b}_{\text{out}}(t) \rangle \equiv \Phi(t), \quad (3.14a)$$

$$\int_{-\infty}^{+\infty} W(t, \omega) dt = S(\omega). \quad (3.14b)$$

Thus by integrating the WDF over the frequency domain, the original flux is obtained because of the correct normalization of the distribution. Whereas integrating the WDF over time gives the total spectrum of the optical field, see equation (3.14b). Last, by integrating in time and frequency, the total number of photons is recovered. In figure 3.7 the reflected total flux $\Phi(t)$ is shown as a function of the simulation time. The flux has been evaluated first, as in section 3.1, by $\langle \hat{b}_{\text{out}}^\dagger(t) \hat{b}_{\text{out}}(t) \rangle$. Whereas, the second curve has been computed by integrating the WDF over the frequency domain. Being superimposed to the previous one, it has proven the WDF correct normalization according to equation (3.14a). The input Gaussian pulse has 15 ps FWHM with average photon number equal to one. The first peak

¹A transform-limited pulse is one that has minimal phase variation over its spectrum and has a minimal time-bandwidth product [26].

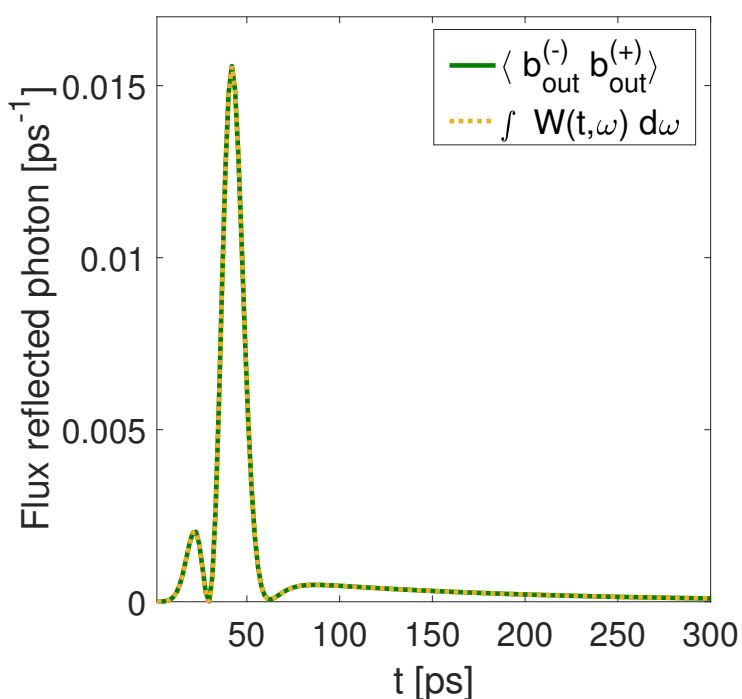


Figure 3.7: Reflected photon flux computed by the output operator and by the Wigner Distribution Function. Differently from figure 3.3a, $\kappa = 200 \mu\text{eV}$, $N_p = 1$.

is due to the reflected field from the top mirror, which interferes destructively with the field reflected from the bottom mirror. The decaying tail corresponds to the quantum emitter emission in the cavity.

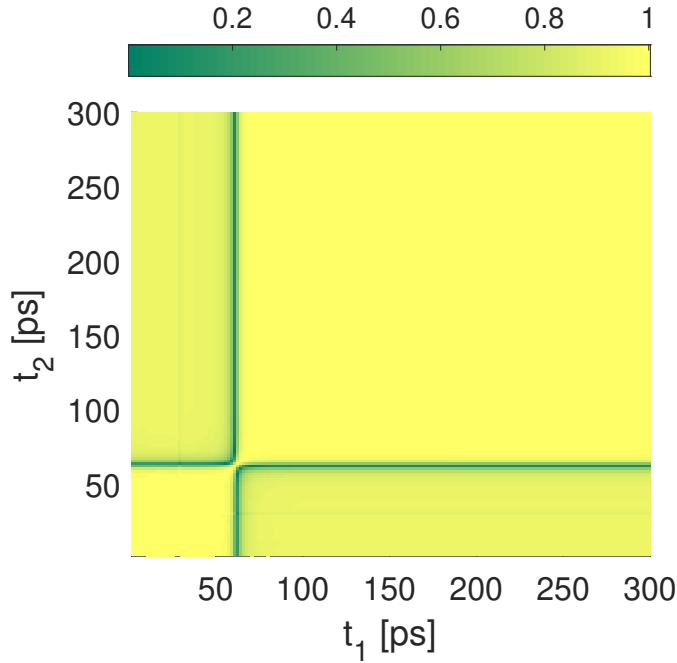


Figure 3.8: Absolute value of the normalized-first order coherence $|g^{(1)}(t_1, t_2)|$ of the reflected field in pulsed wave regime.

Computing the first-order correlation function Being in pulsed regime, two time evolution were required for simulating $g^{(1)}(t_1, t_2)$, shown in figure 3.8. The mathematical details are contained in Appendix A. There is a transition time around 60 ps before which most of the light is induced by the empty-cavity response, and after which most of the light is induced by the slowly-decaying QD signal. The figure can be analyzed according to different time sets:

- Along the diagonal $t_1 = t_2$, the normalized first order correlation is unity by definition. In the yellow region where both t_1 and t_2 are before the transition time, it regards coherence of the empty-cavity reflection with itself, which comes from the laser input: perfect relative coherence is obtained, being $|g^{(1)}(t_1, t_2)| \approx 1$. For the yellow region where both t_1 and t_2 are after the transition time, it regards coherence of the QD-emitted signal with itself, which is also near-unity due to the negligible pure dephasing chosen in the simulation.
- When t_1 is before the transition time and t_2 after, or the reverse, $|g^{(1)}(t_1, t_2)|$ measures the relative coherence of the QD-signal with the directly-reflected laser, showing only partial coherence. This is in accordance with the partial coherence also observed in

figure 3.4 in the CW regime. In general, the QD-emitted light is not fully coherent with the incoming laser.

- The zero coherence lines presumably arise from the specific transition moment where there should be no reflected light at all, due to perfect interference, if the QD signal were entirely coherent. This would happen in the limit of very low power, in addition to no pure dephasing. Since there is some amount of signal at this transition moment, this signal only arises from the incoherent part, and this explains why there is absolutely no coherence at that time.

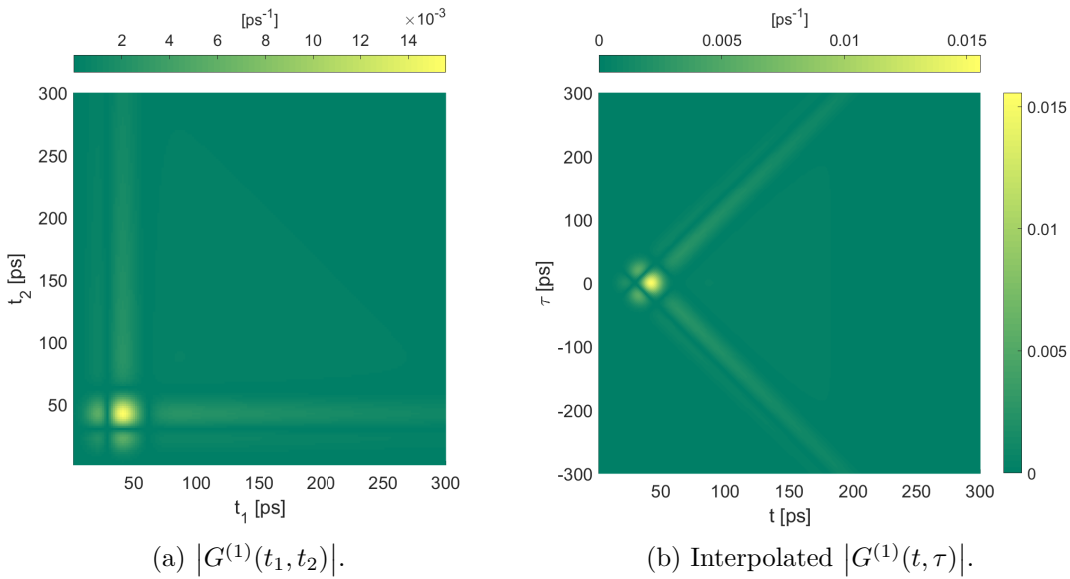


Figure 3.9: First-order correlation function of the reflected field in pulsed wave excitation.

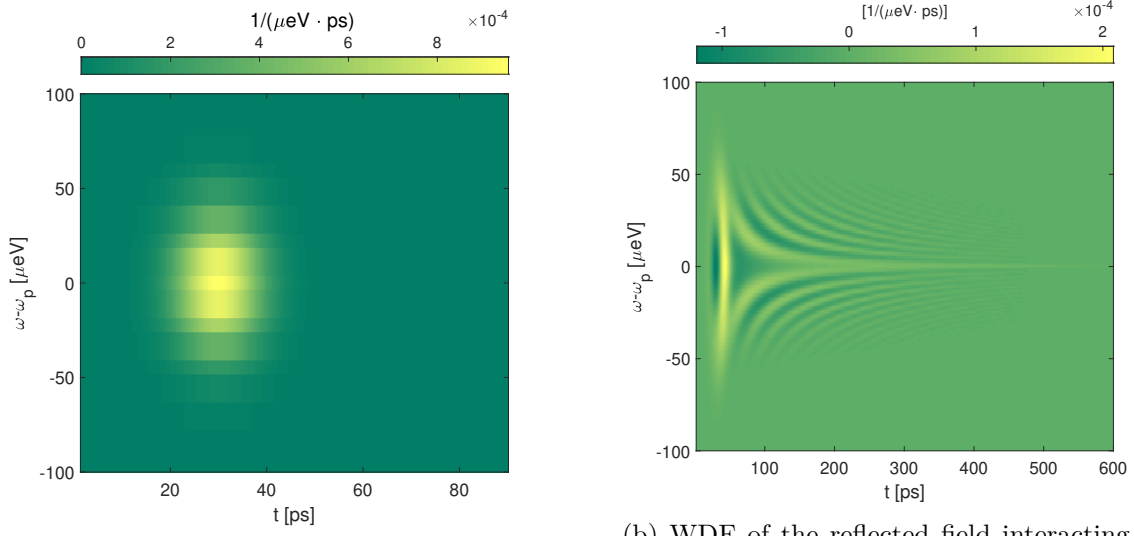
Computing the Wigner Distribution Function In equation (3.13) the WDF is described in terms of time t and delay τ . The latter are related to t_1, t_2 according to the following mapping:

$$\begin{cases} t &= (t_1 + t_2)/2 \\ \tau &= t_2 - t_1. \end{cases}$$

The first-order correlation function $G^{(1)}(t_1, t_2)$ is shown in figure 3.9a, and the corresponding interpolated function $G^{(1)}(t, \tau)$ is shown in 3.9b, where the highest correlation occurs nearby the maximum peak at about 50 ps of the reflected flux in figure 3.7. Comments on the interpolation procedure, and on the computation of the Wigner Distribution Function using the Fast Fourier Transform (FFT) are discussed in Appendix A. Indeed, a new WDF algorithm has been developed independently, because the associated MATLAB® routine (available from R2018b) is designed for single-time series and not correlation functions.

The WDF function, real because of the time-reversal symmetry of the first-order correlation functions, is presented in figure 3.10b. As a function of time, the spectral content is centered at the average pulse frequency. The negative values assumed by the WDF are a consequence

of the so called *Heisenberg–Gabor limit*, which states that one cannot simultaneously sharply localize a signal in both time ad frequency domain. Thus, an averaging along a time or frequency window is necessary to deduce a physical and positive quantity. The WDF of a Gaussian is still a bell-shaped surface which represents the pulse in the time-frequency phase space, see figure 3.10a. In the simulated WDF with the QD-cavity, the effect of the optical cavity and the QD spontaneous emission can be appreciated. The incident Gaussian pulse is divided into a reflected pulse in phase space (weak yellow) and interference fringes because of the many emission sources: the light directly reflected without entering, the light extracted after entering the cavity (but without having interacted with the QD), and finally, the light emitted due to QD decay. In figure 3.11 it is shown the spectrum $S(\omega)$



(a) The WDF of a Gaussian is still a bell-shaped surface. Result obtained from the reflected field by setting $\eta_{\text{top}} \approx 0$.

(b) WDF of the reflected field interacting with the QD-cavity. Interference fringes are due to the multiple light sources present, as explained in the text.

Figure 3.10: Wigner Distribution Functions in time-frequency axes given an input Gaussian pulse.

obtained by integrating along time the WDF. The total spectrum is given by the sum of a coherent and incoherent contribution, with the quantum emitter responsible for the latter.

3.3 Second-order Coherence

The first-order coherence correlation functions do not provide information on the photon statistics, which is contained in the second-order quantum correlation function (at fixed position)

$$g^{(2)}(t, \tau) = \frac{G^{(2)}(t, \tau)}{G^{(1)}(t, t)G^{(1)}(t + \tau, t + \tau)}, \quad (3.15)$$

where

$$G^{(2)}(t, \tau) = \text{tr}(\hat{\rho}\hat{E}^{(-)}(t)\hat{E}^{(-)}(t + \tau)\hat{E}^{(+)}(t + \tau)\hat{E}^{(+)}(t)). \quad (3.16)$$

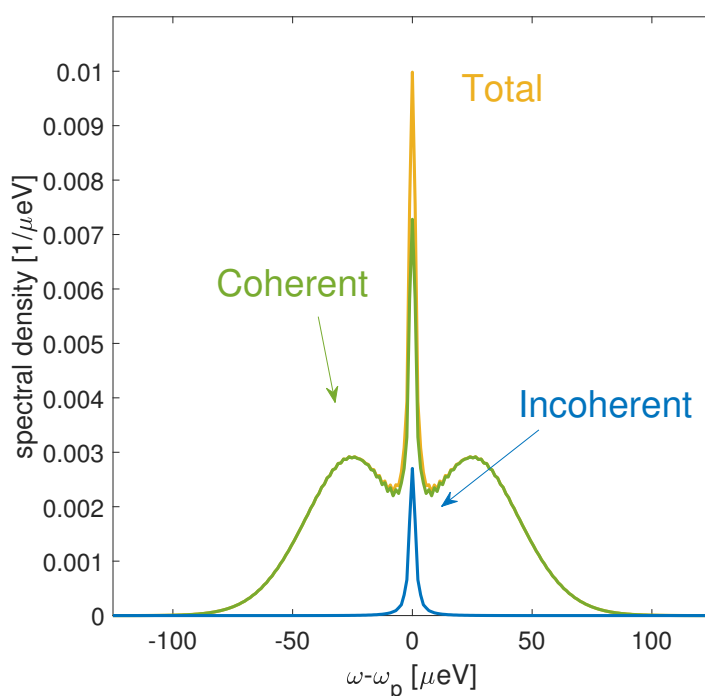
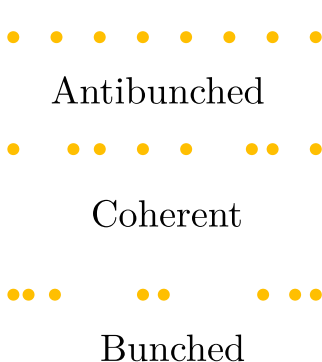
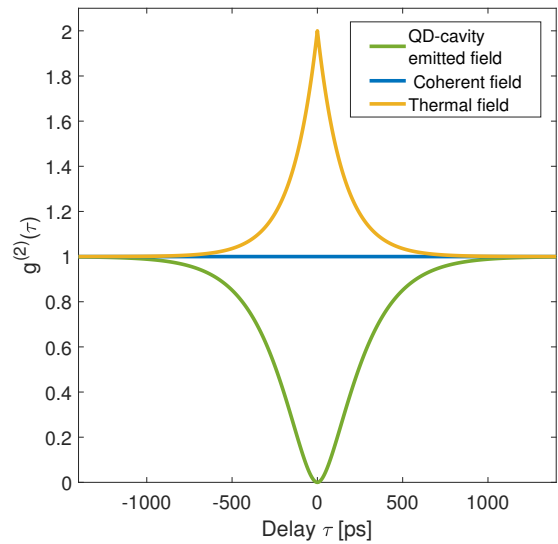


Figure 3.11: Reflected flux spectral density obtained from the Wigner Distribution Function by equation (3.14b). Image discussed in section 3.2.2.

A quantum field is said to be second order coherent if $g^{(2)}(t, t + \tau) = 1$. Equation (3.15) is interpreted as the conditional probability to detect a photon at time $t + \tau$ knowing that a first photon has already been detected at time t , divided by the unconditioned probability. For a coherent multimode state, it can be shown that $g^{(2)}(\tau) = 1$ and thus the photon stream obeys a Poisson distribution. In the case of $g^{(2)}(0) < g^{(2)}(\tau)$, called photon antibunching, photons tend to impinge evenly spaced in time and it represents a non-classical state, figure 3.12a. In figure 3.12b the simulated $g^{(2)}(\tau)$ of the quantum dot spontaneous emission in the cavity is compared with a multimode coherent field and thermal state. Being $g^{(2)}(0) \approx 0$, this represents a non-classical light source as mentioned at the beginning of Chapter 2. To reduce numerical errors in the simulation, it has been



(a) Comparison of the photon streams for antibunched light, coherent light, and bunched light. For the case of coherent light, the Poissonian photon statistics correspond to random time intervals between the photons.



(b) The $g^{(2)}(\tau)$ of the QD emitted field is compared with a thermal (bunched) and a multimode coherent field. $\kappa = 200 \text{ } \mu\text{eV}$ and $P_{\text{in}} = 10 \text{ } \mu\text{W}$.

Figure 3.12: Photon statistics and simulated second-order correlation for the QD spontaneously emitted field.

decided to evaluate the second-order quantum coherence $g^{(2)}(t_2, t_1)$ in terms of a conditional density matrix. The field operator for spontaneous emission is given by $\hat{e} = \sqrt{\gamma_{\text{sp}}} \hat{\sigma}_-$, which projects the excited state $|e\rangle$ into the ground state $|g\rangle$. To physically interpret the results and to get a better numerical convergence, it is computed the system's density matrix just after a detection event at time t . This new *conditional density matrix* $\hat{\rho}'(t_1)$ is given by

$$\hat{\rho}'(t_1) = \frac{\hat{e} \hat{\rho}(t_1) \hat{e}^\dagger}{\text{tr}(\hat{\rho}(t_1) \hat{e}^\dagger \hat{e})}. \quad (3.17)$$

This is a valid density matrix with unit trace, verified by taking the trace in the previous equation and by exploiting the cyclic permutation property. From this density matrix at time $t_1^{(+)}$, right after the first detection at t_1 , one deduces the conditional density

matrix at time t_2 , leading to a density matrix $\hat{\rho}(t_2 | t_1) \equiv \hat{\rho}(t_2, \text{conditioned to a click at } t_1)$. Therefore, the quantity

$$\text{tr}(\hat{e}^\dagger \hat{e} \hat{\rho}(t_2 | t_1)) = \frac{\langle \hat{e}^\dagger(t_1) \hat{e}^\dagger(t_2) \hat{e}(t_2) \hat{e}(t_1) \rangle}{\langle \hat{e}^\dagger(t_1) \hat{e}(t_1) \rangle}. \quad (3.18)$$

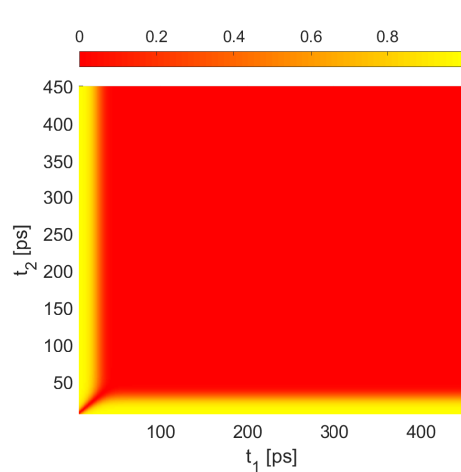
Last, the second term in the denominator of equation (3.15) is given by

$$\langle \hat{e}^\dagger(t_2) \hat{e}(t_2) \rangle = \text{tr}(\hat{e}^\dagger \hat{e} \hat{\rho}(t_2)). \quad (3.19)$$

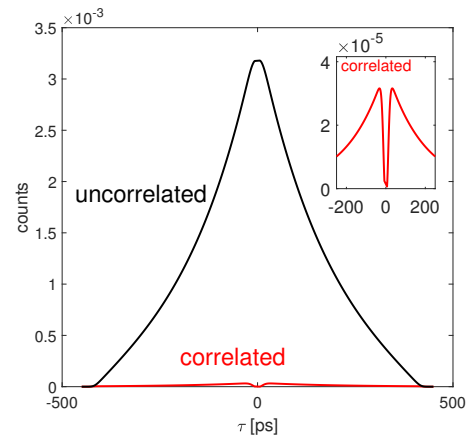
So it is found that the normalized correlation function $g^{(2)}(t_1, t_2)$ is indeed the ratio between two quantities: the photon flux at time t_2 , conditioned by a previous photon detection event at time t_1 , and the photon flux at time t_2 , unconditioned. This is the equivalent experimental definition of the second-order correlation function.

In the CW regime, the second-order quantum coherence function is only a function of the delay, $g^{(2)}(\tau)$, which simplifies the simulation of figure (3.12b) to just one-time evolution.

On the other hand, for PW excitation, the $g^{(2)}(t_1, t_2)$ for the QD emitted light is shown in



(a) $g^{(2)}(t_1, t_2)$ of the quantum dot emitted light.



(b) Correlated and uncorrelated coincidences of the quantum dot emitted light, $\kappa = 400 \mu\text{eV}$. Inset is the correlated count, centered at zero delay.

Figure 3.13: Second order correlation function, correlated and uncorrelated coincidences in pulsed wave excitation.

figure 3.13a. Along the diagonal, so for zero-delay time, $g^{(2)}(t, t) = 0$ as expected: the QD cannot emit a second photon immediately after having emitted a first one, since it has been projected to the ground state. After the pulse arrival time, there is a “dead time” before the laser field drives the electron back into the excited state at which moment another photon may be emitted (yellow region). For longer times, the pulse is mostly extinguished and the conditional probability is null (red region).

Note that in the $g^{(2)}(t_1, t_2)$ the denominator $\langle \hat{e}^\dagger(t_1) \hat{e}(t_1) \rangle \langle \hat{e}^\dagger(t_2) \hat{e}(t_2) \rangle$ represents the rate of *uncorrelated coincidences* corresponding to the expected coincidence rate for photons from

independent sources (or, as usually done in the laboratory, by independent excitation pulses from the same source). In comparison, the numerator $\langle \hat{e}^\dagger(t_1)\hat{e}^\dagger(t_2)\hat{e}(t_2)\hat{e}(t_1) \rangle$ corresponds to the rate of correlated coincidences, that is the expected coincidences rate for photons from the same pulse.

In a HBT experiment in pulsed regime, $g^{(2)}(\tau)$ is obtained by an histogram integrating all the coincidences corresponding to a given delay $\tau = t_2 - t_1$. Here the normalization is chosen such that the area of the $g^{(2)}(\tau)$ peak is unity for uncorrelated coincidences, figure B.4a in Appendix B. The correlated coincidences, figure B.4b, lead to a zero-delay peak corresponding to photons emitted during the same pulse. Both the uncorrelated and correlated coincidences are shown as a function of the delay τ in figure 3.13b, whose experimental counterpart is represented in Appendix B, figure B.5. The purity of the source is linked to the ratio between the correlated and uncorrelated areas. Here the area for the correlated coincidences is almost negligible (inset in figure 3.13b), i.e. negligible probability to have a second photon emitted during the same pulse compared to the correlated case. Thus, this result confirms the very good single-photon purity of the simulated quantum emitter.

Conclusions

In this chapter the custom Cavity QED Quantum Toolbox structure has been presented, showing some quantum optics simulations results. It has been addressed the quantum emitter optical non-linearity which modifies the reflectivity spectra, showing the 2-level atom saturation at higher input power. From the spectrum of the first-order correlation functions in the continuous-wave regime, the Mollow triplet phenomenon has been reproduced as the driving Rabi frequency becomes much larger than the exciton spontaneous emission rate. To investigate the first-order coherence function in the pulsed regime, a custom algorithm for evaluating the Wigner Distribution Function has been presented with the associated results. Last, the single-photon emission property of the artificial atom has been proved by the second-order correlation function, both in continuous and pulsed wave excitation. In the next chapter, the adiabatic elimination of the cavity mode Fock space is discussed, highlighting its advantages for the computational cost and some results, in comparison with the “full” model used in this Chapter.

Chapter 4

Adiabatic Elimination

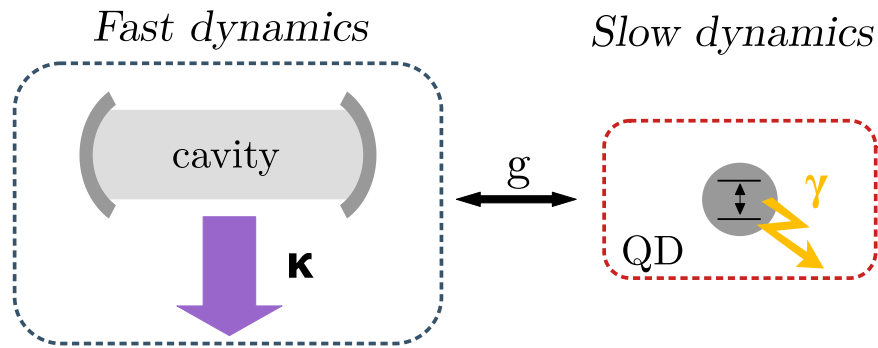


Figure 4.1: A fast sub-system, the cavity, is coupled to the slow sub-system, the neutral QD. The cavity acts as a perturbation and it is adiabatically eliminated.

Adiabatic elimination is an approximation that produces an effective Hamiltonian for the sub-space of interest and it is valid when the cavity damping rate κ is much higher than any other evolution rate: $\kappa \gg g, \gamma_{\text{sp}}, \gamma^*$. This is the so-called *bad cavity* regime and these conditions are always fulfilled for the simulations in this Chapter. As presented in figure 4.1, the cavity is subjected to high losses and its dynamics are much faster than the QD ones. If not stated otherwise, the QD-Cavity system has:

- $\kappa \approx 400 \mu\text{eV}$, leading to a photon lifetime in the cavity of about 1.6 ps. The decay time comes from the Lorentzian cavity spectrum, whose Fourier transform is an exponential decay. The decay rate is $\kappa/(2\hbar)$ for the field amplitude, whereas κ/\hbar for the intensity, i.e. a photon lifetime \hbar/κ . Since $\hbar = 6.582 \cdot 10^{-4} \text{ eV} \cdot \text{ps}$, it explains why κ is denoted alternatively as a cavity linewidth or, by considering $\hbar \equiv 1$ units, as a decay rate.
- $g \approx 17 \mu\text{eV}$, corresponding to 120 ps timescale. Notice that g is related to the period of the vacuum Rabi oscillations illustrated in figure 3.3b. From equation (2.17), the Rabi angular frequency is $2g/\hbar$, with $2g$ the vacuum Rabi splitting between the two first excited eigenstates of the Jaynes-Cummings model.

- $\gamma_{\text{sp}} \approx 0.6 \mu\text{eV}$, about 1 ns of spontaneous emission time in other modes than the cavity mode, with negligible pure dephasing.

In such a case, the photons emitted by the QD in the cavity mode are not stored in the cavity: they quickly escape it. From the QD point of view, there is no difference between the spontaneous emission in the other modes, at the rate γ_{sp} , and the emission in the cavity mode followed by photon escape, at the rate Γ_m . It is reminded that the ratio between the latter and the former defines the Purcell factor, equation (2.10). Two important parameters for the rate of emitted photons in the cavity mode (Γ_m) are:

- the normalized QD-Cavity detuning:

$$\Delta_{\text{QD-C}} \equiv \frac{2(\omega_d - \omega_c)}{\kappa}. \quad (4.1)$$

- the Purcell-enhanced emission rate at zero detuning:

$$\Gamma_0 = \frac{4g^2}{\kappa}. \quad (4.2)$$

One can show that, with these notations and for a 2-level system in a cavity, the following Lorentzian dependence with the detuning is obtained for the Purcell-enhanced emission rate in the cavity mode, Γ_m :

$$\Gamma_m = \frac{\Gamma_0}{1 + \Delta_{\text{QD-C}}^2}. \quad (4.3)$$

With the above given values, at zero detuning it is found that $\Gamma_m = \Gamma_0 = 2.9 \mu\text{eV}$, thus $\Gamma_{\text{tot}} = \Gamma_m + \gamma_{\text{sp}} = 3.5 \mu\text{eV}$. This value is also much lower than κ and corresponds to a total emission time of 180 ps. The coupling factor, proportional to the brightness, is $\beta = 2.9 \mu\text{eV}/3.5 \mu\text{eV} \approx 83\%$ at zero detuning.

Before discussing how the adiabatic model is obtained, in the following table the computation time of the full model is compared with the adiabatic version. As the dimension of the cavity mode Fock space increases, which is required for higher input powers, also the simulations take more time. On the contrary, for the adiabatic model the Fock space has been neglected and taken into account by an effective Hamiltonian. In the following table simulation times for a CW and PW program are shown to illustrate the computational cost reduction of the adiabatic approximation. The average times have been computed over ten simulations for each program, without plotting.

Program	Full model, $N = \dim(\mathcal{H}_{\text{cav}})$			Adiabatic model (s)
	$N = 10$ (s)	$N = 15$ (s)	$N = 20$ (s)	
Reflectivity spectrum in CW	6.9 ± 0.3	11 ± 2	18 ± 1	4.4 ± 0.3
Photon flux evolution and QD occupation in PW	9.6 ± 0.1	16.6 ± 0.5	33 ± 1	1.13 ± 0.05

4.1 Approximations from the “Full Model”

In the general case, the exact calculation starts from the standard CQED Hamiltonian for a CQED system coherently excited by an input field b_{in} , presented in section 2.4. The full Hamiltonian acts both on the QD and the cavity subspaces: the goal of adiabatic elimination is to work *only* within the QD Hilbert space.

In the *fast*, or *bad*, cavity regime, the point is that the variables associated to the cavity mode have no memory of the past. At a given time t they simply adapt to the values of the other important quantities at that time, in particular $b_{\text{in}}(t)$ and $\langle \hat{\sigma}_- \rangle(t)$. Following a similar derivation from [28, sec. 13.2.1], one can use the Heisenberg’s representation for operators $\hat{a}(t)$, $\hat{b}_{\text{in}}(t)$, $\hat{\sigma}_-(t)$ and write in the rotating frame, as Loïc Lanco has done:

$$\begin{aligned} \dot{\hat{a}}(t) &= \left[-\frac{\kappa}{2} - i(\omega_c - \omega) \right] \hat{a}(t) - g \hat{\sigma}_-(t) - \sqrt{\kappa_{\text{top}}} \hat{b}_{\text{in}}(t) \\ &\quad + \text{noise operator averaging to zero.} \end{aligned} \quad (4.4)$$

Finally, integrating this equation gives:

$$\begin{aligned} \hat{a}(t) &= \hat{a}(0) \exp \left\{ - \left[\frac{\kappa}{2} + i(\omega_c - \omega) \right] t \right\} \\ &\quad - g \int_0^t dt' \hat{\sigma}_-(t-t') \exp \left\{ - \left[\frac{\kappa}{2} + i(\omega_c - \omega) \right] t' \right\} \\ &\quad - \sqrt{\kappa_{\text{top}}} \int_0^t dt' \hat{b}_{\text{in}}(t-t') \exp \left\{ - \left[\frac{\kappa}{2} + i(\omega_c - \omega) \right] t' \right\}, \end{aligned} \quad (4.5)$$

where:

- the first (red) term quickly disappears after a fast transient regime;
- the other (blue) terms are almost a Dirac $\delta(t')$ function, up to a coefficient, since κ implies fast decays. Thus, the past times $t - t'$ play no role except for very small values of t' .

Since one can focus on times t' close to zero, at first order

$$\hat{b}_{\text{in}}(t-t') \approx \hat{b}_{\text{in}}(t) \quad (4.6a)$$

$$\hat{\sigma}_-(t-t') \approx \hat{\sigma}_-(t) e^{i(\omega_d - \omega)t'}, \quad (4.6b)$$

where the exponential arises since the QD is detuned from the laser frequency. The simplified integrals over t' lead to

$$\int_0^\infty dt' \exp \left\{ - \left[\frac{\kappa}{2} + i(\omega_c - \omega_d) \right] t' \right\} = \frac{1}{\frac{\kappa}{2} + i(\omega_c - \omega_d)} = \frac{1}{\frac{\kappa}{2} (1 - i\Delta_{\text{QD-C}})}, \quad (4.7a)$$

$$\int_0^\infty dt' \exp \left\{ - \left[\frac{\kappa}{2} + i(\omega_c - \omega) \right] t' \right\} = \frac{1}{\frac{\kappa}{2} + i(\omega_c - \omega)} = \frac{1}{\frac{\kappa}{2} (1 - i\Delta)}, \quad (4.7b)$$

where

$$\Delta \equiv \frac{2(\omega - \omega_c)}{\kappa}. \quad (4.8)$$

Disregarding the noise term, one obtains:

$$\hat{a}(t) = -\frac{g \hat{\sigma}_-(t)}{\frac{\kappa}{2} (1 - i\Delta_{QD-C})} - \frac{\sqrt{\kappa_{top}} \hat{b}_{in}(t)}{\frac{\kappa}{2} (1 - i\Delta)}. \quad (4.9)$$

This also gives the correct equation when one comes back to the Schrödinger's representation:

$$\hat{a} = -\frac{g \hat{\sigma}_-}{\frac{\kappa}{2} (1 - i\Delta_{QD-C})} - \frac{\sqrt{\kappa_{top}} \hat{b}_{in}}{\frac{\kappa}{2} (1 - i\Delta)}. \quad (4.10)$$

It is recalled that when the input field arises from a coherent (laser) light source, one can replace \hat{b}_{in} by $b_{in} \cdot \hat{I}$. Thus, given this last assumption, the quantum fluctuations of the annihilation operator are due to the quantum fluctuations of the QD lowering operator. Note that the adiabatic elimination corresponds to a completely different point of view since now the operator \hat{a} does not act on the cavity subspace, that is not considered, but is viewed only through its effect on the QD subspace, as given by equation (4.10).

4.2 Adiabatic Hamiltonian and Output Operators

In the previous section the annihilation operator has been expressed in terms of the lowering operator and the coherent input field. Equation (4.10) is significant since it states that the cavity field adapts instantaneously to its two sources: the input field and the Purcell-enhanced emission from the QD into the cavity mode. The cavity forgets any previous value it had. From this equation a new input-output equation is deduced

$$\hat{b}_{out} = \hat{b}_{in} + \sqrt{\kappa_{top}} \hat{a} \quad (4.11)$$

↓

$$\hat{b}_{out} = b_{in} \left(1 - \frac{2 \eta_{top}}{1 - i\Delta} \right) \hat{I} - \frac{\sqrt{\Gamma_0 \eta_{top}}}{1 - i\Delta_{QD-C}} \hat{\sigma}_-, \quad (4.12)$$

being \hat{I} the identity operator. Note that equation (4.12) has a direct and fundamental interpretation, where the reflected optical field is directly viewed as the sum of two contributions. The first one, proportional to b_{in} , is the optical field reflected by the empty cavity alone, as would be obtained in the absence of QD. The second term, proportional to $\hat{\sigma}_-$, is the optical field induced by a photon emitted in the cavity mode by the QD, and then quickly extracted out from the cavity through the top mirror. Also note that the operators \hat{I} and $\hat{\sigma}_-$ in equation (4.12) are directly related to the effect that the detection of a reflected photon can have on the QD subspace. If the detected photon comes from the empty-cavity reflection, it does not change the QD state (operator \hat{I}) since this photon was not emitted by the QD. If the detected photon comes from the QD emission, however, this means that the QD has just decayed to the ground state (operator $\hat{\sigma}_-$). The superposition of these two fields in equation (4.12) is also a direct illustration that they can interfere, as already discussed in the interpretation of some of the results obtained in Chapter 3.

At last, one can limit the Hamiltonian to the part acting on the QD subspace, using the above equation for \hat{a} , to obtain a simplified, adiabatic one

$$\hat{H}_{ad} = (\omega_{eff} - \omega) \hat{\sigma}_+ \hat{\sigma}_- - i\sqrt{\Gamma_0 \eta_{top}} \left(\frac{b_{in}}{1 - i\Delta} \hat{\sigma}_+ - \frac{b_{in}^*}{1 + i\Delta} \hat{\sigma}_- \right), \quad (4.13)$$

with

$$\omega_{\text{eff}} = \omega_d + \frac{\Gamma_0 \Delta_{\text{QD-C}}}{2(1 + \Delta_{\text{QD-C}}^2)}. \quad (4.14)$$

The difference $\omega_{\text{eff}} - \omega_d$ is a cavity-induced frequency shift [28]. It is proportional to Γ_m and to the detuning $\Delta_{\text{QD-C}}$. The second term is analogous to the Rabi Hamiltonian for an atom in free space, with the proper amplitude and phase factor describing how the input field excites the QD.

Finally, replacing \hat{a} in the optical Bloch equations and obtaining the time derivatives $\langle \dot{\hat{\sigma}}_- \rangle$, $\langle \dot{\hat{\sigma}}_z \rangle$, it is found that they are consistent with the adiabatic Hamiltonian providing that one modifies the collapse operator for the quantum dot spontaneous emission in the leaky modes

$$\hat{C}_{\text{QD}} = \sqrt{\gamma_{\text{sp}}} \hat{\sigma}_- \longrightarrow \hat{C}_{\text{QD}} = \sqrt{\Gamma_{\text{tot}}} \hat{\sigma}_-. \quad (4.15)$$

As before, $\Gamma_{\text{tot}} = \Gamma_m + \gamma_{\text{sp}}$, so it takes into account QD decay both due to Purcell-enhanced emission via the cavity mode and emission in the leaky modes. In practice, this means that regarding the QD subspace all the dynamics is described by the Hamiltonian in equation (4.13) and the collapse operator in equation (4.15), provided that the adiabatic approximation holds.

4.3 Comparing Adiabatic and Full Model

During this internship, all the programs of the cavity-QED quantum toolbox have been developed with two available options: “full model” or “adiabatic model”. It has been verified each time that the higher the cavity damping rate κ , the quicker the cavity adapts to its environment (i.e. the QD and the external field), and the better the two models coincide. However, the inequality $\kappa \gg g, \gamma_{\text{sp}}, \gamma^*$ should *not* be considered as a sufficient condition for the adiabatic elimination to be valid. What is important is the possibility to approximate as in (4.6), when t' is of the order of the photon lifetime in the cavity.

Out of conciseness, it has been chosen to only focus in the following two examples, highlighting when these approximations may or may not be valid.

4.3.1 Mollow triplets

In the CW regime, the constant input field obviously verifies $b_{in}(t - t') = b_{in}(t)$, but the approximation $\hat{\sigma}_-(t - t') \approx \hat{\sigma}_-(t)e^{i(\omega_d - \omega)t'}$ can fail at high input power. This could lead to discrepancies in the predictions for the first-order coherence $g^{(1)}(\tau)$, and thus also for the predicted spectral densities. In section 3.2.1 it has been shown that under resonance fluorescence, for higher input powers the degeneracy splitting of the uncoupled system eigenstates results in the so-called Mollow triplets spectrum. In this specific simulation, adiabatic elimination is very promising because higher input powers require a larger dimension N of the cavity truncated Fock space. Indeed, by adiabatic elimination, an element of the Fock-Liouville space previously defined has always four components instead of $4 \times N^2$.

In CW regime, given equation (2.17) and assuming zero detuning, all Fock states contribute with the same Rabi frequency $\Omega_R \approx 2g\sqrt{\langle \hat{n} \rangle}$, where $\hat{n} = \hat{a}^\dagger \hat{a}$ is the photon number operator

for the optical mode of interest. By definition, this Rabi frequency is the rate at which the QD state oscillates in the Bloch sphere [16], which is also the rate at which the QD lowering operator is evolving. This means that, for the approximation $\hat{\sigma}_-(t-t') \approx \hat{\sigma}_-(t)e^{i(\omega_d-\omega)t'}$ to be valid when t' is of the order of the cavity photon lifetime, it is required that $\Omega_R \ll \kappa$ for the effective Hamiltonian to be accurate enough. In the semi-classical approximation, which is a very good assumption for higher optical input powers, the average photon number from equation (4.10) is given by

$$n \equiv \langle \hat{n} \rangle = \frac{4\eta_{\text{top}}}{\kappa} b_{\text{in}}^2. \quad (4.16)$$

Since the aim is to obtain an order of magnitude estimate for the adiabatic approximation to be valid, from here on the semi-classical approximation will be taken for granted. Substituting equation (4.16) into the previous inequality regarding the Rabi frequency, and considering that by definition $b_{\text{in}} = \sqrt{\eta_{\text{top}} P_{\text{in}} / (\hbar \omega_c)}$, it is found that:

$$P_{\text{in}} \ll \frac{\hbar \omega_c \kappa^2}{8\eta_{\text{top}}^2 g}. \quad (4.17)$$

Given the usual parameters of this chapter, the input power should be much lower than few

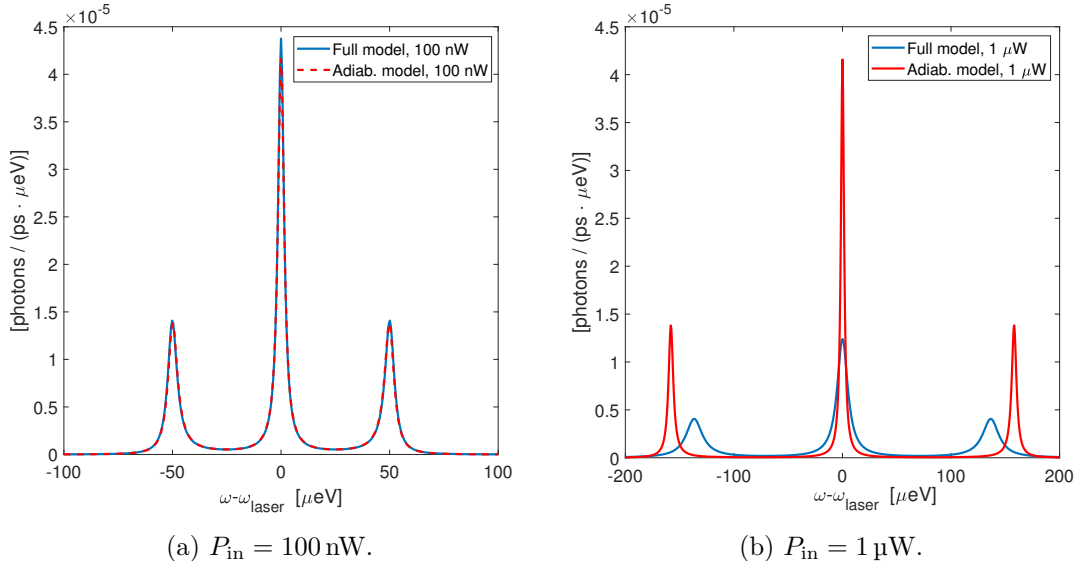


Figure 4.2: Comparing Mollow triplets spectra of the spontaneously emitted field, obtained with adiabatic and full model, for different input powers.

micro-watts. In figure 4.2a the spontaneous emitted spectrum under resonance fluorescence is shown for 100 nW input power, in figure 4.2b at 1 μW . In the former case the adiabatic model curve is superimposed onto the one obtained by the full model. In the second case, in accordance to the newly found rule of thumb, the effective Hamiltonian fails, as the side-peaks distance becomes comparable with the cavity damping rate.

A related phenomenon that the adiabatic model is not able to reproduce is when the QD frequency is detuned from the cavity, the expected asymmetry of the Mollow triplet arises,

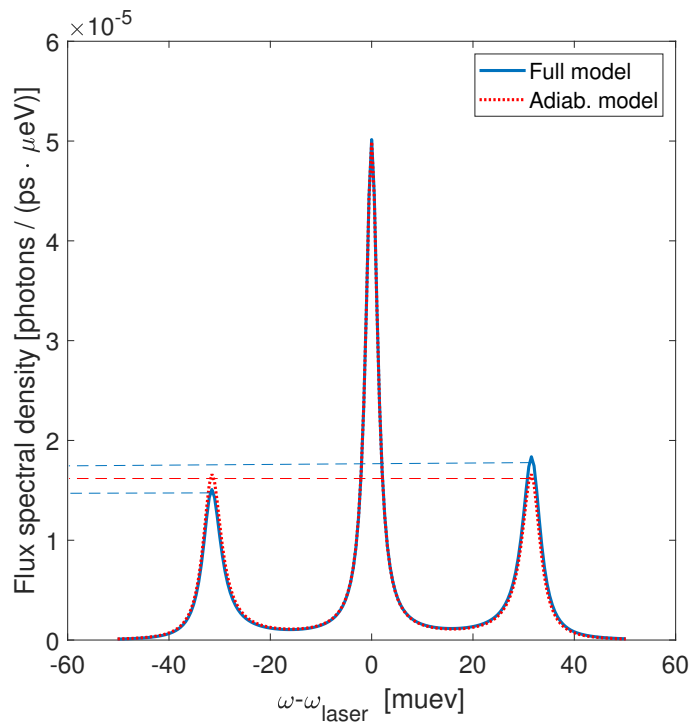


Figure 4.3: Mollow triplets of the emitted field spectrum, for $P_{\text{in}} = 50 \text{ nW}$, detuning between the cavity and the QD, $\omega_d - \omega_c = 100 \mu\text{eV}$ and laser at resonance with the QD. The expected asymmetry in the full model is not recovered in the adiabatic model.

figure 4.3. This is because one side peak emits more in the mode than the other side peak. Indeed, in this case, one side peak has a significantly different normalized detuning with the cavity, compared to the other side-peak that is significantly closer or further away from the cavity mode resonance. This leads to an asymmetry in the values of Γ_m (Purcell-enhanced emission rate in the cavity mode), and thus an asymmetry in the β factor¹ for the two side peaks. The adiabatic model is intrinsically unable to predict such asymmetry since it considers only one value of Γ_m , and thus one value of β , evaluated at the laser frequency and not at the frequency of the side peaks. Still, at lower power, the adiabatic model retrieves its validity since all the peaks, the central one and its two side-peaks, span a small frequency range compared to the cavity damping rate. In this limit, the side-peaks approximately have the same value of the normalized detuning, hence equal Γ_m and β .

4.3.2 Reflectivity in pulsed wave regime

In the following, the optical responses to two incoming Gaussian pulses are compared. The pulses impinge towards the optical micropillar at different delays and with different $FWHM$, keeping constant the average photon number in each pulse. In pulsed wave regime also the approximation $\hat{b}_{in}(t - t') \approx \hat{b}_{in}(t)$ should be considered for the adiabatic model domain of validity.

For the time derivative in the pulsed regime, the important inequality is formally $db_{in}/dt \ll \kappa/2 \times b_{in}$. Indeed, the question is whether $b_{in}(t - t')$ is close to $b_{in}(t)$ in a time-scale t' such that $\kappa/2 \times t' \approx 1$. And on such a time scale one can say that

$$b_{in}(t - t') \approx b_{in}(t) - \frac{db_{in}}{dt} \frac{2}{\kappa}, \quad (4.18)$$

that reduces to $b_{in}(t)$ given the inequality mentioned above. In this case, for a Gaussian pulse, the maximal value of $b_{in}(t)$ time derivative is of the order of the amplitude of b_{in} , divided by the pulse $FWHM$. The condition becomes

$$\frac{\kappa}{2} \times FWHM \gg 1, \quad (4.19)$$

for a Gaussian pulse, where the photon number does not appear because both the signal and its derivative are proportional to it. In the simulation of figure 4.4 the coupling constant g has been set to zero to not have any QD lowering operator contribution. In the case of the short FWHM of 5 ps the effective Hamiltonian is not able to reproduce the reflected flux of the full model because of the too-short time scale for the system to adapt to the Gaussian pulse. Indeed, in the effective Hamiltonian approximation only one peak is obtained instead of two, and almost half the maximum peak value. By substituting the parameters in equation (4.19), it is found that $FWHM \gg 1.3$ ps for the adiabatic model to be valid. The short pulse does not satisfy the inequality, having a $FWHM$ only about four times longer. While the long pulse is better recovered, there is still some visible delay induced by the fact that in the adiabatic model the cavity instantaneously reflects the incoming field, while in

¹Fraction of photons emitted in the cavity mode, compared to the fraction emitted outside the mode, introduced in Chapter 2.

the full model it does store it for a short time before letting it be reflected. It is important to outline that the inequality (4.19) has been obtained for a Gaussian pulse. For instance, the cavity would not be able to respond to a square pulse adiabatically.

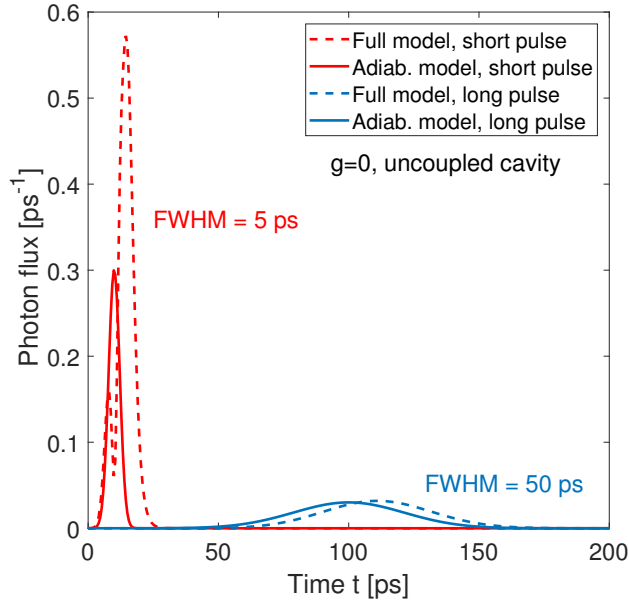


Figure 4.4: Adiabatic and full model comparison of the reflected photon flux in pulsed wave regime, average photon number $N_p = 10$, for different FWHM of the two pulses.

Conclusions

In this chapter, an effective Hamiltonian has been introduced, based on the adiabatic elimination of the cavity mode Hilbert space. This approximation simplifies the computational cost of most of the quantum optics phenomena addressed in the previous chapter, in the weak coupling regime. The quantum fluctuations of the annihilation operator, in the semiclassical approximation for the input field, are related only to the lowering operator. It has been shown that in CW excitation for resonance fluorescence, one condition for the adiabatic elimination validity is that the driving Rabi frequency should be much lower than the cavity damping rate. Moreover, it has been shown that the effective Hamiltonian is not able to reproduce the Mollow triplets asymmetry. The second condition, in PW regime, is that the cavity should be able to follow the input signal time variations.

Chapter 5

Conclusions

In this work, a new custom Cavity QED Quantum Toolbox for a two-level system has been developed to simulate common quantum optics problems, such as non-linear optical properties, first- and second-order correlations, and flux spectral densities for reflected, transmitted, diffracted and emitted fields. While it has been previously established that the Master equation integration based on a pre-existing quantum optics toolbox [23] provides accurate results, given a proper fitting of the experimental parameters, phenomena that require high photon number can be computationally expensive. In this direction, an effective adiabatic Hamiltonian has been implemented to adiabatically eliminate the cavity mode Fock space, and to deal only with the quantum-dot subspace.

The custom cavity QED quantum toolbox took inspiration from pre-existing codes, written by Loïc Lanco, that have been fully revisited. The overall aim has been to find an equilibrium between easiness for future readers and efficiency. An exception is the case of spectral analysis, where the balance has been tipped strongly in favor of efficiency. Indeed, while the fast Fourier transform is much more efficient than the standard definition of the discrete Fourier transform, $\mathcal{O}(N \log N)$ versus $\mathcal{O}(N^2)$, it has required more attention to obtain the proper normalization and phase, in the CW regime as well as in the custom-made Wigner Distribution Function for time-frequency signal analysis.

The adiabatic approximation has shown to be promising in the weak coupling regime, which is the working condition for the deterministic and scalable CQED built at C2N, employed as single-photon source [11] and as an interface between the spin of a single charge and the polarization of a single photon [29]. In the continuous-wave regime, its domain of validity has resulted to be strictly related to the cavity damping rate, responsible for the cavity time scale dynamics. An important parameter has been proven to be the laser input power, that sets the Rabi frequency of the QD sub-system dynamics, which should be much slower than the cavity one for the adiabatic approximation to hold. More studies are required in pulsed-wave excitation for the input pulse shape, because of the limited cavity response time that would prevent the cavity from adapting in time to sudden signal changes.

Among prospects, the most natural one is the generalization to less simple QD systems introducing a charge, spin, and photons polarization, already begun by Clément Millet, Elham Mehdi, and Nathan Coste in the C2N team. Starting from the programs developed

in this work, other physical phenomena such as Mollow triplets in pulsed-wave regime [30] and the quantum Zeno effect [31] could be addressed. Even though the adiabatic elimination has been introduced for an optical micropillar, it would be possible to generalize it in the larger context of dipoles in 1-D photonic crystal waveguides and nanocavities [32]. For future developments, it would be important to translate the scripts from MATLAB® into the open-source **Quantum Toolbox in Python** (QuTiP) package [33], which is used by a larger community and contains several already-implemented routines. Still, however attractive also the idea of having already developed routines in QuTiP, the lower-level programming of this thesis provides useful insights by detailing how each physical quantity is computed, explicitly linking theoretical and experimental results.

Appendix A

Correlations in Time Domain

A.1 First-order Coherence and Quantum Regression Theorem

In section 3.2 the field operator first-order correlation function (3.3) has been introduced to evaluate the frequency dependence of the scattered radiation. The *quantum regression theorem* simplifies the problem of evaluating a two-time correlation function by Lindbladian evolution of a fictitious density matrix. Dropping the hat symbol, here $A(t)$ and $B(t)$ are two system operators (i.e. they do not act on the reservoir coupled to the system) and the system density matrix satisfies the Lindbladian master equation $\partial_t \rho(t) = \mathcal{L}\rho(t)$. In the Heisenberg representation, the quantum regression theorem states that in the long time limit [25]

$$\lim_{t \rightarrow \infty} \langle A(t)B(t + \tau) \rangle = \text{tr}(B \Lambda(\tau)), \quad (\text{A.1})$$

where $\Lambda(t + \tau, t)$ acts as a sort of “fictitious” density matrix with respect to the B operator. As the system density matrix evolves in time, the newly introduced operator evolves along the delay τ according to

$$\frac{d\Lambda}{dt} = \mathcal{L}\Lambda(\tau), \quad (\text{A.2})$$

with initial condition

$$\Lambda(0) = \rho(t \rightarrow \infty) A. \quad (\text{A.3})$$

Here $\rho(t \rightarrow \infty)$ is the density matrix which is obtained in stationary regime, where it is possible to simplify the two-time correlation function as a single-time average. The quantum regression theorem can be applied for the pulsed wave case, but a two-time evolution is then required.

Two-time evolution for pulsed-wave excitation To calculate the first correlation function from equation (3.5), in Heisenberg representation, a general two-time representation is $\langle A(t_1)B(t_2) \rangle$, where for instance $A(t) = U^\dagger(t,0)AU(t,0)$. Here $U(t,0)$ is the unitary time-evolution operator from 0 to t . By exploiting the *composition* and *inversion properties* of

the evolution operator

$$U(t, t')U(t', t'') = U(t, t'') \quad (\text{A.4})$$

$$U^\dagger(t, t') = U(t', t), \quad (\text{A.5})$$

it is found, by calling ρ the density matrix of the system

$$\langle A(t_1)B(t_2) \rangle = \text{tr}(A(t_1)B(t_2)\rho) \quad (\text{A.6})$$

$$= \text{tr}\left(BU(t_2, t_1)\rho(t_1)AU^\dagger(t_2, t_1)\right) \quad (\text{A.7})$$

where $\rho(t_1) = U(t_1, 0)\rho U(t_1, 0)^\dagger$. Therefore, first the density matrix evolves from time 0 to t_1 . Then the density matrix is multiplied on the right by the operator A , obtaining a “fictitious” density matrix that is let evolve from t_1 to t_2 . At last, the latter is used to calculate the expectation value of the operator B .

A.2 Custom Wigner Distribution Function Script

As mentioned in section 3.2, to compute the Wigner Distribution Function of a (e.g. reflected) field it is necessary to map $G^{(1)}(t_1, t_2)$ into $G^{(1)}(t, \tau)$ according to

$$\begin{cases} t &= (t_1 + t_2)/2 \\ \tau &= t_2 - t_1. \end{cases}$$

In the MATLAB® script, $G^{(1)}(t_1, t_2)$ is saved as a matrix $G^{(1)}(t1_index, t2_index)$ with $t1_index, t2_index = 1, \dots, N$, whereas $G^{(1)}(t, \tau)$ in terms of $G^{(1)}(time_index, tau_index)$, being $time_index, tau_index = 1, \dots, 2N - 1$. The coordinate systems are shown in figure A.1. It follows that

$$tau_index = t2_index - t1_index + N, \quad (\text{A.8})$$

$$time_index = t1_index + t2_index - 1, \quad (\text{A.9})$$

where $N \times N$ is the dimension of the square matrix. It is then found that

$$t1_index = (time_index - tau_index + 1 + N)/2 \quad (\text{A.10})$$

$$t2_index = (time_index + tau_index + 1 - N)/2. \quad (\text{A.11})$$

From the previous system it is clear that $G^{(1)}$ must be interpolated at half-integer values of the indices, by averaging with the values of $G^{(1)}(t1_index, t2_index)$ obtained at the closest integer indices.

Fast Fourier transform implementation The fast Fourier transform (FFT) algorithm computes the discrete Fourier transform of a finite sequence $\{x_n\}$, converting in this thesis the signal from time domain to frequency domain. It reduces the computational cost from

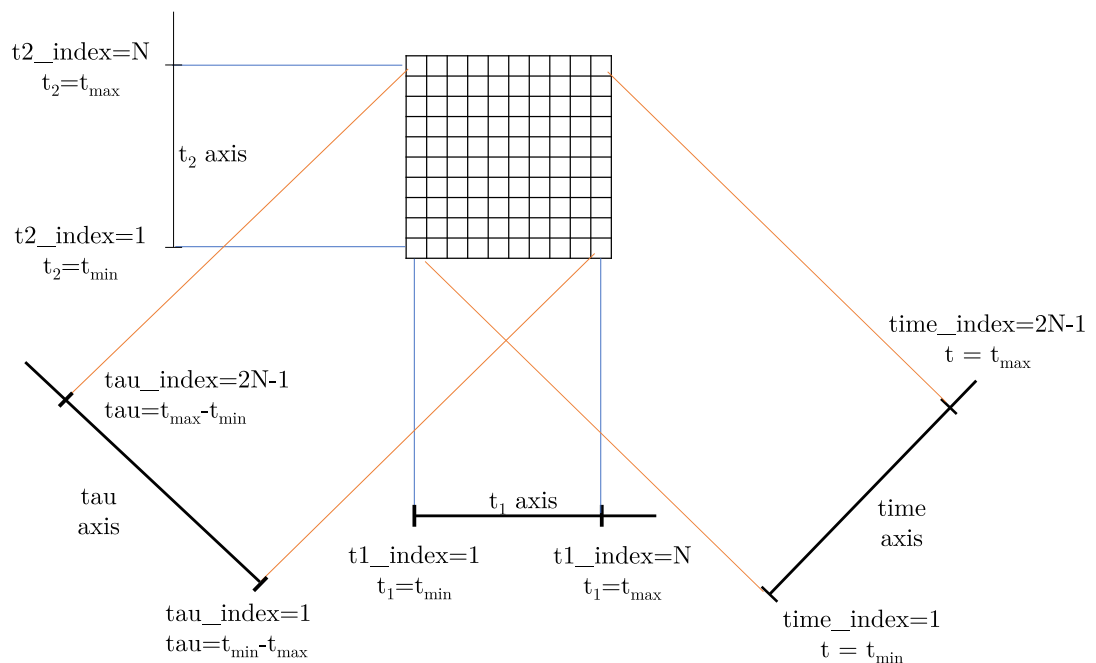


Figure A.1: Discrete first order correlation function $G^{(1)}(t1_index, t2_index)$ in the blue coordinate system. In orange as $G^{(1)}(time_index, tau_index)$.

$\mathcal{O}(N^2)$ to $\mathcal{O}(N \log N)$, where N is the number of elements of the signal, according to the DFT definition

$$X_k \equiv \mathcal{F}(\{x_n\})_k = \sum_{n=0}^{N-1} x_n e^{-i2\pi kn/N} \quad k = 0, \dots, N-1 \quad (\text{A.12})$$

with x_0, \dots, x_{N-1} complex numbers. In the following, the phase shifting and normalization criteria will be illustrated.

Phase shift A first-order correlation function is always anti symmetric in the sense that

$$G^{(1)}(-\tau) = G^{(1)}(\tau)^*. \quad (\text{A.13})$$

This anti symmetry ensures that the spectral density of the optical field, being the Fourier Transform of the first-order correlation function, is a real quantity. Moreover, the integral of the spectral density recovers the photon flux (3.10), i.e. a real physical quantity. In the pulsed-wave regime a similar anti-symmetry relation holds:

$$G^{(1)}(t_1, t_2) = G^{(1)}(t_2, t_1)^*, \quad (\text{A.14})$$

which ensures that the Wigner-Ville function, also denoted Wigner Distribution Function and abbreviated by WDF in this manuscript, is a real quantity - though it can assume negative values.

However, directly applying the FFT algorithm to the correlation functions does not lead to real values, as it is now explained. In the simulations each signal is discrete and stored with positive indices. For instance given a signal x_n defined over $n = -N, -N+1, \dots, N-1, N$, it is treated by the FFT algorithm as it were defined over $n = 1, 2, \dots, 2N+1$. This determines a phase shifted output, which is in general not a problem since one is commonly interested in the absolute values of the Fourier transform (as in a circuit transfer function). Still, it must be corrected if one wants to check the normalization or have the correct WDF. The right phase is recovered by exploiting the *shift theorem* of the DFT, that is

$$\mathcal{F}(\{x_{n-m}\})_k = X_k \cdot e^{-\frac{2\pi i}{N} km}, \quad (\text{A.15})$$

where in this case m is the number of elements associated to negative delays in the first-order correlation function, or the Wigner Distribution Function at each time bin *time_index*. Thus, a circular shift of the input x_n corresponds to multiplying the output X_k by a linear phase.

Normalization Apart from the phase shift, also proper normalization of the FFT result has to be ensured. Parseval's theorem for the DFT states that

$$\sum_{n=0}^{N-1} |x_n|^2 = \frac{1}{N} \sum_{k=0}^{N-1} |X_k|^2. \quad (\text{A.16})$$

The discrepancy occurs when, due to the FFT algorithm optimization, the original signal x_n is padded with zeros so that its length is a power of two. Because of the N dependency in the last equation, Parseval's theorem does not hold anymore for the original signal. To recover it, it can be shown that the output of the FFT must be divided by the sampling frequency. More information can be found in the commented code.

Appendix B

Supplementary Figures

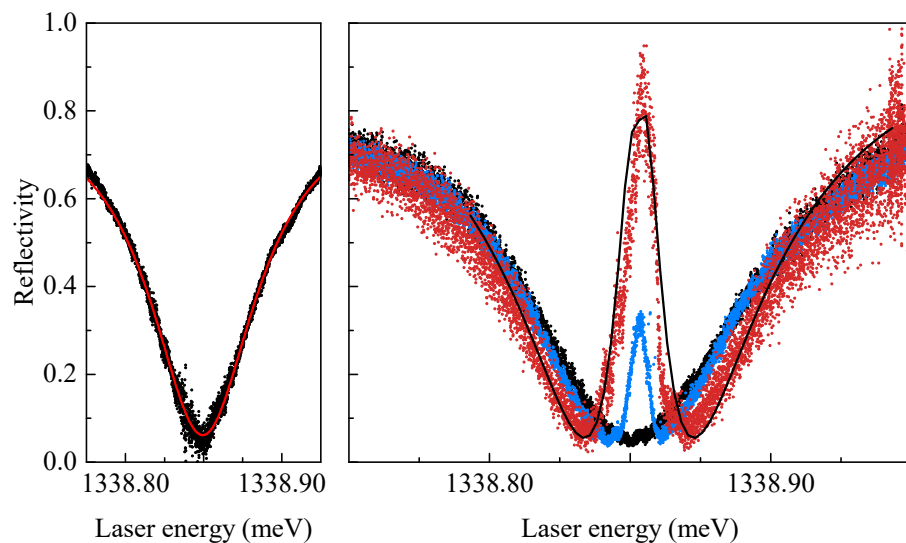


Figure B.1: Experimental (symbols) and simulated (lines) reflectivity as a function of the incident laser energy of (left) an empty cavity, (right) a QD with increasing input power. The black line refers to the lowest power. Image from [19].

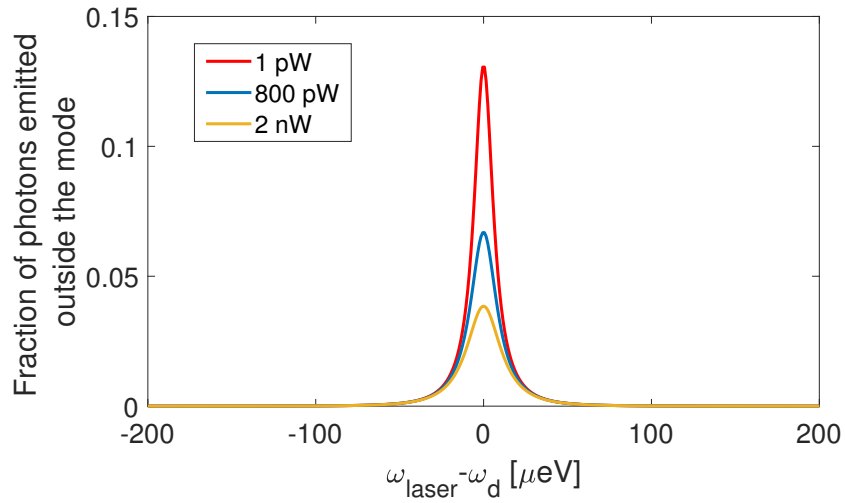


Figure B.2: Fraction of photons emitted outside the mode. Simulation parameters in section 3.1.

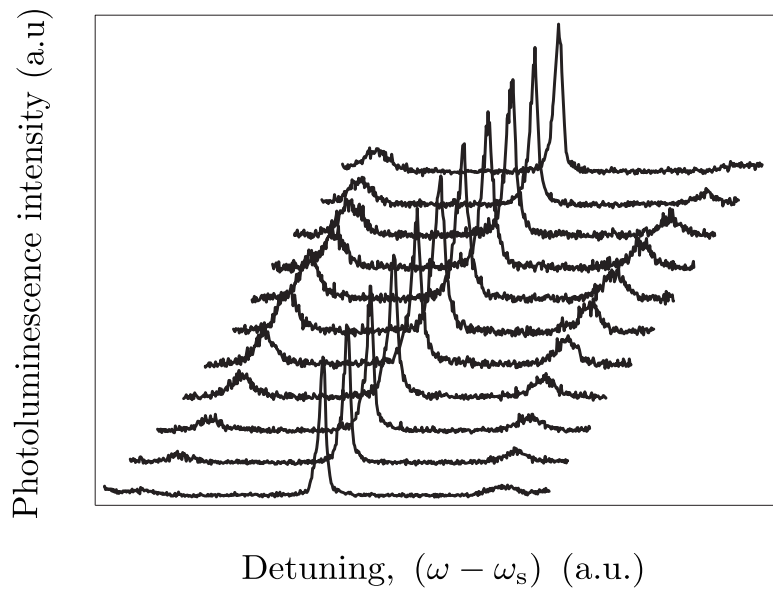
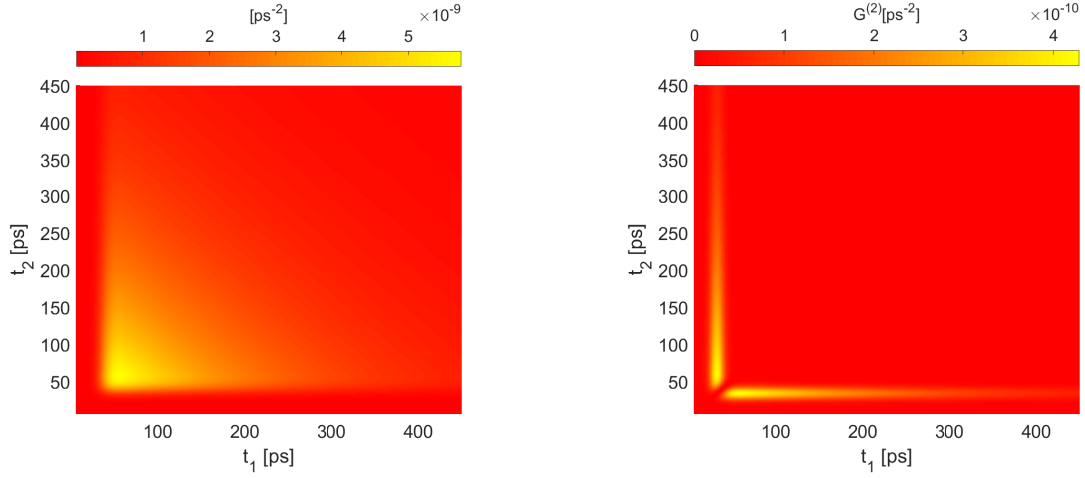


Figure B.3: Laser detuning dependent resonance fluorescence spectra at increasing power, showing Mollow triplets as the power increases. Image from [34].



(a) Uncorrelated coincidences rate of the emitted field. It is the denominator of equation (3.15), but expressed in terms of (t_1, t_2) instead of $t \equiv t_1$ and delay $\tau \equiv t_2 - t_1$.

(b) Correlated coincidences $G^{(2)}$ of the emitted field. It is the numerator of equation (3.15), but expressed in terms of (t_1, t_2) instead of $t \equiv t_1$ and delay $\tau \equiv t_2 - t_1$.

Figure B.4: Correlated and uncorrelated coincidences of the emitted field in pulsed wave excitation, simulation parameters in section 3.3.

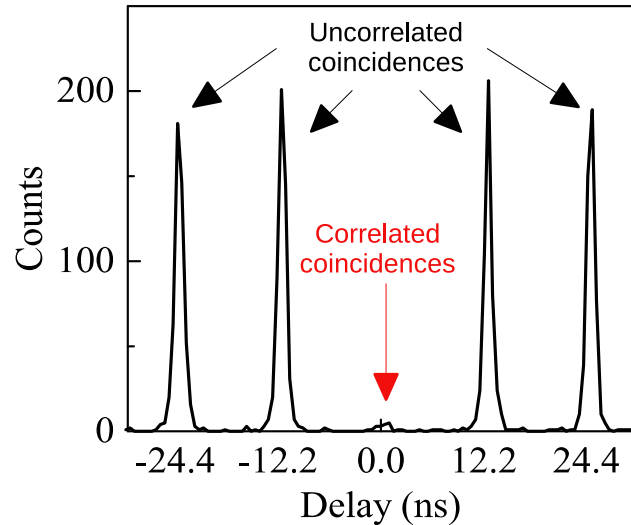


Figure B.5: Experimental second order correlation of the emission from a QD in a micropillar. Image from [19].

Appendix C

MATLAB[®] Scripts

C.1 Main scripts

C.1.1 Reflectivity spectrum in CW

```
1 clear
2 clc
3 %close all
4 %%%%%% Common basis to every programs based "two levels" %%%%%%
5 % Important note: these paths must be modified if needed
6 addpath(genpath('..\QotoolboxV015'));
7 addpath(genpath('..\CQED subprograms'));
8 addpath(genpath('..\CQED device parameters'))
9
10 % In addition, for the mesolve function to operate the executable files
11 % (.exe) and batch files (.bat) contained in '[...] \QotoolboxV015\bin'
12 % have to be copied to a folder that is on the Windows system path, in the
13 % main hard drive where Windows is installed. This can be for example in:
14 % 'C:\Program Files\Matlab\R2014a\bin'.
15
16 % Warning: for the adiabatic version to converge, the tolerance in
17 % mesolve.m function must be reduced compared to the default values. For
18 % example:
19 % ode2file('ode_input.dat',L,rho0,t_list,struct('reltol',7e-8,'abstol',8e
20 % -8));
21 %% %%%%%%%% CW – spectra under stationary resonant excitation %%%%%%
22 % This script indexed "CW" considers a fixed incoming power and a variable
23 % angular frequency for the laser. One calculates the spectral response
24 % associated to the various fields (reflected, transmitted,
25 % diffracted/lost, and spontaneously emitted outside the cavity mode). One
26 % finally verifies the conservation of the total photon flux
27
```

```

28 % Choice of full model 'F' or adiabatic 'A'
29 model = 'F';
30
31 %%% Experimental conditions
32 detuning_QD_C_muev = 0; %Detuning between the QD and cavity frequencies, in
    mueV
33 eta_in = 1; % Injection efficiency for the incoming photons (depends on
    experimentally-achieved spatial coupling)
34 P_in_CW_pW=10;% Incoming continuous-wave power in pW
35
36 %Parameters for the calculation of spectra
37 min_detuning_muev=-100; %minimal detuning (left part of the spectrum), in
    muev
38 max_detuning_muev=100; %maximal detuning (right part of the spectrum), in
    muev
39 nb_points_spectrum=400;
40
41 Init2levelDeviceParametersOngoingTest;
42 Init2levelHilbertSpaceAndOperators;
43 InitLists2levelCWscanLaserFrequency;
44
45 %Incoming power
46 P_in_CW = P_in_CW_pW*1e-12;% Incoming power in W %%
47 b_in_CW = sqrt(eta_in*P_in_CW*1e-24/(hbar*omega_c)); % square root of the
    photon number per unit time, in ps-1/2
48 total_flux_injected_photons=abs(b_in_CW)^2; % total flux of incoming
    photons taking into account eta_in (so only the photons coupled to the
    cavity mode), in ps-1
49
50 % tic % NB: "tic" is used as a "start" time for the measurement of the
51 % computing time between "tic" and "toc"
52
53 %%%%%%%%%%%%%% Start the calculation of spectra %%%%%%%%%%%%%%
54 for omega_index=1:nb_points_spectrum %Loop for frequency scan
55
56     omega_laser=omega_laser_list(omega_index); %Current value of
        omega_laser, in rad/ps
57
58     switch model
59         case 'A' % Adiabatic case
60
61             Delta = 2*(omega_laser-omega_c)/kappa; %normalized laser
                detuning appearing in Eq.12 of the pdf notes
62
63             %%%%%%%%%% Definition of the adiabatic-model Hamiltonian (which
                depends on omega_laser)

```

```

64      H_CW = (omega_eff-omega_laser)*sigma_dag*sigma...
65      - li*sqrt(Gamma_0*eta_top)*(b_in_CW*sigma_dag/(1-li*Delta)-
66      b_in_CW'*sigma/(1+li*Delta)); % Adiabatic Hamiltonian
67
68      %% For the redefinition of the operator "a" acting in the QD
69      %% space
70      % (Eq. 10 of the pdf notes
71      a = -2*g*sigma/(kappa*(1-li*Delta_QDC))-2*sqrt(kappa_top)*
72      b_in_CW*Id/(kappa*(1-li*Delta)); %annihilation operator a
73      % in adiabatic approximation
74
75      % UNUSED HERE: Ansatz for the annihilation operator, obtained
76      % by taking the time derivative of "a" equal to 0
77      % (OK for CW but not for PR (pulsed regime) programs)
78      % a = -2*g*sigma/(kappa*(1-li*Delta))-2*sqrt(kappa_top)*b_in_CW
79      % *Id/(kappa*(1-li*Delta));
80
81      case 'F' % Full model
82
83      %%%%%% Definition of the full-model Hamiltonian (which
84      % depends on omega_laser)
85      H_CW = (omega_d-omega_laser)*sigma_dag*sigma...
86      + (omega_c-omega_laser)*a_dag*a...
87      + li*g*(sigma_dag*a-a_dag*sigma)...
88      - li*sqrt(kappa_top)*b_in_CW*(a_dag-a);
89
90      end % end of the "switch model"
91
92      %Superoperator associated to the coherent processes (Hamiltonian)
93      L_coh = -li * (spre(H_CW) - spost(H_CW));
94
95      %%%%%% Calculation of the Liouvillian superoperator
96      Liouvillian = L_coh + L_incoh; % Total Liouvillian superoperator
97      % including both coherent processes (Hamiltonian) and incoherent
98      % processes (dissipative jumps)
99
100     %%%%%% Calculation of the density matrix corresponding to the
101     % stationary state
102     rhoss_CW = steady(Liouvillian);
103
104     %%%%%% Definition (or re-definition) of the output operators
105     if (model=='A' || omega_index==1) %
106         % In the full model, the output flux operators are not
107         % frequency-dependent and thus need to be defined only the first
108         % time In the adiabatic model the value of "a" is
109         % frequency-dependent and the output operators have to be

```

```

100      % redefined for each frequency
101
102      b_out = b_in_CW*Id + sqrt(kappa_top)*a; % definition of the
103          operator b_out, i.e. the output operator for the reflected
104          light, in ps^(-1/2)
105      c_out = sqrt(kappa_bottom)*a; % definition of the operator c_out, i
106          .e. the output operator for the transmitted light, in ps^(-1/2)
107      d_out = sqrt(kappa_loss)*a; % definition of the operator d_out, i.e
108          . the output operator for the diffracted/lost light, in ps
109          ^(-1/2)
110      % e_out = sqrt(gamma_sp)*sigma; % definition of the operator e_out,
111          i.e. the output operator for the light spontaneously emitted
112          outside the cavity mode, in ps^(-1/2)
113
114      % NB: in the adiabatic model the operators could also have been
115          written directly as:
116
117      % b_out = b_in_CW*Id*(1-2*eta_top/(1-li*Delta))-sqrt(Gamma_0*
118          eta_top)*sigma/(1-li*Delta_QDC); %output flux operator, (eq
119          .12)
120
121      % c_out = -2*g*sqrt(kappa_bottom)*sigma/(kappa*(1-li*Delta_QDC))-2*
122          sqrt(kappa_top*kappa_bottom)*b_in_CW*Id/(kappa*(1-li*Delta));
123
124      % d_out = -2*g*sqrt(kappa_loss)*sigma/(kappa*(1-li*Delta_QDC))-2*
125          sqrt(kappa_top*kappa_loss)*b_in_CW*Id/(kappa*(1-li*Delta));
126
127      % Such formulas are obtained by directly replacing the value of "a"
128      % from the adiabatic model, and are thus equivalent to the above,
129      % more general definitions In addition, e_out is independent on the
130      % experimental conditions and thus defined in the subprogram
131      % "Init_2level_Hilbert_space_and_operators.m". It is given here for
132      % information and clarity purposes only
133
134      end
135
136      %%%%%% Calculation of useful expectation values %%%%%%
137
138      % Calculation of the total photon flux as a function of omega_laser
139      total_flux_reflected_photons_vs_omega(omega_index) = expect(b_out'*
140          b_out,rhoss_CW); % Total reflected flux = <b_out_dag b_out>, in ps
141          ^(-1)
142      total_flux_transmitted_photons_vs_omega(omega_index) = expect(c_out'*
143          c_out,rhoss_CW); % Total transmitted flux = <c_out_dag c_out>, in
144          ps^(-1)
145      total_flux_diffracted_photons_vs_omega(omega_index) = expect(d_out'*
146          d_out,rhoss_CW);% Total diffracted/lost flux = <d_out_dag d_out>,
147          in ps^(-1)

```

```

126 total_flux_emitted_photons_vs_omega(omega_index) = expect(e_out'*e_out,
    rhoss_CW);% Total flux of spontaneously-emitted photons outside the
    mode = <e_out_dag e_out>, in ps^(-1)
127
128 occupation_excited_state_vs_omega(omega_index) = expect(sigma_dag*sigma
    ,rhoss_CW); % Occupation probability for the excited state |e>
129 occupation_ground_state_vs_omega(omega_index) = expect(sigma*sigma_dag,
    rhoss_CW); % Occupation probability for the ground state |g>
130 end % end of the frequency scan
131
132 % toc
133 % NB: "toc" is used as a "stop" time for the measurement of the computing
    time between "tic" and "toc"
134
135 % Normalization: coefficients of reflectivity, transmission, diffracted/
    lost part, and spontaneously-emitted part
136 R_vs_omega = total_flux_reflected_photons_vs_omega /
    total_flux_injected_photons;
137 T_vs_omega = total_flux_transmitted_photons_vs_omega /
    total_flux_injected_photons;
138 D_vs_omega = total_flux_diffracted_photons_vs_omega /
    total_flux_injected_photons;
139 E_vs_omega = total_flux_emitted_photons_vs_omega /
    total_flux_injected_photons;
140
141 %% %%%%%%%% Plots %%%%%%%
142 % For plot selection:
143 % – Reflected photons : 'R'
144 % – Transmitted + diffracted/lost photons : 'T'
145 % – Photons emitted outside the mode : 'E'
146 % – Occupation probabilities : 'O'
147
148 % plot_choice = ['T'];
149 plot_choice = ['T';'R';'E';'O'];
150 Plot2levelCWvsLaserFrequency;

```

C.1.2 Photon flux evolution and QD occupation in PW

```

1 clear
2 clc
3 %close all
4 %% Important note: these paths must be modified if needed
5 addpath(genpath('..\QotoolboxV015'));
6 addpath(genpath('..\CQED subprograms'));
7 addpath(genpath('..\CQED device parameters'))
8 savepath

```

```
9
10 % In addition, for the mesolve function to operate the executable files
11 % (.exe) and batch files (.bat) contained in '[...] \QotoolboxV015\bin'
12 % have to be copied to a folder that is on the Windows system path, in the
13 % main hard drive where Windows is installed. This can be for example in:
14 % 'C:\Program Files\Matlab\R2014a\bin'.
15
16 % Warning: for the adiabatic version to converge, the tolerance in
17 % mesolve.m function must be reduced compared to the default values. For
18 % example:
19 % ode2file('ode_input.dat',L,rho0,t_list,struct('reltol',7e-8,'abstol',8e
20 % -8));
21 %% %%%%%%%%%%%%%% Pulsed regime %%%%%%%%%%%%%%
22 %%%%%% %%%%%% %%%%%% %%%%%% %%%%%% %%%%%%
23 % This section indexed "PR" computes the time evolution of the photon flux
24 % for various fields, and of the exciton occupation, in response to a
25 % coherent laser pulse with a fixed center frequency, temporal width, and
26 % average number of photons. One finally verifies that the total photon
27 % flux has been conserved after the simulation.
28 %%%%%% %%%%%% %%%%%% %%%%%% %%%%%% %%%%%%
29
30 %% Choice of full model 'F' or adiabatic model 'A'
31 model = 'F';
32
33 %% Experimental conditions
34 detuning_QD_C_muev = 10; %Detuning between the QD and cavity frequencies,
35 % in mueV
35 detuning_pulse_QD_muev = 0; %Detuning between the pulse central frequency
36 % and the QD frequency, in mueV
36 eta_in = 1; % Injection efficiency for the incoming photons (depends on
37 % experimentally-achieved spatial coupling)
37 Nb_photons = 10; % Average number of incoming photons in a pulse. This
38 % quantity should be multiplied by eta_in to know the number of incoming
39 % photons actually coupled to the optical mode
38 FWHM = 15; %in ps, full width at half-maximum of the incoming Gaussian
40 % pulse intensity (unit: ps since angular frequencies are in rad/ps)
40
41 %% %Initialization of parameters, operators, arrays, etc...
42 Init2levelDeviceParametersOngoingTest;
43 Init2levelHilbertSpaceAndOperators;
44 InitLists2levelPRvsTime;
45
46 % Definition of the input field in ps^(-1/2), in the form of a fseries (
47 % necessary for integrating the master equation)
```

```
47 Standard_deviation_b_in_PR = FWHM/(2*sqrt(log(2))); %Deduced from the
   properties of a Gaussian function
48 b_in_fn = fn('gauss',t_delay,Standard_deviation_b_in_PR) * sqrt( eta_in*
   Nb_photons / ( sqrt(pi) * Standard_deviation_b_in_PR ) ); % square root
   of the incoming photon number per time unit, in ps-1/2
49 b_in_vs_time = fsval(b_in_fn,t_list); %scalar array representing b_in vs
   time
50
51 % Initial density matrix before the pulse has started
52 switch model
53   case 'F' %Full model
54     psi0 = tensor(Vacuum_state,g_ket); % Initial state: tensorial
       product of photonic vacuum and QD ground state
55     rho0 = psi0*psi0'; % Density matrix corresponding to the initial
       pure state
56   case 'A' % Adiabatic model
57     rho0 = g_ket*g_ket'; % Density matrix corresponding to the initial
       pure state
58 end
59
60 %%% UNUSED HERE: to describe a non-resonant excitation experiment where the
61 % exciton state |e> is populated at time zero, one can simply change psi0
62 % and use a very small value for N_in, like 0.0001, to ensure that the
63 % output fields are almost entirely induced by the initial excitation. In
64 % such a case we use (e.g. for the full model):
65 % psi0=tensor(Vacuum_state,e_ket); % Initial state: tensorial product of
       photonic vacuum and QD excited state
66 % rho0=psi0*psi0'; % Density matrix corresponding to the initial pure state
67
68 %%%%%%%% System Hamiltonian and time-dependent operators %%%%%%%%
69 %
70 % The system Hamiltonian is time-dependent due to the function b_in_fn
71 % describing the input field b_in(t).
72
73 % In addition, in the case of adiabatic elimination of the cavity mode an
74 % effective operator $a$ is defined, acting on the QD subspace, based on
75 % the formula for adiabatic elimination (Eq. 10 of the pdf notes). Since
76 % this formula depends on b_in(t), we define a time-dependent quantity
77 % "a_vs_time", which is an array containing, for each time of t_list, the
78 % corresponding operator "a". In the full model case, to simplify the
79 % following calculations, we define the same quantity a_vs_time, yet this
80 % time this array contains the same operator (annihilation operator "a"
81 % acting on the cavity subspace), replicated for all times of t_list.
82
83
84 switch model
```

```

85      case 'A' % Adiabatic model
86
87      Delta = 2*(omega_pulse-omega_c)/kappa; %normalized laser
88      detuning appearing in Eq.12 of the pdf notes
89
90      %%%%%% Definition of the adiabatic-model Hamiltonian (which
91      % depends on omega_pulse)
92      H_PR = (omega_eff-omega_pulse)*sigma_dag*sigma - li*sqrt(
93          Gamma_0*eta_top)*...
94          ((1-li*Delta)^(-1)*b_in_fn*sigma_dag-(1+li*Delta)^(-1)*
95          b_in_fn'*sigma); % Hamiltonian (eq.13)
96
97      %% For the redefinition of the operator "a" acting in the QD
98      %% space vs time (Eq. 10 of the pdf notes)
99      a_vs_time = -2*(kappa*(1-li*Delta_QDC))^(-1)*g*sigma*Id_vs_time
100     -2*sqrt(kappa_top)*(kappa*(1-li*Delta))^(-1)*fsval(b_in_fn,
101     t_list).*Id_vs_time; %annihilation operator a in adiabatic
102     approximation (eq.10), as fseries
103
104
105
106
107
108
109
110
111
112
113
114
115
116
117
118
119

```

```

120
121 %%%%%%%%%%%%%% Definition of the output operators %%%%%%%%%%%%%%
122 % These are general formulas for both the adiabatic and full model,
123 % depending on "a_vs_time"
124 b_out_vs_time = b_in_vs_time*Id_vs_time + sqrt(kappa_top)*a_vs_time; %
125 % definition of the operator b_out, i.e. the output operator for the
126 % reflected light, in ps^(-1/2)
127 c_out_vs_time = sqrt(kappa_bottom)*a_vs_time; % definition of the operator
128 % c_out_vs_time, i.e. the output operator for the transmitted light, in
129 % ps^(-1/2)
130 d_out_vs_time = sqrt(kappa_loss)*a_vs_time; % definition of the operator
131 % d_out_vs_time, i.e. the output operator for the diffracted/lost light,
132 % in ps^(-1/2)
133 % e_out = sqrt(gamma_sp)*sigma % output operator for the light
134 % spontaneously emitted outside the cavity mode, in ps^(-1/2), already
135 % defined in Init_2level_Hilbert_space_and_operators.m
136 a_dag_vs_time = a_vs_time'; % definition of describing a_dag(t)
137
138 % Calculation of the state population
139 expect_sigma_dag_sigma_vs_time = expect(sigma_dag*sigma,rho_vs_time); %
140 % List describing <sigma_dag sigma>(t), i.e. the excited state population
141 expect_sigma_sigma_dag_vs_time = expect(sigma*sigma_dag,rho_vs_time); %
142 % List describing <sigma sigma_dag>(t), i.e. the ground state population
143
144 % Calculation of the total photon flux as a function of time
145 flux_injected_photons_vs_time = b_in_vs_time.^2; % total flux of injected
146 % photons taking into account eta_in (so only the photons coupled to the
147 % cavity mode), in ps(-1)
148 flux_reflected_photons_vs_time = real(expect(b_out_vs_time'*b_out_vs_time,
149 %flux in ps^(-1))
150 rho_vs_time));%flux in ps^(-1)
151 flux_transmitted_photons_vs_time = real(expect(c_out_vs_time'*c_out_vs_time
152 ,rho_vs_time));%flux in ps^(-1)
153 flux_diffracted_photons_vs_time = real(expect(d_out_vs_time'*d_out_vs_time,
154 rho_vs_time)); %flux in ps^(-1)
155 flux_emitted_photons_vs_time = real(expect(e_out'*e_out,rho_vs_time));%flux
156 % in ps^(-1)
157 %% %%%%%%%%%%%%%% Plots %%%%%%%%%%%%%%
158 %%%%%% For plot selection:
159 % – photon fluxes vs time vs delay : 'F'
160 % – occupation probabilities vs time: 'O'
161
162 plot_choice = ['F';'O'];
163 Plot2levelPRvsTime;

```

C.1.3 First-order correlation and spectral densities in CW

```

1 clear
2 clc
3 close all
4
5 %% Important note: these paths must be modified if needed
6 addpath(genpath('..\QotoolboxV015'));
7 addpath(genpath('..\CQED subprograms'));
8 addpath(genpath('..\CQED device parameters'))
9 savepath
10
11 % In addition, for the mesolve function to operate the executable files
12 % (.exe) and batch files (.bat) contained in '[...]\QotoolboxV015\bin'
13 % have to be copied to a folder that is on the Windows system path, in the
14 % main hard drive where Windows is installed. This can be for example in:
15 % 'C:\Program Files\Matlab\R2014a\bin'.
16
17 % Warning: for the adiabatic version to converge, the tolerance in
18 % mesolve.m function must be reduced compared to the default values. For
19 % example:
20 % ode2file('ode_input.dat',L,rho0,t_list,struct('reltol',7e-8,'abstol',8e
21 % -8));
22 %%
23 %%%%%%%% g1SDCW : g1(tau) and spectral densities in CW
24 %
25 %%%%%%
26 % This section called "g1SDCW" evaluates the first order temporal coherence
27 % g(1) as a function of the delay tau, for the various fields. It indicates
28 % the fractions of the coherent and incoherent contributions to the photon
29 % flux for each field. It also computes the Fourier transform of the
30 % incoherent contribution to g(1)(tau) as a function of omega, which gives
31 % the spectral density of flux for the incoherent part of the optical
32 % field. It verifies that the integral of the spectral densities
33 % corresponds to the photon flux (incoherent part only).
34 %
35 %%% Choice of full model 'F' or adiabatic model 'A'
36 model = 'F';

```

```
37 % Warning: in the full model 'F', the size of the Fock state must be large
38 % enough to ensure that the last Fock state is negligibly occupied.
39 % Artifacts can otherwise arise, especially when increasing the incoming
40 % power.
41
42 %%% Experimental conditions
43 detuning_QD_C_muev = 0; %Detuning between the QD and cavity frequencies, in
    mueV
44 detuning_laser_QD_muev = 0; %Detuning between the pulse central frequency
    and the QD frequency, in mueV
45 eta_in = 1; % Injection efficiency for the incoming photons (depends on
    experimentally-achieved spatial coupling)
46 P_in_CW_pW = 10;% Incoming continuous-wave power in pW
47
48 % Parameters for the evaluation of the temporal evolution
49 %
50 % NB1: the maximum delay "tau_max" will also dictate the frequency
51 % resolution of the spectra, given by the angular frequency step
52 % "omega_step". The corresponding angular frequency lists are defined in
53 % the "Init_lists_..." subprogram (see also below details on the
54 % calculation and Fast Fourier Transform (FFT) algorithm)
55 %
56 % NB2: one should be careful that tau_max is large enough to include a good
57 % approximation of "infinite delays" (check that the g1(tau) function has
58 % had enough time to truly converge), while keeping a number of points
59 % large enough to ensure a good temporal resolution. This is especially
60 % important for high input powers where artifacts can appear.
61
62 tau_max = 4000; %maximum positive delay in ps
63 nb_points_delay = 2^13 + 1; % Number of points in the list of positive
    delays (tau_list).
64 % —> This must be of the form 2^N+1 for FFT optimization. For example:
    2^13+1=8193
65
66 % Parameter defining the observed spectral window, in mueV, to avoid
67 % plotting and calculating spectra over an inadequately large angular
68 % frequency ranges. NB: should not exceed the size of the full FFT
69 % spectrum, which depends on the temporal time step and thus on tau_max and
70 % nb_points_delay.
71
72 width_spectral_window_muev = 300; % width of the spectral window to be
    displayed, centered on omega_laser
73
74 %%%%%%%% Plots %%%%%%%
75 % For plot selection:
76 % — g1(tau) : 'G'
```

```

77 % -- Spectral densities of flux : 'S'
78 %
79 % plot_choice = ['G'];
80 plot_choice = ['G'; 'S'];
81
82 %%
83 % Initialization of parameters, operators, arrays, etc...
84 Init2levelDeviceParametersOngoingTest;
85 Init2levelHilbertSpaceAndOperators;
86 InitLists2levelG1SDCWvsDelayAndFrequency;
87
88 % Incoming power
89 P_in_CW = P_in_CW_pW*1e-12;% Incoming power of the CW laser, in W %%
90 b_in_CW = sqrt(eta_in*P_in_CW*1e-24/(hbar*omega_c)); % square root of the
    photon number per unit time, in ps-1/2
91 flux_injected_photons = abs(b_in_CW)^2; % total flux of injected photons,
    taking into account eta_in (so only the photons coupled to the cavity
    mode), in ps-1
92
93 switch model
94     case 'A' % Adiabatic elimination model
95
96         Delta = 2*(omega_laser-omega_c)/kappa; % Normalized laser-cavity
            detuning
97
98         % Hamiltonian including the QD operators, the cavity effect being
            included by adiabatic elimination
99         Hamiltonian_CW = (omega_eff-omega_laser)*sigma_dag*sigma...
100             - li*sqrt(Gamma_0*eta_top)*(b_in_CW*sigma_dag/(1-li*
                Delta)-b_in_CW'*sigma/(1+li*Delta)); %
                    Hamiltonian
101
102         % Definition of the operator "a" acting in the QD subspace,
            % following adiabatic elimination (Eq. 10 of the pdf notes)
103         a = -2*g*sigma/(kappa*(1-li*Delta_QDC))-2*sqrt(kappa_top)*b_in_CW*
            Id/(kappa*(1-li*Delta)); % annihilation operator a in adiabatic
            approximation
104
105
106         % UNUSED HERE: Ansatz for the annihilation operator, obtained by
            taking the time derivative of "a" equal to 0
107         % (OK for CW but not for PR (pulsed regime) programs)
108         % a = -2*g*sigma/(kappa*(1-li*Delta))-2*sqrt(kappa_top)*b_in_CW*Id
            /(kappa*(1-li*Delta));
109
110     case 'F' % Full model
111

```

```

112 % Hamiltonian including both QD and cavity operators
113 Hamiltonian_CW = (omega_d-omega_laser)*sigma_dag*sigma...
114 + (omega_c-omega_laser)*a_dag*a...
115 + li*g*(sigma_dag*a-a_dag*sigma)...
116 - li*sqrt(kappa_top)*b_in_CW*(a_dag-a);
117
118 end % end of the "switch model"
119
120 %Superoperator associated with the coherent processes (Hamiltonian)
121 L_coh = -li * (spre(Hamiltonian_CW) - spost(Hamiltonian_CW));
122
123 %%%%%%%% Calculation of the Liouvillian superoperator
124 Liouvillian = L_coh + L_incoh; % Total Liouvillian superoperator including
125 both coherent processes (Hamiltonian) and incoherent processes (
126 dissipative jumps)
127
128 %%%%%%%% Calculation of the density matrix corresponding to the stationary
129 state
130 density_matrix_stationary_state = steady(Liouvillian);
131
132 %%%%%%%%%%%%%% Definition of the output operators %%%%%%%%%%%%%%
133 % These are general formulas for both the adiabatic and full model
134 b_out = b_in_CW*Id + sqrt(kappa_top)*a; % definition of the operateur b_out
135 , i.e. the output operator for the reflected light, in ps^{(-1/2)}
136 c_out = sqrt(kappa_bottom)*a; % definition of the operateur c_out, i.e. the
137 output operator for the transmitted light, in ps^{(-1/2)}
138 d_out = sqrt(kappa_loss)*a; % definition of the operateur d_out, i.e. the
139 output operator for the diffracted/lost light, in ps^{(-1/2)}
140 % e_out = sqrt(gamma_sp)*sigma; % definition of the operateur e_out, i.e.
141 the output operator for the light spontaneously emitted outside the
142 cavity mode, in ps^{(-1/2)}
143
144 % NB: in the adiabatic model the operators could also have been written
145 % directly as a contribution from the empty cavity (term proportionnal to
146 % the identity operator "Id") and a contribution describing QD emission
147 % (term proportionnal to the decay operator "sigma"):
148 % b_out = b_in_CW*Id*(1-2*eta_top/(1-li*Delta))-sqrt(Gamma_0*eta_top)*sigma
149 % /(1-li*Delta_QDC); %output flux operator, (eq.12)
150 % c_out = -2*g*sqrt(kappa_bottom)*sigma/(kappa*(1-li*Delta_QDC))-2*sqrt(
151 % kappa_top*kappa_bottom)*b_in_CW*Id/(kappa*(1-li*Delta));
152 % d_out = -2*g*sqrt(kappa_loss)*sigma/(kappa*(1-li*Delta_QDC))-2*sqrt(
153 % kappa_top*kappa_loss)*b_in_CW*Id/(kappa*(1-li*Delta)); %annihilation
154 operator a in adiabatic approximation
155 %
156 % Such formulas are obtained by directly replacing the value of "a" from

```

```
146 % the adiabatic model, and are thus equivalent to the above, more general
147 % definitions. In addition, e_out is independent on the experimental
148 % conditions and thus defined in the subprogram
149 % "Init_2level_Hilbert_space_and_operators.m". It is given here for
150 % information and clarity purposes
151
152
153 % Total photon flux for the various fields, i.e. expectation values of the
154 % form
155 % < b'b >, including both coherent and incoherent contributions to the
156 % optical flux
157 flux_reflected_photons=real(expect(b_out'*b_out,
158     density_matrix_stationary_state)); %flux in ps^(-1)
159 flux_transmitted_photons=real(expect(c_out'*c_out,
160     density_matrix_stationary_state)); %flux in ps^(-1)
161 flux_diffracted_photons=real(expect(d_out'*d_out,
162     density_matrix_stationary_state)); %flux in ps^(-1)
163 flux_emitted_photons=real(expect(e_out'*e_out,
164     density_matrix_stationary_state)); %flux in ps^(-1)
165
166 % Coherent part of the photon flux, i.e. expectation values of the form <
167 % b' > < b >, corresponding to the fraction of light that has a
168 % well-defined amplitude and phase (characterized by the complex field
169 % amplitude < b > ), with respect to the incoming monochromatic laser.
170 flux_reflected_photons_laser_coherent = abs(expect(b_out,
171     density_matrix_stationary_state))^2; %flux in ps^(-1)
172 flux_transmitted_photons_laser_coherent = abs(expect(c_out,
173     density_matrix_stationary_state))^2;%flux in ps^(-1)
174 flux_diffracted_photons_laser_coherent = abs(expect(d_out,
175     density_matrix_stationary_state))^2;%flux in ps^(-1)
176 flux_emitted_photons_laser_coherent = abs(expect(e_out,
177     density_matrix_stationary_state))^2;%flux in ps^(-1)
178
179 % Incoherent part of the photon flux, corresponding to the fraction of the
180 % optical flux which has no well-defined phase with respect to the incoming
181 % laser, and thus cannot interfere with it.
182 flux_reflected_photons_incoh = flux_reflected_photons-
183     flux_reflected_photons_laser_coherent;%flux in ps^(-1)
184 flux_transmitted_photons_incoh = flux_transmitted_photons-
185     flux_transmitted_photons_laser_coherent;%flux in ps^(-1)
186 flux_diffracted_photons_incoh = flux_diffracted_photons-
187     flux_diffracted_photons_laser_coherent;%flux in ps^(-1)
188 flux_emitted_photons_incoh = flux_emitted_photons-
189     flux_emitted_photons_laser_coherent;%flux in ps^(-1)
190
191 %% %%%%%%%%%%%%%%
```

```
178 %%%%%%%%%%%%%%%% Evaluation of g1(tau) %%%%%%%%%%%%%%%%
179 %%%%%%%%%%%%%%%% %%%%%%%%%%%%%%%% %%%%%%%%%%%%%%%%
180 %
181 % For a given output field operator b, the two-time first-order
182 % auto-correlation function, g1(t1,t2), also called the "degree of
183 % first-order coherence", is defined by:
184 %     g1(t1,t2)= < b'(t2) b(t1) > / sqrt[ <b'b>(t2) <b'b>(t1) ]
185 % Such a quantity plays a major role in any experiment using an
186 % interference between two time-delayed components of an optical field (as
187 % in a Michelson or Mach-Zender setup ensuring the interference of a short
188 % and long path). It also plays a huge role in the calculation of optical
189 % spectra (as in photoluminescence or resonance fluorescence experiments),
190 % due to the Wiener-Kinchine theorem which directly links the optical
191 % spectra with the Fourier Transform of the first-order autocorrelation
192 % function.
193 %
194 % To calculate such a quantity, one needs to use the "Quantum Regression
195 % Theorem". This theorem allows making the link between the Heisenberg
196 % representation of a two-time correlation function < A(t2) B(t1) >, where
197 % operators A and B are time-dependant, and the Schrodinger approach that
198 % we have to use here (where the density matrix varies). The "recipe" to
199 % deduce < A(t2)B(t1) > consists in:
200 %     – Letting the density matrix evolve from time 0 to t1
201 %     – Replacing rho(t1) by a fictitious density matrix B*rho(t1)
202 %     – Computing the evolution of this fictitious density matrix between
203 %         times t1 and t2
204 %– Calculating the expectation value of operator A using this fictitious
205 %   density matrix
206 %
207 % Note that even if B*rho(t1) is not a real/valid density matrix (it's not
208 % even Hermitian), we can at least make it of the order of unity, to ensure
209 % an optimal numerical convergence (especially important in the pulsed
210 % regime where for example the operator b_out is extremely small at the
211 % beginning of the pulse). Looking at the definition of g1(t1,t2), we see
212 % that this is readily obtained by taking the operator B as b/sqrt( <b'b>),
213 % with the consequence that operator A has to be taken equal to b'/sqrt(
214 % <b'b>).
215 %
216 % NB1: To read more about the Quantum Regression Theorem, and the validity
217 % of the "recipe": —>
218 % http://atomoptics-nas.uoregon.edu/~dsteck/teaching/quantum-optics/quantum
219 % -optics-notes.pdf
220 %     (see in particular Sec. 5.7.3, page 199)
221 % —> "Quantum Noise" by Gardiner & Zoller
222 %     (see in particular Eq. 5.2.11 and an alternative formulation in Sec.
223 %      5.2.3)
```

```
222 % --> "Statistical Methods in Quantum Optics 1" by H. J. Carmichael
223 %     (see in particular Sec. 1.5 up to equations 1.97 and 1. 98)
224
225 % NB2: The approach used in the "g2CW_vs_delay" and "g2PR_vs_t1_t2"
226 % programs, to calculate second-order autocorrelation functions, is more
227 % focused on the physical/experimental definition of these quantities. It
228 % also makes use of real/normalized/valid density matrices, contrary to the
229 % fictitious density matrices used below. But the theory behind is also
230 % entirely linked to the use of the Quantum Regression Theorem.
231
232 % NB3: In the stationary regime, under CW excitation, one can take any
233 % initial time as time 0, and consider the density matrix of the stationary
234 % state at this time. Also, the flux  $\langle b'b \rangle$  does not depend on time, hence
235 % the degree of coherence only depends on the delay tau through:
236 %      $g_1(\tau) = \langle b'(\tau) b(0) \rangle / \langle b'b \rangle(0)$ 
237 % From this formula one can directly see that at zero delay  $g_1(0)$  has to be
238 % equal to unity, indeed:
239 %      $g_1(0) = \langle b'b \rangle / \langle b'b \rangle = 1$ 
240 % In addition, for very long delays one can guess that the field at delay
241 %  $\tau = \text{infty}$  is completely uncorrelated from the field at delay zero, and we
242 % find that  $g_1(\text{infty})$  has to be equal to the coherent fraction of the
243 % optical field, corresponding to the fraction of light that has a
244 % well-defined amplitude and phase with respect to the incoming
245 % monochromatic laser. Indeed:
246 %      $g_1(\text{infty}) = \langle b' \rangle \langle b \rangle / \langle b'b \rangle$ 
247 % where we used  $\langle b'(\text{infty}) b(0) \rangle = \langle b'(\text{infty}) \rangle \langle b(0) \rangle$  (uncorrelated
248 % fields). Conversely, the difference between  $g_1(0)$  and  $g_1(\text{infty})$  gives the
249 % incoherent fraction of the optical field, i.e the fraction of intensity
250 % with no well-defined phase with respect to the incoming laser.
251
252
253 % Evaluation of  $g_1(\tau)$  for positive delays only, starting from the
254 % stationary-state density matrix at time 0.
255
256 tic %Start timer to evaluate the computation time
257 g_1_reflected_vs_tau = expect(b_out'/sqrt(flux_reflected_photons),mesolve(
    Liouvillian,b_out/sqrt(flux_reflected_photons)*
    density_matrix_stationary_state,tau_list)); %Equivalent to <
    b_out_normalized_dag(t) b_out_normalized(t+tau)> for t--> infinity
258 g_1_transmitted_vs_tau = expect(c_out'/sqrt(flux_transmitted_photons),
    mesolve(Liouvillian,c_out/sqrt(flux_transmitted_photons)*
    density_matrix_stationary_state,tau_list)); %Equivalent to <
    c_out_normalized_dag(t) c_out_normalized(t+tau)> for t--> infinity
```

```

259 g_1_emitted_vs_tau = expect(e_out'/sqrt(flux_emitted_photons),mesolve(
    Liouvillian,e_out/sqrt(flux_emitted_photons)*
    density_matrix_stationary_state,tau_list)); %Equivalent to <
    e_out_normalized_dag(t) e_out_normalized(t+tau)> for t→infinity
260 toc % Stop timer
261
262 % Evaluation of g1(tau) for both negative and positive delays (
    full_tau_list).
263 full_g1_reflected_vs_tau = [fliplr(conj (g_1_reflected_vs_tau(2:end-1)))
    g_1_reflected_vs_tau ];
264 full_g1_transmitted_vs_tau = [fliplr(conj (g_1_transmitted_vs_tau(2:end-1)
    )) g_1_transmitted_vs_tau ];
265 full_g1_emitted_vs_tau = [fliplr(conj (g_1_emitted_vs_tau(2:end-1)))
    g_1_emitted_vs_tau ];
266 % NB: It is ensured that the total number of points is a power of 2, as
    required for
267 % the calculation of spectra using the Fast Fourier Transform algorithm
268
269
270 %% %%%%%%%%%%%%%% Spectral densities of flux %%%%%%%%%%%%%%
271 %%%%%%%%%%%%%% Spectral densities of flux %%%%%%%%%%%%%%
272 %%%%%%%%%%%%%% Spectral densities of flux %%%%%%%%%%%%%%
273
274 % The optical spectrum of a CW optical field is characterized by its
275 % "spectral density of flux", S(omega), whose integral over the whole
276 % spectrum gives the total photon flux. Computing such a spectrum requires
277 % using the "Wiener–Khinchine theorem", which states that the spectral
278 % density of flux, for a field described by operator "b", is the Fourier
279 % Transform of the non-normalized autocorrelation function vs delay :
280 %  $S(\omega) = (1/2\pi) * \int \langle b'(\tau) b(0) \rangle \exp(-i\omega\tau) d\tau$ 
281 % The normalization of this quantity implies that indeed the integral of
282 %  $S(\omega)$  is the total flux:
283 %  $\int S(\omega) d\omega = \langle b'(0) b(0) \rangle = \text{total flux}$ 
284 %
285 % As we saw above, however, the quantity  $\langle b'(\tau) b \rangle$  is the sum of two
286 % contributions:
287 % – A contribution  $\langle b' \rangle \langle b \rangle$ , corresponding to the coherent part of
288 % the flux.
289 % For monochromatic (i.e. infinitely coherent) CW laser excitation,
290 % this contribution never decays even at infinite delay (constant value
291 %  $\langle b' \rangle \langle b \rangle$ ).
292 % – Complementary, a contribution  $\langle b'(\tau)b \rangle - \langle b' \rangle \langle b \rangle$ , induced
293 % by the incoherent
294 % part of the flux. This contribution tends towards zero for large
295 % delays.
296 %

```

```
297 % Thus, after Fourier transforming < b'(tau) b > to obtain the spectrum:  
298 %   – The first constant contribution leads to a delta function centered on  
299 %     omega_laser,  
300 %       with an area given by < b' > < b >: this is the coherent part of the  
301 %       optical field, which is monochromatic and oscillating at the same  
302 %       frequency as the laser (with a phase and amplitude given by the  
303 %       complex number < b > ).  
304 %   – The decaying contribution leads to a continuous spectrum, which can  
305 %     not interfere  
306 %       with the incoming laser since it is not monochromatic: this is the  
307 %       spectrum of the incoherent part of the optical field, whose total  
308 %       area is the incoherent flux <b'b> – <b'><b>. Typically, in the  
309 %       weak-coupling regime this incoherent spectrum has the shape of a  
310 %       single Lorentzian peak at low power, but of a Mollow triplet at high  
311 %       power. This is this incoherent part of the spectrum that is  
312 %       calculated here, by Fourier transforming < b'(tau) b > – < b' >< b >  
313 %       as a function of the delay tau.  
314 %  
315 % NB1: To know more about Wiener–Khinchin theorem and the computation of  
316 % optical spectra:  
317 % --> http://atomoptics-nas.uoregon.edu/~dstreck/teaching/quantum-optics/quantum-optics-notes.pdf  
318 %       (see in particular Chap. 2 for Wiener–Khinchin theorem, and Sec. 5.7  
319 %       for resonance fluorescence)  
320 % --> "The Quantum Theory of Light" by Rodney Loudon  
321 %       (see in particular Chap. 3 for classical optics, and Chap. 8 for  
322 %       resonance fluorescence spectra)  
323 % --> "Statistical Methods in Quantum Optics 1" by Howard Carmichael  
324 %       (see in particular Sec. Z.3.4)  
325 %  
326 % NB2: We choose to define a spectral density in terms of the photon energy  
327 % (in mueV), instead of frequency (in ps-1) or angular frequency (in  
328 % rad/ps). As a flux is measured here in ps-1 (number of photons per unit  
329 % time), the dimension of our spectral densities has to be in ps-1 / mueV.  
330 % Indeed each spectral contribution to the total flux is obtained through  
331 % multiplying the spectral density of flux (in ps-1 / mueV) by the photon  
332 % energy step (in mueV).  
333 %  
334 % NB3: The default technique used here is the Fast Fourier Transform (FFT)  
335 % algorithm, which can provide accurate spectra in a very fast way provided  
336 % we use a number of points that is a power of 2 (same number of points in  
337 % the time and frequency domain). The spectral width of the FFT spectrum  
338 % (here denoted as "FFT_sampling_frequency") and its resolution (here  
339 % related to the step in angular frequency, "omega_step") are fixed by the  
340 % width and resolution used in in the time domain (related to "tau_max" and  
341 % "tau_step" characterizing the "full_tau_list"). In practice, we are
```

```
342 % interested only in a spectral window of width
343 % "width_spectral_window_muev", and the list of angular frequencies omega
344 % in "omega_list" (that we use to plot quantities "versus omega" and
345 % calculate integrals) is just a subset of the full FFT spectrum, centered
346 % on omega_laser. Also note that the raw FFT spectra have to be adequately
347 % transformed into real physical quantities:
348 %   a) Proper normalization of the FFT result has to be ensured, so that
349 %       the integral of the
350 %           spectral density indeed corresponds to the optical flux in ps^-1
351 %           (or more precisely the incoherent component of the optical flux, as
352 %           discussed above).
353 %   b) One needs to ensure that the optical spectra are centered on the
354 %       laser frequency/photon
355 %           energy, to take into account the fact that we worked in the
356 %           rotating frame at this laser frequency. Using the "fftshift"
357 %           function just ensures that the first half of the FFT spectrum
358 %           corresponds to negative frequencies, and the second half to
359 %           positive frequencies. In addition, we ensure that the lists of
360 %           angular frequencies ("omega_list_full_spectrum" for the complete
361 %           list in rad/ps, "omega_list" for the selected spectral window in
362 %           rad/ps, and "omega_list_eV" for the selected energy window in eV)
363 %           are defined to be centered. on the laser frequency/photon energy.
364 %   c) The list of delays in "full_tau_list" includes negative and
365 %       positive
366 %           delays, with the
367 %               zero delay in the middle of the list. But the FFT algorithm
368 %               considers that this is the first point of the list which is the
369 %               time zero, which leads to a frequency-dependent phase shift along
370 %               the full FFT spectrum. This phase shift has to be compensated (the
371 %               spectral density of flux is a real quantity), which is done through
372 %               a multiplication by "phase_shift_compensation_full_FFT_spectrum".
373 %   --> All the angular frequency lists and quantities related to the
374 %       calculation of the FFT spectra
375 %           are defined in the "Init_lists_..." subprogram, for clarity.
376
377 % Computing the spectral densities of flux over the full frequency spectrum
378 spectral_density_flux_reflected_photons_incoh_full_spectrum = 1/(2*pi)*
    fftshift(fft(full_g_1_reflected_vs_tau*flux_reflected_photons-
    flux_reflected_photons_laser_coherent,nb_points_full_spectrum)./
    phase_shift_compensation_vs_omega_full_spectrum)/FFT_sampling_frequency
    * (ev/hbar*1e-18); % spectral density in ps^-1 / muev
```

```

379 spectral_density_flux_transmitted_photons_incoh_full_spectrum = 1/(2*pi)*
    fftshift(fft(full_g_1_transmitted_vs_tau*flux_transmitted_photons-
    flux_transmitted_photons_laser_coherent,nb_points_full_spectrum)./
    phase_shift_compensation_vs_omega_full_spectrum)/FFT_sampling_frequency
    * (ev/hbar*1e-18); % spectral density in ps^-1 / mueV
380 spectral_density_flux_emitted_photons_incoh_full_spectrum = 1/(2*pi)*
    fftshift(fft(full_g_1_emitted_vs_tau*flux_emitted_photons-
    flux_emitted_photons_laser_coherent,nb_points_full_spectrum)./
    phase_shift_compensation_vs_omega_full_spectrum)/FFT_sampling_frequency
    * (ev/hbar*1e-18); % spectral density in ps^-1 / mueV
381
382 % Spectral densities of flux as a function of omega, limited to the
383 % selected spectra window (range of angular frequencies defined by "omega
384 % list")
385 spectral_density_flux_reflected_photons_incoh_vs_omega =
    spectral_density_flux_reflected_photons_incoh_full_spectrum(
    index_min_zoomed_spectrum:index_max_zoomed_spectrum); % spectrum
    restricted to the selected spectral window, in ps^-1 / mueV
386 spectral_density_flux_transmitted_photons_incoh_vs_omega =
    spectral_density_flux_transmitted_photons_incoh_full_spectrum(
    index_min_zoomed_spectrum:index_max_zoomed_spectrum); % spectrum
    restricted to the selected spectral window, ps^-1 / mueV
387 spectral_density_flux_emitted_photons_incoh_vs_omega =
    spectral_density_flux_emitted_photons_incoh_full_spectrum(
    index_min_zoomed_spectrum:index_max_zoomed_spectrum);% spectrum
    restricted to the selected spectral window, in ps^-1 / mueV
388
389
390 %%
391 % %%% Alternative method: Fourier transform by explicit calculation of the
392 % Fourier integrals % This method is very inefficient in terms of computing
393 % time, yet is crucial to allow verifying % the results obtained with the
394 % FFT algorithm: it must give the same result as the FFT method.
395 %
396 % tic % Start timer to evaluate the computation
397 %
398 % for omega_index=1:nb_points_spectrum
399 %     spectral_density_flux_reflected_photons_incoh_vs_omega(omega_index) =
        1/(2*pi)* sum ( (full_g_1_reflected_vs_tau*flux_reflected_photons-
        flux_reflected_photons_laser_coherent) .* exp(-li* (omega_list(
        omega_index) - omega_laser) .*full_tau_list ) ) * tau_step * (ev/hbar*1e
        -18) ; % spectral density in ps^-1 / mueV

```

```

400 %     spectral_density_flux_transmitted_photons_incoh_vs_omega(omega_index)
        = 1/(2*pi)* sum ( (full_g_1_transmitted_vs_tau*
        flux_transmitted_photons–flux_transmitted_photons_laser_coherent) .*%
        exp(-li* (omega_list(omega_index) – omega_laser) .*full_tau_list )) *%
        tau_step *(ev/hbar*1e-18); % spectral density in ps^-1 / mueV
401 %     spectral_density_flux_emitted_photons_incoh_vs_omega(omega_index) =
        1/(2*pi)* sum ( (full_g_1_emitted_vs_tau*flux_emitted_photons-
        flux_emitted_photons_laser_coherent) .* exp(-li* (omega_list(
        omega_index) – omega_laser) .*full_tau_list )) * tau_step *(ev/hbar*1e
        -18); % spectral density in ps^-1 / mueV
402 % end
403 %
404 % toc    % Stop timer
405
406
407 %% %%%%%%%%%%%%%% Plots %%%%%%%%%%%%%%
408
409 Plot2LevelG1SDCWvsDelayAndFrequency;

```

C.1.4 First-order correlation and Wigner Distribution Function in PW

```

1 clear
2 clc
3 close all
4
5 %% Important note: these paths must be modified if needed
6 addpath(genpath('..\QotoolboxV015'));
7 addpath(genpath('..\CQED subprograms'));
8 addpath(genpath('..\CQED device parameters'))
9 savepath
10
11 % In addition, for the mesolve function to operate the executable files
12 % (.exe) and batch files (.bat) contained in '[...] \QotoolboxV015\bin'
13 % have to be copied to a folder that is on the Windows system path, in the
14 % main hard drive where Windows is installed. This can be for example in:
15 % 'C:\Program Files\Matlab\R2014a\bin'.
16
17 % Warning: for the adiabatic version to converge, the tolerance in
18 % mesolve.m function must be reduced compared to the default values. For
19 % example:
20 % ode2file('ode_input.dat',L,rho0,t_list,struct('reltol',7e-8,'abstol',8e
21 % -8));
22
23 %% %%%%%%%%%%%%%% %%%%%%%%%%%%%%

```

```

24 %%%%%%%% g1SDPR : g1(t1,t2) and spectral densities in PR %%%%%%
25 %%%%%%
26 %This section labeled "g1SDPR" studies the resonant resonance fluorescence
27 %spectra in pulsed regime, by prior evaluation of the normalized
28 %correlation function g1(t1,t2). By setting t=(t1-t2)/2 and tau = t2-t1, an
29 %interpolated (unnormalized) G1(t,tau) is computed from G1(t1,t2). The
30 %Fourier Transform is evaluated over tau to find the associated
31 %Wigner–Ville–Distribution WDF(t,omega). To check its normalization,
32 %WDF(t,omega) is integrated over omega and compared with the photon fluxes.
33 %WDF is integrated over t for determining the spectral energy density
34 %ESD(omega), which is what is measured by the spectrometer. It is verified
35 %that the area of this spectrum gives the total number of photons. At last,
36 %the spectra of the total and the coherent component of the fluxes are
37 %compared for the reflected, transmitted, diffracted and emitted fields.
38 %%%%%%
39
40 %% Choice of full model 'F' or adiabatic model 'A'
41 model = 'A';
42
43 %% Experimental conditions (to be edited)
44 detuning_QD_C_muev = 0; %Detuning between the QD and cavity frequencies, in
        mueV
45 detuning_pulse_QD_muev = 0; %Detuning between the pulse central frequency
        and the QD frequency, in mueV
46 eta_in = 1; % Injection efficiency for the incoming photons (depends on
        experimentally–achieved spatial coupling)
47 Nb_photons_pulse = 1; % Average number of incoming photons in a pulse.
        This quantity should be multiplied by eta_in to know the number of
        incoming photons actually coupled to the optical mode
48 FWHM_pulse = 15; %in ps, full width at half–maximum of the incoming
        Gaussian pulse intensity (unit: ps since angular frequencies are in rad
        /ps)
49 % Parameters for the evaluation of the temporal evolution
50 %
51 % NB1: the maximum delay "t_max_ps" will also dictate the frequency
52 % resolution of the spectra, given by the angular frequency step
53 % "omega_step". The corresponding angular frequency lists are defined in
54 % the "Init_lists_..." subprogram (see also below details on the
55 % calculation and Fast Fourier Transform (FFT) algorithm)
56 %
57 % NB2: one should be careful that "t_max_ps" is large enough to include a
58 % good approximation of "infinite delays" (check that the g1(tau) function
59 % has had enough time to truly converge), while keeping a number of points
60 % large enough to ensure a good temporal resolution. This is especially
61 % important for high input powers where artifacts can appear.

```

```

62 t_delay = 2*FWHM_pulse; % Time at which the pulse is maximally intense, so
    % that the computation starts when the pulse has not arrived yet
63 t_max_ps = (t_delay + 4*FWHM_pulse)*5; % Final time where we stop the
    % computation and plots of time evolutions
64 nb_points_time = 2^7; % Time resolution/Number of iterations / <100000
    % otherwise the integrating the master equation gets difficult (odesolve)
    %
65 % --- This should be such that 4*nb_points_time-3 is less than a power of 2
66 % if one wants to reduce the amount of zero padding, the latter being
67 % required for FFT optimization.
68 t_min = 0.1*FWHM_pulse; % Initial time considered for the computations and
    % plots of time evolutions
69 width_spectral_window_muev = 300; % width of the spectral window to be
    % displayed, centered on omega_pulse
70 %% Initialization of parameters, operators, arrays, etc...
71 Init2levelDeviceParametersOngoingTest;
72 Init2levelHilbertSpaceAndOperators;
73 InitMaps2levelG1wdfPR;
74 %%
75 % Definition of the input field in ps^{(-1/2)}, in the form of a fseries (
    % necessary for integrating the master equation)
76 Standard_deviation_b_in_PR = FWHM_pulse/(2*sqrt(log(2))); %Deduced from the
    % properties of a Gaussian function
77 b_in_fn = fn('gauss',t_delay,Standard_deviation_b_in_PR) * sqrt( eta_in*
    % Nb_photons_pulse / ( sqrt(pi) * Standard_deviation_b_in_PR ) ); %
    % square root of the incoming photon number per time unit, in ps^{-1/2}
78 b_in_vs_time = fsval(b_in_fn,t_list); %scalar array representing b_in vs
    % time
79
80 % Initial density matrix before the pulse has started
81 switch model
82     case 'F' %Full model
83         psi0 = tensor(Vacuum_state,g_ket); % Initial state: tensorial
            % product of photonic vacuum and QD ground state
84         rho0 = psi0*psi0'; % Density matrix corresponding to the initial
            % pure state
85     case 'A' % Adiabatic model
86         rho0 = g_ket*g_ket'; % Density matrix corresponding to the initial
            % pure state
87 end
88
89 %% %%%%%%%%%%%%%% System Hamiltonian and time-dependent operators %%%%%%%%%%%%%%
90 %
91 % The system Hamiltonian is time-dependent due to the function b_in_fn
92 % describing the input field b_in(t).
93

```

```
94 % In addition, in the case of adiabatic elimination of the cavity mode an
95 % effective
96 % operator "a" is defined, acting on the QD subspace, based on the formula
97 % for
98 % adiabatic elimination. Since this formula depends
99 % on b_in(t), we define a time-dependent quantity "a_vs_time", which is an
100 % array containing, for each time of t_list, the corresponding operator
101 % "a".
102 % In the full model case, to simplify the following calculations, we define
103 % the
104 % same quantity a_vs_time, yet this time this array contains the same
105 % operator
106 % (annihilation operator "a" acting on the cavity subspace), replicated for
107 % all
108 % times of t_list.
109
110 switch model
111     case 'A' % Adiabatic model
112
113         Delta = 2*(omega_pulse-omega_c)/kappa; %normalized pulse
114             detuning
115
116             %%%%%% Definition of the adiabatic-model Hamiltonian (in the
117             % frame rotating at angular frequency omega_pulse)
118             H_PR = (omega_eff-omega_pulse)*sigma_dag*sigma - li*sqrt(
119                 Gamma_0*eta_top)*...
120                 ((1-li*Delta)^(-1)*b_in_fn*sigma_dag-(1+li*Delta)^(-1)*
121                     b_in_fn'*sigma); % Hamiltonian
122
123             %% Definition of the time-dependent operator "a_vs_time"
124             % acting in the QD subspace
125             a_vs_time = -2*(kappa*(1-li*Delta_QDC))^(−1)*g*sigma*Id_vs_time
126                 -2*sqrt(kappa_top)*(kappa*(1-li*Delta))^(−1)*fsval(b_in_fn,
127                     t_list).*Id_vs_time; %annihilation operator a in adiabatic
128                     approximation, as fseries
129
130         case 'F' % Full model
131
132             %%%%%% Definition of the full-model Hamiltonian (in the
133             % frame rotating at angular frequency omega_pulse)
134             H_PR = (omega_d-omega_pulse)*sigma_dag*sigma...
135                 + (omega_c-omega_pulse)*a_dag*a...
136                 + li*g*(sigma_dag*a-a_dag*sigma)...
137                 - li*sqrt(kappa_top)*b_in_fn*(a_dag-a);
138
139
140
141
142
143
144
```

```
125 % Definition of the operator a_vs_time, even though "a" is
126 % constant in the full model, to reduce the number of "switch
127 % " in the following code
128 a_vs_time = a*Id_vs_time;
129
130 end % end of the "switch model"
131
132 %Superoperator associated to the coherent processes (Hamiltonian)
133 L_coh = -1i * (spre(H_PR) - spost(H_PR));
134
135 %%%%%%%% Calculation of the Liouvillian superoperator
136 Liouvillian = L_coh + L_incoh; % Total Liouvillian superoperator including
137 % both coherent processes (Hamiltonian) and incoherent processes (
138 % dissipative jumps)
139
140 %%%%%%%% Numerical Integration of the Master Equation %%%%%%%
141
142 % Computation of preliminary time evolution, between 0 (long before the
143 % pulse)
144 % and t_min (time at which we want to start plotting and integrating the
145 % physical
146 % quantities. Such a computation can be performed with very low time
147 % resolution,
148 % i.e. the corresponding t_list_before_t_min has a very low number of
149 % points,
150 % since the density matrix almost doesn't evolve between 0 and t_min.
151 %
152 % NB: such a preliminary time evolution is mandatory to avoid having
153 % strictly
154 % zero expectation values for some quantities (such as the input or output
155 % fields),
156 % during the following time evolution between t_min and t_max). Indeed,
157 % zero
158 % expectation values lead to NaN errors when used in normalizing physical
159 % quantities, such as conditional density matrices (see below), or
160 % Stokes/Bloch coordinates in the Poincare'/Bloch sphere.
161
162 density_matrix_vs_time_before_t_min = mesolve(Liouvillian,rho0,
163 t_list_before_t_min); %master equation solver based on odesolve: first
164 % evolution of the system
165 density_matrix_at_t_min = density_matrix_vs_time_before_t_min{
166 nb_points_time_before_t_min};
167
168 % Computation of the density matrix vs time with t_list, i.e. between t_min
169 % and t_max, requiring a large enough time resolution.
```

```

156 density_matrix_vs_time = mesolve(Liouvillian,density_matrix_at_t_min,t_list
157 ); % second evolution of the system
158 %%%%%%%%%%%%%%%%%%%%%%%%%%%%%%%%%%%%%% Definition of the output operators %%%%%%%%%%%%%%
159 % These are general formulas for both the adiabatic and full model,
160 % depending on "a_vs_time"
161 b_out_vs_time = b_in_vs_time*Id_vs_time + sqrt(kappa_top)*a_vs_time; %
162 % definition of the operator b_out, i.e. the output operator for the
163 % reflected light, in ps^{(-1/2)}
164 c_out_vs_time = sqrt(kappa_bottom)*a_vs_time; % definition of the operator
165 % c_out_vs_time, i.e. the output operator for the transmitted light, in
166 % ps^{(-1/2)}
167 d_out_vs_time = sqrt(kappa_loss)*a_vs_time; % UNUSED HERE: definition of
168 % the operator d_out_vs_time, i.e. the output operator for the diffracted
169 % /lost light, in ps^{(-1/2)}
170 % e_out = sqrt(gamma_sp)*sigma % output operator for the light
171 % spontaneously emitted outside the cavity mode, in ps^{(-1/2)}, already
172 % defined in Init_2level_Hilbert_space_and_operators.m
173
174 % Calculation of the total photon flux as a function of time, for the
175 % various optical fields
176 flux_injected_photons_vs_time = b_in_vs_time.^2; % total flux of injected
177 % photons taking into account eta_in (so only the photons coupled to the
178 % cavity mode), in ps{(-1)}
179 flux_reflected_photons_vs_time = real(expect(b_out_vs_time'*b_out_vs_time,
180 %flux in ps^{(-1)}
181 density_matrix_vs_time)); %flux in ps^{(-1)}
182 flux_transmitted_photons_vs_time = real(expect(c_out_vs_time'*c_out_vs_time
183 ,density_matrix_vs_time)); %flux in ps^{(-1)}
184 flux_diffracted_photons_vs_time = real(expect(d_out_vs_time'*d_out_vs_time,
185 density_matrix_vs_time)); %flux in ps^{(-1)}
186 flux_emitted_photons_vs_time = real(expect(e_out'*e_out,
187 density_matrix_vs_time)); %flux in ps^{(-1)}
188
189 % Calculation of the total coherent photon flux as a function of time, for
190 % the various optical fields
191 flux_reflected_photons_pulse_coherent_vs_time= abs(expect(b_out_vs_time,
192 % coherent flux = <b_out'(t)><b_out(t)> in
193 density_matrix_vs_time)).^2; % coherent flux = <b_out'(t)><b_out(t)> in ps^{(-1)}
194 flux_transmitted_photons_pulse_coherent_vs_time=abs(expect(c_out_vs_time,
195 % coherent flux = <c_out'(t1)><c_out(t2)>
196 density_matrix_vs_time)).^2; % coherent flux = <c_out'(t1)><c_out(t2)>
197 in ps^{(-1)}
198 flux_diffracted_photons_pulse_coherent_vs_time=abs(expect(d_out_vs_time,
199 % coherent flux = <d_out'(t1)><d_out(t2)>
200 density_matrix_vs_time)).^2; % coherent flux = <d_out'(t1)><d_out(t2)>
201 in ps^{(-1)}
```

```
177 flux_emitted_photons_pulse_coherent_vs_time=abs(expect(e_out,
    density_matrix_vs_time)).^2; % coherent flux =  $\langle e_{out}'(t_1) \rangle \langle e_{out}(t_2) \rangle$ 
    in ps^{-1}
178
179 %Computing the number of reflected/transmitted/emitted photons, by
    integrating over all times in t_list
180 Nb_reflected_photons = trapz(t_list,flux_reflected_photons_vs_time);
181 Nb_transmitted_photons = trapz(t_list,flux_transmitted_photons_vs_time);
182 Nb_diffracted_photons = trapz(t_list,flux_diffracted_photons_vs_time);
183 Nb_emitted_photons = trapz(t_list,flux_emitted_photons_vs_time);
184
185 %%
    %%%%%%%%%%%%%%%%
186 %%%%%% Evaluation of g1(t1,t2)
    %%%%%%
187 %
    %%%%%%
188 %
189 % For a given output field operator b, the two-time first-order auto-
    correlation function,
190 % g1(t1,t2), also called the "degree of first-order coherence", is defined
    by:
191 %      $g1(t1,t2) = \langle b'(t1) b(t2) \rangle / \sqrt{\langle b'(t1) \rangle \langle b(t2) \rangle}$ 
192 %
193 % To calculate such a quantity, one can use the Heisenberg representation
    of a two-time
194 % correlation function  $\langle A(t1) B(t2) \rangle$ , where operators A and B are time-
    dependent, and
195 % the Schroedinger approach that we have to use here (where the density
    matrix varies).
196 % The "recipe" to deduce  $\langle A(t1) B(t2) \rangle$  consists in:
197 %     – Letting the density matrix evolve from time 0 to t1
198 %     – Replacing rho(t1) by a fictitious density matrix rho(t1)*A
199 %     – Computing the evolution of this fictitious density matrix between
    times t1 and t2
200 %     – Calculating the expectation value of operator B using this
    fictitious density matrix
201 %
202 % Note that even if rho(t1)*A is not a real/valid density matrix (it's not
    even Hermitian),
203 % we can at least make it of the order of unity, to ensure an optimal
    numerical convergence
204 % (especially important in the pulsed regime where for example the operator
    b_out is
```

```
205 % extremely small at the beginning of the pulse). Looking at the definition
206 % of g1(t1,t2),
207 % we see that this is readily obtained by taking the operator B as b/sqrt(
208 % <b'b>), with
209 % the consequence that operator A has to be taken equal to b'/sqrt( <b'b> )
210 %
211 % NB1: The approach used in the "g2CW_vs_delay" and "g2PR_vs_t1_t2"
212 % programs, to calculate
213 % second-order autocorrelation functions, is more focused on the physical/
214 % experimental
215 % definition of these quantities. It also makes use of real/normalized/
216 % valid density matrices,
217 % contrary to the fictitious density matrices used below. But the theory
218 % behind is also
219 % entirely linked to the use of the Quantum Regression Theorem.
220 %
221 %%%%%%%% Calculation of fictitious density matrix rho(t1)*A %%%%%%
222 % In the following the "density_matrix_times_OPERATOR_dag_vs_t1"-s are
223 % defined for each value of time t1 in t_list.
224 %
225 % NB: notice the normalization b'/sqrt( <b'b> ) to optimize numerical
226 % convergence
227 density_matrix_times_b_out_dag_vs_t1 = density_matrix_vs_time*b_out_vs_time
228 % ./sqrt(flux_reflected_photons_vs_time);
229 density_matrix_times_c_out_dag_vs_t1 = density_matrix_vs_time*c_out_vs_time
230 % ./sqrt(flux_transmitted_photons_vs_time);
231 density_matrix_times_d_out_dag_vs_t1 = density_matrix_vs_time*d_out_vs_time
232 % ./sqrt(flux_diffracted_photons_vs_time);
233 density_matrix_times_e_out_dag_vs_t1 = density_matrix_vs_time*e_out'./sqrt(
234 % flux_emitted_photons_vs_time);
235 %
236 % NB: "tic" is used as a "start" time for the measurement of the computing
237 % time between "tic" and "toc"
238 %tic
239 %
240 %Cycle over all times t1 in t_list, corresponding to the moment where a
241 % first click occurred
242 for t1_index = 1:nb_points_time
243 %
244 % Both t1 and t2 are values in t_list. However, to compute the
245 % "fictitious density matrix B*rho(t1)" vs t2, we consider
246 % only t2 >= t1, and we need to deal with the fact that there are less
247 % and less remaining values of t2 in t_list, when t1 increases. To keep
248 % all quantities defined in the full t_list, for each time t1 < t2 we
249 % have a "zero" density matrix, i.e. a fictitious density matrix with
```

```
238 % only zero elements–
239
240 % Incrementing the array of zero density matrices, each time t1_index
241 % is increased, to fill the density matrix for times t1 < t2
242
243 if (t1_index >=2) % No need to include a zero density matrix at the
244     first value of t1
245     zero_density_matrix_vs_t2_before_t1{t1_index-1} = 0*Id; %null
246         density matrix with the same dimensions of the involved Hilbert
247         space
248 end
249
250 % Array of normalized density matrices, conditioned on the detection of
251 % a
252 % click at time t1, as a function of t2 >= t1 (and zero otherwise)
253
254 % NB: notice the normalization b'/sqrt( <b'b> ) to optimize numerical
255 % convergence
256 density_matrix_times_b_out_dag_vs_t2 = [
257     zero_density_matrix_vs_t2_before_t1 mesolve(Liouvillian,
258         density_matrix_times_b_out_dag_vs_t1{t1_index},t_list(t1_index:end)
259         )]./sqrt(flux_reflected_photons_vs_time);
260 density_matrix_times_c_out_dag_vs_t2 = [
261     zero_density_matrix_vs_t2_before_t1 mesolve(Liouvillian,
262         density_matrix_times_c_out_dag_vs_t1{t1_index},t_list(t1_index:end)
263         )]./sqrt(flux_transmitted_photons_vs_time);
264 density_matrix_times_d_out_dag_vs_t2 = [
265     zero_density_matrix_vs_t2_before_t1 mesolve(Liouvillian,
266         density_matrix_times_d_out_dag_vs_t1{t1_index},t_list(t1_index:end)
267         )]./sqrt(flux_diffracted_photons_vs_time);
268 density_matrix_times_e_out_dag_vs_t2 = [
269     zero_density_matrix_vs_t2_before_t1 mesolve(Liouvillian,
270         density_matrix_times_e_out_dag_vs_t1{t1_index},t_list(t1_index:end)
271         )]./sqrt(flux_emitted_photons_vs_time);
272
273
274 % Evaluation of g1(t1,t2) as described in the general notes above, for
275 % t2 >= t1 (and zero otherwise)
276 % NB: the normalization by the photon flux is already considered in
277 % density_matrix_times_OPERATOR_dag_vs_t2
278 g1_reflected_vs_t1_t2(t1_index,:) = expect(b_out_vs_time,
279     density_matrix_times_b_out_dag_vs_t2);
280 g1_transmitted_vs_t1_t2(t1_index,:) = expect(c_out_vs_time,
281     density_matrix_times_c_out_dag_vs_t2);
282 g1_diffracted_vs_t1_t2(t1_index,:) = expect(d_out_vs_time,
283     density_matrix_times_d_out_dag_vs_t2);
```

```

263     g1_emitted_vs_t1_t2(t1_index,:) = expect(e_out,
264         density_matrix_times_e_out_dag_vs_t2);
265    end
266    %% Completion of previous partially-calculated maps vs t1,t2, to include
267    %% the case where t2 < t1
268    % Due to the symmetry between t1 and t2, we have to use properties like g1(
269    % t1,t2)=g1(t2,t1)* to fill
270    % the voids in the quantities that we have only partially calculated yet
271    % (since we systematically considered a zero value when t2 < t1. For each
272    % map function of t1 and t2, this completion is obtained by adding it to
273    % its transpose conjugate (to replace the zeros at t2 < t1) and dividing by
274    % 2 the elements along the diagonal (to avoid counting twice the case where
275    % t2=t1). This is done via an ad-hoc matrix idx below:
276    idx = ones(nb_points_time)-0.5*diag(ones(nb_points_time,1)); % to divide by
277    %% 2 the elements along the diagonal
278    % Completed g1(t1,t2) for the various optical fields
279
280    g1_reflected_vs_t1_t2 = (g1_reflected_vs_t1_t2+g1_reflected_vs_t1_t2').*idx
281    ;
282    g1_transmitted_vs_t1_t2 = (g1_transmitted_vs_t1_t2+g1_transmitted_vs_t1_t2
283    ').*idx;
284    g1_diffracted_vs_t1_t2 = (g1_diffracted_vs_t1_t2+g1_diffracted_vs_t1_t2').*
285    %% idx;
286    g1_emitted_vs_t1_t2 = (g1_emitted_vs_t1_t2+g1_emitted_vs_t1_t2').*idx;
287
288    % G1 correlation vs (t1,t2), e.g. <b_out'(t1) b_out(t2)>
289    G1_reflected_vs_t1_t2 = g1_reflected_vs_t1_t2.*(
290        flux_reflected_photons_vs_time'*flux_reflected_photons_vs_time).^0.5;
291    G1_transmitted_vs_t1_t2 = g1_transmitted_vs_t1_t2.*(
292        flux_transmitted_photons_vs_time'*flux_transmitted_photons_vs_time)
293        .^0.5;
294    G1_diffracted_vs_t1_t2 = g1_diffracted_vs_t1_t2.*(
295        flux_diffracted_photons_vs_time'*flux_diffracted_photons_vs_time).^0.5;
296    G1_emitted_vs_t1_t2 = g1_emitted_vs_t1_t2.*((flux_emitted_photons_vs_time'*
297        flux_emitted_photons_vs_time).^0.5;
298
299    % coherent component cross product, e.g <b_out'(t1)> <b_out(t2)>
300    expect_b_out_dag_t1_times_expect_b_out_t2 = expect(b_out_vs_time',
301        density_matrix_vs_time).*expect(b_out_vs_time,density_matrix_vs_time);
302    expect_c_out_dag_t1_times_expect_c_out_t2 = expect(c_out_vs_time',
303        density_matrix_vs_time).*expect(c_out_vs_time,density_matrix_vs_time);

```

```
294 expect_d_out_dag_t1_times_expect_d_out_t2 = expect(d_out_vs_time',
295     density_matrix_vs_time).*expect(d_out_vs_time,density_matrix_vs_time);
296 expect_e_out_dag_t1_times_expect_e_out_t2 = expect(e_out',
297     density_matrix_vs_time).*expect(e_out,density_matrix_vs_time);
298 %% %%%%%%%%%%%%%%%% Wigner distribution function%%%%%%%%%%%%%%%
299 %The Wigner distribution function (WDF) is used in signal processing as a
300 %transform in time–frequency analysis. the Wigner distribution function
301 %provides the highest possible temporal vs frequency resolution which is
302 %mathematically possible within the limitations of uncertainty in quantum
303 %wave theory. Given a non–stationary autocorrelation function C(t1,t2), by
304 %defining t=(t1+t2)/2 and tau= t2–t1, Fourier transforming the lag is
305 %obtained :
306 %WDF(t,omega) = \int C(t+tau/2,t-tau/2)*exp(-i*tau*omega) d\tau.
307 %More info can be found at https://en.wikipedia.org/wiki/Wigner\_distribution\_function
308 %Notice that tau is defined based on the definition of C(t1,t2) in this
309 %script, with opposite sign with respect to the wiki page one.
310 %% Mapping C(t1,t2) into C(t,tau)
311 %The Fourier transform of the WDF will be performed over tau/2 and not
312 %simply tau. This implies that in addition to mapping C(t1,t2) into
313 %C(t,tau), C(t1,t2) must be interpolated also not only over time and tau,
314 %but also
315 %over the tau/2. If this were not done, aliasing would occur due to
316 %under sampling. For more information, section "More about" at
317 % https://www.mathworks.com/help/signal/ref/wvd.html
318 interpolation_2level_g1SDPR_vs_t1_t2;
319
320 %Side note: MATLAB has implemented its own WDF since R2018b, however it is
321 %defined for a single time series signal x(t) and not C(t1,t2). Still, it
322 %can be used for comparison to evaluate the WDF of the coherent component
323 %of the flux. Below it is shown how it is done for the reflected coherent
324 %field.
325
326 % expect_b_out_vs_time_dag = expect(b_out_vs_time',density_matrix_vs_time);
327 % sampling_frequency = 1/t_step; % Sampling frequency ps^(-1)
328 % [WVD_b_out_vs_time_coherent,frequency_WVD,t_list_WVD] = wvd(
329 %     expect_b_out_vs_time_dag,sampling_frequency); %returns the smoothed
330 % pseudo Wigner–Ville distribution
331 % nb_points_WVD_spectrum = nb_points_time;
332 % omega_step_WVD = 2*pi*(sampling_frequency/2)/nb_points_WVD_spectrum;
333 % omega_step_WVD_muev = omega_step_WVD/ev*hbar/1e-18; %in mueV
334 % omega_spectrum_WVD = omega_pulse + frequency_WVD*2*pi; % rad/ps, arrays
335 % of angular frequencies. Obs: the zero value from fft corresponds to
336 % omega_laser
```

```
331 % omega_spectrum_WVD_muev = omega_spectrum_WVD/ev*hbar/1e-18; % mueV,  
    arrays of angular frequencies, zero-centered  
332 % figure,  
333 % surf(t_list_WVD,omega_spectrum_WVD_muev - omega_pulse_ev*1e6,  
    WVD_b_out_vs_time_coherent/(2*pi/ev*hbar/1e-18),'EdgeColor','none')  
334 % xlabel('time [ps]')  
335 % ylabel('\omega-\omega_p [\mu eV]')  
336 % title('Wigner-Ville distribution reflected coherent photons - MATLAB')  
337 % view(2)  
338 % colorbar  
339  
340 %% Fourier Transforming over the delay tau to obtain the WDF  
341 % The technique used here for the Fourier Transform is the Fast Fourier  
    Transform (FFT) algorithm, which  
342 % can provide accurate spectra in a very fast way provided we use a number  
    of points that is  
343 % a power of 2 (same number of points in the time and frequency domain).  
    The spectral width of  
344 % the FFT spectrum (here denoted as "FFT_sampling_frequency") and its  
    resolution (here related  
345 % to the step in angular frequency, "omega_step") are fixed by the width  
    and resolution used in  
346 % in the time domain (related to "t_max_ps" and "t_delay" characterizing  
    the "full_tau_list").  
347 % In practice, we are interested only in a spectral window of width "  
    width_spectral_window_muev",  
348 % and the list of angular frequencies omega in "omega_list" (that we use to  
    plot quantities  
349 % "versus omega" and calculate integrals) is just a subset of the full FFT  
    spectrum, centered on  
350 % omega_pulse. Also note that the raw FFT spectra have to be adequately  
    transformed into real  
351 % physical quantities:  
352 %     a) Proper normalization of the FFT result has to be ensured, so that  
        the integral of the  
353 %         spectral density indeed corresponds to the optical flux in ps^-1 (or  
        more precisely  
354 %         the incoherent component of the optical flux, as discussed above).  
355 %     b) One needs to ensure that the optical spectra are centered on the  
        laser frequency/photon  
356 %         energy, to take into account the fact that we worked in the  
        rotating frame at this laser  
357 %         frequency. Using the "fftshift" function just ensures that the  
        first half of the FFT  
358 %         spectrum corresponds to negative frequencies, and the second half  
        to positive frequencies.
```

```
359 %      In addition, we ensure that the lists of angular frequencies ("omega_list_full_spectrum"
360 %      for the complete list in rad/ps, "omega_list" for the selected
361 %      spectral window in rad/ps,
362 %      and "omega_list_eV" for the selected energy window in eV) are
363 %      defined to be centered.
364 %      on the laser frequency/photon energy.
365 %      c) The list of delays in "full_tau_list" include negative and positive
366 %      delays, with the
367 %      zero delay in the middle of the list. But the FFT algorithm
368 %      considers that this is the
369 %      first point of the list which is the time zero, which leads to a
370 %      frequency-dependent
371 %      phase shift along the full FFT spectrum. This phase shift has to be
372 %      compensated (the
373 %      spectral density of flux is a real quantity), which is done through
374 %      a multiplication
375 %      by "phase_shift_compensation_full_FFT_spectrum".
376 % --> All the angular frequency lists and quantities related to the
377 %      calculation of the FFT spectra
378 %      are defined in the "Init_lists_..." subprogram, for clarity.
379 %WDF-s for reflected field
380 WDF_interpolated_G1_reflected_vs_time_tau_full_spectrum = 1/(2*pi)*fftshift
381     (fft(interpolated_G1_reflected_vs_time_tau,nb_points_full_spectrum,2)
382     ,2)./(FFT_sampling_frequency)./
383     phase_shift_compensation_vs_omega_full_spectrum*(ev/hbar*1e-18); % 1/
384     (mueV*ps)
385 WDF_interpolated_reflected_coherent_vs_time_tau_full_spectrum = 1/(2*pi)*
386     fftshift(fft(interpolated_reflected_coherent_vs_time_tau,
387     nb_points_full_spectrum,2),2)./(FFT_sampling_frequency)./
388     phase_shift_compensation_vs_omega_full_spectrum*(ev/hbar*1e-18); % 1/
389     (mueV*ps)
390 WDF_interpolated_G1_reflected_vs_time_tau =
391     WDF_interpolated_G1_reflected_vs_time_tau_full_spectrum(:,%
392     index_min_zoomed_spectrum:index_max_zoomed_spectrum); % 1/(mueV*ps)
393 WDF_interpolated_reflected_coherent_vs_time_tau =
394     WDF_interpolated_reflected_coherent_vs_time_tau_full_spectrum(:,%
395     index_min_zoomed_spectrum:index_max_zoomed_spectrum); % 1/(mueV*ps)
396
397 %WDF-s for transmitted field
398 WDF_interpolated_G1_transmitted_vs_time_tau_full_spectrum = 1/(2*pi)*
399     fftshift(fft(interpolated_G1_transmitted_vs_time_tau,
400     nb_points_full_spectrum,2),2)./(FFT_sampling_frequency)./
401     phase_shift_compensation_vs_omega_full_spectrum*(ev/hbar*1e-18); % 1/
402     (mueV*ps)
```

```

379 WDF_interpolated_transmitted_coherent_vs_time_tau_full_spectrum = 1/(2*pi)*
    fftshift(fft(interpolated_transmitted_coherent_vs_time_tau,
    nb_points_full_spectrum,2),2)./(FFT_sampling_frequency)./
    phase_shift_compensation_vs_omega_full_spectrum*(ev/hbar*1e-18); % 1/(
    mueV*ps)
380 WDF_interpolated_G1_transmitted_vs_time_tau =
    WDF_interpolated_G1_transmitted_vs_time_tau_full_spectrum(:,,
    index_min_zoomed_spectrum:index_max_zoomed_spectrum);% 1/(mueV*ps)
381 WDF_interpolated_transmitted_coherent_vs_time_tau =
    WDF_interpolated_transmitted_coherent_vs_time_tau_full_spectrum(:,,
    index_min_zoomed_spectrum:index_max_zoomed_spectrum);% 1/(mueV*ps)
382
383 %WDF-s for emitted field
384 WDF_interpolated_G1_emitted_vs_time_tau_full_spectrum = 1/(2*pi)*fftshift(
    fft(interpolated_G1_emitted_vs_time_tau,nb_points_full_spectrum,2),2)
    ./(FFT_sampling_frequency)./
    phase_shift_compensation_vs_omega_full_spectrum*(ev/hbar*1e-18); % 1/(
    mueV*ps)
385 WDF_interpolated_emitted_coherent_vs_time_tau_full_spectrum = 1/(2*pi)*
    fftshift(fft(interpolated_emitted_coherent_vs_time_tau,
    nb_points_full_spectrum,2),2)./(FFT_sampling_frequency)./
    phase_shift_compensation_vs_omega_full_spectrum*(ev/hbar*1e-18); % 1/(
    mueV*ps)
386 WDF_interpolated_G1_emitted_vs_time_tau =
    WDF_interpolated_G1_emitted_vs_time_tau_full_spectrum(:,,
    index_min_zoomed_spectrum:index_max_zoomed_spectrum);% 1/(mueV*ps)
387 WDF_interpolated_emitted_coherent_vs_time_tau =
    WDF_interpolated_emitted_coherent_vs_time_tau_full_spectrum(:,,
    index_min_zoomed_spectrum:index_max_zoomed_spectrum);% 1/(mueV*ps)
388
389 %WDF-s for diffracted field
390 WDF_interpolated_G1_diffracted_vs_time_tau_full_spectrum = 1/(2*pi)*
    fftshift(fft(interpolated_G1_diffracted_vs_time_tau,
    nb_points_full_spectrum,2),2)./(FFT_sampling_frequency)./
    phase_shift_compensation_vs_omega_full_spectrum*(ev/hbar*1e-18); % 1/(
    mueV*ps)
391 WDF_interpolated_diffracted_coherent_vs_time_tau_full_spectrum = 1/(2*pi)*
    fftshift(fft(interpolated_diffracted_coherent_vs_time_tau,
    nb_points_full_spectrum,2),2)./(FFT_sampling_frequency)./
    phase_shift_compensation_vs_omega_full_spectrum*(ev/hbar*1e-18); % 1/(
    mueV*ps)
392 WDF_interpolated_G1_diffracted_vs_time_tau =
    WDF_interpolated_G1_diffracted_vs_time_tau_full_spectrum(:,,
    index_min_zoomed_spectrum:index_max_zoomed_spectrum);% 1/(mueV*ps)

```

```

393 WDF_interpolated_diffracted_coherent_vs_time_tau =
394     WDF_interpolated_diffracted_coherent_vs_time_tau_full_spectrum(:,%
395     index_min_zoomed_spectrum:index_max_zoomed_spectrum);% 1/(mueV*ps)
396
397 %% Spectral energy density and spectral energy flux
398 % The projection property (see Wiki page linked above) of the WDF(t,omega)
399 % guarantees that its
400 % integral over the spectrum omega gives the photon flux as a function of
401 % time, whereas the integral of WDF over time gives the energy spectral
402 % density of the flux, which is shown in the spectrometer.
403 %
404 % As we saw above, however, the quantity  $\langle b'(t,\tau) b(t) \rangle$  is the sum of
405 % two contributions:
406 % – A contribution  $\langle b'(t,\tau) \rangle \langle b(t) \rangle$ , corresponding to the coherent
407 % part of the flux.
408 % – Complementary, a contribution  $\langle b'(t,\tau)b(t) \rangle - \langle b'(t,\tau) \rangle \langle b(t)$ 
409 %  $\rangle$ , induced by the incoherent
410 % part of the flux. This contribution tends towards zero for large
411 % delays.
412
413 ESD_reflected_photons_vs_omega = real(sum(
414     WDF_interpolated_G1_reflected_vs_time_tau,1))*time_step; % 1/mueV
415 ESD_coherent_reflected_photons_laser_vs_omega = real(sum(
416     WDF_interpolated_reflected_coherent_vs_time_tau,1))*time_step; % 1/mueV
417 ESD_transmitted_photons_vs_omega = real(sum(
418     WDF_interpolated_G1_transmitted_vs_time_tau,1))*time_step; % 1/mueV
419 ESD_coherent_transmitted_photons_laser_vs_omega = real(sum(
420     WDF_interpolated_transmitted_coherent_vs_time_tau,1))*time_step; % 1/
421     mueV
422 ESD_emitted_photons_vs_omega = real(sum(
423     WDF_interpolated_G1_emitted_vs_time_tau,1))*time_step; % 1/mueV
424 ESD_coherent_emitted_photons_laser_vs_omega = real(sum(
425     WDF_interpolated_emitted_coherent_vs_time_tau,1))*time_step; % 1/mueV
426 ESD_diffracted_photons_vs_omega = real(sum(
427     WDF_interpolated_G1_diffracted_vs_time_tau,1))*time_step; % 1/mueV
428 ESD_coherent_diffracted_photons_laser_vs_omega = real(sum(
429     WDF_interpolated_diffracted_coherent_vs_time_tau,1))*time_step; % 1/
430     mueV
431
432 %% %%%%%%%%%%%%%%%%
433 %% %%%%%%%%%%%%%%%%
434 %% %%%%%%%%%%%%%%%%
435 %% %%%%%%%%%%%%%%%%
436 %% %%%%%%%%%%%%%%%%
437 %% %%%%%%%%%%%%%%%%
438 %% %%%%%%%%%%%%%%%%
439 %% %%%%%%%%%%%%%%%%
440 % For plot selection:
441 % – g1 vs (t1,t2) : 'g'
442 % – G1 vs (t1,t2) : 'G'

```

```

423 % - interpolated G1 vs (time, tau): 'I'
424 % - WDF vs (time, omega) : 'W'
425 % - photon fluxes : 'F'
426
427 % - plot_choice = ['G'];
428 plot_choice = ['g';'G';'I';'W';'F'];
429 Plot2levelG1wdfPR;

```

C.1.5 Second-order correlation in CW

```

1 clear
2 clc
3 close all
4 %% %%%%%% Common basis to every programs based "two levels" %%%%%%
5 % Important note: these paths must be modified if needed
6 addpath(genpath('..\QotoolboxV015'));
7 addpath(genpath('..\CQED_subprograms'));
8 addpath(genpath('..\CQED device parameters'))
9 savepath
10
11 % In addition, for the mesolve function to operate the executable
12 % files (.exe) and batch files (.bat) contained in '[...] \QotoolboxV015\
13 % bin'
14 % have to be copied to a folder that is on the Windows system path,
15 % in the main hard drive where Windows is installed. This can be
16 % for example in: 'C:\Program Files\Matlab\R2014a\bin'.
17
18 % Warning: for the adiabatic version to converge, the tolerance in
19 % mesolve.m function must be reduced compared to the default values. For
20 % example:
21 % ode2file('ode_input.dat',L,rho0,t_list,struct('reltol',7e-8,'abstol',8e
22 % -8));
23
24 %% %%%%%%%% g2CW : photon-photon correlations under CW excitation %%%%%%
25 %%%%%%%% This section indexed "g2CW" computes the intensity correlations as a
26 % This section indexed "g2CW" computes the intensity correlations as a
27 % function of delay, i.e g2(tau), for the various optical fields. One
28 % checks that values of g2(0) and g2(infty) correspond to the
29 % expected ones, and that the photons emitted outside the mode are single
30 % photons (g2(0)=0). Depending on the detuning large bunchings with
31 % g2(0)>>1 can also be observed, on the transmitted field for example (cf
32 % PRL 101, 203602 2008) or in the strong-coupling regime (see for example
33 % Nature 575, 622–627(2019)).
34

```

```
35 % Warning: g2CW may not always lead to a proper numerical convergence,
36 % especially for very low incoming powers: this can be seen when we obtain
37 % absurd negative values of g(2) and/or noisy values of g2(infty) (instead
38 % of a smooth convergence to unity), and/or abrupt discontinuities in the
39 % g2(tau) function. This can usually be solved by adjusting the incoming
40 % power and/or the Fock space and/or the mesolve function (mainly the
41 % tolerances, and potentially the calculation algorithm). But it seems that
42 % the use of normalized density matrices (normalized = unity trace, even
43 % for conditional density matrices obtained after a detection event) is
44 % crucial to get the best numerical convergence.
45
46 % Choice of full model 'F' or adiabatic 'A'
47 model = 'F';
48
49 %%% Experimental conditions
50 detuning_QD_C_muev = 0; %Detuning between the QD and cavity frequencies, in
    mueV
51 eta_in = 1; % Injection efficiency for the incoming photons (depends on
    experimentally-achieved spatial coupling)
52 P_in_CW_pW=1000;% Incoming continuous-wave power in pW
53
54 Init2levelDeviceParametersOngoingTest;
55 Init2levelHilbertSpaceAndOperators;
56
57 %Incoming power
58 P_in_CW = P_in_CW_pW*1e-12;% Incoming power in W %%
59 b_in_CW = sqrt(eta_in*P_in_CW*1e-24/(hbar*omega_c)); % square root of the
    photon number per unit time, en ps-1/2
60
61 % Angular frequency of the incoming CW laser (fixed)
62 omega_laser_ev = omega_d_ev; % in eV
63 omega_laser = omega_laser_ev*ev/hbar*1e-12; % in rad/ps
64
65 %Parameters for the calculation of the time dynamics of g(2)(tau)
66 tau_max=800; % Maximal delay in ps (the minimal delay is fixed to 0 for
    calculations)
67 nb_points_time_g2CW=20000; %% Time resolution/number of iterations for the
    curves G(2)(tau)
68 tau_step_g2CW=(tau_max)/(nb_points_time_g2CW-1); % Duration of a time step
69 tau_list_g2CW = linspace(0,tau_max,nb_points_time_g2CW); % list of all the
    positive delays considered in the computation and plots
70 full_tau_list_g2CW = [fliplr(-tau_list_g2CW(2:end)) , tau_list_g2CW ]; %
    list of all negative and positive delays for the plots
71
72 % tic NB: "tic" is used as a "start" time for the measurement of the
73 % computing time between "tic" and "toc"
```

```

74
75 switch model
76     case 'A' % Adiabatic case
77
78         Delta = 2*(omega_laser-omega_c)/kappa; %normalized laser
79             detuning appearing in Eq.12 of the pdf notes
80
81         %%%%%%% Definition of the adiabatic-model Hamiltonian (which
82             depends on omega_laser)
83         H_CW = (omega_eff-omega_laser)*sigma_dag*sigma...
84             - li*sqrt(Gamma_0*eta_top)*(b_in_CW*sigma_dag/(1-li*Delta)
85             - b_in_CW'*sigma/(1+li*Delta)); % Hamiltonian (Eq.13 of
86             the pdf notes)
87
88
89         %% For the redefinition of the operator "a" acting in the QD
90             space
91         % (Eq. 10 of the pdf notes
92         a = -2*g*sigma/(kappa*(1-li*Delta_QDC))-2*sqrt(kappa_top)*
93             b_in_CW*Id/(kappa*(1-li*Delta)); %annihilation operator a
94             in adiabatic approximation
95
96         % UNUSED HERE: Ansatz for the annihilation operator, obtained
97             by taking the time derivative of "a" equal to 0
98             % (OK for CW but not for PR (pulsed regime) programs)
99             % a = -2*g*sigma/(kappa*(1-li*Delta))-2*sqrt(kappa_top)*b_in_CW
100                *Id/(kappa*(1-li*Delta));
101
102     case 'F' % Full model
103
104         %%%%%% Definition of the full-model Hamiltonian (which
105             depends on omega_laser)
106         H_CW = (omega_d-omega_laser)*sigma_dag*sigma...
107             + (omega_c-omega_laser)*a_dag*a...
108             + li*g*(sigma_dag*a-a_dag*sigma)...
109             - li*sqrt(kappa_top)*b_in_CW*(a_dag-a);
110
111 end % end of the "switch model"
112
113 %Superoperator associated with the coherent processes (Hamiltonian)
114 L_coh = -li * (spre(H_CW) - spost(H_CW));
115
116 %%%%%% Calculation of the Liouvillian superoperator
117 Liouvillian = L_coh + L_incoh; % Total Liouvillian superoperator including
118             both coherent processes (Hamiltonian) and incoherent processes (
119             dissipative jumps)

```

```
108
109 %%%%%%%% Calculation of the density matrix corresponding to the stationary
110 % state
111 rhoss_CW = steady(Liouvillian);
112 %%%%%%%% Definition of the output operators. These are general formulas
113 % for both the adiabatic and full model, depending on the choice of "a"
114 b_out = b_in_CW*Id + sqrt(kappa_top)*a; % definition of the operator b_out,
115 % i.e. the output operator for the reflected light, in ps^(-1/2)
116 c_out = sqrt(kappa_bottom)*a; % definition of the operator c_out, i.e. the
117 % output operator for the transmitted light, in ps^(-1/2)
118 d_out = sqrt(kappa_loss)*a; % definition of the operator d_out, i.e. the
119 % output operator for the diffracted/lost light, in ps^(-1/2)
120 % e_out = sqrt(gamma_sp)*sigma; % definition of the operator e_out, i.e.
121 % the output operator for the light spontaneously emitted outside the
122 % cavity mode, in ps^(-1/2), already defined in "
123 % Init_2level_Hilbert_space_and_operators.m"
124 % NB: in the adiabatic model the operators could also have been written
125 % directly as:
126 % b_out = b_in_CW*Id*(1-2*eta_top/(1-li*Delta))-sqrt(Gamma_0*eta_top)*sigma
127 % /(1-li*Delta_QDC); %output flux operator, (eq.12)
128 % c_out = -2*g*sqrt(kappa_bottom)*sigma/(kappa*(1-li*Delta_QDC))-2*sqrt(
129 % kappa_top*kappa_bottom)*b_in_CW*Id/(kappa*(1-li*Delta));
130 % d_out = -2*g*sqrt(kappa_loss)*sigma/(kappa*(1-li*Delta_QDC))-2*sqrt(
131 % kappa_top*kappa_loss)*b_in_CW*Id/(kappa*(1-li*Delta)); %annihilation
132 % operator a in adiabatic approximation
133 % Such formulas are obtained by directly replacing the value of "a" from
134 % the adiabatic model, and are thus equivalent to the above, more general
135 % definitions In addition, e_out is independent on the experimental
136 % conditions and thus defined in the subprogram
137 % "Init_2level_Hilbert_space_and_operators.m". It is given here for
138 % information and clarity purposes only
139
140 % Calculation of the total photon flux as a function of omega_laser
141 total_flux_injected_photons=abs(b_in_CW)^2; % total flux of injected
142 % photons taking into account eta_in (so only the photons coupled to the
143 % cavity mode), in ps-1
144 total_flux_reflected_photons=expect(b_out'*b_out,rhoss_CW);%flux in ps^(-1)
145 total_flux_transmitted_photons=expect(c_out'*c_out,rhoss_CW);%flux in ps
146 %^(-1)
147 total_flux_diffracted_photons=expect(d_out'*d_out,rhoss_CW);%flux in ps
148 %^(-1)
149 total_flux_emitted_photons=expect(e_out'*e_out,rhoss_CW);%flux in ps^(-1)
150
151 %%
```

```
139 %%%%%%%% Intensity correlations %%%%%%%%
140 % (method ensuring the best numerical convergence, using normalized density
141 % matrices in the mesolve functions)
142
143 %%% General notes on calculating two-time correlation functions, valid in
144 %%% PR and CW %%%
145
146 % Experimentally, the second order correlation function g2(t1,t2) is the
147 % ratio between two probabilities:
148 %   – the probability of detecting a photon at time t2 conditioned by a
149 %   first photon detected at time t1
150 %   – the probability of detecting a photon at time t2 without any
151 %   information on previous detections
152 % On the theory side, the standard definition of a normalized correlation
153 % function g2(t1,t2) is:
154 %    $g2(t1,t2) = \langle b'(t1)b'(t2)b(t2)b(t1) \rangle / \langle b'(t2)b(t2) \rangle \langle b'(t1)b(t1) \rangle$ 
155 % We thus need to make the link between both views, and derive a way to
156 % practically compute such quantities with the physical interpretation in
157 % mind.
158 % As a preliminary remark, the theoretical notations above consider the
159 % Heisenberg representation, where the operators vary in time but the
160 % density matrix is constant (equal to its initial value at t=0). For
161 % example:
162 %    $\langle b'(t1)b(t1) \rangle = \text{Trace} [ b'(t1)b(t1) * \rho(0) ]$ 
163 % Fortunately, to go to the Schrodinger evolution we can use a very useful
164 % rule, which tells us that we can put the time evolution in the density
165 % matrix (instead of the operators) to calculate any average value:
166 %    $\langle b'(t1)b(t1) \rangle = \text{Trace} [ b'(0)b(0) * \rho(t1) ]$ 
167 % In this Schrodinger representation the operators are constant and thus
168 % equal to their value at time 0, so that :
169 %    $\langle b'(t1)b(t1) \rangle = \text{Trace} [ b'b * \rho(t1) ]$ 
170 % This is why, to calculate  $\langle b'(t1)b(t1) \rangle$  we just have to start at t=0
171 % and make  $\rho(t)$  evolve up to time t1 using mesolve, then calculate the
172 % expectation value of  $b'b$ :
173 %    $\langle b'(t1)b(t1) \rangle = \text{expect} ( b'b, \rho(t1) )$ 
174
175 % Now, to calculate g2(t1,t2) we also have to switch from the
176 % Heisenberg definition to a practical quantity we can calculate, i.e. the
177 % expectation value of some operator on some density matrix. By definition
178 % in the Heisenberg representation:
179 %    $\langle b'(t1) b'(t2) b(t2) b(t1) \rangle = \text{Trace} [ b'(t1) b'(t2) b(t2) b(t1) * \rho(0) ]$ 
180 % But with a circular permutation inside the Trace this can also be seen as
181 %   :
182 %    $\langle b'(t1) b'(t2) b(t2) b(t1) \rangle = \text{Trace} [ b'(t2) b(t2) * b(t1)\rho(0)b'(t1) ]$ 
```

```
182 % This gives us some hint that the correlation function, in the Heisenberg
183 % representation, can be seen as the expectation value of b'b at time t2,
184 % starting at time t1 from a fictitious density matrix b(t1)rho(0)b'(t1).
185 % In the Schrodinger representation, however, the operators b and b' are
186 % constant and only the density matrix evolves between times 0 and t1, and
187 % between times t1 and t2. But we can also take into account the effect of
188 % a photon detection event at time t1, which leads to an abrupt change of
189 % the system density matrix between two times:
190 %     – time t=t1^(-): after evolution between 0 and t1, but just before a
191 %         click (photon detection event)
192 %     – time t=t1^(+): just after a click at time t1
193 % With this in mind, the idea is to compute < b'(t1) b'(t2) b(t2) b(t1) >
194 % thanks to three steps:
195 %     – evolution from 0 to t1^(-), leading to a density matrix rho(t1)
196 %         "just before a click"
197 %     – modification of the system state due to the detection event at t1,
198 %         leading to a different density matrix "just after a click"
199 %     – further evolution of the system between times t1^(+) and t2
200
201 % However, to physically interpret the results and to get a nice numerical
202 % convergence, we should not work with the fictitious density matrix
203 % b(t1)rho(0)b'(t1) in the Heisenberg representation, nor its equivalent in
204 % the Shrodinger representation b rho(t1) b', since it is not normalized
205 % (its trace is not unity). Instead we define the real/normalized density
206 % matrix obtained just after a detection event at time t1:
207 %     rho(t1, just after a click) = b rho(t1) b' / expect [ b'b , rho(t1)
208 % ]
209 % This is a valid density matrix since the denominator is :
210 %     expect [ b'b , rho(t1) ] = Trace [ b'b * rho(t1) ] = Trace [ b rho(
211 % t1) b' ],
212 % and thus "rho(t1, just after a click)" is well normalized with unity
213 % trace. This division by expect [ b'b , rho(t1) ] also makes sense since
214 % this quantity is equal to <b'b(t1)>, i.e. one of the two terms in the
215 % denominator of g2(t1,t2). From this density matrix at time t1^(+), we can
216 % then deduce the density matrix at time t2, leading to a density matrix
217 % "rho(t2, conditioned to a click at t1)". With these notations the
218 % quantity < b'(t1) b'(t2) b(t2) b(t1) > / < b'b(t1) > is equivalent to :
219 %     < b'(t1) b'(t2) b(t2) b(t1) > / < b'b'(t1) > = Trace[ b'b * rho(t2,
220 % conditioned to a click at t1) ]
221 % And with similar notations the quantity < b'b(t2) > is equivalent to:
222 %     < b'b'(t2) > = Trace [ b'b * rho(t2) ]
223 % So we find that the normalized correlation function g2(t1,t2) is indeed
224 % the ratio between two quantities:
225 %     – the photon flux at time t2, conditioned by a previous photon
226 %         detection event at time t1
227 %     – the photon flux at time t2, unconditioned
```

```

225 % This is exactly the experimentalist's definition of g2(t1,t2). Note that
226 % in CW we usually take t1 = 0 and t2 = tau, and we take the stationary
227 % density matrix state both for rho(t1) and rho (t2), since by definition
228 % it does not evolve with time: only the density matrix "rho(tau,
229 % conditioned to a click at time 0)", being different from the stationary
230 % state's density matrix, does evolve with the delay tau
231
232 % Normalized (unity trace) density matrices just after a click at time 0,
233 % for the various optical fields:
234 density_matrix_just_after_reflected_photon_detection=b_out*rhoss_CW*b_out'/
    total_flux_reflected_photons; % Density matrix just after a reflected
    photon click at time 0
235 density_matrix_just_after_transmitted_photon_detection=c_out*rhoss_CW*c_out'
    '/total_flux_transmitted_photons; % Density matrix just after a
    transmitted photon click at time 0
236 density_matrix_just_after_emitted_photon_detection=e_out*rhoss_CW*e_out'/
    total_flux_emitted_photons;% Density matrix just after an emitted (
    outside the mode) photon click at time 0
237
238 % Normalized density matrices as a function of the (positive) delay tau,
239 % conditioned on the detection of a click at time 0
240 density_matrix_vs_delay_after_reflected_photon_detection=mesolve(
    Liouvillian,density_matrix_just_after_reflected_photon_detection,
    tau_list_g2CW); %Density matrix at time tau, conditioned on a reflected
    photon click at time 0
241 density_matrix_vs_delay_after_transmitted_photon_detection=mesolve(
    Liouvillian,density_matrix_just_after_transmitted_photon_detection,
    tau_list_g2CW); %Density matrix at time tau, conditioned on a
    transmitted photon click at time 0
242 density_matrix_vs_delay_after_emitted_photon_detection=mesolve(Liouvillian,
    density_matrix_just_after_emitted_photon_detection,tau_list_g2CW); %
    Density matrix at time tau, conditioned on an emitted (outside the mode
    ) photon click at time 0
243
244 % Calculation of the normalized auto-correlation functions g2(tau), for
245 % positive delays and various optical fields
246 g2_reflected_vs_delay=expect(b_out'*b_out,
    density_matrix_vs_delay_after_reflected_photon_detection)/
    total_flux_reflected_photons; %Auto-correlation g(2)(tau) for the
    reflected light
247 g2_transmitted_vs_delay=expect(c_out'*c_out,
    density_matrix_vs_delay_after_transmitted_photon_detection)/
    total_flux_transmitted_photons; %Auto-correlation g(2)(tau) for the
    transmitted light

```

```

248 g2_emitted_vs_delay=expect(e_out'*e_out,
    density_matrix_vs_delay_after_emitted_photon_detection)/
    total_flux_emitted_photons; %Auto-correlation g(2)(tau) for the light
    emitted outside the mode
249
250 % Calculation of g2(tau) for both negative and positive delays
251 full_g2_reflected_vs_delay= [fliplr(g2_reflected_vs_delay(2:end) )
    g2_reflected_vs_delay ];
252 full_g2_transmitted_vs_delay= [fliplr(g2_transmitted_vs_delay(2:end) )
    g2_transmitted_vs_delay ];
253 full_g2_emitted_vs_delay= [fliplr(g2_emitted_vs_delay(2:end) )
    g2_emitted_vs_delay ];
254
255 % Calculation of the conditional occupation probabilities, as a function
256 % of the delay tau after a photon detection event
257 occupation_ground_vs_delay_after_reflected_photon_detection=expect(sigma*
    sigma_dag,density_matrix_vs_delay_after_reflected_photon_detection);
258 occupation_excited_vs_delay_after_reflected_photon_detection=expect(
    sigma_dag*sigma,
    density_matrix_vs_delay_after_reflected_photon_detection);
259 occupation_ground_vs_delay_after_transmitted_photon_detection=expect(sigma*
    sigma_dag,density_matrix_vs_delay_after_transmitted_photon_detection);
260 occupation_excited_vs_delay_after_transmitted_photon_detection=expect(
    sigma_dag*sigma,
    density_matrix_vs_delay_after_transmitted_photon_detection);
261 occupation_ground_vs_delay_after_emitted_photon_detection=expect(sigma*
    sigma_dag,density_matrix_vs_delay_after_emitted_photon_detection);
262 occupation_excited_vs_delay_after_emitted_photon_detection=expect(sigma_dag*
    *sigma,density_matrix_vs_delay_after_emitted_photon_detection);
263
264 %toc
265
266 %% UNUSED HERE: alternative method with non-normalized conditional density
267 %% matrices
268 % NB: we denote G2(tau) (with a capital "G") the non-normalized intensity
269 % correlations of the form  $\langle b'(0) b'(\tau) b(\tau) b(0) \rangle$ , where the output
270 % fields are in  $\{1/2\}$ . Complementary, we denote g2(tau) the normalized
271 % intensity correlations  $\langle b'(0) b'(\tau) b(\tau) b(0) \rangle / \langle b' b \rangle \langle b' b \rangle$ 
272
273 % rho_vs_delay_if_rho0_equal_a_rhooss_a_dag=mesolve(Liouvillian,a*rhooss_CW*
    a_dag,tau_list_g2CW); % Sufficient to calculate correlations for c_out
    =sqrt(kappa_bottom)a et d_out=sqrt(kappa_loss)a
274 % rho_vs_delay_if_rho0_equal_sigma_rhooss_sigma_dag=mesolve(Liouvillian,
    sigma*rhooss_CW*sigma_dag,tau_list_g2CW); % Sufficient to calculate
    correlations of e_out=sqrt(gamma_sp) sigma

```

```

275 % rho_vs_delay_if_rho0_equal_rhoss_a_dag=mesolve(Liouvillian,rhoss_CW*a_dag
276 % ,tau_list_g2CW); % Necessary to calculate correlations of b_out=b_in+
277 % sqrt(kappa_top) a
278 % rho_vs_delay_if_rho0_equal_a_rhoss=mesolve(Liouvillian,a*rhoss_CW,
279 % tau_list_g2CW); % Necessary to calculate correlations of b_out=b_in+
280 % sqrt(kappa_top) a
281 %
282 % G2_reflected_vs_tau= kappa_top*expect(b_out'*b_out,
283 % rho_vs_delay_if_rho0_equal_a_rhoss_a_dag)...
284 % + abs(b_in_CW)^2*expect(b_out'*b_out,rhoss_CW)...
285 % + sqrt(kappa_top)*b_in_CW*expect(b_out'*b_out,
286 % rho_vs_delay_if_rho0_equal_a_rhoss)...+
287 % sqrt(kappa_top)*conj(b_in_CW)*expect(b_out'*b_out,
288 % rho_vs_delay_if_rho0_equal_rhoss_a_dag);
289 % G2_transmitted_vs_tau=kappa_bottom*expect(c_out'*c_out,
290 % rho_vs_delay_if_rho0_equal_a_rhoss_a_dag);
291 % G2_diffracted_vs_tau=kappa_loss*expect(d_out'*d_out,
292 % rho_vs_delay_if_rho0_equal_a_rhoss_a_dag);
293 % G2_emitted_vs_tau=gamma_sp*expect(e_out'*e_out,
294 % rho_vs_delay_if_rho0_equal_sigma_rhoss_sigma_dag);
295 %
296 %
297 % %%% Calculation of the G(2) for all delays, through the symmetrization
298 % G2(tau) = conj(G2(-tau))
299 % full_G2_reflected_vs_tau = [fliplr(G2_reflected_vs_tau(2:end) )
300 % G2_reflected_vs_tau ];
301 % full_G2_transmitted_vs_tau = [fliplr(G2_transmitted_vs_tau(2:end) )
302 % G2_transmitted_vs_tau ];
303 % full_G2_diffracted_vs_tau = [fliplr(G2_diffracted_vs_tau(2:end) )
304 % G2_diffracted_vs_tau ];
305 % full_G2_emitted_vs_tau = [fliplr(G2_emitted_vs_tau(2:end) )
306 % G2_emitted_vs_tau ];
307 %
308 % %%% Calculation of the normalized g(2) for all delays
309 % full_g2_reflected_vs_delay = full_G2_reflected_vs_tau/(
310 % total_flux_reflected_photons)^2;
311 % full_g2_transmitted_vs_tau = full_G2_transmitted_vs_tau/(
312 % total_flux_transmitted_photons)^2;
313 % full_g2_diffracted_vs_tau = full_G2_diffracted_vs_tau/(
314 % total_flux_diffracted_photons)^2;
315 % full_g2_emitted_vs_tau = full_G2_emitted_vs_tau/(
316 % total_flux_emitted_photons^2);
317 %
318 %
319 % %%%%%%%% Plots %%%%%%%
320 % For plot selection:

```

```
302 % – g2 from reflected photons : 'R'  
303 % – g2 from transmitted + diffracted/lost photons : 'T'  
304 % – g2 from photons emitted outside the mode : 'E'  
305 % – associated conditioned occupation probabilities : 'O'  
306  
307 %plot_choice = ['T'];  
308 plot_choice = ['T';'R';'E';'O'];  
309 Plot2LevelG2CWvsDelay;
```

C.1.6 Second-order correlation in PW

```
1 clear  
2 clc  
3 %close all  
4  
5 %% Important note: these paths must be modified if needed  
6 addpath(genpath('..\QotoolboxV015'));  
7 addpath(genpath('..\CQED subprograms'));  
8 addpath(genpath('..\CQED device parameters'))  
9 savepath  
10  
11 % In addition, for the mesolve function to operate the executable files  
12 % (.exe) and batch files (.bat) contained in '[...] \QotoolboxV015\bin'  
13 % have to be copied to a folder that is on the Windows system path, in the  
14 % main hard drive where Windows is installed. This can be for example in:  
15 % 'C:\Program Files\Matlab\R2014a\bin'.  
16  
17 % Warning: for the adiabatic version to converge, the tolerance in  
18 % mesolve.m function must be reduced compared to the default values. For  
19 % example:  
20 % ode2file('ode_input.dat',L,rho0,t_list,struct('reltol',7e-8,'abstol',8e  
-8));  
21  
22  
23 %%  
24 %%%%%%%% Intensity correlations in the pulsed regime  
25 %  
26 % This section indexed "g2PR_vs_t1_t2" computes the intensity correlations  
27 % in the pulsed regime, as a function of the detection times t1 and t2 in  
two
```

```
28 % detectors, for the various optical fields. The normalized function g2(t1,
29 % t2)
30 % is computed, as well as the coincidence maps determining the probability
31 % of
32 % having double-clicks, one at time t1 and the other at time t_2, during
33 % the same
34 % pulse or for uncorrelated pulses. The conditional occupation
35 % probabilities,
36 % modified by the detection of a first photon at time t1, are also computed
37 % , as
38 % well as the normalized g2 as a function of delay tau = t2 – t1, and the
39 % averaged
40 % g2(0), i.e. the area of the zero-delay peak of the normalized g2 function
41 %
42 %%%%%%%%%%%%%%%%
43 %
44 %
45 %
46 %
47 %
48 %
49 %
50 %
51 %
52 %
53 %
54 % Initialization of parameters, operators, arrays, etc...
```

```

55 Init2levelDeviceParametersOngoingTest;
56 Init2levelHilbertSpaceAndOperators;
57 InitMaps2LevelG2PRvsT1T2;
58
59 % Definition of the input field in ps^{(-1/2)}, in the form of a fseries (
    % necessary for integrating the master equation)
60 Standard_deviation_b_in_PR = FWHM_pulse/(2*sqrt(log(2))); %Deduced from the
    % properties of a gaussian function
61 b_in_fn = fn('gauss',t_delay,Standard_deviation_b_in_PR) * sqrt( eta_in*
    % Nb_photons_pulse / ( sqrt(pi) * Standard_deviation_b_in_PR ) );
    % square root of the incoming photon number per time unit, in ps^{-1/2}
62 b_in_vs_time = fsval(b_in_fn,t_list); %scalar array representing b_in vs
    % time
63
64 % Initial density matrix before the pulse has started
65 switch model
66     case 'F' %Full model
67         psi0 = tensor(Vacuum_state,g_ket); % Initial state: tensorial
            % product of photonic vacuum and QD ground state
68         rho0 = psi0*psi0'; % Density matrix corresponding to the initial
            % pure state
69     case 'A' % Adiabatic model
70         rho0 = g_ket*g_ket'; % Density matrix corresponding to the initial
            % pure state
71 end
72
73 %% %%%%%%%% System Hamiltonian and time-dependent operators %%%%%%%%
74 %
75 % The system Hamiltonian is time-dependent due to the function b_in_fn
76 % describing the input field b_in(t).
77
78 % In addition, in the case of adiabatic elimination of the cavity mode an
    % effective
79 % operator $a$ is defined, acting on the QD subspace, based on the formula
    % for
80 % adiabatic elimination (Eq. 10 of the pdf notes). Since this formula
    % depends
81 % on b_in(t), we define a time-dependent quantity "a_vs_time", which is an
82 % array containing, for each time of t_list, the corresponding operator
83 % "a".
84 % In the full model case, to simplify the following calculations, we define
    % the
85 % same quantity a_vs_time, yet this time this array contains the same
    % operator
86 % (annihilation operator "a" acting on the cavity subspace), replicated for
    % all

```

```

87 % times of t_list.
88
89
90 switch model
91     case 'A' % Adiabatic model
92
93         Delta = 2*(omega_pulse-omega_c)/kappa; %normalized laser
94             detuning appearing in Eq.12 of the pdf notes
95
96         %%%%%% Definition of the adiabatic-model Hamiltonian (in the
97             frame rotating at angular frequency omega_pulse)
98         H_PR = (omega_eff-omega_pulse)*sigma_dag*sigma - li*sqrt(
99             Gamma_0*eta_top)*...
100                ((1-li*Delta)^(-1)*b_in_fn*sigma_dag-(1+li*Delta)^(-1)*
101                    b_in_fn'*sigma); % Hamiltonian (eq.13)
102
103
104         %% Definition of the time-dependant operator "a_vs_time"
105             acting in the QD subspace (Eq. 10 of the pdf notes)
106         a_vs_time = -2*(kappa*(1-li*Delta_QDC))^( -1)*g*sigma*Id_vs_time
107             -2*sqrt(kappa_top)*(kappa*(1-li*Delta))^( -1)*fsval(b_in_fn,
108                 t_list).*Id_vs_time; %annihilation operator a in adiabatic
109                 approximation (eq.10), as fseries
110
111     case 'F' % Full model
112
113
114         %%%%%% Definition of the full-model Hamiltonian (in the
115             frame rotating at angular frequency omega_pulse)
116         H_PR = (omega_d-omega_pulse)*sigma_dag*sigma...
117             + (omega_c-omega_pulse)*a_dag*a...
118             + li*g*(sigma_dag*a-a_dag*sigma)...
119             - li*sqrt(kappa_top)*b_in_fn*(a_dag-a);
120
121
122         % Definition of the operator a_vs_time, even though "a" is
123             constant in the full model, to reduce the number of "switch
124             " in the following code
125         a_vs_time = a*Id_vs_time;
126
127
128 end % end of the "switch model"
129
130
131 %Superoperator associated to the coherent processes (Hamiltonian)
132 L_coh = -li * (spre(H_PR) - spost(H_PR));
133
134
135 %%%%%% Calculation of the Liouvillian superoperator
136 Liouvillian = L_coh + L_incoh; % Total Liouvillian superoperator including
137             both coherent processes (Hamiltonian) and incoherent processes (
138                 dissipative jumps)

```

```
120
121 %%%%%%%% Numerical Integration of the Master Equation %%%%%%%
122
123 % Computation of preliminary time evolution, between 0 (long before the
124 % pulse)
125 % and t_min (time at which we want to start plotting and integrating the
126 % physical
127 % quantities. Such a computation can be performed with very low time
128 % resolution,
129 % i.e. the corresponding t_list_before_t_min has a very low number of
130 % points,
131 % since the density matrix almost doesn't evolve between 0 and t_min.
132 %
133 % NB: such a preliminary time evolution is mandatory to avoid having
134 % strictly
135 % zero expectation values for some quantities (such as the input or output
136 % fields),
137 % during the following time evolution between t_min and t_max). Indeed,
138 % zero
139 % expectation values lead to NaN errors when used in normalizing physical
140 % quantities, such as conditional density matrices (see below), or
141 % Stokes/Bloch coordinates in the Poincare'/Bloch sphere.
142
143
144
145 %%%%%%%% Definition of the output operators %%%%%%%
146 % These are general formulas for both the adiabatic and full model,
147 % depending on "a_vs_time"
148 b_out_vs_time = b_in_vs_time*Id_vs_time + sqrt(kappa_top)*a_vs_time; %
149 % definition of the operator b_out, i.e. the output operator for the
150 % reflected light, in ps^(-1/2)
151 c_out_vs_time = sqrt(kappa_bottom)*a_vs_time; % definition of the operator
152 % c_out_vs_time, i.e. the output operator for the transmitted light, in
153 % ps^(-1/2)
```

```

150 % d_out_vs_time = sqrt(kappa_loss)*a_vs_time; % UNUSED HERE: definition of
      the operator d_out_vs_time, i.e. the output operator for the diffracted
      /lost light, in ps^(-1/2)
151 % e_out = sqrt(gamma_sp)*sigma % output operator for the light
      spontaneously emitted outside the cavity mode, in ps^(-1/2), already
      defined in Init_2level_Hilbert_space_and_operators.m
152
153 % Calculation of the total photon flux as a function of time, for the
      various optical fields
154 flux_injected_photons_vs_time = b_in_vs_time.^2; % total flux of injected
      photons taking into account eta_in (so only the photons coupled to the
      cavity mode), in ps(-1)
155 flux_reflected_photons_vs_time = real(expect(b_out_vs_time'*b_out_vs_time,
      density_matrix_vs_time)); %flux in ps^(-1)
156 flux_transmitted_photons_vs_time = real(expect(c_out_vs_time'*c_out_vs_time
      ,density_matrix_vs_time)); %flux in ps^(-1)
157 % flux_diffracted_photons_vs_time = real(expect(d_out_vs_time'*d_out_vs_time,
      rho_vs_time)); %flux in ps^(-1)
158 flux_emitted_photons_vs_time = real(expect(e_out'*e_out,
      density_matrix_vs_time)); %flux in ps^(-1)
159
160 %Computing the number of reflected/transmitted/emitted photons, by
      integrating over all times in t_list
161 Nb_reflected_photons = trapz(t_list,flux_reflected_photons_vs_time);
162 Nb_transmitted_photons = trapz(t_list,flux_transmitted_photons_vs_time);
163 % Nb_diffracted_photons = trapz(t_list,flux_diffracted_photons_vs_time);
164 Nb_emitted_photons = trapz(t_list,flux_emitted_photons_vs_time);
165
166
167 %% %%%%%%%%%%%%%%%%%%%%%%%%%%%%%%%%%%%%%%%%%%%%%%%%%%%%%%%%%%%%%%%%%%%%%%
168 %%%%%%%%%% Intensity correlations and conditional probabilities
      %%%%%%%%%%
169 %
      %%%%%%%%%%
170 % (method ensuring the best numerical convergence, using normalized density
171 % matrices in the mesolve functions)
172
173 %%% General notes on calculating two-time correlation functions, valid in
174 %%% PR (pulsed regime) and CW
175 %
176 % Experimentally, the second order correlation function g2(t1,t2) is the
177 % ratio between two probabilities:

```

```
178 % — the probability of detecting a photon at time t2 conditioned by a
179 % first
180 % — photon detected at time t1
180 % — the probability of detecting a photon at time t2 without any
181 % information
181 % on previous detections
182 %
183 % On the theory side, the standard definition of a normalized correlation
184 % function g2(t1,t2) is:
185 %      $g2(t1,t2) = \langle b'(t1)b'(t2)b(t2)b(t1) \rangle / \langle b'(t2)b(t2) \rangle \langle b'(t1)b(t1) \rangle$ 
186 %
187 % We thus need to make the link between both views, and derive a way to
188 % practically compute such quantities with the physical interpretation in
189 % mind.
190
191
192 % As a preliminary remark, the theoretical notations above consider the
193 % Heisenberg representation, where the operators vary in time but the
194 % density matrix is constant (equal to its initial value at t=0). For
195 % example:
196 %      $\langle b'(t1)b(t1) \rangle = \text{Trace} [ b'(t1)b(t1) * \rho(0) ]$ 
197 % Fortunately, to go to the Schrodinger evolution we can use a very useful
198 % rule, which tells us that we can put the time evolution in the density
199 % matrix (instead of the operators) to calculate any average value:
200 %      $\langle b'(t1)b(t1) \rangle = \text{Trace} [ b'(0)b(0) * \rho(t1) ]$ 
201 % In this Schrodinger representation the operators are constant and thus
202 % equal to their value at time 0, so that :
203 %      $\langle b'(t1)b(t1) \rangle = \text{Trace} [ b'b * \rho(t1) ]$ 
204 % This is why, to calculate  $\langle b'(t1)b(t1) \rangle$  we just have to start at t=0
205 % and make  $\rho(t)$  evolve up to time t1 using mesolve, then calculate the
206 % expectation value of  $b'b$ :
207 %      $\langle b'(t1)b(t1) \rangle = \text{expect} ( b'b, \rho(t1) )$ 
208
209 % Now, to calculate  $g2(t1,t2)$  we also also have to switch from the
210 % Heisenberg definition to a practical quantity we can calculate, i.e. the
211 % expectation value of some operator on some density matrix. By definition
212 % in the Heisenberg representation:
213 %      $\langle b'(t1) b'(t2) b(t2) b(t1) \rangle = \text{Trace} [ b'(t1) b'(t2) b(t2) b(t1) * \rho(0) ]$ 
214 % But with a circular permutation inside the Trace this can also be seen as
214 % :
215 %      $\langle b'(t1) b'(t2) b(t2) b(t1) \rangle = \text{Trace} [ b'(t2) b(t2) * b(t1)\rho(0)b'(t1) ]$ 
216
217 % This gives us some hint that the correlation function, in the Heisenberg
218 % representation, can be seen as the expectation value of  $b'b$  at time t2,
```

```
219 % starting at time t1 from a fictitious density matrix b(t1)rho(0)b'(t1).
220 % In the Schrodinger representation, however, the operators b and b' are
221 % constant and only the density matrix evolves between times 0 and t1, and
222 % between times t1 and t2. But we can also take into account the effect of
223 % a photon detection event at time t1, which leads to an abrupt change of
224 % the system density matrix between two times:
225 % — time t=t1^(-): after evolution between 0 and t1, but just before a
226 % click (photon detection event)
227 % — time t=t1^(+): just after a click at time t1
228 % With this in mind, the idea is to compute < b'(t1) b'(t2) b(t2) b(t1) >
229 % thanks to three steps:
230 % — evolution from 0 to t1^(-), leading to a density matrix rho(t1)
231 % "just before a click"
232 % — modification of the system state due to the detection event at t1,
233 % leading to a different density matrix "just after a click"
234 % — further evolution of the system between times t1^(+) and t2
235
236 % However, to physically interpret the results and to get a nice numerical
237 % convergence, we should not work with the fictitious density matrix
238 % b(t1)rho(0)b'(t1) in the Heisenberg representation, nor its equivalent in
239 % the Shrodinger representation b rho(t1) b', since it is not normalized
240 % (its trace is not unity). Instead we define the real/normalized density
241 % matrix obtained just after a detection event at time t1:
242 %     rho(t1, just after a click) = b rho(t1) b' / expect [ b'b , rho(t1
243 % ) ]
244 % This is a valid density matrix since the denominator is :
245 %     expect [ b'b , rho(t1) ] = Trace [ b'b * rho(t1) ] = Trace [ b rho(
246 % t1) b' ],
247 % and thus "rho(t1, just after a click)" is well normalized with unity
248 % trace. This division by expect [ b'b , rho(t1) ] also makes sense since
249 % this quantity is equal to <b'b(t1)>, i.e. one of the two terms in the
250 % denominator of g2(t1,t2). From this density matrix at time t1^(+), we can
251 % then deduce the density matrix at time t2, leading to a density matrix
252 % "rho(t2, conditioned to a click at t1)". With these notations the
253 % quantity < b'(t1) b'(t2) b(t2) b(t1) > / < b'b(t1) > is equivalent to :
254 %     < b'(t1) b'(t2) b(t2) b(t1) > / < b'b(t1) > = Trace[ b'b * rho(t2,
255 % conditioned to a click at t1) ]
256 % And with similar notations the quantity < b'b(t2) > is equivalent to:
257 %     < b'b(t2) > = Trace [ b'b * rho(t2) ]
258 % So we find that the normalized correlation function g2(t1,t2) is indeed
259 % the ratio between two quantities:
260 % — the photon flux at time t2, conditioned by a previous photon
261 % detection
```

```
262 % in CW we usually take t1 = 0 and t2 = tau, and we take the stationary
263 % density matrix state "rhoss" both for rho(t1) and rho (t2), since by
264 % definition rhoss does not evolve with time: only the density matrix
265 % "rho(tau, conditioned to a click at time 0)", being different from rhoss,
266 % does evolve with the delay tau
267 %%%%%%%%%%%%%%%%%%%%%%%%%%%%%%%%%%%%%%
268
269 %%%%%%%%%%%%%% Calculation of conditional density matrices
270 %%%%%%%%%%%%%%
271 % In the following the "density_matrix_vs_t1_just_after_click_OPERATOR"s
272 % are
273 % defined for each value of time t1 in t_list. Their N-th element represent
274 % the normalized density matrix just after a click has occurred at the N-th
275 % time.
276
277 %NB: "tic" is used as a "start" time for the measurement of the computing
278 % time between "tic" and "toc"
279 %tic
280
281 %Cycle over all times t1 in t_list, corresponding to the moment where a
282 % first click occurred
283 for t1_index = 1:nb_points_time
284
285 % Both t1 and t2 are values in t_list. However, to compute the
286 % normalized density matrices vs t2 after a click at t1, we consider
287 % only t2 >= t1, and we need to deal with the fact that there are less
288 % and less remaining values of t2 in t_list, when t1 increases. To keep
289 % all quantities defined in the full t_list, for each time t1 < t2 we
290 % have a "zero" density matrix, i.e. a fictitious density matrix with
291 % only zero elements-
292
293 % Incrementing the array of zero density matrices, each time t1_index
294 % is increased, to fill the density matrix for times t1 < t2
295 if (t1_index >=2) % No need to include a zero density matrix at the
296 % first value of t1
```

```

296     zero_density_matrix_vs_t2_before_t1{t1_index-1} = 0*Id; %null
         density matrix with the same dimensions of the involved Hilbert
         space
297 end
298
299 % Array of normalized density matrices, conditioned on the detection of
   a
300 % click at time t1, as a function of t2 >= t1 (and zero otherwise)
301 density_matrix_vs_t2_after_click_b_out_at_t1 = [
302     zero_density_matrix_vs_t2_before_t1 mesolve(Liouvillian,
303     density_matrix_vs_t1_just_after_click_b_out{t1_index},t_list(
304     t1_index:end))];
302 density_matrix_vs_t2_after_click_c_out_at_t1 = [
303     zero_density_matrix_vs_t2_before_t1 mesolve(Liouvillian,
304     density_matrix_vs_t1_just_after_click_c_out{t1_index},t_list(
305     t1_index:end))];
303 density_matrix_vs_t2_after_click_e_out_at_t1 = [
304     zero_density_matrix_vs_t2_before_t1 mesolve(Liouvillian,
305     density_matrix_vs_t1_just_after_click_e_out{t1_index},t_list(
306     t1_index:end))];
304
305 % Evaluation of g2(t1,t2) as described in the general notes above, for
   t2 >= t1 (and zero otherwise)
306 g2_reflected_vs_t1_t2(t1_index,:) = expect(b_out_vs_time'*b_out_vs_time
   ,density_matrix_vs_t2_after_click_b_out_at_t1)./
   flux_reflected_photons_vs_time; %Auto-correlation g(2)(tau) for the
   reflected light
307 g2_transmitted_vs_t1_t2(t1_index,:) = expect(c_out_vs_time'*
   c_out_vs_time,density_matrix_vs_t2_after_click_c_out_at_t1)./
   flux_transmitted_photons_vs_time; %Auto-correlation g(2)(tau) for the
   transmitted light
308 g2_emitted_vs_t1_t2(t1_index,:) = expect(e_out'*e_out,
   density_matrix_vs_t2_after_click_e_out_at_t1)./
   flux_emitted_photons_vs_time; %Auto-correlation g(2)(tau) for the
   light emitted outside the mode
309
310 % Calculation of the conditional occupation probabilities at time t2
   after
311 % a photon detection event at t1, for t2 >= t1 (and zero otherwise)
312 occupation_ground_vs_t1_vs_t2_after_click_b_out_at_t1(t1_index,:) =
   expect(sigma*sigma_dag,density_matrix_vs_t2_after_click_b_out_at_t1
   );
313 occupation_excited_vs_t1_vs_t2_after_click_b_out_at_t1(t1_index,:) =
   expect(sigma_dag*sigma,density_matrix_vs_t2_after_click_b_out_at_t1
   );

```

```

314     occupation_ground_vs_t1_vs_t2_after_click_c_out_at_t1(t1_index,:) =
315         expect(sigma*sigma_dag,density_matrix_vs_t2_after_click_c_out_at_t1
316             );
315     occupation_excited_vs_t1_vs_t2_after_click_c_out_at_t1(t1_index,:) =
316         expect(sigma_dag*sigma,density_matrix_vs_t2_after_click_c_out_at_t1
317             );
316     occupation_ground_vs_t1_vs_t2_after_click_e_out_at_t1(t1_index,:) =
317         expect(sigma*sigma_dag,density_matrix_vs_t2_after_click_e_out_at_t1
318             );
317     occupation_excited_vs_t1_vs_t2_after_click_e_out_at_t1(t1_index,:) =
318         expect(sigma_dag*sigma,density_matrix_vs_t2_after_click_e_out_at_t1
319             );
319
320 %toc
321
322 %%
323 %%%%% Completion of previous partially-calculated maps vs t1,t2, to include
324     the case where t2 < t1
325
325 % Due to the symmetry between t1 and t2 (we don't know which detector will
326 % click first), we have to use properties like g2(t1,t2)=g2(t2,t1) to fill
327 % the voids in the quantities that we have only partially calculated yet
328 % (since we systematically considered a zero value when t2 < t1. For each
329 % map function of t1 and t2, this completion is obtained by adding it to
330 % its transpose (to replace the zeros at t2 < t1) and dividing by 2 the
331 % elements along the diagonal (to avoid counting twice the case where
332 % t2=t1). This is done via an ad-hoc matrix idx below:
333
334 idx = ones(nb_points_time)-0.5*diag(ones(nb_points_time,1)); % to divide by
335     2 the elements along the diagonal
335
336 % Completed g2(t1,t2) for the various optical fields
337 g2_emitted_vs_t1_t2 = real((g2_emitted_vs_t1_t2+g2_emitted_vs_t1_t2.')).*
338     idx;
338 g2_reflected_vs_t1_t2 = real((g2_reflected_vs_t1_t2+g2_reflected_vs_t1_t2
339     .')).*idx;
339 g2_transmitted_vs_t1_t2 = real((g2_transmitted_vs_t1_t2+
340     g2_transmitted_vs_t1_t2.')).*idx;
341
341 %Completed conditional occupation probabilities for the excited and ground
342     state
342 occupation_ground_vs_t1_vs_t2_after_click_b_out_at_t1 = (
343     occupation_ground_vs_t1_vs_t2_after_click_b_out_at_t1+
344     occupation_ground_vs_t1_vs_t2_after_click_b_out_at_t1.').*idx;

```

```

343 occupation_excited_vs_t1_vs_t2_after_click_b_out_at_t1 = (
    occupation_excited_vs_t1_vs_t2_after_click_b_out_at_t1+
    occupation_excited_vs_t1_vs_t2_after_click_b_out_at_t1.*idx;
344 occupation_ground_vs_t1_vs_t2_after_click_c_out_at_t1 = (
    occupation_ground_vs_t1_vs_t2_after_click_c_out_at_t1+
    occupation_ground_vs_t1_vs_t2_after_click_c_out_at_t1.*idx;
345 occupation_excited_vs_t1_vs_t2_after_click_c_out_at_t1 = (
    occupation_excited_vs_t1_vs_t2_after_click_c_out_at_t1+
    occupation_excited_vs_t1_vs_t2_after_click_c_out_at_t1.*idx;
346 occupation_ground_vs_t1_vs_t2_after_click_e_out_at_t1 = (
    occupation_ground_vs_t1_vs_t2_after_click_e_out_at_t1+
    occupation_ground_vs_t1_vs_t2_after_click_e_out_at_t1.*idx;
347 occupation_excited_vs_t1_vs_t2_after_click_e_out_at_t1 = (
    occupation_excited_vs_t1_vs_t2_after_click_e_out_at_t1+
    occupation_excited_vs_t1_vs_t2_after_click_e_out_at_t1.*idx;
348
349
350 %% %%%%%%%%%%%%%%%%
351 %%%%%% Coincidence maps as a function of t1, t2 %%%%%%
352 %%%%%%
353
354 % This part computes quantities such as :
355 % - < b_out'(t1) b_out'(t2) b_out(t2) b_out(t1) >, which is proportional
356 % to the probability of detecting two reflected photons at time t1 and
357 % t2
358 % in two detectors, during the same pulse (correlated clicks)
359 % - < b_out'(t1) b_out(t1) > < b_out'(t2) b_out(t2) >, which is
360 % proportional
361 % to the probability of detecting two reflected photons at time t1 and
362 % t2
363 % in two detectors, but for different pulses (uncorrelated clicks)
364
365 % Uncorrelated photon_coincidences vs (t1,t2), e.g. <b_out'(t1)b_out(t1)> <
366 % b_out'(t2)b_out(t2)>
367 emitted_photon_coincidences_vs_t1_vs_t2_uncorrelated_pulses = real(expect(
    e_out'*e_out,density_matrix_vs_time))*real(expect(e_out'*e_out,
    density_matrix_vs_time));
368 reflected_photon_coincidences_vs_t1_vs_t2_uncorrelated_pulses = real(expect(
    (b_out_vs_time'*b_out_vs_time,density_matrix_vs_time))*real(expect(
    b_out_vs_time'*b_out_vs_time,density_matrix_vs_time));
369 transmitted_photon_coincidences_vs_t1_vs_t2_uncorrelated_pulses = real(
    expect(c_out_vs_time'*c_out_vs_time,density_matrix_vs_time))*real(
    expect(c_out_vs_time'*c_out_vs_time,density_matrix_vs_time));
370
371 % Correlated photon_coincidences vs (t1,t2), e.g. <b_out'(t1) b_out'(t2)
372 % b_out(t2) b_out(t1)>

```

```

368 emitted_photon_coincidences_vs_t1_vs_t2 = g2_emitted_vs_t1_t2.*  

    emitted_photon_coincidences_vs_t1_vs_t2_uncorrelated_pulses;  

369 reflected_photon_coincidences_vs_t1_vs_t2 = g2_reflected_vs_t1_t2.*  

    reflected_photon_coincidences_vs_t1_vs_t2_uncorrelated_pulses;  

370 transmitted_photon_coincidences_vs_t1_vs_t2 = g2_transmitted_vs_t1_t2.*  

    transmitted_photon_coincidences_vs_t1_vs_t2_uncorrelated_pulses;  

371  

372 %% %%%%%%%%%%%%%%% %%%%%%%%%%%%%%% %%%%%%%%%%%%%%% %%%%%%%%%%%%%%% %%%%%%%%%%%%%%%  

373 %%%%%%%%%%%%%%% Normalized g2(tau) %%%%%%%%%%%%%%% %%%%%%%%%%%%%%% %%%%%%%%%%%%%%%  

374 %%%%%%%%%%%%%%% %%%%%%%%%%%%%%% %%%%%%%%%%%%%%% %%%%%%%%%%%%%%% %%%%%%%%%%%%%%%  

375 %  

376 % As in a standard HBT experiment in the pulsed regime, g2(tau) is obtained  

377 % by defining an histogram integrating all the coincidences corresponding  

378 % to a given delay tau (with tau = t2 – t1 being positive or negative). The  

379 % normalization choice here is that the area of the g2(tau) peak is unity  

380 % for uncorrelated coincidences, i.e. for all peaks except the zero-delay  

381 % peak.  

382  

383 % Normalized g2 (tau) for the zero-delay peak, corresponding to photons  

    emitted  

384 % within the same pulse. It is obtained from the correlated coincidence  

    map  

385 %  $\langle b'(t_1)b'(t_2)b(t_2)b(t_1) \rangle$ , by integrating over all values corresponding to  

    a  

386 % given delay tau = t2 – t1, with a time bin t_step, and normalizing by  

    Nb_photons^2.  

387 % Note that tau = 0 for t1=t2, corresponding to the diagonal elements of  

    the  

388 % g2(t1,t2) map, while non-zero delays are obtained outside the diagonal.  

389 for j = 1:nb_points_time  

390     normalized_g2_vs_delay_emitted(j) = real(sum(diag(  

        emitted_photon_coincidences_vs_t1_vs_t2,j)))*t_step/  

        Nb_emitted_photons^2;  

391     normalized_g2_vs_delay_reflected(j) = real(sum(diag(  

        reflected_photon_coincidences_vs_t1_vs_t2,j)))*t_step/  

        Nb_reflected_photons^2;  

392     normalized_g2_vs_delay_transmitted(j) = real(sum(diag(  

        transmitted_photon_coincidences_vs_t1_vs_t2,j)))*t_step/  

        Nb_transmitted_photons^2;  

393 end  

394  

395 % Normalized g2 (tau) for the other peaks, corresponding to photons emitted  

396 % within different pulses. It is obtained from the uncorrelated coincidence  

    map  

397 %  $\langle b'(t_2)b(t_2) \rangle \langle b'(t_1)b(t_1) \rangle$ , by integrating over all values corresponding  

    to a

```

```

398 % given delay tau = t2 - t1, with a time bin t_step, and normalizing by
  Nb_photons^2.
399 for j = 1:nb_points_time
400     normalized_g2_vs_delay_uncorrelated_emitted(j) = real(sum(diag(
        emitted_photon_coincidences_vs_t1_vs_t2_uncorrelated_pulses,j)))*
        t_step/Nb_emitted_photons^2;
401     normalized_g2_vs_delay_uncorrelated_reflected(j) = real(sum(diag(
        reflected_photon_coincidences_vs_t1_vs_t2_uncorrelated_pulses,j)))*
        t_step/Nb_reflected_photons^2;
402     normalized_g2_vs_delay_uncorrelated_transmitted(j) = real(sum(diag(
        transmitted_photon_coincidences_vs_t1_vs_t2_uncorrelated_pulses,j)))
        )*t_step/Nb_transmitted_photons^2;
403 end
404
405 %% %%%%%%%%%%%%%% Mean g2 for the zero delay peak %%%%%%%%%%%%%%
406 %%%%%%%%%%%%%% Mean g2 for the zero delay peak %%%%%%%%%%%%%%
407 %%%%%%%%%%%%%% Mean g2 for the zero delay peak %%%%%%%%%%%%%%
408
409 % In the pulsed regime, what experimentalists usually call the g2(0) is in
410 % fact the mean value of g2(tau) for the zero-delay peak, or more precisely
411 % the area of the normalized g2(tau) curve for the zero-delay peak, as
  compared
412 % to the unity area obtained for the other uncorrelated peaks.
413
414 % Area of normalized g2(tau) for the zero-delay/correlated peak
415 mean_g2_zero_delay_peak_reflected_photons = trapz(full_tau_list,[flip(
    normalized_g2_vs_delay_reflected(2:end))
    normalized_g2_vs_delay_reflected]);
416 mean_g2_zero_delay_peak_transmitted_photons = trapz(full_tau_list,[flip(
    normalized_g2_vs_delay_transmitted(2:end))
    normalized_g2_vs_delay_transmitted]);
417 mean_g2_zero_delay_peak_emitted_photons = trapz(full_tau_list,[flip(
    normalized_g2_vs_delay_emitted(2:end)) normalized_g2_vs_delay_emitted])
  ;
418
419 % Area of normalized g2(tau) for the zero-delay/correlated peak
420 mean_g2_uncorrelated_peaks_reflected_photons = trapz(full_tau_list,[flip(
    normalized_g2_vs_delay_uncorrelated_reflected(2:end))
    normalized_g2_vs_delay_uncorrelated_reflected]);
421 mean_g2_uncorrelated_peaks_transmitted_photons = trapz(full_tau_list,[flip(
    normalized_g2_vs_delay_uncorrelated_transmitted(2:end))
    normalized_g2_vs_delay_uncorrelated_transmitted]);
422 mean_g2_uncorrelated_peaks_emitted_photons = trapz(full_tau_list,[flip(
    normalized_g2_vs_delay_uncorrelated_emitted(2:end))
    normalized_g2_vs_delay_uncorrelated_emitted]);
423

```

```
424
425
426
427 %% %%%%%%%%%%%%%%%%
428 %%%%%%%%%%%%%% Plots %%%%%%%%%%%%%%
429 %%%%%%%%%%%%%%%%
430
431 % For plot selection:
432 % – g2 vs (t1,t2) : 'G'
433 % – photon coincidences (correlated and not) vs (t1,t2) : 'C'
434 % – ground state occupations vs (t1,t2) : 'O'
435 % – photon fluxes vs time & g2 vs delay : 'F'
436
437 % plot_choice = ['G'];
438 plot_choice = ['G';'C';'O';'F'];
439 Plot2LevelG2PRvsT1T2;
```

C.2 CQED device parameters

```
1 if ~ismember(model,['F'; 'A'])
2     f = errordlg('Not valid input for full / adiabatic model selection.','
3                 Error');
4 end
5 %%% Physical constants (do not change) %%%
6 ev=1.60217646e-19;h=6.626068e-34; hbar=h/(2*pi);
7
8 % Parameters: energies of the mode ("c" for "cavity" and of the QD ("d" for
9 % "dot") in eV. NB: all variable names have to end in "_ev" when they are
10 % in electron–volts. Afterwards the energies in electron–volts will all be
11 % converted in angular frequencies in rad/ps for subsequent calculations.
12 omega_c_ev = 1.329810; % Cavity mode energy
13 omega_d_ev = omega_c_ev + detuning_QD_C_muev*1e-6; % QD transition energy
14
15 % Parameters of the QD (in ueV as indicated by the name ending by "_muev"
16 g_muev = 17; % Light matter coupling in mueV
17 gamma_sp_muev = 0.6; %Spontaneous emission of leaky modes (i.e. not in the
18 %cavity mode)
19 gamma_puredephasing_muev = 0; %Pure dephasing in mueV
20 gamma_decoherence_muev = gamma_sp_muev/2 + gamma_puredephasing_muev;
21
22 %Parameters of the cavity
23 kappa_muev = 400; % Cavity intensity decay rate, in ueV
24 eta_top = 0.7; %Extraction efficiency for the top Bragg mirror
25 eta_bottom = 0.1; %Extraction efficiency for the bottom Bragg mirror
```

```

26 eta_loss = 1-eta_top-eta_bottom; %Losses induced by lateral diffraction or
27 % absorption
28 % Conversions in rad/ps
29 omega_c = omega_c_ev*ev/hbar*1e-12; %in rad/ps
30 omega_d = omega_d_ev*ev/hbar*1e-12; %in rad/ps
31 g = g_muev*10^-6*ev/hbar*1e-12; %in rad/ps
32 gamma_decoherence = gamma_decoherence_muev*1e-6*ev/hbar*1e-12; %in rad/ps
33 gamma_sp = gamma_sp_muev*1e-6*ev/hbar*1e-12; %in rad/ps
34 gamma_puredephasing = gamma_puredephasing_muev*1e-6*ev/hbar*1e-12; %in rad
35 %/ps
36 kappa = kappa_muev*1e-6*ev/hbar*1e-12; %in rad/ps
37 kappa_top = kappa*eta_top; %in rad/ps
38 kappa_bottom = kappa*eta_bottom; %in rad/ps
39 kappa_loss = kappa*eta_loss; %in rad/ps
40 if strcmp(model,'F')
41     N=10; %Maximal number of photons in the cavity mode (troncature of the
42 % Fock space if complete model is used)
43 end
44 % Parameters useful for physical interpretation of data, and required for
45 % the "adiabatic elimination" model
46 Delta_QDC = 2*(omega_d-omega_c)/kappa; %normalized QD-cavity detuning
47 Gamma_0 = 4*g^2/kappa; %Purcell-enhanced emission rate at zero detuning
48 Gamma_m = Gamma_0/(1 + Delta_QDC^2); % Purcell-enhanced emission rate
49 Gamma_tot = Gamma_m + gamma_sp; %total emission rate
50 omega_eff = omega_d + 0.5*Gamma_0*Delta_QDC/(1 + Delta_QDC^2); %cavity
      induced frequency shift

```

C.3 Subprograms

C.3.1 mesolve

```

1 % Function developed by Sze Meng Tan. A quantum optics toolbox, 1999
2 function [rho] = mesolve(L,rho0,t_list)
3 %%%%%%%%%%%%%%% L : Liouvillian use in the Master Equation
4 %%%%%%%%%%%%%%% rho 0 : Initial Condition for the solving of the ME
5 %%%%%%%%%%%%%%% t_list : time list containing each time value where the
6 %%%%%%%%%%%%%%% Density Matrix will be calculated thanks to the routine
7
8 %%%%%%%%%%%% Numerical Integration of the Master Equation %%%%%%
9
10
11 ode2file('ode_input.dat',L,rho0,t_list,struct('reltol',7e-8,'abstol',8e-7))
    ; % Writes the data into a file

```

```

12 odesolve('ode_input.dat','ode_output.dat'); % Solve/Integration (here Adams
    method by default)
13 fid = fopen('ode_output.dat','rb');
14 rho = qoread(fid,dims(rho0),size(t_list));
15 fclose(fid);
16 %%%%%%%%%%%%%%%% rho : list of the Density Matrix calculated for each
17 %%%%%%%%%%%%%%%% time specified in the list

```

C.3.2 Init 2level Hilbert space and operators

```

1 switch model
2   case 'F'
3     %%%%%%%%%%%%%%%% Sub-space "quantum dot" %%%%%%%%%%%%%%%
4
5     %Basis states for the quantum dot (g for "ground", e for "excited")
6     g_ket=qo([1;0]); %% Quantum object "ket" associated to the ground
      state
7     g_bra=g_ket'; %% Quantum object "bra" associated to the ground
      state
8     e_ket=qo([0;1]); %% Quantum object "ket" associated to the excited
      state
9     e_bra=e_ket'; %% Quantum object "bra" associated to the excited
      state
10
11    %Operators acting in the sub-space of the 2-level QD system (2x2
      matrixs)
12    id_QD=e_ket*e_bra+g_ket*g_bra; % Quantum object "Identity operator"
13    sigma_QD=g_ket*e_bra; % Quantum object "de-excitation of the 2-
      level system"
14    sigma_dag_QD=sigma_QD'; % Quantum object "excitation of the 2-level
      system"
15
16    %%%%%%%%%%%%%%%% Sub-space "cavity" %%%%%%%%%%%%%%%
17    %N denotes the maximal number of photons in the truncated Fock
      space (see above)
18    id_cav = identity(N); % Quantum object "Identity operator" (
      matrix NxN)
19    destroy_cav=destroy(N);% Quantum object "annihilation operator" (
      matrix NxN)
20    Vacuum_state=basis(N,1); % State corresponding to photon vacuum |0>
      (Nx1)
21
22    last_Fock_state_ket = basis(N,N);% State corresponding to the last
      Fock state |N-1>, to control its occupation probability
23

```

```

24 %
%%%%%
25 %%%%%% Operators acting in the product space cavity-quantum dot
26 % (matrices 2Nx2N)
27 Id= tensor(id_cav,id_QD); % Tensorial product of identities in the
28 % cavity and QD subspace
29 sigma = tensor(id_cav,sigma_QD); % De-excitation operator from the
30 % excited QD state to the ground QD state
31 sigma_dag = sigma'; % De-excitation operator from the ground QD
32 % state to the excited QD state
33
34 a=tensor(destroy_cav,id_QD); % Annihilation operator for a photon
35 % in the cavity mode
36 a_dag=a'; % Creation operator for a photon in the cavity mode
37 n=a_dag*a; % Intracavity photon number operator
38
39 occupation_last_Fock_state=tensor(last_Fock_state_ket*
40 %%%%%% operator for the occupation of
41 % the last Fock state, to control that it remains low
42
43 %%%%%% Definition of Collapse operators
44 %%%%%%
45 C_cav = sqrt(kappa)*a; %Collapse operator for the cavity
46 C_sp = sqrt(gamma_sp)*sigma; % Collapse operator for a spontaneous
47 % emission outside the cavity mode
48 C_pure_dephasing = sqrt(2*gamma_puredephasing)*sigma_dag*sigma; %
49 % Collapse operator for pure dephasing
50
51 % Lindblad operators associated to each incoherent process
52 L_cav = 1/2 * (2*spre(C_cav)*spost(C_cav') - spre(C_cav'*C_cav) -
53 % 1st terme: cavity dumping
54 spost(C_cav'*C_cav));%
55 L_sp = 1/2 * (2*spre(C_sp)*spost(C_sp') - spre(C_sp'*C_sp) - spost(
56 % 2nd terme: exciton lifetime
57 C_sp'*C_sp));%
58 L_pure_dephasing = 1/2 * (2*spre(C_pure_dephasing)*spost(
59 % 3rd term: pure dephasing
60 C_pure_dephasing') - spre(C_pure_dephasing'*C_pure_dephasing) -
61 spost(C_pure_dephasing'*C_pure_dephasing));%
62
63 % Lindblad operator associated to all the incoherent processes
64 L_incoh=L_cav+L_sp+L_pure_dephasing;
65
66 case 'A'
67 %%%%%% space "quantum dot" %%%%%%

```

```

53
54      %Basis states for the quantum dot (g for "ground", e for "excited")
55      g_ket=qo([1;0]); %% Quantum object "ket" associated to the ground
56          state
57      g_bra=g_ket'; %% Quantum object "bra" associated to the ground
58          state
59      e_ket=qo([0;1]); %% Quantum object "ket" associated to the excited
60          state
61      e_bra=e_ket'; %% Quantum object "bra" associated to the excited
62          state
63
64      %Operators acting in the sub-space of the 2-level QD system (2x2
65          matrixs)
66      Id=e_ket*e_bra+g_ket*g_bra; % Quantum object "Identity operator"
67      sigma=g_ket*e_bra; % Quantum object "de-excitation of the 2-level
68          system"
69      sigma_dag=sigma'; % Quantum object "excitation of the 2-level
70          system"
71
72      %%%%%%%%%%%%%% Definition of Collapse operators
73      %%%%%%%%%%%%%%
74      C_QD = sqrt(Gamma_tot)*sigma; % Collapse operator for a spontaneous
75          emission outside the cavity mode (eq.15)
76      C_pure_dephasing = sqrt(2*gamma_puredephasing)*sigma_dag*sigma; %
77          Collapse operator for pure dephasing
78
79      % Lindblad operators associated to each incoherent process
80      L_QD = 1/2 * (2*spre(C_QD)*spost(C_QD') - spre(C_QD'*C_QD) ...
81          - spost(C_QD'*C_QD));% exciton lifetime
82      L_pure_dephasing = 1/2 * (2*spre(C_pure_dephasing)*spost(
83          C_pure_dephasing') - spre(C_pure_dephasing'*C_pure_dephasing) -
84          spost(C_pure_dephasing'*C_pure_dephasing));% 3rd term: pure
85          dephasing
86
87      % Lindblad operator associated to all the incoherent processes
88      L_incoh=L_QD+L_pure_dephasing;
89
90      % NB: in the adiabatic model L_QD includes both the emission
91          outside the mode
92      % and the Purcell-enhanced emission through the cavity mode, hence
93          the
94      % "Gamma_tot" term in the definition of C_QD
95
96      end
97
98

```

```

83 %%%%%%%% Constant output operator used to describe the field emitted
84     outside the mode
85 e_out=sqrt(gamma_sp)*sigma; % Output flux operator in ps^(-1/2)
86
87 % NB: the other output flux operators can be power-dependent or frequency-
88     dependent, depending on the model used
89 % (full or adiabatic). They are thus defined in the main file. Also note
90     that e_out is equal to C_sp, but we use
91 % a different notation to insist on its use as an output operator,
92     analogous to the other output operators b_out,
93 % c_out, and d_out, respectively describing the reflected, transmitted, and
94     diffracted/lost photon field.

```

C.3.3 Init lists 2level CW scan laser frequency

```

1 %Parameters for the calculation of spectra
2 omega_laser_min_ev=omega_d_ev+min_detuning_muev*1e-6;
3 omega_laser_max_ev=omega_d_ev+max_detuning_muev*1e-6;
4
5 %%% Initialization of lists to calculate and plot the spectra as a
6     function of omega_laser
6 omega_laser_list_ev = linspace(omega_laser_min_ev,omega_laser_max_ev,
7     nb_points_spectrum);% list of laser photon energies for the plots in eV
7 omega_laser_list = omega_laser_list_ev*ev/hbar*1e-12;% list of laser
8     angular frequencies in rad/ps, the unit used for calculations
8 omega_step = (max(omega_laser_list) - min(omega_laser_list)) / (
9     nb_points_spectrum-1); %in rad/ps, step for the calculation of
10    integrals
10
11 % List to plot the spectra as a function of the detuning omega_laser-
12     omega_d, in mueV
11 detuning_list_muev = (omega_laser_list_ev - omega_d_ev)*1e6;
12
13 %%%%%%%%%%%%%%
14 % Memory preallocation (allows gaining in calculation time)
15 % The "_vs_omega" indicates here that this is a list of values related to
16     the defferent_values of omega_laser
16
17 total_flux_reflected_photons_vs_omega = zeros(1,length(omega_laser_list));
18     %flux in ps^(-1)
18 total_flux_transmitted_photons_vs_omega = zeros(1,length(omega_laser_list))
19     ; %flux in ps^(-1)
19 total_flux_diffracted_photons_vs_omega = zeros(1,length(omega_laser_list));
20     %flux in ps^(-1)
20 total_flux_emitted_photons_vs_omega = zeros(1,length(omega_laser_list)); %
21     flux in ps^(-1)

```

```
21
22 occupation_excited_state_vs_omega = zeros(1,length(omega_laser_list)); %
   for the occupation of the excited state
23 occupation_ground_state_vs_omega = zeros(1,length(omega_laser_list)); % for
   the occupation of the ground state
24
25
26 %%%% OPTIONAL : Memory preallocation for the coherent part of the output
   fields
27 % Here the term "laser_coherent" means that it corresponds to the part of
   the flux that is
28 % coherent with the incoming excitation laser, and not the "total" flux.
   Obviously the incoherent part
29 % is just given by substrating the "laser_coherent" part from the "total"
   flux
30
31 flux_reflected_photons_laser_coherent_vs_omega = zeros(1,length(
   omega_laser_list)); %flux in ps^(-1)
32 flux_transmitted_photons_laser_coherent_vs_omega = zeros(1,length(
   omega_laser_list)); %flux en s^(-1)
33 flux_diffracted_photons_laser_coherent_vs_omega = zeros(1,length(
   omega_laser_list)); %flux en s^(-1)
34 flux_emitted_photons_laser_coherent_vs_omega = zeros(1,length(
   omega_laser_list)); %flux en s^(-1)
```

C.3.4 Init lists 2level PW vs time

```
1 % Parameters of the incoming gaussian pulse
2 omega_pulse_ev=omega_d_ev+detuning_pulse_QD_muev*1e-6; %center energy of
   the incoming pulse, in eV
3 omega_pulse=omega_pulse_ev*ev/hbar*1e-12; %in rad/ps
4
5 % Parameters for the computation of time evolutions
6 t_delay = 2*FWHM; % Time at which the pulse is maximally intense, so that
   the computation starts when the pulse has not arrived yet
7 t_max_ps=t_delay + 4*FWHM +0.5/gamma_sp; % Final time where we stop the
   computation and plots of time evolutions
8 nb_points_time = 1000; % Time resolution/Number of iterations / <100000
   otherwise the integrating the master equation gets difficult (odesolve)
   )
9 t_min = 0*FWHM; % Initial time considered for the computations and plots of
   time evolutions
10 t_step=(t_max_ps-t_min)/(nb_points_time-1); % Duration of a time step
11 t_list=linspace(t_min,t_max_ps,nb_points_time); % list of all the times
   considered in the computation and plots
12
```

```

13 % Initialization of qo array of identity operator
14 Id_vs_time = qo;
15 for time_index = 1:nb_points_time
16     Id_vs_time{time_index} = Id;
17 end

```

C.3.5 Init lists 2level g1SD CW vs delay and frequency

```

1 %M Laser frequency (fixed)
2
3 omega_laser_ev = omega_d_ev + detuning_laser_QD_muev*1e-6;
4 omega_laser = omega_laser_ev*ev/hbar*1e-12; % laser angular frequency in
      rad/ps, the unit used for calculations
5
6
7 %% Parameters and lists for the evaluation of the temporal evolution as a
      function of the delay tau
8
9 tau_step = (tau_max)/(nb_points_delay-1); %size of the time step, in ps
10 tau_list = linspace(0,tau_max,nb_points_delay); % array containg the non-
      negative time steps
11 full_tau_list = [fliplr(-tau_list(2:end-1)) , tau_list ];% array containing
      both positive and negative time steps
12
13
14 %% Parameters for the calculation of spectral densities through the Fast
      Fourier Transform (FFT) algorithm
15 %
16 % NB1: See comments in the main program for a definition of spectral
      densities and main concepts involved
17 %
18 % NB2: For more information in the matlab FFT function, see:
19 % https://fr.mathworks.com/help/matlab/ref/fft.html
20 % A discussion on the proper normalization of the FFT signal (which should
      be performed by
21 % dividing the fft function's result by the signal's sampling frequency)
      can be found here:
22 % https://math.stackexchange.com/questions/636847/understanding-fourier-
      transform-example-in-matlab
23 % Such a normalization choice allows respecting the Parseval's theorem, i.e
      .:
24 %      sum_{n=0}^{N-1} |x[n]|^2 = 1/N*sum_{k=0}^{N-1} |X[k]|^2,
25 % with x[n] the signal and X[k] its discrete Fourier Transform, n and k
      being positive
26 % indices between 0 and N-1. Indeed, Parseval's theorem is at the heart of
      our normalization

```

```
27 % choice that the integral of the spectra density of flux should be the
28 % total flux.
29 %
30 % NB3: To get a really fast algorithm, the number of points used in the
31 % time and frequency domain should be a power of 2.
32
33 FFT_sampling_frequency = 1/tau_step; % sampling frequency, also called "
34     % sampling rate", in ps^(-1)
35 nb_points_full_spectrum = 2^nextpow2(length(full_tau_list)); % ensuring a
36     % power of 2 for optimized FFT performance
37
38 omega_step = 2*pi*FFT_sampling_frequency/nb_points_full_spectrum; % angular
39     % frequency step in the spectrum, in rad/ps
40 omega_step_muev = omega_step/ev*hbar/1e-18; % photon energy step in mueV
41
42 omega_list_full_spectrum = omega_laser + (-nb_points_full_spectrum/2:
43     % nb_points_full_spectrum/2-1)*omega_step; % array of angular frequencies
44     % in rad/ps
45 % spectrum centered around omega_laser, since we work in the frame rotating
46     % at this angular frequency)
47
48 % Parameters for the zoomed spectrum, i.e. the list of angular frequencies
49     % of interest in the selected spectral window.
50 %
51 % NB: This zoomed spectrum is simply a subset of the previous one, between
52     % a minimal index
53 % and a maximal one that are defined below.
54
55 index_min_zoomed_spectrum = nb_points_full_spectrum/2+1-round(
56     % width_spectral_window_muev/omega_step_muev/2);
57 index_max_zoomed_spectrum = nb_points_full_spectrum/2+1+round(
58     % width_spectral_window_muev/omega_step_muev/2);
59
60 omega_list = linspace(omega_list_full_spectrum(index_min_zoomed_spectrum),
61     % omega_list_full_spectrum(index_max_zoomed_spectrum),
62     % index_max_zoomed_spectrum=index_min_zoomed_spectrum+1); % list of
63     % angular frequencies, in rad/ps over the full FFT spectrum
64
65 nb_points_spectrum = length(omega_list);
66
67 %
68 % Parameters for the zoomed spectrum expressed in photon energy
69 %
70 omega_list_ev = omega_list/ev*hbar/1e-12; % selected list of photon
71     % energies, in eV
```

```
59
60
61 %% Parameters for the compensation of the FFT phase shift compensation
62 %
63 % NB: a first-order autocorrelation function is always anti-symmetric in
64 %      the sense that:
65 %          g1(-tau) = g1(tau)*
66 % This antisymmetry ensures that its Fourier Transform, and thus the
67 % corresponding spectral
68 % density, gives a real physical quantity. However, as discussed in the
69 % main program the fft
70 % function considers that the first signal point corresponds to time 0,
71 %      while in our case
72 % the full_tau_list contains both negative and positive delays, and the
73 %      antisymmetry point
74 % (tau=0) is shifted to the middle of the spectrum. This is a very general
75 % issue arising
76 % from the fact that MATLAB arrays have only positive indices, so a signal
77 %      x[n] defined over
78 % n = -N, -N+1, ..., 0, ... N-1, N is treated by the fft function as it
79 %      were defined over
80 % n = 1 , 2 , ... , 2*N+1. Such a translation of the x[n] signal leads, in
81 %      its Fourier
82 % Transform X[k], to a phase shift which linearly increases with the index
83 %      k. In our case,
84 % the phase shift will depend on the angular frequency omega, and has to be
85 %      compensated by
86 % by a phase term denoted "phase_shift_compensation_vs_omega_full_spectrum
87 %      ".
88 % For more info on the phase shift compensation, see:
89 % https://www.mathworks.com/matlabcentral/answers/94874-why-is-the-fft-of-
90 %      an-anti-symmetric-signal-not-correct
91
92
93 %% Memory preallocation (allows gaining in calculation time)
94 % NB: The "_vs_omega" indicates here that this is a list of values related
95 %      to the different
96 % values of omega, in rad/ps, in omega_list
97
98 spectral_density_flux_reflected_photons_incoh_vs_omega = zeros(1,length(
99 omega_list));
```

```

88 spectral_density_flux_transmitted_photons_incoh_vs_omega = zeros(1,length(
     omega_list));
89 spectral_density_flux_emitted_photons_incoh_vs_omega = zeros(1,length(
     omega_list));

```

C.3.6 Init maps 2level g1 WDF PW

```

1 % Parameters of the incoming gaussian pulse
2 omega_pulse_ev=omega_d_ev+detuning_pulse_QD_muev*1e-6; %center energy of
   the incoming pulse, in eV
3 omega_pulse=omega_pulse_ev*ev/hbar*1e-12; %in rad/ps
4
5 % Parameters for the computation of time evolutions
6 t_step=(t_max_ps-t_min)/(nb_points_time-1); % Duration of a time step
7 t_list=linspace(t_min,t_max_ps,nb_points_time); % list of all the times
   considered in the computation and plots
8
9 % Steps in time and delay for the Wigner Distribution Function (WDF).
10 % Notice that even though tau = t2-t1, its step here is half the step in
11 % the density matrix evolution to correctly Fourier transform over
12 % frequency later, according to the WDF definition. More info in the "main"
13 % script.
14
15 tau_step = t_step/2; %important to avoid aliasing
16 time_step = t_step/2;
17
18 time_list = (t_list(1):time_step:t_list(end));
19 tau_list = (t_list(1)-t_list(end):tau_step:t_list(end)-t_list(1));
20 %%
21 % Parameters for the computation of preliminary time evolution,
22 % between 0 (long before the pulse) and t_min (time at which we want
23 % to start plotting and integrating the physical quantities
24 nb_points_time_before_t_min = 5; % (Low) time resolution for first
   evolution of the system for initialization
25 t_list_before_t_min = linspace(0,t_min,nb_points_time_before_t_min); % time
   array for first evolution of the sistem
26
27 % Initialization of qo array of identity operator
28 Id_vs_time = qo;
29 for t1_index = 1:nb_points_time
30     Id_vs_time{t1_index} = Id;
31 end
32
33 %% Preallocation of the memory to save computing time
34
35 % Initialization of g1 vs (t1,t2)

```

```
36 g1_reflected_vs_t1_t2 = zeros(nb_points_time,nb_points_time);
37 g1_transmitted_vs_t1_t2 = zeros(nb_points_time,nb_points_time);
38 g1_diffracted_vs_t1_t2 = zeros(nb_points_time,nb_points_time);
39 g1_emitted_vs_t1_t2 = zeros(nb_points_time,nb_points_time);
40
41 % Initialization of the "zero" density matrix which will be used to fill
   the
42 % conditional density matrices, using 0 values for t2 < t1
43 zero_density_matrix_vs_t2_before_t1 = q0;
44 %% Parameters for the calculation of Fourier Transform over tau through the
   Fast Fourier Transform (FFT) algorithm
45 %
46 % NB1: See comments in the main program for a definition of spectral
   densities and main concepts involved
47 %
48 % NB2: For more information in the matlab FFT function, see:
49 % https://fr.mathworks.com/help/matlab/ref/fft.html
50 % A discussion on the proper normalization of the FFT signal (which should
   be performed by
51 % dividing the fft function's result by the signal's sampling frequency)
   can be found here:
52 % https://math.stackexchange.com/questions/636847/understanding-fourier-
   transform-example-in-matlab
53 % Such a normalization choice allows respecting the Parseval's theorem, i.e
   ..
54 %      sum_{n=0}^{N-1} |x[n]|^2 = 1/N*sum_{k=0}^{N-1} |X[k]|^2,
55 % with x[n] the signal and X[k] its discrete Fourier Transform, n and k
   being positive
56 % indices between 0 and N-1. Indeed, Parseval's theorem is at the heart of
   our normalization
57 % choice that the integral of the spectra density of flux should be the
58 % total flux.
59 %
60 % NB3: To get a really fast algorithm, the number of points used in the
61 % time and frequency domain should be a power of 2. However, in this
62 % specific program the number of elements is 4*nb_points_time-3, so zero
63 % padding is performed by the fft-s defined in the main.
64
65 FFT_sampling_frequency = 1/t_step; % sampling frequency, also called "
   sampling rate", in ps^(-1)
66 nb_points_full_spectrum = 2^nextpow2(length(tau_list)); % ensuring a power
   of 2 for for optimized FFT performance
67 omega_step = 2*pi*FFT_sampling_frequency/nb_points_full_spectrum; % angular
   frequency step in the spectrum, in rad/ps
68 omega_step_muev = omega_step/ev*hbar/1e-18; % photon energy step in mueV
69
```

```
70 omega_list_full_spectrum = omega_pulse + (-nb_points_full_spectrum/2:
    nb_points_full_spectrum/2-1)*omega_step; % array of angular frequencies
    in rad/ps
71 omega_list_full_spectrum_muev = omega_list_full_spectrum/ev*hbar/1e-18;
72 % spectrum centered around omega_pulse, since we work in the frame rotating
    at this angular frequency)
73
74 %% Parameters for the zoomed spectrum, i.e. the list of angular frequencies
    of interest in the selected spectral window.
75 %
76 % NB: This zoomed spectrum is simply a subset of the previous one, between
    a minimal index
77 % and a maximal one that are defined below.
78
79 index_min_zoomed_spectrum = nb_points_full_spectrum/2+1-round(
    width_spectral_window_muev/omega_step_muev/2);
80 index_max_zoomed_spectrum = nb_points_full_spectrum/2+1+round(
    width_spectral_window_muev/omega_step_muev/2);
81
82 omega_list = linspace(omega_list_full_spectrum(index_min_zoomed_spectrum),
    omega_list_full_spectrum(index_max_zoomed_spectrum),
    index_max_zoomed_spectrum-index_min_zoomed_spectrum+1); % list of
    angular frequencies, in rad/ps over the full FFT spectrum
83
84 nb_points_spectrum = length(omega_list);
85
86 %% Parameters for the zoomed spectrum expressed in photon energy
87
88 omega_list_ev = omega_list/ev*hbar/1e-12; % selected list of photon
    energies, in eV
89
90 %% Parameters for the compensation of the FFT phase shift compensation
91 %
92 % NB: WVD gives a real quantity. However, as discussed in the main program
    the fft
93 % function considers that for each row, the first signal point corresponds
    to delay 0, while in our case
94 % each row contains both negative and positive delays. This is a very
    general issue arising
95 % from the fact that MATLAB arrays have only positive indices, so a signal
    x[n] defined over
96 % n = -N, -N+1, ..., 0, ... N-1, N is treated by the fft function as if it
    were defined over
97 % n = 1, 2, ..., 2*N+1. Such a translation of the x[n] signal leads, in
    its Fourier
```

```

98 % Transform X[k], to a phase shift which linearly increases with the index
99 % k. In our case,
100 % the phase shift will depend on the angular frequency omega, and has to be
101 % compensated by
102 % by a phase term denoted "phase_shift_compensation_vs_omega_full_spectrum"
103 %
104 k = 0:(nb_points_full_spectrum-1);
105 %NB 1: the command "repmat" is used since the fft returns a matrix to be
106 %phaseshifted only along the rows. Therefore, "repmat" is used to generate
107 %a matrix with identical rows.
108 %NB 2: "length(tau_list)-1)/2" is the number of negative delay elements for
109 %each row
110 phase_shift_compensation_vs_omega_full_spectrum = repmat(exp(-1j*2*pi*((
    length(tau_list)-1)/2)*k/length(k)),2*nb_points_time-1,1);

```

C.3.7 Interpolation 2level G1 WDF PR

```

1 %% Memory preallocation (allows gaining in calculation time)
2 interpolated_G1_reflected_vs_time_tau = 0*time_list'*tau_list;
3 interpolated_reflected_coherent_vs_time_tau = 0*time_list'*tau_list;
4 interpolated_G1_transmitted_vs_time_tau = 0*time_list'*tau_list;
5 interpolated_transmitted_coherent_vs_time_tau = 0*time_list'*tau_list;
6 interpolated_G1_emitted_vs_time_tau = 0*time_list'*tau_list;
7 interpolated_emitted_coherent_vs_time_tau = 0*time_list'*tau_list;
8 interpolated_G1_diffracted_vs_time_tau = 0*time_list'*tau_list;
9 interpolated_diffracted_coherent_vs_time_tau = 0*time_list'*tau_list;
10
11 %From the definition of time = (t1+t2)/2 and tau=t2-t1, it is found that
12 %for a
13 %matrix tau_index = t2_index-t1_index + N and time_index =
14 %t1_index+t2_index-1. Therefore, it is obtained that t1_index =
15 %(time_index-tau_index+1+1)/2 and t2_index = (time_index+tau_index+1-N)/2.
16 %NB: The following interpolation is based on a simple arithmetic mean
17 % between
18 % consecutives values at half-integer values. "Fancier" interpolations
19 % would surely increase the overall accuracy.
20 for time_index = 1:length(time_list)
21     for tau_index = 1:length(tau_list)

```

```

22     t1_index = (time_index-((tau_index+1)/2)+1+nb_points_time)/2; %obs:
23         tau_index from the previous formula is acually "(tau_index+1)
24             /2" since we have set tau_step = t_step/2
25     t2_index = (time_index+((tau_index+1)/2)+1-nb_points_time)/2; %same
26         as above
27
28     if t1_index <= nb_points_time && t1_index >= 1 && t2_index <=
29         nb_points_time && t2_index >= 1
30
31         if floor(t1_index)==t1_index && floor(t2_index)==t2_index
32             interpolated_G1_reflected_vs_time_tau(time_index, tau_index
33                 ) = G1_reflected_vs_t1_t2(t1_index, t2_index);
34             interpolated_reflected_coherent_vs_time_tau(time_index,
35                 tau_index) = expect_b_out_dag_t1_times_expect_b_out_t2(
36                 t1_index, t2_index);
37             interpolated_G1_transmitted_vs_time_tau(time_index,
38                 tau_index) = G1_transmitted_vs_t1_t2(t1_index, t2_index
39                 );
40             interpolated_transmitted_coherent_vs_time_tau(time_index,
41                 tau_index) = expect_c_out_dag_t1_times_expect_c_out_t2(
42                 t1_index, t2_index);
43             interpolated_G1_emitted_vs_time_tau(time_index, tau_index
44                 ) = G1_emitted_vs_t1_t2(t1_index, t2_index);
45             interpolated_emitted_coherent_vs_time_tau(time_index,
46                 tau_index) = expect_e_out_dag_t1_times_expect_e_out_t2(
47                 t1_index, t2_index);
48             interpolated_G1_diffracted_vs_time_tau(time_index,
49                 tau_index) = G1_diffracted_vs_t1_t2(t1_index, t2_index)
50                 ;
51             interpolated_diffracted_coherent_vs_time_tau(time_index,
52                 tau_index) = expect_d_out_dag_t1_times_expect_d_out_t2(
53                 t1_index, t2_index);
54
55         elseif floor(t1_index)==t1_index && floor(t2_index)~= t2_index
56             interpolated_G1_reflected_vs_time_tau(time_index, tau_index
57                 ) = (G1_reflected_vs_t1_t2(t1_index, floor(t2_index)) +
58                 G1_reflected_vs_t1_t2(t1_index, ceil(t2_index)))/2;
59             interpolated_reflected_coherent_vs_time_tau(time_index,
60                 tau_index) = (expect_b_out_dag_t1_times_expect_b_out_t2(
61                 t1_index, floor(t2_index)) +
62                 expect_b_out_dag_t1_times_expect_b_out_t2(t1_index,
63                 ceil(t2_index)))/2;
64             interpolated_G1_transmitted_vs_time_tau(time_index,
65                 tau_index) = (G1_transmitted_vs_t1_t2(t1_index, floor(
66                 t2_index)) + G1_transmitted_vs_t1_t2(t1_index, ceil(
67                 t2_index)))/2;

```

```

41     interpolated_transmitted_coherent_vs_time_tau(time_index,
42         tau_index) = (expect_c_out_dag_t1_times_expect_c_out_t2
43             (t1_index, floor(t2_index)) +
44             expect_c_out_dag_t1_times_expect_c_out_t2(t1_index,
45                 ceil(t2_index)))/2;
46     interpolated_G1_emitted_vs_time_tau(time_index, tau_index)
47         = (G1_emitted_vs_t1_t2(t1_index, floor(t2_index)) +
48             G1_emitted_vs_t1_t2(t1_index, ceil(t2_index)))/2;
49     interpolated_emitted_coherent_vs_time_tau(time_index,
50         tau_index) = (expect_e_out_dag_t1_times_expect_e_out_t2
51             (t1_index, floor(t2_index)) +
52             expect_e_out_dag_t1_times_expect_e_out_t2(t1_index,
53                 ceil(t2_index)))/2;
54     interpolated_G1_diffracted_vs_time_tau(time_index,
55         tau_index) = (G1_diffracted_vs_t1_t2(t1_index, floor(
56             t2_index)) + G1_diffracted_vs_t1_t2(t1_index, ceil(
57                 t2_index)))/2;
58     interpolated_diffracted_coherent_vs_time_tau(time_index,
59         tau_index) = (expect_d_out_dag_t1_times_expect_d_out_t2
60             (t1_index, floor(t2_index)) +
61             expect_d_out_dag_t1_times_expect_d_out_t2(t1_index,
62                 ceil(t2_index)))/2;
63
64     elseif floor(t2_index)==t2_index && floor(t1_index)~= t1_index
65         interpolated_G1_reflected_vs_time_tau(time_index, tau_index)
66             = (G1_reflected_vs_t1_t2(floor(t1_index), t2_index)+
67                 G1_reflected_vs_t1_t2(ceil(t1_index), t2_index))/2;
68         interpolated_reflected_coherent_vs_time_tau(time_index,
69             tau_index) = (expect_b_out_dag_t1_times_expect_b_out_t2
70                 (floor(t1_index), t2_index)+
71                 expect_b_out_dag_t1_times_expect_b_out_t2(ceil(t1_index
72                     ), t2_index))/2;
73         interpolated_G1_transmitted_vs_time_tau(time_index,
74             tau_index) = (G1_transmitted_vs_t1_t2(floor(t1_index),
75                 t2_index)+G1_transmitted_vs_t1_t2(ceil(t1_index),
76                 t2_index))/2;
77         interpolated_transmitted_coherent_vs_time_tau(time_index,
78             tau_index) = (expect_c_out_dag_t1_times_expect_c_out_t2
79                 (floor(t1_index), t2_index)+
80                 expect_c_out_dag_t1_times_expect_c_out_t2(ceil(t1_index
81                     ), t2_index))/2;
82         interpolated_G1_emitted_vs_time_tau(time_index, tau_index)
83             = (G1_emitted_vs_t1_t2(floor(t1_index), t2_index)+
84                 G1_emitted_vs_t1_t2(ceil(t1_index), t2_index))/2;

```

```
53     interpolated_emitted_coherent_vs_time_tau(time_index,
      tau_index) = (expect_e_out_dag_t1_times_expect_e_out_t2
      (floor(t1_index), t2_index)+
      expect_e_out_dag_t1_times_expect_e_out_t2(ceil(t1_index)
      ), t2_index))/2;
54     interpolated_G1_diffracted_vs_time_tau(time_index,
      tau_index) = (G1_diffracted_vs_t1_t2(floor(t1_index),
      t2_index)+G1_diffracted_vs_t1_t2(ceil(t1_index),
      t2_index))/2;
55     interpolated_diffracted_coherent_vs_time_tau(time_index,
      tau_index) = (expect_b_out_dag_t1_times_expect_d_out_t2
      (floor(t1_index), t2_index)+
      expect_b_out_dag_t1_times_expect_d_out_t2(ceil(t1_index)
      ), t2_index))/2;
56   else
57     interpolated_G1_reflected_vs_time_tau(time_index, tau_index
      ) = (G1_reflected_vs_t1_t2(floor(t1_index), floor(
      t2_index))+G1_reflected_vs_t1_t2(ceil(t1_index), floor(
      t2_index))+G1_reflected_vs_t1_t2(floor(t1_index), ceil(
      t2_index))+G1_reflected_vs_t1_t2(ceil(t1_index), ceil(
      t2_index)))/4;
58     interpolated_reflected_coherent_vs_time_tau(time_index,
      tau_index) = (expect_b_out_dag_t1_times_expect_b_out_t2
      (floor(t1_index), floor(t2_index))+
      expect_b_out_dag_t1_times_expect_b_out_t2(ceil(t1_index)
      ), floor(t2_index)) +
      expect_b_out_dag_t1_times_expect_b_out_t2(floor(
      t1_index), ceil(t2_index))+
      expect_b_out_dag_t1_times_expect_b_out_t2(ceil(t1_index)
      ), ceil(t2_index)))/4;
59     interpolated_G1_transmitted_vs_time_tau(time_index,
      tau_index) = (G1_transmitted_vs_t1_t2(floor(t1_index),
      floor(t2_index))+G1_transmitted_vs_t1_t2(ceil(t1_index)
      , floor(t2_index))+G1_transmitted_vs_t1_t2(floor(
      t1_index), ceil(t2_index))+G1_transmitted_vs_t1_t2(ceil(
      t1_index), ceil(t2_index)))/4;
60     interpolated_transmitted_coherent_vs_time_tau(time_index,
      tau_index) = (expect_c_out_dag_t1_times_expect_c_out_t2
      (floor(t1_index), floor(t2_index))+
      expect_c_out_dag_t1_times_expect_c_out_t2(ceil(t1_index)
      ), floor(t2_index)) +
      expect_c_out_dag_t1_times_expect_c_out_t2(floor(
      t1_index), ceil(t2_index))+
      expect_c_out_dag_t1_times_expect_c_out_t2(ceil(t1_index)
      ), ceil(t2_index)))/4;
```

```

61     interpolated_G1_emitted_vs_time_tau(time_index, tau_index)
62         = (G1_emitted_vs_t1_t2(floor(t1_index), floor(t2_index))
63             +G1_emitted_vs_t1_t2(ceil(t1_index), floor(t2_index))+
64             G1_emitted_vs_t1_t2(floor(t1_index), ceil(t2_index))+
65             G1_emitted_vs_t1_t2(ceil(t1_index), ceil(t2_index)))/4;
66     interpolated_emitted_coherent_vs_time_tau(time_index,
67         tau_index) = (expect_e_out_dag_t1_times_expect_e_out_t2
68             (floor(t1_index), floor(t2_index))+
69             expect_e_out_dag_t1_times_expect_e_out_t2(ceil(t1_index)
70                 , floor(t2_index)) +
71                 expect_e_out_dag_t1_times_expect_e_out_t2(floor(
72                     t1_index), ceil(t2_index))+
73                     expect_e_out_dag_t1_times_expect_e_out_t2(ceil(t1_index)
74                         , ceil(t2_index)))/4;
75     interpolated_G1_diffracted_vs_time_tau(time_index,
76         tau_index) = (G1_diffracted_vs_t1_t2(floor(t1_index),
77             floor(t2_index))+G1_diffracted_vs_t1_t2(ceil(t1_index),
78                 floor(t2_index))+G1_diffracted_vs_t1_t2(floor(t1_index)
79                     , ceil(t2_index))+G1_diffracted_vs_t1_t2(ceil(t1_index)
80                         , ceil(t2_index)))/4;
81     interpolated_diffracted_coherent_vs_time_tau(time_index,
82         tau_index) = (expect_d_out_dag_t1_times_expect_d_out_t2
83             (floor(t1_index), floor(t2_index))+
84             expect_d_out_dag_t1_times_expect_d_out_t2(ceil(t1_index)
85                 , floor(t2_index)) +
86                 expect_d_out_dag_t1_times_expect_d_out_t2(floor(
87                     t1_index), ceil(t2_index))+
88                     expect_d_out_dag_t1_times_expect_d_out_t2(ceil(t1_index)
89                         , ceil(t2_index)))/4;
90     end
91 end
92 end
93 end
94 end

```

C.3.8 Init maps 2level g2 PR vs t1 t2

```

1 % Parameters of the incoming gaussian pulse
2 omega_pulse_ev=omega_d_ev+detuning_pulse_QD_muev*1e-6; %center energy of
3 %the incoming pulse, in eV
4 omega_pulse=omega_pulse_ev*ev/hbar*1e-12; %in rad/ps
5 % Parameters for the computation of time evolutions
6 t_step=(t_max_ps-t_min)/(nb_points_time-1); % Duration of a time step
7 t_list=linspace(t_min,t_max_ps,nb_points_time); % list of all the times
8 % considered in the computation and plots

```

```
9 % Parameters for the computation of preliminary time evolution,
10 % between 0 (long before the pulse) and t_min (time at which we want
11 % to start plotting and integrating the physical quantities
12 nb_points_time_before_t_min = 5; % (Low) time resolution for first
    evolution of the system for initialization
13 t_list_before_t_min = linspace(0,t_min,nb_points_time_before_t_min); % time
    array for first evolution of the sistem
14
15
16
17 % Initialization of qo array of identity operator
18 Id_vs_time = qo;
19 for time_index = 1:nb_points_time
20     Id_vs_time{time_index} = Id;
21 end
22
23
24 full_tau_list = [-flip(t_list(2:end)) t_list(1:end)]; %t_list with both
    negative and positive delays for plotting
25
26 %%% Preallocation of the memory to save computing time
27
28 % Initialization of g2 vs (t1,t2)
29 g2_reflected_vs_t1_t2 = zeros(nb_points_time,nb_points_time);
30 g2_transmitted_vs_t1_t2 = zeros(nb_points_time,nb_points_time);
31 g2_emitted_vs_t1_t2 = zeros(nb_points_time,nb_points_time);
32
33 % Initialization of conditional occupation probabilities vs (t1,t2)
34 occupation_ground_vs_t1_vs_t2_after_click_b_out_at_t1 = zeros(
    nb_points_time,nb_points_time);
35 occupation_excited_vs_t1_vs_t2_after_click_b_out_at_t1 = zeros(
    nb_points_time,nb_points_time);
36 occupation_ground_vs_t1_vs_t2_after_click_c_out_at_t1 = zeros(
    nb_points_time,nb_points_time);
37 occupation_excited_vs_t1_vs_t2_after_click_c_out_at_t1 = zeros(
    nb_points_time,nb_points_time);
38 occupation_ground_vs_t1_vs_t2_after_click_e_out_at_t1 = zeros(
    nb_points_time,nb_points_time);
39 occupation_excited_vs_t1_vs_t2_after_click_e_out_at_t1 = zeros(
    nb_points_time,nb_points_time);
40
41 % Initialization of the "zero" density matrix which will be used to fill
    the
42 % conditional density matrices, using 0 values for t2 < t1
43 zero_density_matrix_vs_t2_before_t1 = qo;
44
```

```

45 % Initialization of correlated normalized g2(tau)
46 normalized_g2_vs_delay_emitted = zeros(1,nb_points_time);
47 normalized_g2_vs_delay_reflected = zeros(1,nb_points_time);
48 normalized_g2_vs_delay_transmitted = zeros(1,nb_points_time);
49
50 % Initialization of uncorrelated normalized g2(tau)
51 normalized_g2_vs_delay_uncorrelated_emitted = zeros(1,nb_points_time);
52 normalized_g2_vs_delay_uncorrelated_reflected = zeros(1,nb_points_time);
53 normalized_g2_vs_delay_uncorrelated_transmitted = zeros(1,nb_points_time);

```

C.3.9 plot 2level CW vs laser frequency

```

1 switch model
2   case 'F'
3     text_legend_model='full model';
4   case 'A'
5     text_legend_model='adiabatic model';
6 end
7
8 % Parameters for the text displayed in figure legends
9 text_legend_QD=['g=', num2str(g_muev) ' muev \gamma_{sp}=' num2str(
10   gamma_sp_muev) 'muev \gamma^{*}' num2str(gamma_puredephasing_muev) ' '
11   muev];
12 text_legend_cav=['\kappa=' num2str(kappa_muev) '\mu ev \eta_{top}='
13   num2str(eta_top) ' C=' num2str(g^2/kappa/gamma_decoherence,3)];
14 text_legend_P_in=['P_{in}'= num2str(P_in_CW_pW) 'pW n_0=' num2str(4*
15   eta_top*abs(b_in_CW)^2/kappa,2) ' n_c=' num2str(gamma_decoherence*
16   gamma_sp/(4*g^2),2)];
17 text_legend={text_legend_QD,text_legend_cav,text_legend_P_in};
18 % NB: C is the cooperativity and n_c the critical photon number, both
19 % depend only on the cavity-QED parameters.
20 % On the contrary, n_0 depends on the incoming power P_in since it is the
21 % calculated number of intracavity photons
22 % in the absence of QD (i.e. when g=0). When n_0 is much lower than n_c we
23 % are in the weak excitation limit.
24
25 % Verification of the conservation of total photon flux
26 fprintf(['CW - ' text_legend_model ' ': Maximal relative error on the
27   conservation of photon flux: ' num2str(max(abs(1-R_vs_omega-T_vs_omega-
28   D_vs_omega-E_vs_omega))) '\n\n'])
29
30 %%%%%%%% Plots %%%%%%%
31
32
33 if ismember('R',plot_choice)

```

```

25 %Color code : Refl in red, Transm + Diffrr/lost in blue, Spont. Em. in
26 magenta
27 figure('Name',[ 'CW - ' text_legend_model ' ' ' - Reflectivity vs laser
28 photon energy - Pin = ' num2str(P_in_CW_pW) ' pW'], 'NumberTitle', 'off')
29 %%% UNUSED HERE: allows comparing total part and coherent part
30 % plot(omega_laser_list_ev_CW,real(R_vs_omega),'r',
31 % omega_laser_list_ev_CW,real(R_coh_vs_omega),'r--');
32 % legend('Fraction of reflected photons','Fraction of coherent
33 % reflected photons')
34 plot(detuning_list_muev,real(R_vs_omega),'r');
35 xlabel('\omega_{laser}-\omega_d [\mu eV]'); ylabel('Reflectivity');
36 ylim([0 1]);
37 text(detuning_list_muev(ceil(nb_points_spectrum*0.55)),0.8, text_legend,
38 'FontSize',9)
39 legend('Reflected photons','Location','Northeast')
40 end
41
42
43 if ismember('T',plot_choice)
44 figure('Name',[ 'CW - ' text_legend_model ' ' ' - Transmission vs laser
45 photon energy - Pin = ' num2str(P_in_CW_pW) ' pW'], 'NumberTitle', 'off')
46 %%% UNUSED HERE: allows comparing total part and coherent part
47 % plot(omega_laser_list_ev_CW,real(T_vs_omega+D_vs_omega),'b',
48 % omega_laser_list_ev_CW,real(T_coh_vs_omega+D_coh_vs_omega),'b--');
49 % legend('Fraction of transmitted + diffracted photons','Fraction of
50 % coherent transmitted/diffracted photons')
51 plot(detuning_list_muev,real(T_vs_omega+D_vs_omega),'b');
52 xlabel('\omega_{laser}-\omega_d [\mu eV]'); ylabel('Transmission +
53 diffraction/losses');
54 ylim([0 1]);
55 text(detuning_list_muev(ceil(nb_points_spectrum*0.55)),0.12, text_legend
56 , 'FontSize',9)
57 legend('Transmitted + diffracted photons','Location','Northeast')
58 end
59
60
61 if ismember('E',plot_choice)
62 figure('Name',[ 'CW - ' text_legend_model ' ' ' - Spontaneous emission
63 outside the mode vs laser photon energy - Pin = ' num2str(
64 P_in_CW_pW) ' pW'], 'NumberTitle', 'off')
65 %%% UNUSED HERE: allows comparing total part and coherent part
66 % plot(omega_laser_list_ev_CW,real(E_vs_omega),'m',
67 % omega_laser_list_ev_CW,real(E_coh_vs_omega),'m--');

```

```

56 % legend('Fraction of spontaneously emitted photons','Fraction of
      coherent spontaneously-emitted photons');
57 plot(detuning_list_muev,real(E_vs_omega),'m');
58 % xlabel('\omega_{laser}-\omega_d [\mu eV]'); ylabel('Fraction of
      photons emitted outside the mode');
59 ylim([0 1]);
60 text(detuning_list_muev(ceil(nb_points_spectrum*0.55)),0.8,text_legend,
      'FontSize',9)
61 legend('Photons emitted outside the mode','Location','Northeast')
62 end
63
64
65
66 if ismember('0',plot_choice)
67 figure('Name',['CW - ' text_legend_model ' - Occupation
      probabilities vs laser photon energy - Pin = ' num2str(P_in_CW_pW)
      ' pW'],'NumberTitle','off')
68 plot(detuning_list_muev,real(occupation_excited_state_vs_omega),'r',...
       detuning_list_muev,real(occupation_ground_state_vs_omega),'b');
69 xlabel('\omega_{laser}-\omega_d [\mu eV]'); ylabel('Occupation
      probability');
70 ylim([-0.05 1.05]);
71 text(detuning_list_muev(ceil(nb_points_spectrum*0.55)),0.7,text_legend,
      'FontSize',9)
72 legend('Occupation state |e>','Occupation state |g>','Location','best')
73 end
74

```

C.3.10 plot 2level PW vs time

```

1 switch model
2   case 'F'
3     text_legend_model='Full model';
4   case 'A'
5     text_legend_model='Adiabatic model';
6 end
7
8 fprintf([text_legend_model ' - Average number of injected photons per pulse
      : ' num2str(abs(sum(flux_injected_photons_vs_time)*t_step)) '\n'])
9 fprintf([text_legend_model ' - Average number of reflected photons per
      pulse : ' num2str(abs(sum(flux_reflected_photons_vs_time)*t_step)) '\n
      '])
10 fprintf([text_legend_model ' - Average number of transmitted photons per
      pulse : ' num2str(abs(sum(flux_transmitted_photons_vs_time)*t_step)) '\n'])

```

```

11 fprintf([text_legend_model ' – Average number of diffracted photons per
12   pulse : ' num2str(abs(sum(flux_diffracted_photons_vs_time)*t_step)) ' \
13   n'])
14 fprintf([text_legend_model ' – Average number of spontaneously-emitted
15   photons per pulse : ' num2str(abs(sum(flux_emitted_photons_vs_time)*
16   t_step)) ' \n \n'])
17 %Verification of the conservation of photon number
18 fprintf([text_legend_model ' – Verification – relative error on the
19   conservation of photon number : ' num2str(abs(sum(
20   flux_reflected_photons_vs_time+flux_transmitted_photons_vs_time+
21   flux_diffracted_photons_vs_time+flux_emitted_photons_vs_time-
22   flux_injected_photons_vs_time)/sum(flux_injected_photons_vs_time))) ' \
23   n \n'])
24 %Verification of the maximal photon number in the last Fock state (for full
25 %model only)
26 if model == 'F'
27   last_Fock_state_ket = basis(N,N);
28   occupation_last_Fock_state=tensor(last_Fock_state_ket*
29     last_Fock_state_ket',id_QD);
30   expect_occupation_last_Fock_state_vs_time=expect(
31     occupation_last_Fock_state,rho_vs_time); %
32   fprintf(['Full model – Verification – maximal occupation of the last
33     Fock state : ' num2str(max(abs(
34     expect_occupation_last_Fock_state_vs_time))) ' \n'])
35 end
36 %%%%%%%% Plots %%%%%%%
37 % Parameters for the text displayed in figure legends
38 text_legend_QD = ['g=', num2str(g_muev) ' muev \gamma_{sp}=' num2str(
39   gamma_sp_muev) 'muev \gamma^{*}' num2str(gamma_puredephasing_muev) ' '
40   muev'];
41 text_legend_cav = ['\kappa=' num2str(kappa_muev) 'muev \eta_{top}='
42   num2str(eta_top) ' C=' num2str(g^2/kappa/gamma_decoherence,3)];
43 text_legend_pulse = ['N_{in}=' num2str(Nb_photons) ' FWHM_{pulse}='
44   num2str(FWHM) 'ps'];
45 text_legend = {text_legend_QD,text_legend_cav,text_legend_pulse};
46 % NB: C is the cooperativity
47
48 if ismember('F',plot_choice)
49   figure('Name',[ 'PR – ' text_legend_model ' – Photon flux vs time – N_in
50   = ' num2str(Nb_photons) ' – Pulse FWHM = ' num2str(FWHM) ' ps –
51   pulsation laser = ' num2str(omega_pulse_ev) ' eV'], 'NumberTitle', 'off')

```

```

36 plot(t_list,real(flux_reflected_photons_vs_time), 'r',t_list,real(
37     flux_transmitted_photons_vs_time+flux_diffracted_photons_vs_time), 'b',
38 legend('Flux of reflected photons','Flux of transmitted + diffracted/
39     lost photons', 'Flux of photons spontaneously-emitted outside the
40 mode')
41 xlabel('Time t [ps]');ylabel('Photon flux [ps^{-1}]');
42 text(t_list(floor(nb_points_time*0.6)),0.7*max(
43     flux_reflected_photons_vs_time),text_legend,'FontSize',9)
44 end
45
46 if ismember('0',plot_choice)
47     figure('Name',[ 'PR - ' text_legend_model ' - Occupation probabilities
48         vs time - N_in = ' num2str(Nb_photons) ' - Pulse FWHM = ' num2str(
49             FWHM) ' ps - pulsation laser = ' num2str(omega_pulse_ev) ' eV'], 'NumberTitle','off')
50 plot(t_list,real(expect_sigma_dag_sigma_vs_time), 'r',t_list,real(
51     expect_sigma_dag_vs_time), 'k')
52 legend('Occupation of excited state |e>','Occupation of ground state |g
53     >')
54 xlabel('Time t [ps]');ylabel('Occupation probability');
55 ylim([0 1])
56 text(t_list(floor(nb_points_time*0.6)),0.7,text_legend,'FontSize',9)
57 end

```

C.3.11 plot 2level g1SD CW vs delay and frequency

```

1 switch model
2     case 'F'
3         text_legend_model='full model';
4     case 'A'
5         text_legend_model='adiabatic model';
6 end
7
8 % Parameters for the text displayed in figure legends
9 text_legend_QD = [ 'g=' num2str(g_muev) ' muev \gamma_{sp}=' num2str(
10     gamma_sp_muev) 'muev \gamma^{*}=' num2str(gamma_puredephasing_muev) ' muev' ];
11 text_legend_cav = [ '\kappa=' num2str(kappa_muev) 'muev \eta_{top}='
12     num2str(eta_top) ' C=' num2str(g^2/kappa/gamma_decoherence,3)];
13 text_legend_P_in = [ 'P_{in}=' num2str(P_in_CW_pw) 'pw n_0=' num2str(4*
14     eta_top*abs(b_in_CW)^2/kappa,2) ' n_c=' num2str(gamma_decoherence*
15     gamma_sp/(4*g^2),2)];
16 text_legend_omega = [ ' \omega_{laser}-\omega_d=' num2str(
17     detuning_laser_QD_muev) ' muev' ];

```

```

13 text_legend = {text_legend_QD, text_legend_cav, text_legend_P_in,
    text_legend_omega};
14 % NB: C is the cooperativity and n_c the critical photon number, both
    depend only on the cavity-QED parameters.
15 % On the contrary, n_0 depends on the incoming power P_in since it is the
    calculated number of intracavity photons
16 % in the absence of QD (i.e. when g=0). When n_0 is much lower than n_c we
    are in the weak excitation limit.
17
18 %Verification of the maximal photon number in the last Fock state (for full
    model only)
19 if model == 'F'
20     fprintf(['Full model – Verification – maximal occupation of the last
        Fock state : ' num2str(abs(expect(occupation_last_Fock_state,
            density_matrix_stationary_state))) ' \n \n'])
21 end
22
23 % Verification of photon flux conservation
24 fprintf(['g1SDCW – ' text_legend_model ': Relative error on photon flux
    conservation: ' num2str(abs(flux_injected_photons-
        flux_reflected_photons-flux_transmitted_photons-flux_diffracted_photons-
        flux_emitted_photons)/flux_injected_photons) ' \n \n'])
25
26 % Verifications on the extreme values of g1(tau) functions at zero and "
    infinite" delay
27 fprintf(['g1SDCW – ' text_legend_model ': Relative error on g1(0) = 1: ' '
    num2str(abs(1-g_1_reflected_vs_tau(1))) ' \n'])
28 fprintf(['g1SDCW – ' text_legend_model ': Relative error on g1(0) = 1: ' '
    num2str(abs(1-g_1_transmitted_vs_tau(1))) ' \n'])
29 fprintf(['g1SDCW – ' text_legend_model ': Relative error on g1(0) = 1: ' '
    num2str(abs(1-g_1_emitted_vs_tau(1))) ' \n \n'])
30 fprintf(['g1SDCW – ' text_legend_model ': Relative error on g1(infty) =
    coherent fraction for reflected photons: ' num2str(abs(
        flux_reflected_photons_laser_coherent/flux_reflected_photons-
        g_1_reflected_vs_tau(nb_points_delay))) ' \n'])
31 fprintf(['g1SDCW – ' text_legend_model ': Relative error on g1(infty) =
    coherent fraction for transmitted photons: ' num2str(abs(
        flux_transmitted_photons_laser_coherent/flux_transmitted_photons-
        g_1_transmitted_vs_tau(nb_points_delay))) ' \n'])
32 fprintf(['g1SDCW – ' text_legend_model ': Relative error on g1(infty) =
    coherent fraction for emitted photons: ' num2str(abs(
        flux_emitted_photons_laser_coherent/flux_emitted_photons-
        g_1_emitted_vs_tau(nb_points_delay))) ' \n \n'])
33
34 % Verification of spectral density normalization for the various fields (
    incoherent part only). Its integral over

```

```

35 % the whole spectrum must correspond to the incoherent photon flux,
    considering that each spectral density is measured
36 % in ps-1/muev, which gives a flux in ps-1 when multiplying by the photon
    energy step in mueV (omega_step_ev*1e-6)
37 fprintf(['g1SDCW - ' text_legend_model ': Relative error on the spectral
    density normalization - reflected photons (incoherent part) : ' num2str
    (abs(sum(spectral_density_flux_reflected_photons_incoh_vs_omega*(

    omega_step_muev))-flux_reflected_photons_incoh)/
    flux_reflected_photons_incoh) ' \n'])
38 fprintf(['g1SDCW - ' text_legend_model ': Relative error on the spectral
    density normalization - transmitted photons (incoherent part) :'
    num2str(abs(sum(
    spectral_density_flux_transmitted_photons_incoh_vs_omega*(

    omega_step_muev))-flux_transmitted_photons_incoh)/
    flux_reflected_photons_incoh) ' \n'])
39 fprintf(['g1SDCW - ' text_legend_model ': Relative error on the spectral
    density normalization - emitted photons (incoherent part) : ' num2str(
    abs(sum(spectral_density_flux_emitted_photons_incoh_vs_omega*(

    omega_step_muev))-flux_emitted_photons_incoh)/
    flux_emitted_photons_incoh) ' \n \n'])
40
41
42 %%%%%%%%%%%%%% Plots of g(1)(tau) %%%%%%%%%%%%%%
43 if ismember('G',plot_choice)
44     figure('Name',[ 'g1SDCW - ' text_legend_model ' - |(g1)| vs tau -
        reflected photons - Pin = ' num2str(P_in_CW_pW) ' pW - Pulsation
        laser = ' num2str(omega_laser_ev) ' eV' ],'NumberTitle','off')
45     plot(full_tau_list,abs(full_g_1_reflected_vs_tau),'r');
46     xlabel('Delay \tau [ps]'); ylabel('|(g1)| - reflected photons');
47     xlim([min(full_tau_list) max(full_tau_list)]); ylim([0 real(max(
        full_g_1_reflected_vs_tau))]);
48     text(full_tau_list(ceil(nb_points_delay/20)),0.2*max(
        full_g_1_reflected_vs_tau),text_legend,'FontSize',9)
49     annotation('textbox',[.15 .65 .2 .2],'String',[ 'Coherent : ' num2str(
        abs(100*flux_reflected_photons_laser_coherent/
        flux_reflected_photons)) ' %'], 'FitBoxToText','on');
50     annotation('textbox',[.15 .55 .2 .2],'String',[ 'Incoherent : ' num2str(
        abs(100*flux_reflected_photons_incoh/flux_reflected_photons)) ' %
        ], 'FitBoxToText','on');
51
52     figure('Name',[ 'g1SDCW - ' text_legend_model ' - |(g1)| vs tau -
        transmitted photons - Pin = ' num2str(P_in_CW_pW) ' pW - Pulsation
        laser = ' num2str(omega_laser_ev) ' eV' ],'NumberTitle','off')
53     plot(full_tau_list,abs(full_g_1_transmitted_vs_tau),'r');
54     xlabel('Delay \tau [ps]'); ylabel('|(g1)| - transmitted photons');

```

```

55     xlim([min(full_tau_list) max(full_tau_list)]); ylim([0 real(max(
56         full_g_1_transmitted_vs_tau))]);
57     text(full_tau_list(ceil(nb_points_delay/20)),0.2*max(
58         full_g_1_transmitted_vs_tau),text_legend,'FontSize',9)
59     annotation('textbox',[.15 .65 .2 .2], 'String',[ 'Coherent : ' num2str(
60         abs(100*flux_transmitted_photons_laser_coherent/
61             flux_transmitted_photons)) ' %'], 'FitBoxToText','on');
62     annotation('textbox',[.15 .55 .2 .2], 'String',[ 'Incoherent : ' num2str(
63         abs(100*flux_transmitted_photons_incoh/flux_transmitted_photons)) ' %
64         '], 'FitBoxToText','on');
65
66     figure('Name',[ 'g1SDCW - ' text_legend_model ' -real |(g1)| vs tau -
67         emitted photons in leaky modes - Pin = ' num2str(P_in_CW_pW) ' pW -
68         Pulsation laser = ' num2str(omega_laser_ev) ' eV' ],'NumberTitle',
69         'off')
70     plot(full_tau_list,abs(full_g_1_emitted_vs_tau),'r');
71     xlabel('Delay \tau [ps]'); ylabel('|(g1)| - emitted photons');
72     xlim([min(full_tau_list) max(full_tau_list)]); ylim([0 real(max(
73         full_g_1_emitted_vs_tau))]);
74     text(full_tau_list(ceil(nb_points_delay/20)),0.2*max(
75         full_g_1_emitted_vs_tau),text_legend,'FontSize',9)
76     annotation('textbox',[.15 .65 .2 .2], 'String',[ 'Coherent : ' num2str(
77         abs(100*flux_emitted_photons_laser_coherent/flux_emitted_photons)) ' %
78         '], 'FitBoxToText','on');
79     annotation('textbox',[.15 .55 .2 .2], 'String',[ 'Incoherent : ' num2str(
80         abs(100*flux_emitted_photons_incoh/flux_emitted_photons)) ' %'], 'FitBoxToText','on');
81
82     end
83 %%%%%%%%%%%%%% Plotting of spectra densities %%%%%%%%%%%%%%
84
85 if ismember('S',plot_choice)
86
87     figure('Name',[ 'g1SDCW - ' text_legend_model ' - Spectral density of
88         flux - Incoherent reflected photons - Pin = ' num2str(P_in_CW_pW) ' pW -
89         Pulsation laser = ' num2str(omega_laser_ev) ' eV' ],'NumberTitle',
90         'off')
91     plot((omega_list_ev-omega_laser_ev)*1e6,abs(
92         spectral_density_flux_reflected_photons_incoh_vs_omega));
93     xlabel('\omega-\omega_{laser} [muev]'); ylabel('Flux spectral density [
94         photons / ps / mueV]');
95     text(1e6*(omega_list_ev(ceil(nb_points_spectrum/20))-omega_laser_ev),
96         ,0.9*real(max(abs(
97             spectral_density_flux_reflected_photons_incoh_vs_omega))),text_legend,'FontSize',9)
98     title('Flux spectral density - incoherent part of the reflected field')
99
100

```

```

77 figure('Name',[ 'g1SDCW - ' text_legend_model ' - Spectral density of
    flux - Incoherent transmitted photons - Pin = ' num2str(P_in_CW_pW)
    ' pW - Pulsation laser = ' num2str(omega_laser_ev) ' eV' ],'
    NumberTitle','off')
78 plot((omega_list_ev-omega_laser_ev)*1e6,abs(
    spectral_density_flux_transmitted_photons_incoh_vs_omega));
79 xlabel('\omega-\omega_{laser} [muev]');ylabel('Flux spectral density [
    photons / ps / mueV]');
80 text(1e6*(omega_list_ev(ceil(nb_points_spectrum/20))-omega_laser_ev)
    ,0.9*real(max(abs(
        spectral_density_flux_transmitted_photons_incoh_vs_omega))),text_legend,'FontSize',9)
81 title('Flux spectral density - incoherent part of the transmitted field
    ')
82
83 figure('Name',[ 'g1SDCW - ' text_legend_model ' - Spectral density of
    flux - Incoherent emitted photons - Pin = ' num2str(P_in_CW_pW)
    ' pW - Pulsation laser = ' num2str(omega_laser_ev) ' eV' ],'
    NumberTitle','off')
84 plot((omega_list_ev-omega_laser_ev)*1e6, abs(
    spectral_density_flux_emitted_photons_incoh_vs_omega));
85 xlabel('\omega-\omega_{laser} [muev]');ylabel('Flux spectral density [
    photons / ps / mueV]');
86 text(1e6*(omega_list_ev(ceil(nb_points_spectrum/20))-omega_laser_ev)
    ,0.9*real(max(abs(
        spectral_density_flux_emitted_photons_incoh_vs_omega))),text_legend
    ,'FontSize',9)
87 title('Flux spectral density - incoherent part of the emitted field')
88 end

```

C.3.12 plot 2level g1 WDF PW

```

1 %Verification of the photon number conservation
2 fprintf(['RFTR: relative error of the photon number conservation: ' num2str
    (abs(Nb_reflected_photons+Nb_transmitted_photons+Nb_diffracted_photons+
    Nb_emitted_photons-Nb_photons_pulse)/Nb_photons_pulse) '\n'])
3 %
4 switch model
5 case 'F'
6     text_legend_model='full model';
7 case 'A'
8     text_legend_model='adiabatic model';
9 end
10 %% plotting g1(t1,t2)
11
12 if ismember('g',plot_choice)

```

```
13
14 figure('Name',['g1 reflected vs (t1,t2) – ' text_legend_model],'
15     NumberTitle,'off')
16 surf(flip(t_list),t_list,flip(abs(g1_reflected_vs_t1_t2),2),'LineStyle'
17     , 'none')
18 xlabel('t_1 [ps]')
19 ylabel('t_2 [ps]')
20 title('reflected |g^{(1)}(t_1,t_2)|')
21 view(2)
22 colorbar
23
24 figure('Name',['g1 diffracted vs (t1,t2) – ' text_legend_model],'
25     NumberTitle,'off')
26 surf(flip(t_list),t_list,flip(abs(g1_diffracted_vs_t1_t2),2),'LineStyle'
27     , 'none')
28 xlabel('t_1 [ps]')
29 ylabel('t_2 [ps]')
30 title('diffracted |g^{(1)}(t_1,t_2)|')
31 view(2)
32 colorbar
33
34 figure('Name',['g1 transmitted vs (t1,t2) – ' text_legend_model],'
35     NumberTitle,'off')
36 surf(flip(t_list),t_list,flip(abs(g1_transmitted_vs_t1_t2),2),'LineStyle'
37     , 'none')
38 xlabel('t_1 [ps]')
39 ylabel('t_2 [ps]')
40 title('transmitted |g^{(1)}(t_1,t_2)|')
41 view(2)
42 colorbar
43
44 figure('Name',['g1 emitted vs (t1,t2) – ' text_legend_model],'
45     NumberTitle,'off')
46 surf(flip(t_list),t_list,flip(abs(g1_emitted_vs_t1_t2),2),'LineStyle',
47     'none')
48 xlabel('t_1 [ps]')
49 ylabel('t_2 [ps]')
50 title('emitted |g^{(1)}(t_1,t_2)|')
51 view(2)
52 colorbar
53
54 end
55 %% plotting G1 vs(t1,t2)
56 if ismember('G',plot_choice)
57
58 figure('Name',['G1 reflected vs (t1,t2) – ' text_legend_model],'
59     NumberTitle,'off')
```

```

50 surf(flip(t_list),t_list,flip(abs(G1_reflected_vs_t1_t2),2), 'LineStyle'
51     , 'none')
52 xlabel('t_1 [ps]')
53 ylabel('t_2 [ps]')
54 title('|<b_{out}''(t_1) b_{out}(t_2)>| ')
55 view(2)
56 colorbar
57
58 figure('Name',[ 'G1 transmitted vs (t1,t2) - ' text_legend_model], 'NumberTitle','off')
59 surf(flip(t_list),t_list,flip(abs(G1_transmitted_vs_t1_t2),2), 'LineStyle',
60     'none')
61 xlabel('t_1 [ps]')
62 ylabel('t_2 [ps]')
63 title('|<c_{out}''(t_1) c_{out}(t_2)>| ')
64 view(2)
65 colorbar
66
67 figure('Name',[ 'G1 diffracted vs (t1,t2) - ' text_legend_model], 'NumberTitle','off')
68 surf(flip(t_list),t_list,flip(abs(G1_diffracted_vs_t1_t2),2), 'LineStyle
69     ', 'none')
70 xlabel('t_1 [ps]')
71 ylabel('t_2 [ps]')
72 title('|<d_{out}''(t_1) d_{out}(t_2)>| ')
73 view(2)
74 colorbar
75
76 figure('Name',[ 'G1 emitted vs (t1,t2) - ' text_legend_model], 'NumberTitle','off')
77 surf(flip(t_list),t_list,flip(abs(G1_emitted_vs_t1_t2),2), 'LineStyle', '
78     none)
79 xlabel('t_1 [ps]')
80 ylabel('t_2 [ps]')
81 title('|<e_{out}''(t_1) e_{out}(t_2)>| ')
82 view(2)
83 colorbar
84
85 end
86 % Parameters for the text displayed in figure legends
87 text_legend_QD = [ 'g=' num2str(g_muev) ' muev \gamma_{sp}'= num2str(
88     gamma_sp_muev) 'muev \gamma^{**}' num2str(gamma_puredephasing_muev) 'muev'];
89 text_legend_cav = [ '\kappa=' num2str(kappa_muev) 'muev \eta_{top}'=
90     num2str(eta_top) ' C=' num2str(g^2/kappa/gamma_decoherence,3)];
91 text_legend_pulse = [ 'N_{in}'= num2str(Nb_photons_pulse) ' FWHM_{pulse}'=
92     num2str(FWHM_pulse) 'ps'];

```

```

85 text_legend = {text_legend_QD,text_legend_cav,text_legend_pulse};
86 % NB: C is the cooperativity
87
88 %% plotting interpolated G1(time,tau)
89 if ismember('I',plot_choice)
90     figure('Name',[ 'interpolated G1 reflected vs time tau - '
91             text_legend_model ' - Nb_photons = ' num2str(Nb_photons_pulse)],'
92             'NumberTitle','off')
93     surf(time_list,tau_list, abs(interpolated_G1_reflected_vs_time_tau'),'
94             'LineStyle','none')
95     axis xy
96     colorbar
97     xlabel('t, origin at beginning of 1st evolution [ps]', 'FontSize',14)
98     ylabel('\tau [ps]', 'FontSize',14)
99     title('interpolated G1 reflected vs time tau')
100    view(2)
101
102    figure('Name',[ 'interpolated G1 transmitted vs time tau - '
103            text_legend_model ' - Nb_photons = ' num2str(Nb_photons_pulse)],'
104            'NumberTitle','off')
105    surf(time_list,tau_list, abs(interpolated_G1_transmitted_vs_time_tau'),'
106            'LineStyle','none')
107    axis xy
108    colorbar
109    xlabel('t, origin at beginning of 1st evolution [ps]', 'FontSize',14)
110    ylabel('\tau [ps]', 'FontSize',14)
111    title('interpolated G1 transmitted vs time tau')
112    view(2)
113
114    figure('Name',[ 'interpolated G1 emitted vs time tau - '
115            text_legend_model ' - Nb_photons = ' num2str(Nb_photons_pulse)],'
116            'NumberTitle','off')
117    surf(time_list,tau_list, abs(interpolated_G1_emitted_vs_time_tau'),'
118            'LineStyle','none')

```

```

119 axis xy
120 colorbar
121 xlabel('t, origin at beginning of 1st evolution [ps]', 'FontSize', 14)
122 ylabel('\tau [ps]', 'FontSize', 14)
123 title('interpolated G1 diffracted vs time tau')
124 view(2)
125 end
126 %% Plotting WDF
127 if ismember('W', plot_choice)
128     figure('Name', ['WDF reflected photons - ' text_legend_model ' -
129         Nb_photons = ' num2str(Nb_photons_pulse)], 'NumberTitle', 'off')
130     imagesc(time_list, (omega_list_full_spectrum_muev - omega_pulse_ev*1e6),
131             real(WDF_interpolated_G1_reflected_vs_time_tau_full_spectrum));
132     axis xy
133     colorbar
134     xlabel('t, origin at beginning of 1st evolution [ps]')
135     ylabel('\omega-\omega_p [\mu eV]', 'FontSize', 14)
136     title('Wigner distribution reflected [1/(\mu eV\cdot\cdot\cdot)]')
137
138     figure('Name', ['WDF reflected photons - zoomed spectrum - ' -
139         text_legend_model ' - Nb_photons = ' num2str(Nb_photons_pulse)], ' -
140         NumberTitle', 'off')
141     imagesc(time_list, (omega_list_ev - omega_pulse_ev)*1e6, real(
142         WDF_interpolated_G1_reflected_vs_time_tau));
143     axis xy
144     colorbar
145     xlabel('t, origin at beginning of 1st evolution [ps]')
146     ylabel('\omega-\omega_p [\mu eV]', 'FontSize', 14)
147     title('zoomed Wigner distribution reflected [1/(\mu eV\cdot\cdot\cdot)]')
148
149     figure('Name', ['WDF transmitted photons - ' text_legend_model ' -
150         Nb_photons = ' num2str(Nb_photons_pulse)], 'NumberTitle', 'off')
151     imagesc(time_list, (omega_list_full_spectrum_muev - omega_pulse_ev*1e6),
152             real(WDF_interpolated_G1_transmitted_vs_time_tau_full_spectrum));
153     ;
154     axis xy
155     colorbar
156     xlabel('t, origin at beginning of 1st evolution [ps]')
157     ylabel('\omega-\omega_p [\mu eV]', 'FontSize', 14)
158     title('Wigner distribution transmitted [1/(\mu eV\cdot\cdot\cdot)]')
159
160     figure('Name', ['WDF transmitted photons - zoomed spectrum - ' -
161         text_legend_model ' - Nb_photons = ' num2str(Nb_photons_pulse)], ' -
162         NumberTitle', 'off')
163     imagesc(time_list, (omega_list_ev - omega_pulse_ev)*1e6, real(
164         WDF_interpolated_G1_transmitted_vs_time_tau));

```

```

154 axis xy
155 colorbar
156 xlabel('t, origin at beginning of 1st evolution [ps]')
157 ylabel('\omega-\omega_p [\mu eV]', 'FontSize', 14)
158 title('zoomed Wigner distribution transmitted [1/(\mu eV\cdot\cdot\cdot)]')
159
160 figure('Name', ['WDF emitted photons - ' text_legend_model ' -
    Nb_photons = ' num2str(Nb_photons_pulse)], 'NumberTitle', 'off')
161 imagesc(time_list, (omega_list_full_spectrum_muev - omega_pulse_ev*1e6),
    real(WDF_interpolated_G1_emitted_vs_time_tau_full_spectrum));
162 axis xy
163 colorbar
164 xlabel('t, origin at beginning of 1st evolution [ps]')
165 ylabel('\omega-\omega_p [\mu eV]', 'FontSize', 14)
166 title('Wigner distribution emitted [1/(\mu eV\cdot\cdot\cdot)]')
167
168 figure('Name', ['WDF emitted photons - zoomed spectrum - ' -
    text_legend_model ' - Nb_photons = ' num2str(Nb_photons_pulse)], ' -
    NumberTitle', 'off')
169 imagesc(time_list, (omega_list_ev - omega_pulse_ev)*1e6, real(
    WDF_interpolated_G1_emitted_vs_time_tau'));
170 axis xy
171 colorbar
172 xlabel('t, origin at beginning of 1st evolution [ps]')
173 ylabel('\omega-\omega_p [\mu eV]', 'FontSize', 14)
174 title('zoomed Wigner distribution emitted [1/(\mu eV\cdot\cdot\cdot)]')
175
176 figure('Name', ['WDF diffracted photons - ' text_legend_model ' -
    Nb_photons = ' num2str(Nb_photons_pulse)], 'NumberTitle', 'off')
177 imagesc(time_list, (omega_list_full_spectrum_muev - omega_pulse_ev*1e6),
    real(WDF_interpolated_G1_diffracted_vs_time_tau_full_spectrum));
178 axis xy
179 colorbar
180 xlabel('t, origin at beginning of 1st evolution [ps]')
181 ylabel('\omega-\omega_p [\mu eV]', 'FontSize', 14)
182 title('Wigner distribution diffracted [1/(\mu eV\cdot\cdot\cdot)]')
183
184 figure('Name', ['WDF diffracted photons - zoomed spectrum - ' -
    text_legend_model ' - Nb_photons = ' num2str(Nb_photons_pulse)], ' -
    NumberTitle', 'off')
185 imagesc(time_list, (omega_list_ev - omega_pulse_ev)*1e6, real(
    WDF_interpolated_G1_diffracted_vs_time_tau));
186 axis xy
187 colorbar
188 xlabel('t, origin at beginning of 1st evolution [ps]')
189 ylabel('\omega-\omega_p [\mu eV]', 'FontSize', 14)

```

```

190     title('zoomed Wigner distribution diffracted [1/(\mu_eV\cdot\omega)]')
191 end
192 %% Plotting photon fluxes
193 if ismember('F',plot_choice)
194     figure('Name',[ 'Flux reflected photons vs time - Nb_photons = ' num2str
195         (Nb_photons_pulse)],'NumberTitle','off')
196     plot(t_list, flux_reflected_photons_vs_time,'r', time_list, real(sum(
197         WDF_interpolated_G1_reflected_vs_time_tau_full_spectrum,2))*%
198         omega_step_muev,'g--', t_list,
199         flux_reflected_photons_pulse_coherent_vs_time,'k',time_list, real(
200             sum(WDF_interpolated_reflected_coherent_vs_time_tau_full_spectrum
201                 ,2))*omega_step_muev,'m--');
202     xlabel('Time t [ps]');ylabel('Flux reflected photon [ps^{-1}]');
203     legend('<b_{out}>''b_{out}>', 'total flux by WDF(t,\omega)', '<b_{out}><
204         b_{out}>', 'total coherent flux by WDF(t,\omega)');
205     text(t_list(floor(nb_points_time*0.6)),0.2*max(
206         flux_reflected_photons_vs_time),text_legend,'FontSize',9)
207
208     figure('Name',[ 'Flux transmitted photons vs time - Nb_photons = ' num2str
209         (Nb_photons_pulse)],'NumberTitle','off')
210     plot(t_list, flux_transmitted_photons_vs_time,'r', time_list, real(sum(
211         WDF_interpolated_G1_transmitted_vs_time_tau_full_spectrum,2))*%
212         omega_step_muev,'g--', t_list,
213         flux_transmitted_photons_pulse_coherent_vs_time,'k',time_list, real(
214             sum(
215                 WDF_interpolated_transmitted_coherent_vs_time_tau_full_spectrum,2))
216             *omega_step_muev,'m--');
217     xlabel('Time t [ps]');ylabel('Flux transmitted photon [ps^{-1}]');
218     legend('<c_{out}>''c_{out}>', 'total flux by WDF(t,\omega)', '<c_{out}><
219         c_{out}>', 'total coherent flux by WDF(t,\omega)');
220     text(t_list(floor(nb_points_time*0.6)),0.2*max(
221         flux_transmitted_photons_vs_time),text_legend,'FontSize',9)
222
223     figure('Name',[ 'Flux emitted photons vs time - Nb_photons = ' num2str
224         (Nb_photons_pulse)],'NumberTitle','off')
225     plot(t_list, flux_emitted_photons_vs_time,'r', time_list, real(sum(
226         WDF_interpolated_G1_emitted_vs_time_tau_full_spectrum,2))*%
227         omega_step_muev,'g--', t_list,
228         flux_emitted_photons_pulse_coherent_vs_time,'k',time_list, real(sum(
229             (WDF_interpolated_emitted_coherent_vs_time_tau_full_spectrum,2))*%
230                 omega_step_muev,'m--');
231     xlabel('Time t [ps]');ylabel('Flux emitted photon [ps^{-1}]');
232     legend('<d_{out}>''d_{out}>', 'total flux by WDF(t,\omega)', '<d_{out}><
233         d_{out}>', 'total coherent flux by WDF(t,\omega)');
234     text(t_list(floor(nb_points_time*0.6)),0.2*max(
235         flux_emitted_photons_vs_time),text_legend,'FontSize',9)

```

```

211
212 figure('Name',[ 'Flux diffracted photons vs time – Nb_photons = '
213     num2str(Nb_photons_pulse)],'NumberTitle','off')
214 plot(t_list, flux_diffracted_photons_vs_time,'r', time_list, real(sum(
215     WDF_interpolated_G1_diffracted_vs_time_tau_full_spectrum,2))*omega_step_muev,'g--', t_list,
216     flux_diffracted_photons_pulse_coherent_vs_time,'k',time_list, real(
217     sum(WDF_interpolated_diffracted_coherent_vs_time_tau_full_spectrum
218     ,2))*omega_step_muev,'m--');
219 xlabel('Time t [ps]');ylabel('Flux diffracted photon [ps^{-1}]');
220 legend('<e_{out}''e_{out}>', 'total flux by WDF(t,\omega)', '<e_{out}><
221     e_{out}>', 'total coherent flux by WDF(t,\omega)');
222 text(t_list(floor(nb_points_time*0.6)),0.2*max(
223     flux_diffracted_photons_vs_time),text_legend,'FontSize',9)
224
225
226 figure('Name',[ 'Spectral density reflected photons vs omega –
227     Nb_photons = ' num2str(Nb_photons_pulse)],'NumberTitle','off')
228 plot((omega_list_ev – omega_pulse_ev)*1e6, real(
229     ESD_reflected_photons_vs_omega) , 'r',(omega_list_ev –
230     omega_pulse_ev)*1e6, real(
231     ESD_coherent_reflected_photons_laser_vs_omega), 'g',(omega_list_ev –
232     omega_pulse_ev)*1e6, real(ESD_reflected_photons_vs_omega)–real(
233     ESD_coherent_reflected_photons_laser_vs_omega), 'b');
234 xlim([min(omega_list_ev – omega_pulse_ev)*1e6 max(omega_list_ev –
235     omega_pulse_ev)*1e6]);
236 xlabel('\omega-\omega_p [\mu eV]');ylabel('Reflected field spectral
237     density');
238 legend('WDF(\omega) – total reflected flux', 'WDF(\omega) coherent flux
239     ', 'WDF(\omega) – incoherent flux')
240 text(omega_list_ev(1) – omega_pulse_ev,0.7*max(
241     ESD_reflected_photons_vs_omega),text_legend,'FontSize',9)
242
243
244 figure('Name',[ 'Spectral density transmitted photons vs omega –
245     Nb_photons = ' num2str(Nb_photons_pulse)],'NumberTitle','off')
246 plot((omega_list_ev – omega_pulse_ev)*1e6, real(
247     ESD_transmitted_photons_vs_omega) , 'r',(omega_list_ev –
248     omega_pulse_ev)*1e6, real(
249     ESD_coherent_transmitted_photons_laser_vs_omega), 'g',(omega_list_ev –
250     omega_pulse_ev)*1e6, real(ESD_transmitted_photons_vs_omega)–real(
251     ESD_coherent_transmitted_photons_laser_vs_omega), 'b');
252 xlim([min(omega_list_ev – omega_pulse_ev)*1e6 max(omega_list_ev –
253     omega_pulse_ev)*1e6]);
254 xlabel('\omega-\omega_p [\mu eV]');ylabel('Reflected field spectral
255     density');

```

```

230 legend('WDF(\omega) — total transmitted flux', 'WDF(\omega) coherent
231     flux', 'WDF(\omega) — incoherent flux')
232 text(omega_list_ev(1) — omega_pulse_ev,0.7*max(
233     ESD_transmitted_photons_vs_omega),text_legend,'FontSize',9)
234 figure('Name',[ 'Spectral density emitted photons vs omega — Nb_photons
235     = ' num2str(Nb_photons_pulse)],'NumberTitle','off')
236 plot((omega_list_ev — omega_pulse_ev)*1e6, real(
237     ESD_emitted_photons_vs_omega) , 'r',(omega_list_ev — omega_pulse_ev)
238 *1e6, real(ESD_coherent_emitted_photons_laser_vs_omega), 'g',((
239     omega_list_ev — omega_pulse_ev)*1e6, real(
240     ESD_emitted_photons_vs_omega)—real(
241     ESD_coherent_emitted_photons_laser_vs_omega), 'b');
242 xlim([min(omega_list_ev — omega_pulse_ev)*1e6 max(omega_list_ev —
243     omega_pulse_ev)*1e6]);
244 xlabel('\omega-\omega_p [\mu eV]');ylabel('Reflected field spectral
245     density');
246 legend('WDF(\omega) — total emitted flux', 'WDF(\omega) coherent flux',
247     'WDF(\omega) — incoherent flux')
248 text(omega_list_ev(1) — omega_pulse_ev,0.7*max(
249     ESD_emitted_photons_vs_omega),text_legend,'FontSize',9)
250 figure('Name',[ 'Spectral density diffracted photons vs omega — '
251     text_legend_model ' — Nb_photons = ' num2str(Nb_photons_pulse)],'
252     'NumberTitle','off')
253 plot((omega_list_ev — omega_pulse_ev)*1e6, real(
254     ESD_diffracted_photons_vs_omega) , 'r',(omega_list_ev —
255     omega_pulse_ev)*1e6, real(
256     ESD_coherent_diffracted_photons_laser_vs_omega), 'g',(omega_list_ev
257 — omega_pulse_ev)*1e6, real(ESD_diffracted_photons_vs_omega)—real(
258     ESD_coherent_diffracted_photons_laser_vs_omega), 'b');
259 xlim([min(omega_list_ev — omega_pulse_ev)*1e6 max(omega_list_ev —
260     omega_pulse_ev)*1e6]);
261 xlabel('\omega-\omega_p [\mu eV]');ylabel('Reflected field spectral
262     density');
263 legend('WDF(\omega) — total diffracted flux', 'WDF(\omega) coherent
264     flux', 'WDF(\omega) — incoherent flux')
265 text(omega_list_ev(1) — omega_pulse_ev,0.7*max(
266     ESD_diffracted_photons_vs_omega),text_legend,'FontSize',9)
267 end
268 %% Checking normalization of ESDs
269 fprintf(['Relative error over normalization of spectral density — reflected
270     field: ' num2str(abs(sum(ESD_reflected_photons_vs_omega)*
271     omega_step_muev-Nb_reflected_photons)/Nb_reflected_photons) ' \n'])

```

```

250 fprintf(['Relative error over normalization of spectral density –
    transmitted field: ' num2str(abs(sum(ESD_transmitted_photons_vs_omega)*
        omega_step_muev–Nb_transmitted_photons)/Nb_transmitted_photons) '\n'])
251 fprintf(['Relative error over normalization of spectral density – emitted
    field: ' num2str(abs(sum(ESD_emitted_photons_vs_omega)*omega_step_muev–
        Nb_emitted_photons)/Nb_emitted_photons) '\n'])
252 fprintf(['Relative error over normalization of spectral density –
    diffracted field: ' num2str(abs(sum(ESD_diffracted_photons_vs_omega)*
        omega_step_muev–Nb_diffracted_photons)/Nb_diffracted_photons) '\n'])

```

C.3.13 plot 2level g2 CW vs delay

```

1 switch model
2     case 'F'
3         text_legend_model='full model';
4     case 'A'
5         text_legend_model='adiabatic model';
6 end
7
8 % Parameters for the text displayed in figure legends
9 text_legend_QD=['g= ', num2str(g_muev) ' muev \gamma_{sp}= ' num2str(
    gamma_sp_muev) ' muev \gamma^{**}= ' num2str(gamma_puredephasing_muev) ' '
    muev'];
10 text_legend_cav=[ '\kappa= ' num2str(kappa_muev) ' muev \eta_{top}= ' num2str(
    eta_top) ' C= ' num2str(g^2/kappa/gamma_decoherence,3)];
11 text_legend_P_in=['P_{in}= ' num2str(P_in_CW_pW) ' pW n_c= ' num2str(
    gamma_decoherence*gamma_sp/(4*g^2),2)];
12 text_legend_omega=[ '\omega_{laser}–\omega_d= ' num2str(1e6*(omega_laser_ev–
    omega_d_ev),3) ' muev \omega_d–\omega_c= ' num2str(1e6*(omega_d_ev–
    omega_c_ev),3) ' muev'];
13 text_legend={text_legend_QD,text_legend_cav,text_legend_P_in,
    text_legend_omega};
14 % NB: C is the cooperativity and n_c the critical photon number, both
    depend only on the cavity-QED parameters.
15 % On the contrary, n_0 depends on the incoming power P_in since it is the
    calculated number of intracavity photons
16 % in the absence of QD (i.e. when g=0). When n_0 is much lower than n_c we
    are in the weak excitation limit.
17
18
19 ##### Verifications #####
20
21 % Verification on the conservation of photon flux

```



```

46
47 %%%%%%%% Plots of the normalized g(2)(tau)
48 %%%%%%
49 if ismember('R',plot_choice)
50 figure('Name',[ 'g2CW ' text_legend_model ' – g2 vs tau – reflected
51 photons – Pin = ' num2str(P_in_CW_pW) ' pW – Laser photon energy =
52 ' num2str(omega_laser_ev) ' eV' ],'NumberTitle','off')
53 plot(full_tau_list_g2CW,full_g2_reflected_vs_delay,'r');
54 xlabel('Delay \tau [ps]'); ylabel('g^2 – reflected photons');
55 xlim([min(full_tau_list_g2CW) max(full_tau_list_g2CW)]);
56 text(full_tau_list_g2CW(ceil(nb_points_time_g2CW/20)),0.8*max(
57 full_g2_reflected_vs_delay),text_legend,'FontSize',9)
58
59 if ismember('O',plot_choice)
60 figure('Name',[ 'g2CW ' text_legend_model ' – occupation
61 probabilities conditioned to a reflected photon detecton – Pin
62 = ' num2str(P_in_CW_pW) ' pW – Laser photon energy = ' num2str(
63 omega_laser_ev) ' eV' ],'NumberTitle','off')
64 plot(tau_list_g2CW,
65 occupation_ground_vs_delay_after_reflected_photon_detection,'r'
66 ,...
67 tau_list_g2CW,
68 occupation_excited_vs_delay_after_reflected_photon_detection
69 , 'b');
70 xlabel('Delay \tau [ps]'); ylabel('Conditionnal occupation
71 probabilities');
72 xlim([min(tau_list_g2CW) max(tau_list_g2CW)]); ylim([0 1]);
73 text(tau_list_g2CW(ceil(nb_points_time_g2CW/10)),0.7,text_legend,
74 'FontSize',9)
75 legend('Occupation of |g> conditioned on a reflected photon
76 detection','Occupation of |e> conditioned on a reflected photon
77 detection','Location','best');
78
79 end
80
81 end
82
83 if ismember('T',plot_choice)
84 figure('Name',[ 'g2CW ' text_legend_model ' – g2 vs tau – transmitted
85 photons – Pin = ' num2str(P_in_CW_pW) ' pW – Pulsation laser =
86 ' num2str(omega_laser_ev) ' eV' ],'NumberTitle','off')
87 plot(full_tau_list_g2CW,full_g2_transmitted_vs_delay,'b');
88 xlabel('Delay \tau [ps]'); ylabel('g^2 – transmitted photons');
89 xlim([min(full_tau_list_g2CW) max(full_tau_list_g2CW)]);
90 text(full_tau_list_g2CW(ceil(nb_points_time_g2CW/20)),0.8*max(
91 full_g2_transmitted_vs_delay),text_legend,'FontSize',9)
92
93

```

```

74 if ismember('O',plot_choice)
75     figure('Name',[ 'g2CW ' text_legend_model ' - occupation
    probabilities conditioned to a transmitted photon detecton -
    Pin = ' num2str(P_in_CW_pW) ' pW - Laser photon energy = '
    num2str(omega_laser_ev) ' eV' ],'NumberTitle','off')
76 plot(tau_list_g2CW,
    occupation_ground_vs_delay_after_transmitted_photon_detection,'r',...
77     tau_list_g2CW,
        occupation_excited_vs_delay_after_transmitted_photon_detection
        , 'b');
78 xlabel('Delay \tau [ps]'); ylabel('Conditionnal occupation
    probabilities');
79 xlim([min(tau_list_g2CW) max(tau_list_g2CW)]); ylim([0 1]);
80 text(tau_list_g2CW(ceil(nb_points_time_g2CW/10)),0.7,text_legend,
    'FontSize',9)
81 legend('Occupation of |g> conditioned on a transmitted photon
    detection','Occupation of |e> conditioned on a transmitted
    photon detection','Location','best');
82 end
83 end
84 if ismember('E',plot_choice)
85
86     figure('Name',[ 'g2CW ' text_legend_model ' - g2 vs tau - photons
    emitted outside the mode - Pin = ' num2str(P_in_CW_pW) ' pW -
    Pulsation laser = ' num2str(omega_laser_ev) ' eV' ],'NumberTitle',
    'off')
87 plot(full_tau_list_g2CW,full_g2_emitted_vs_delay,'g');
88 xlabel('Delay \tau [ps]'); ylabel('g^2 - photons emitted outside the
    mode');
89 xlim([min(full_tau_list_g2CW) max(full_tau_list_g2CW)]);
90 text(full_tau_list_g2CW(ceil(nb_points_time_g2CW/20)),0.3*max(
    full_g2_emitted_vs_delay),text_legend,'FontSize',9)
91 if ismember('O',plot_choice)
92     figure('Name',[ 'g2CW ' text_legend_model ' - occupation
    probabilities conditioned to an emitted photon detecton - Pin =
    ' num2str(P_in_CW_pW) ' pW - Laser photon energy = ' num2str(
    omega_laser_ev) ' eV' ],'NumberTitle','off')
93 plot(tau_list_g2CW,
    occupation_ground_vs_delay_after_emitted_photon_detection,'r',
    ...
94     tau_list_g2CW,
        occupation_excited_vs_delay_after_emitted_photon_detection
        , 'b');
95

```

```

96     xlabel('Delay \tau [ps]'); ylabel('Conditionnal occupation
97         probabilities');
98     xlim([min(tau_list_g2CW) max(tau_list_g2CW)]); ylim([0 1]);
99     text(tau_list_g2CW(ceil(nb_points_time_g2CW/10)),0.7,text_legend,
100        'FontSize',9)
101    legend('Occupation of |g> conditioned on an emitted photon
102        detection','Occupation of |e> conditioned on an emitted photon
103        detection','Location','best');
104    end
105 end

```

C.3.14 plot 2level g2 PR vs t1 t2

```

1 switch model
2   case 'F'
3     text_legend_model='full model';
4   case 'A'
5     text_legend_model='adiabatic model';
6 end
7
8 % Parameters for the text displayed in figure legends
9 text_legend_QD = ['g=' num2str(g_muev) ' muev \gamma_{sp}=' num2str(
10    gamma_sp_muev) 'muev \gamma^{*=' num2str(gamma_puredephasing_muev) '
11    muev'];
12 text_legend_cav = ['\kappa=' num2str(kappa_muev) 'muev \eta_{top}='
13    num2str(eta_top) ' C=' num2str(g^2/kappa/gamma_decoherence,3)];
14 text_legend_pulse = ['N_{in}=' num2str(Nb_photons_pulse) ' FWHM_{
15    pulse}= num2str(FWHM_pulse) 'ps'];
16 text_legend = {text_legend_QD, text_legend_cav, text_legend_pulse};
17 % NB: C is the cooperativity
18 %% g2 vs (t1,t2)
19 if ismember('G',plot_choice)
20   figure('Name',['g2 emitted vs (t1,t2) - ' text_legend_model],'
21     'NumberTitle','off')
22   surf(flip(t_list),t_list,flip(real(g2_emitted_vs_t1_t2),2))
23   xlabel('t_1 [ps]')
24   ylabel('t_2 [ps]')
25   title('emitted photon g^{(2)}(t_1,t_2)')
26   view(2)
27   colorbar
28
29   figure('Name',['g2 reflected vs (t1,t2) - ' text_legend_model],'
30     'NumberTitle','off')
31   surf(flip(t_list),t_list,flip(real(g2_reflected_vs_t1_t2),2))
32   xlabel('t_1 [ps]')
33   ylabel('t_2 [ps]')

```

```
28 title('reflected photon g^{(2)}(t_1,t_2)')
29 view(2)
30 colorbar
31
32 figure('Name',[ 'g2 transmitted vs (t1,t2) - ' text_legend_model],'
33     'NumberTitle','off')
34 surf(flip(t_list),t_list,flip(real(g2_transmitted_vs_t1_t2),2))
35 xlabel('t_1 [ps]')
36 ylabel('t_2 [ps]')
37 title('transmitted photon g^{(2)}(t_1,t_2)')
38 view(2)
39 colorbar
40 end
41 %% Photon coincidences
42 if ismember('C',plot_choice)
43 % photon coincidences uncorrelated
44 figure('Name',[ 'Uncorrelated coincidences emitted photons vs (t1,t2) - '
45     ' text_legend_model], 'NumberTitle','off')
46 surf(flip(t_list),t_list,flip(real(
47     emitted_photon_coincidences_vs_t1_vs_t2_uncorrelated_pulses),2))
48 xlabel('t_1 [ps]')
49 ylabel('t_2 [ps]')
50 title('<e_{out}>''(t_1) e_{out}(t_1)> <e_{out}>''(t_2) e_{out}(t_2)>')
51 view(2)
52 colorbar
53
54 figure('Name',[ 'Uncorrelated coincidences reflected photons vs (t1,t2)'
55     ' - ' text_legend_model], 'NumberTitle','off')
56 surf(flip(t_list),t_list,flip(real(
57     reflected_photon_coincidences_vs_t1_vs_t2_uncorrelated_pulses),2))
58 xlabel('t_1 [ps]')
59 ylabel('t_2 [ps]')
60 title('<b_{out}>''(t_1) b_{out}(t_1)> <b_{out}>''(t_2) b_{out}(t_2)>')
61 view(2)
62 colorbar
63
64 figure('Name',[ 'Uncorrelated coincidences transmitted photons vs (t1,t2)'
65     ' ) - ' text_legend_model], 'NumberTitle','off')
66 surf(flip(t_list),t_list,flip(real(
67     transmitted_photon_coincidences_vs_t1_vs_t2_uncorrelated_pulses),2)
68 )
69 xlabel('t_1 [ps]')
70 ylabel('t_2 [ps]')
71 title('<c_{out}>''(t_1) c_{out}(t_1)> <c_{out}>''(t_2) c_{out}(t_2)>')
72 colorbar
73
```

```

66 % photon coincidences correlated
67 figure('Name',[ 'Correlated coincidences emitted photons vs (t1,t2) –
68     text_legend_model], 'NumberTitle','off')
69 surf(flip(t_list),t_list,flip(real(
70     emitted_photon_coincidences_vs_t1_vs_t2),2))
71 xlabel('t_1 [ps]')
72 ylabel('t_2 [ps]')
73 title('<e_{out}''(t_1) e_{out}''(t_2) e_{out}(t_2) e_{out}(t_1)>')
74 view(2)
75 colorbar
76
77 figure('Name',[ 'Correlated coincidences reflected photons vs (t1,t2) –
78     text_legend_model], 'NumberTitle','off')
79 surf(flip(t_list),t_list,flip(real(
80     reflected_photon_coincidences_vs_t1_vs_t2),2))
81 xlabel('t_1 [ps]')
82 ylabel('t_2 [ps]')
83 title('<b_{out}''(t_1) b_{out}''(t_2) b_{out}(t_2) b_{out}(t_1)>')
84 view(2)
85 colorbar
86
87 figure('Name',[ 'Correlated coincidences transmitted photons vs (t1,t2)
88     – text_legend_model], 'NumberTitle','off')
89 surf(flip(t_list),t_list,flip(real(
90     transmitted_photon_coincidences_vs_t1_vs_t2),2))
91 xlabel('t_1 [ps]')
92 ylabel('t_2 [ps]')
93 title('<c_{out}''(t_1) c_{out}''(t_2) c_{out}(t_2) c_{out}(t_1)>')
94 view(2)
95 colorbar
96
97 end
98 %% conditioned occupations
99 if ismember('0',plot_choice)
100 figure('Name',[ 'Occupation ground after reflected photon vs (t1,t2) –
101     text_legend_model], 'NumberTitle','off')
102 surf(flip(t_list),t_list,flip(real(
103     occupation_ground_vs_t1_vs_t2_after_click_b_out_at_t1),2))
104 xlabel('t_1 [ps]')
105 ylabel('t_2 [ps]')
106 title('Occupation ground after reflected photon')
107 view(2)
108 colorbar
109
110 % figure('Name',[ 'Occupation excited after reflected photon vs (t1,t2)
111     – text_legend_model], 'NumberTitle','off')

```

```
102 %     surf(flip(t_list),t_list,flip(real(          occupation_excited_vs_t1_vs_t2_after_click_b_out_at_t1),2))  
103 %     xlabel('t_1 [ps]')  
104 %     ylabel('t_2 [ps]')  
105 %     title('Occupation excited after reflected photon')  
106 %     view(2)  
107 %     colorbar  
108  
109 figure('Name',['Occupation ground after transmitted photon vs (t1,t2) –  
    ' text_legend_model], 'NumberTitle','off')  
110 surf(flip(t_list),t_list,flip(real(          occupation_ground_vs_t1_vs_t2_after_click_c_out_at_t1),2))  
111 xlabel('t_1 [ps]')  
112 ylabel('t_2 [ps]')  
113 title('Occupation ground after transmitted photon')  
114 view(2)  
115 colorbar  
116  
117 %     figure('Name',['Occupation excited after transmitted photon vs (t1,t2)  
    ') – ' text_legend_model], 'NumberTitle','off')  
118 %     surf(flip(t_list),t_list,flip(real(          occupation_excited_vs_t1_vs_t2_after_click_c_out_at_t1),2))  
119 %     xlabel('t_1 [ps]')  
120 %     ylabel('t_2 [ps]')  
121 %     title('Occupation excited after transmitted photon')  
122 %     view(2)  
123 %     colorbar  
124  
125 figure('Name',['Occupation ground after emitted photon vs (t1,t2) – '  
    ' text_legend_model], 'NumberTitle','off')  
126 surf(flip(t_list),t_list,flip(real(          occupation_ground_vs_t1_vs_t2_after_click_e_out_at_t1),2))  
127 xlabel('t_1 [ps]')  
128 ylabel('t_2 [ps]')  
129 title('Occupation ground after emitted photon')  
130 view(2)  
131 colorbar  
132  
133 %     figure('Name',['Occupation excited after emitted photon vs (t1,t2) –  
    ') – ' text_legend_model], 'NumberTitle','off')  
134 %     surf(flip(t_list),t_list,flip(real(          occupation_excited_vs_t1_vs_t2_after_click_e_out_at_t1),2))  
135 %     xlabel('t_1 [ps]')  
136 %     ylabel('t_2 [ps]')  
137 %     title('Occupation excited after emitted photon')  
138 %     view(2)
```

```

139 %     colorbar
140 end
141 %% photon fluxes
142 if ismember('F',plot_choice)
143     figure('Name',[ 'Photons flux vs t1 - ' text_legend_model], 'NumberTitle'
144         , 'off')
145     plot(t_list,flux_injected_photons_vs_time,'k','Displayname','incoming')
146     hold on
147     plot(t_list,flux_reflected_photons_vs_time,'r','Displayname','reflected
148         ')
149     plot(t_list,flux_transmitted_photons_vs_time,'b','Displayname','
150         transmitted')
151     plot(t_list,flux_emitted_photons_vs_time,'g','Displayname','emitted')
152     hold off
153     title(['Photon flux - Nb = ' num2str(Nb_photons_pulse)])
154     xlabel('t_1 [ps]')
155     ylabel('[1/ps]')
156     legend
157     text(t_list(ceil(nb_points_time*0.05)),0.95*max(
158         flux_injected_photons_vs_time),text_legend,'FontSize',9)
159
160     figure('Name',[ 'Normalized g2 vs delay, photon emission - '
161         text_legend_model], 'NumberTitle', 'off')
162     plot(full_tau_list,[flip(normalized_g2_vs_delay_emitted(2:end))
163         normalized_g2_vs_delay_emitted],'g','Displayname', 'correlated')
164     hold on
165     plot(full_tau_list,[flip(normalized_g2_vs_delay_uncorrelated_emitted(2:
166         end)) normalized_g2_vs_delay_uncorrelated_emitted],'-g','
167         Displayname', 'uncorrelated')
168     title('Histogram < g^{(2)}(\tau) > emitted photons')
169     xlabel('\tau [ps]')
170     ylabel('counts')
171     legend('Location','northeast');
172     text(full_tau_list(ceil(nb_points_time*0.05)),max(
173         normalized_g2_vs_delay_uncorrelated_emitted)*0.9,text_legend,
174         'FontSize',9)
175
176     figure('Name',[ 'Normalized g2 vs delay, photon reflection - '
177         text_legend_model], 'NumberTitle', 'off')
178     plot(full_tau_list,[flip(normalized_g2_vs_delay_reflected(2:end))
179         normalized_g2_vs_delay_reflected],'r','Displayname', 'correlated')
180     hold on
181     plot(full_tau_list,[flip(normalized_g2_vs_delay_uncorrelated_reflected
182         (2:end)) normalized_g2_vs_delay_uncorrelated_reflected],'-r','
183         Displayname', 'uncorrelated')
184     title('Histogram < g^{(2)}(\tau) > reflected photons')

```

```

171 xlabel('\tau [ps]')
172 ylabel('counts')
173 legend('Location','northeast');
174 text(full_tau_list(ceil(nb_points_time*0.05)),max(
    normalized_g2_vs_delay_uncorrelated_reflected)*0.95,text_legend,
    'FontSize',9)
175
176 figure('Name',[ 'Normalized g2 vs delay, photon transmission - '
    text_legend_model], 'NumberTitle', 'off')
177 plot(full_tau_list,[flip(normalized_g2_vs_delay_transmitted(2:end))
    normalized_g2_vs_delay_transmitted], 'b', 'Displayname', 'correlated'
    )
178 hold on
179 plot(full_tau_list,[flip(
    normalized_g2_vs_delay_uncorrelated_transmitted(2:end))
    normalized_g2_vs_delay_uncorrelated_transmitted], '—b', 'Displayname
    ', 'uncorrelated')
180 title('Histogram < g^{(2)}(\tau) > transmitted photons')
181 xlabel('\tau [ps]')
182 ylabel('counts')
183 legend('Location','northeast');
184 text(full_tau_list(ceil(nb_points_time*0.05)),max(
    normalized_g2_vs_delay_uncorrelated_transmitted)*0.95,text_legend,
    'FontSize',9)
185 end
186 %%
187
188 % Displaying the mean g2(0), i.e. the area of the correlated HBT peak
189 fprintf(['PR - ' text_legend_model ' ': Area of mean g2(0) from reflected
    photons: ' num2str(mean_g2_zero_delay_peak_reflected_photons) '\n'])
190 fprintf(['PR - ' text_legend_model ' ': Area of mean g2(0) from
    transmitted photons: ' num2str(
    mean_g2_zero_delay_peak_transmitted_photons) '\n'])
191 fprintf(['PR - ' text_legend_model ' ': Area of mean g2(0) from emitted
    photons: ' num2str(mean_g2_zero_delay_peak_emitted_photons) '\n'])
192
193
194 % Verification of the area of the uncorrelated HBT peaks, that should be
195 % normalized to unity
196 fprintf(['PR - ' text_legend_model ' ': Relative error on the area of
    mean g2 for uncorrelated peaks, for reflected photons: ' num2str((-1 +
    mean_g2_uncorrelated_peaks_reflected_photons)*100 ) '%% \n'])
197 fprintf(['PR - ' text_legend_model ' ': Relative error on the area of
    mean g2 for uncorrelated peaks, for transmitted photons: ' num2str((-1 +
    mean_g2_uncorrelated_peaks_transmitted_photons)*100 ) '%% \n'])

```

```
198 fprintf(['PR - ' text_legend_model ' ': Relative error on the area of
    mean g2 for uncorrelated peaks, for emitted photons: ' num2str((-1 +
    mean_g2_uncorrelated_peaks_emitted_photons)*100 ) '%% \n'])
199
200
201 % Basic verifications on the intensity correlations
202 if min(normalized_g2_vs_delay_uncorrelated_transmitted)<0 || min(
    normalized_g2_vs_delay_reflected)<0 || min(
    normalized_g2_vs_delay_emitted)<0
203     fprintf(' \n \n !!!!!!! Warning: non-physical negative values in g2
        vs delay !!!!!!! \n \n');
204 end
```


Bibliography

- [1] Jonathan P. Dowling and Gerard J. Milburn. Quantum technology: the second quantum revolution. *Philosophical Transactions of the Royal Society of London. Series A: Mathematical, Physical and Engineering Sciences*, 361(1809):1655–1674, jun 2003. doi: 10.1098/rsta.2003.1227.
- [2] H. J. Kimble. The quantum internet. *Nature*, 453(7198):1023–1030, jun 2008. doi: 10.1038/nature07127.
- [3] Hatim Azzouz, Sander N. Dorenbos, Daniel De Vries, Esteban Bermúdez Ureña, and Valery Zwiller. Efficient single particle detection with a superconducting nanowire. *AIP Advances*, 2(3):032124, sep 2012. doi: 10.1063/1.4740074.
- [4] Peter Michler, editor. *Quantum Dots for Quantum Information Technologies*. Springer-Verlag GmbH, 2017. ISBN 978-3-319-56378-7.
- [5] David Press, Thaddeus D. Ladd, Bingyang Zhang, and Yoshihisa Yamamoto. Complete quantum control of a single quantum dot spin using ultrafast optical pulses. *Nature*, 456(7219):218–221, nov 2008. doi: 10.1038/nature07530.
- [6] A. Dousse, L. Lanco, J. Suffczyński, E. Semenova, A. Miard, A. Lemaître, I. Sagnes, C. Roblin, J. Bloch, and P. Senellart. Controlled light-matter coupling for a single quantum dot embedded in a pillar microcavity using far-field optical lithography. *Physical Review Letters*, 101(26), dec 2008. doi: 10.1103/physrevlett.101.267404.
- [7] A. Dousse, J. Suffczyński, R. Braive, A. Miard, A. Lemaître, I. Sagnes, L. Lanco, J. Bloch, P. Voisin, and P. Senellart. Scalable implementation of strongly coupled cavity-quantum dot devices. *Applied Physics Letters*, 94(12):121102, mar 2009. doi: 10.1063/1.3100781.
- [8] Adrien Dousse, Jan Suffczyński, Alexios Beveratos, Olivier Krebs, Aristide Lemaître, Isabelle Sagnes, Jacqueline Bloch, Paul Voisin, and Pascale Senellart. Ultrabright source of entangled photon pairs. *Nature*, 466(7303):217–220, jul 2010. doi: 10.1038/nature09148.
- [9] O. Gazzano, S. Michaelis de Vasconcellos, C. Arnold, A. Nowak, E. Galopin, I. Sagnes, L. Lanco, A. Lemaître, and P. Senellart. Bright solid-state sources of indistinguishable single photons. *Nature Communications*, 4(1), feb 2013. doi: 10.1038/ncomms2434.

BIBLIOGRAPHY

- [10] N. Somaschi, V. Giesz, L. De Santis, J. C. Loredo, M. P. Almeida, G. Hornecker, S. L. Portalupi, T. Grange, C. Antón, J. Demory, C. Gómez, I. Sagnes, N. D. Lanzillotti-Kimura, A. Lemaître, A. Auffeves, A. G. White, L. Lanço, and P. Senellart. Near-optimal single-photon sources in the solid state. *Nature Photonics*, 10(5):340–345, mar 2016. doi: 10.1038/nphoton.2016.23.
- [11] Hélène Ollivier, Ilse Maillette de Buy Wenniger, Sarah Thomas, Stephen C. Wein, Abdelmounaim Harouri, Guillaume Coppola, Paul Hilaire, Clément Millet, Aristide Lemaître, Isabelle Sagnes, Olivier Krebs, Loïc Lanço, Juan C. Loredo, Carlos Antón, Niccolo Somaschi, and Pascale Senellart. Reproducibility of high-performance quantum dot single-photon sources. *ACS Photonics*, 7(4):1050–1059, mar 2020. doi: 10.1021/acsphotonics.9b01805.
- [12] Jürgen T. Stockburger. Stochastic and numerical approaches to dissipative quantum dynamics: path integrals and beyond. *physica status solidi (b)*, 237(1):146–158, may 2003. doi: 10.1002/pssb.200301796.
- [13] Pierre Meystre. *Elements of quantum optics*. Springer, Berlin New York, 2007. ISBN 9783540742111.
- [14] Howard Carmichael. *An open systems approach to quantum optics : lectures presented at the Université libre de Bruxelles, October 28 to November 4, 1991*. Springer-Verlag, Berlin New York, 1993. ISBN 9783540566342.
- [15] Rémi Azouit. *Adiabatic elimination for open quantum systems*. PhD thesis, PSL Research University, 2017.
- [16] C. C. Gerry. *Introductory quantum optics*. Cambridge University Press, Cambridge, UK New York, 2005. ISBN 9780511791239.
- [17] Mark Fox. *Quantum Optics*. Oxford University Press, 2006. ISBN 0198566735.
- [18] Peter Michler, editor. *Single Semiconductor Quantum Dots*. Springer-Verlag GmbH, 2009. ISBN 3540874461.
- [19] Lorenzo De Santis. *Single photon generation and manipulation with semiconductor quantum dot devices*. PhD thesis, Université Paris-Saclay, 03 2018.
- [20] Howard Carmichael. *Statistical Methods in Quantum Optics 1 : Master Equations and Fokker-Planck Equations*. Springer Berlin Heidelberg, Berlin, Heidelberg, 1999. ISBN 9783662038758.
- [21] C. W. Gardiner and M. J. Collett. Input and output in damped quantum systems: Quantum stochastic differential equations and the master equation. *Physical Review A*, 31(6):3761–3774, jun 1985. doi: 10.1103/physreva.31.3761.
- [22] Loïc Lanço. *Enhancing photon-photon and spin-photon interactions with quantum-dot based light-matter interfaces*. Habilitation à diriger des recherches, University Paris Diderot - Paris VII, 2017.
- [23] Sze Meng Tan. A quantum optics toolbox for matlab 5, 1999.

BIBLIOGRAPHY

- [24] Vivien Loo. *Excitation résonante et non-linéarité à faible nombre de photons d'une boîte quantique en microcavité*. PhD thesis, Paris 7, 2012.
- [25] D.A. Steck. Quantum and atom optics. 2007.
- [26] Baldassare Bartolo. *Spectroscopy of systems with spatially confined structures : Proceedings of the NATO Advanced Study Institute on Spectroscopy of Systems with Spatially Confined Structures Erice, Sicily, Italy 15-30 June 2001*. Springer, Dordrecht, 2003. ISBN 9789401002875.
- [27] Ilan Shlesinger, Pascale Senellart, Loïc Lanco, and Jean-Jacques Greffet. Time-frequency encoded single-photon sources and broadband quantum memories based on a tunable one-dimensional atom. 05 2019.
- [28] Howard J. Carmichael. *Statistical Methods in Quantum Optics 2*. Springer-Verlag GmbH, 2009. ISBN 9783540713203.
- [29] Carlos Antón, Paul Hilaire, Christian A. Kessler, Justin Demory, Carmen Gómez, Aristide Lemaître, Isabelle Sagnes, Norberto Daniel Lanzillotti-Kimura, Olivier Krebs, Niccolo Somaschi, Pascale Senellart, and Loïc Lanco. Tomography of the optical polarization rotation induced by a single quantum dot in a cavity. *Optica*, 4(11):1326, oct 2017. doi: 10.1364/optica.4.001326.
- [30] Chris Gustin, Ross Manson, and Stephen Hughes. Spectral asymmetries in the resonance fluorescence of two-level systems under pulsed excitation. *Optics Letters*, 43(4):779, feb 2018. doi: 10.1364/ol.43.000779.
- [31] T. Nakanishi, K. Yamane, and M. Kitano. Absorption-free optical control of spin systems: The quantum zeno effect in optical pumping. *Physical Review A*, 65(1), dec 2001. doi: 10.1103/physreva.65.013403.
- [32] S. Hughes. Enhanced single-photon emission from quantum dots in photonic crystal waveguides and nanocavities. *Optics Letters*, 29(22):2659, nov 2004. doi: 10.1364/ol.29.002659.
- [33] J.R. Johansson, P.D. Nation, and Franco Nori. QuTiP 2: A python framework for the dynamics of open quantum systems. *Computer Physics Communications*, 184(4):1234–1240, apr 2013. doi: 10.1016/j.cpc.2012.11.019.
- [34] A. Ulhaq, S. Weiler, S. M. Ulrich, R. Roßbach, M. Jetter, and P. Michler. Cascaded single-photon emission from the mollow triplet sidebands of a quantum dot. *Nature Photonics*, 6(4):238–242, feb 2012. doi: 10.1038/nphoton.2012.23.